THE PHOTOCHEMISTRY OF METHOXY-SUBSTITUTED POLY(ACRYLOPHENONES)

by

Alfredo Paul Ceccarelli ©

An M.Sc. Thesis submitted to the Department of Chemistry in partial fulfillment of the requirements for admittance to the Degree of Master of Science.

Lakehead University

Thunder Bay, Ontario, Canada

May, 1995

ISBN 0-612-09199-6

ABSTRACT

Poly(*p*-methoxyacrylophenone) (PMAP), poly(3,4-dimethoxyacrylophenone) (P34DMAP) and poly(3,5-dimethoxyacrylophenone) (P35DMAP) were exposed in the form of dilute solutions and thin films to long-wave UV radiation ($\lambda \geq 300$ nm) under high vacuum at 25 ± 1°C. Photoreactions of these polymers occurred predominantly from the carbonyl triplets. In addition, the photophysical observations were consistent with the formation of low-lying π,π^* triplets which, in turn, was the result of substitution of the aromatic ketones by electron-donating methoxy groups. Quenching by both naphthalene and *cis*-1,3-pentadiene conformed to Stern-Volmer kinetics. In all cases, methane and ethane were formed, the quantum yields for their formation being lower in solution than those observed for the solid state photolysis. This resulted from methyl radicals formed by O-CH_3 fission. The principal photoreaction in solution was a Norrish type II decomposition which resulted in random chain scission. The polymers also underwent colouration (yellow), and this was attributed to the formation of quinonoid entities, their precursors being the phenoxy radicals formed by O-CH_3 fission. The effects on chain scission of a number of additives with varying transfer activities were found to be complex as rates of chain scission decreased but not to the extent that would be expected if H-transfer alone was occurring. Solvent quality and polarity were also important. Similarly, the rate of chain scission decreased with increasing polymer concentration, and

this has been attributed to inhibition of separation of macrofragments (from the Norrish II reaction) due to polymer entanglement.

ACKNOWLEDGEMENTS

I wish to express my sincere appreciation to Dr. N.A. Weir for his advice and direction in the research and preparation of this thesis. I would also like to thank Dr. J. Arct for his laboratory assistance and aid in the characterization of the polymers. In addition, I would like to thank Dr. Barbara Arct for her invaluable help in synthesizing the polymers. I also wish to thank Mr. K. Pringnitz for his help in the spectroscopic analysis of the polymers.

I also wish to thank the technical staff of the Faculty of Science at Lakehead University with special reference to Mr. D. Corbett and Mr. A. Bharath for their technical assistance.

In addition, I gratefully acknowledge the generous support provided by the Centres of Excellence (Mechanical and Chemi-Mechanical Pulps Network).

TABLE OF CONTENTS

LIST OF ILLUSTRATIONS

Figures

Tables

I. INTRODUCTION

The photochemical field covers all processes which involve chemical change brought about by the interaction of light with matter. Upon absorption of light (photons), the electronically excited molecule can undergo several photophysical processes which compete with the photochemical processes to return the excited species to the ground state.[1,2] The energy associated with a photon of radiation is of the same order as the bond energies of many of the bonds present in organic molecules. It is therefore not surprising that absorption of light can result in chemical reactions. According to the Grotthus-Draper law, only the light absorbed by a molecule can produce a photochemical change in that molecule.[1] This, however, does not mean that the absorption of one quantum of light will bring about a photochemical change in the system as there may well be other more favourable processes for the system to dissipate energy to return to its ground state.[1]

The light absorbed by a molecule has energy equal to the energy difference between the electronic states of the absorbing species. The energy imparted to a molecule, E, by absorption of light is expressed as follows:

$$\Delta E = h\nu = E_1 - E_0$$

where E_1 and E_0 are the energies of the electronic excited state and the electronic ground state respectively, h is Planck's constant and ν is the photon frequency.

The standard molecular orbital model considers that an excited state is derived from the ground state via promotion of an electron from an occupied orbital to a vacant, higher energy orbital. If all the electrons are spin-paired in the ground state, which is usually the case for organic molecules, a one-electron promotion creates two singly occupied orbitals. If the electrons in these two orbitals are spin antiparallel, a singlet state results. In triplet states the two electron spins are parallel. According to Hund's rule, the electronic configuration with the higher spin multiplicity is more stable; therefore, a triplet state has a lower energy than the corresponding singlet state[1] and this can be explained in terms of the Pauli Exclusion Principle. If the two electrons have parallel spin, they cannot occupy the same molecular orbital; therefore, they will tend to avoid each other and, hence, the energy of repulsion will be reduced.[2] This results in a lowering of the energy of the triplet state relative to the corresponding singlet state in which the electrons can exist in the same region in space simultaneously.

The absorption of light results in the excitation of an electron from an electronic ground state (S_0) to an electronic excited state (S_1) of higher energy (Figure 1.1).

$$S_0 + h\nu \rightarrow S_1$$

According to the Franck-Condon principle, the time required for this electronic transition is so short that the internuclear distance remains unchanged. As electronic

transitions are so fast (10^{-15} - 10^{-16} s) compared to molecular vibrations (10^{-13} s), the nuclei have practically the same relative positions and velocities immediately after the transition as they did just before the transition. This implies that the transition is vertical and may be represented by a vertical line connecting the two potential energy surfaces (Figure 1.2), and the most probable transition will be to that vibrational level with the same geometry.[3] One consequence of this is that molecules in the S_1 state frequently possess a number of vibrational quanta.

A. **Photophysical Processes**

After the absorption of a photon, the electronically excited molecule is energetically unstable with respect to the ground state. It generally has a short lifetime since there are a number of different processes which lead to its deactivation to the ground state. Photochemical processes produce chemically distinguishable products while photophysical processes, as seen in Figure 1.1, allow electronically excited molecules to dissipate their energy either by the emission of a photon (luminescence) or by the transfer of energy to other forms (usually to the vibrational modes of the system).[1] Different physical changes are experienced by the electronically excited molecules in photophysical processes; however, the species are the same chemically. The most favourable pathways for energy dissipation are determined by the structure of the molecule

and the nature of its excited state.

1. **Vibrational Relaxation and Internal Conversion**. These two processes are radiationless decays between various vibrational levels of a given electronic state; therefore, no change in multiplicity occurs. Vibrational relaxation results in a decay from a high vibrational level of a given electronic state to the lowest vibrational level of that same electronic state. Organic photochemistry is mostly conducted in solution; as a result, the excess vibrational energy is dissipated as heat due to collisions between the excited molecule and solvent molecules.[2]

On account of the characteristics of the potential energy surfaces for excited and ground state species, there is overlap between the energies of the higher vibrational levels of lower electronic states and lower vibrational levels of higher electronic states; as a result, internal conversion of electronic to vibrational energy is possible. Therefore, internal conversion results in a decay between vibrational levels of two different electronic states of the same multiplicity with no change in the total energy of the molecule. By a combination of vibrational relaxation and internal conversion, an excited molecule at ordinary pressures can drop very quickly to the lowest vibrational level of the first excited electronic state and, in a similar fashion, can subsequently return to the ground state.[1]

2. **Intersystem Crossing**. This radiationless transition

occurs between vibrational levels of two electronic states of different multiplicity with no change in the total energy of the molecule. Intersystem crossing provides the most favourable route to the triplet state when the energy difference between singlet and triplet excited states is not large. Intersystem crossing is made possible by the intersecting of potential energy surfaces for singlet and triplet states. On its first vibration, the initially formed singlet state crosses over to the potential energy surface for the triplet, the process being adiabatic.

$$S_1 \rightarrow \text{Intersystem Crossing} \rightarrow T_1$$

The reverse process of intersystem crossing, triplet to singlet, is highly unlikely since the most stable form of the triplet is lower in energy than the corresponding singlet state.[1] The time for intersystem crossing from a singlet to a triplet state ranges from 10^{-8} to 10^{-11} seconds.[4]

3. **Fluorescence**. Fluorescence is a radiative transition between electronic states of the same multiplicity. Rapid vibrational relaxation and internal conversion allows fluorescence to occur between the lowest vibrational levels of the first excited singlet state and several vibrational levels of the electronic ground state.

$$S_1 \rightarrow S_0 + h\nu'$$

If the vibrational spacings in the excited singlet state are similar to those in the electronic ground state, i.e. similar geometry, there will be a mirror image relationship between

the bands of the fluorescence spectrum and the absorption spectrum. However, owing to differences in dipole orientations, hydrogen bonding and differences in geometry between the ground and excited states, an imperfect mirror relationship frequently results and this is reflected by a definite Stokes shift.[5] Due to the lack of change in multiplicity, this process is very fast (10^{-6} to 10^{-11} s).

4. **Delayed Fluorescence**. Delayed fluorescence, in which the luminescence decays more slowly than normal fluorescence from the same molecule, can arise by several mechanisms of which the most closely investigated are triplet-triplet annihilation and thermally-activated delayed fluorescence. First, delayed fluorescence can be the result of the thermal excitation of a molecule in the lowest excited triplet state back to the lowest excited singlet state (i.e. reverse intersystem crossing). Fluorescence of this newly populated singlet state should be spectrally similar to normal fluorescence, but its lifetime will be that corresponding to the excited triplet. This unimolecular process is known as E-type delayed fluorescence.[1]

$$T_1 \rightarrow \text{Intersystem Crossing} \rightarrow S_1 \rightarrow S_0 + h\nu'$$

The thermal repopulation of the lowest excited singlet state is therefore displayed only by certain molecules which have a small energy gap between the lowest excited singlet and triplet states.

Delayed fluorescence also arises when the triplet

lifetimes of two excited molecules are sufficiently long that an encounter occurs between them. This triplet-triplet annihilation results in the thermal excitation of one molecule to the lowest excited singlet state from which fluorescence can occur, and the internal conversion of the other molecule to the electronic ground state.[5]

$$T_1 + T_1 \rightarrow S_0 + S_1 \rightarrow S_0 + h\nu'$$

This bimolecular process known as P-type delayed fluorescence may occur in molecules with substantial differences in energy between the lowest excited singlet and triplet states. Furthermore, this type of process can result in the formation of excimers (involving both singlet and triplet states) and exciplexes. An energy transfer between chromophores from identical molecules (i.e. excited state molecules with identical ground state molecules) produces an excimer; however, an energy transfer between chromophores from different molecules produces an exciplex.[4]

5. **Phosphorescence**. Phosphorescence is a radiative transition between electronic states of differing multiplicities and occurs between the lowest vibrational level of the first excited triplet state and several vibrational levels of the electronic ground state.

$$T_1 \rightarrow S_0 + h\nu''$$

Due to a change in multiplicity, phosphorescence is longer lived than fluorescence (10^{-5} to 10 s); as a result, several photophysical processes in solution compete effectively with

phosphorescence for deactivation of the first excited triplet state. Except for the shortest lived phosphorescences, collisional deactivation by solvent molecules, quenching by paramagnetic species, photochemical reactions and energy transfer processes prevent the observation of phosphorescence in solution.[5] Phosphorescence is therefore studied in the glassy state at liquid nitrogen temperature where collisional processes cannot completely deactivate the triplet state.

B. **Photochemical Processes**

In addition to the photophysical processes discussed, photochemical processes may arise from a molecule in an excited electronic state (singlet or triplet). In general, photochemical processes can be divided into two categories depending upon the wavelength of the incident radiation. Wavelengths in the 200-300 nm region are used in short-wave photolysis while wavelengths greater than 300 nm are used in long-wave photolysis. The latter of the two has more significance as long-wave radiation represents solar radiation received by the earth; as a result, long-wave photolysis is of more interest in the study of outdoor weathering of many polymer systems.

A photochemical process involves the initially excited molecule along with one or more reactive intermediates. Two general processes can be distinguished, i.e., those arising from the direct reaction of the initially excited species and those associated with the reactive species formed. The types

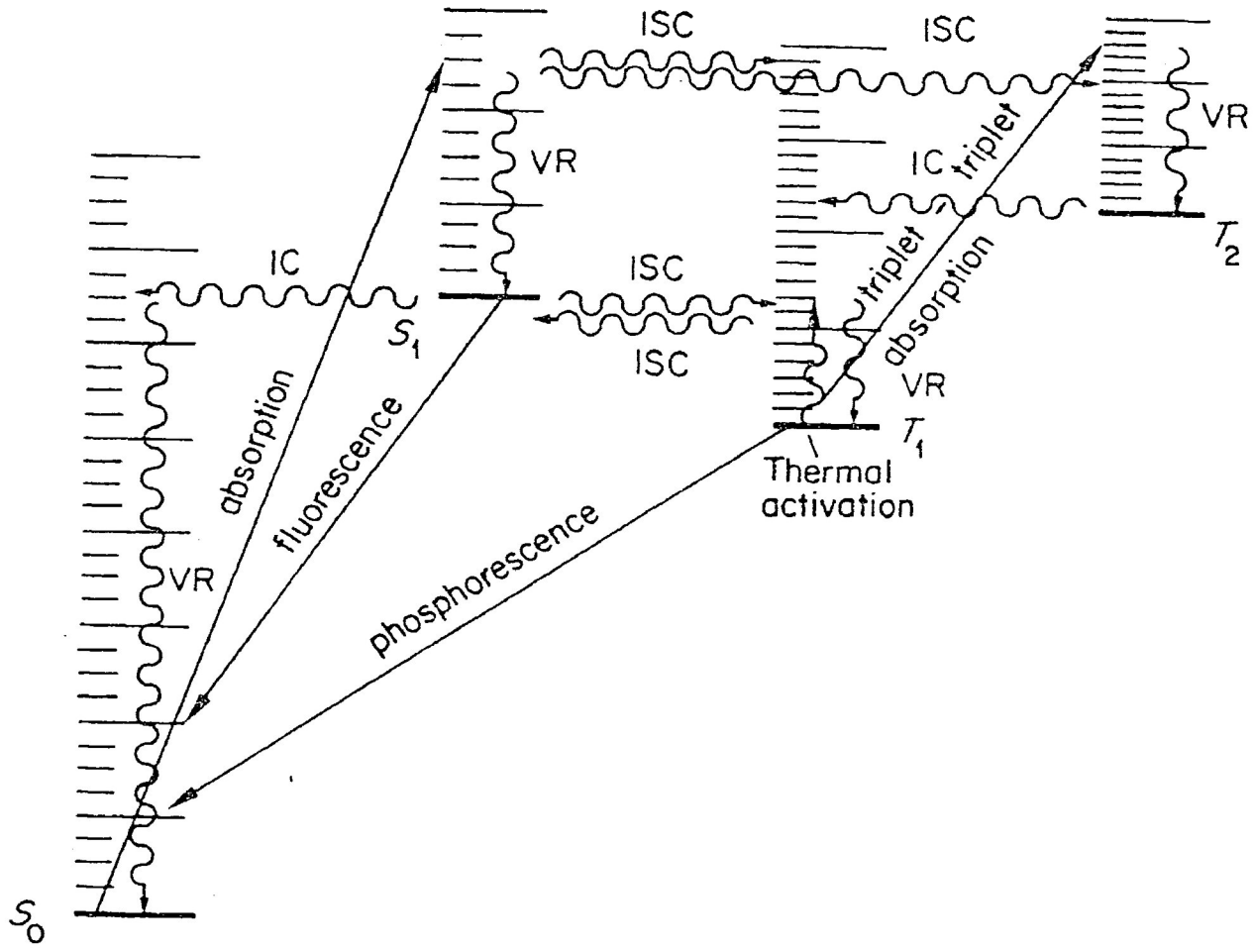

Figure 1.1. Jablonski Diagram Illustrating the Photophysical Transitions in a Photoluminescent System.[6] Bold Lines Indicate Radiative Decay; Wavy Lines Indicate Radiationless Decay (VR = Vibrational Relaxation; IC = Internal Conversion; ISC = Intersystem Crossing).

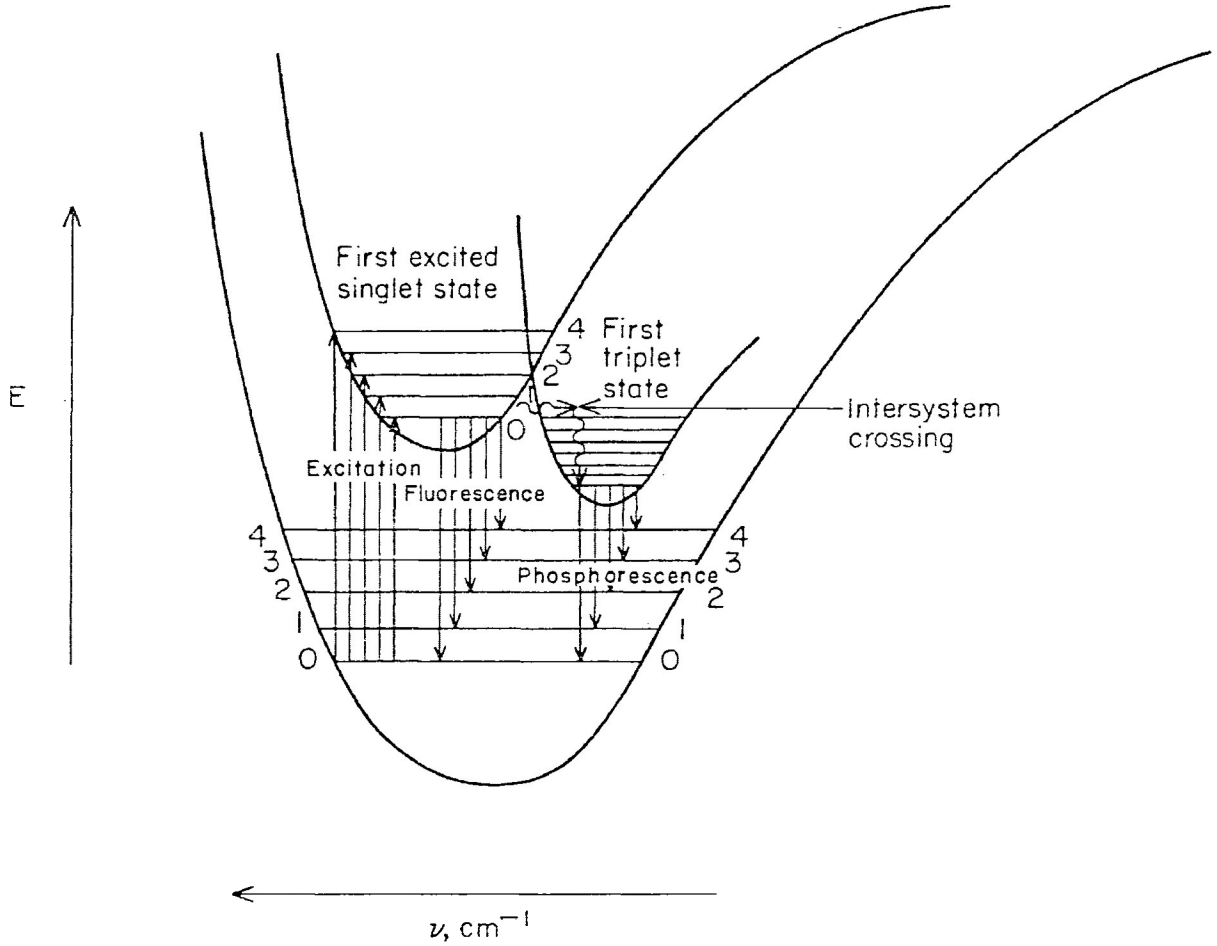

Figure 1.2. Potential Energy Diagram Displaying Excitation and Radiative Deactivation.[3]

of intermediates involved in photochemical reactions include excited state complexes, radicals, radical ions, and compounds of limited thermal and photochemical stability, these giving rise to products by some secondary photochemical process.[2] The lifetimes of these intermediates are quite variable and can range from seconds to picoseconds.

C. **Photochemistry of Ketones**

The study of photoreactions of small ketonic molecules over the past generation have led to a better understanding of their reaction mechanisms; furthermore, this has resulted in a greater understanding of the reaction mechanisms that occur in larger ketonic molecules. The carbonyl chromophore is quite interesting, photochemically speaking, as it is photochemically labile, thermally stable and capable of absorbing light within the range of terrestrial sunlight radiation (near ultraviolet region).[1] These absorptions correspond to the excitation of a non-bonding electron on oxygen from an orbital localized in the plane of the carbonyl group into the higher energy anti-bonding π^*-orbitals delocalized over the carbonyl group (Figure 1.3).

Because the π^*-orbitals and the non-bonding orbitals of oxygen are orthogonal, $n \rightarrow \pi^*$ transitions are considered to be symmetry forbidden and, therefore, of low intensity (typically $\epsilon \leq 150$ dm^3 mol^{-1} cm^{-1}).[2] Aliphatic ketones typically produce a single absorption in the near ultraviolet region (280 nm) which corresponds to the $n \rightarrow \pi^*$ transition of the carbonyl

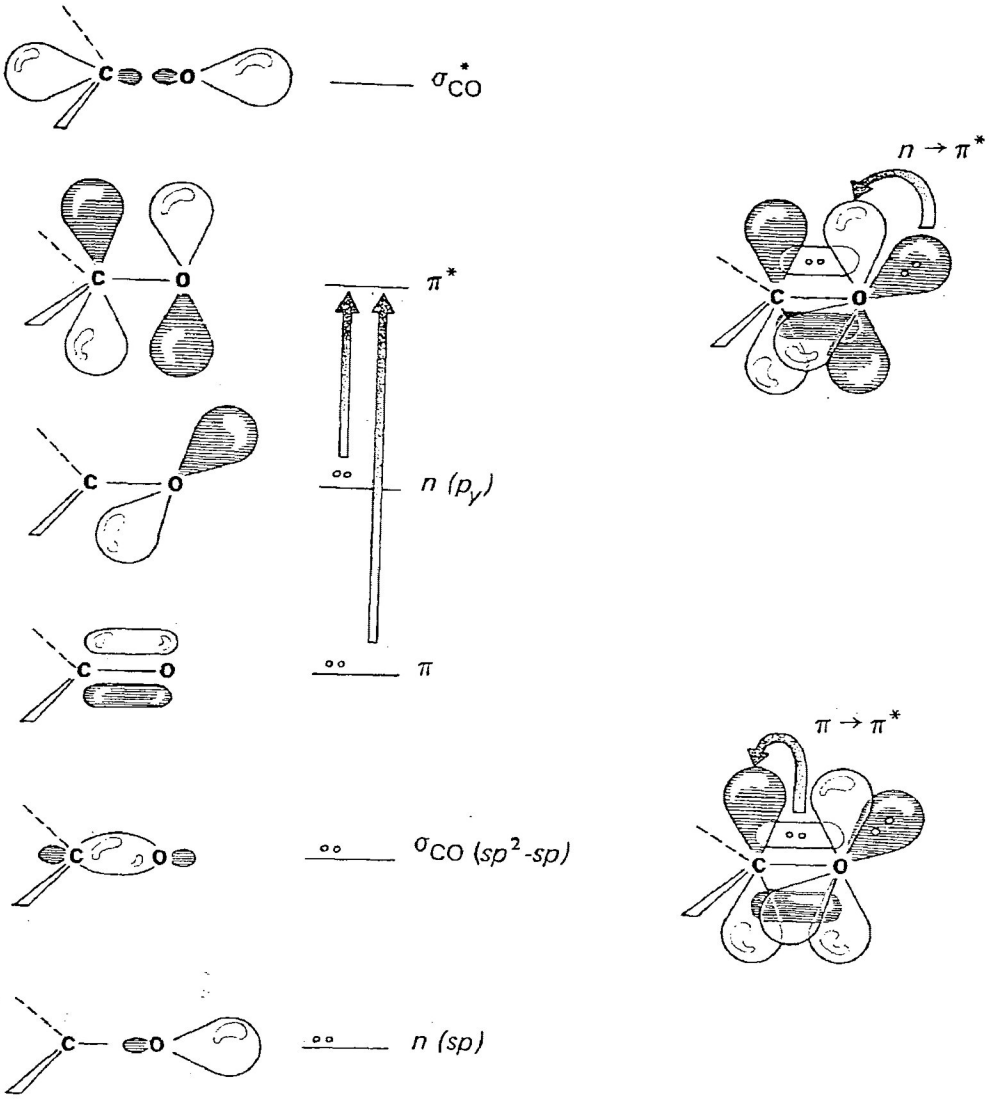

Figure 1.3. Electronic Transitions of the Carbonyl Group.[7]

group. Because the energy distribution in both singlet and triplet n,π^* states is similar, photoreactions of aliphatic ketones may proceed from the singlet or triplet state. Aromatic ketones, however, produce two absorptions. The first absorption occurs around 320 nm and corresponds to the $n \rightarrow \pi^*$ transition of the carbonyl group while the second absorption occurs around 280 nm (and lower) and corresponds to the longest wave $\pi \rightarrow \pi^*$ transition of the aromatic ring. The bathochromic shift shown by $n \rightarrow \pi^*$ transitions in aromatic ketones is due to the inductive effect of the aromatic ring which lowers the energy between the ground and excited states of the carbonyl group.[2]

The electron density at the carbonyl group is increased by the presence of the $\pi \rightarrow \pi^*$ transition of the aromatic ring. Therefore, electron-donating substituents in conjugation with the carbonyl group stabilize the π,π^* triplet state and destabilize the n,π^* triplet state. Electron-withdrawing substituents in conjugation with the carbonyl group, however, destabilize the π,π^* triplet state and stabilize the n,π^* triplet state. Because the quantum yield for intersystem crossing is unity or very close to unity, photoreactions of aromatic ketones mainly proceed from the triplet state.[1,2]

Photoreactions of ketones can be classified as either α-Cleavage (Norrish Type I Reaction) or Hydrogen Abstraction Reactions which include many reactions such as the Norrish Type II Reaction, photoreduction, photoisomerization and other

inter- and intramolecular hydrogen abstraction reactions.[8]

1. **α-Cleavage (Norrish Type I Reaction)**. This reaction arises as a result of localization of the excitation energy, as vibrational energy, in the weaker of the σ-bonds attached to the carbonyl group. The result of this photochemical reaction (shown below) is the fission of a bond adjacent to the excited carbonyl group producing two free radicals.[1,2]

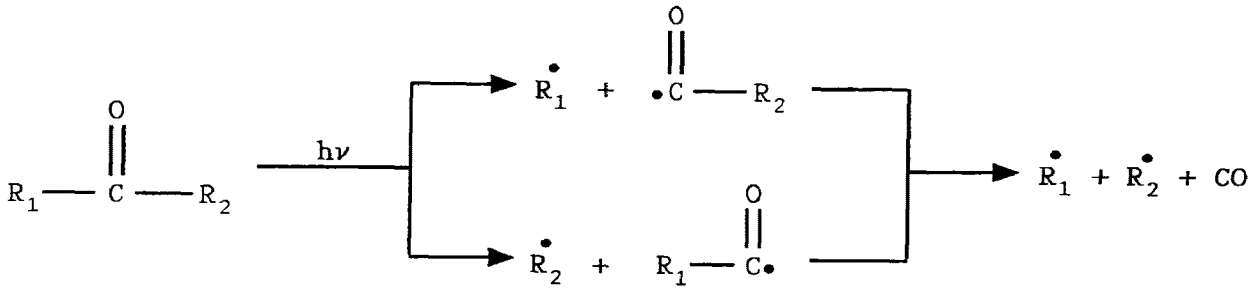

Norrish Type I Reaction (α-Cleavage)

Radical stabilization greatly influences the reaction pathway, and the cleavage occurs mainly at the α-carbon bearing the greater number of alkyl or aryl substituents.[1] On the basis of orbital symmetry correlations, these reactions occur predominantly from the triplet state.

The fate of the radicals formed depends upon the experimental conditions. If the reaction takes place in a solvent which has an easily abstractable hydrogen atom, the radicals then react with the solvent. If the reaction is carried out with solid or liquid phase ketones, the radicals

can then abstract a hydrogen atom from another ketone molecule.[1,2] The point of abstraction, though, depends upon the strength of the carbon-hydrogen bond and, with it, the stability of the newly formed radical. Tertiary hydrogens are abstracted more readily than secondary hydrogens which are in turn preferred to primary hydrogens. Alkyl radicals typically also undergo disproportionation and combination reactions.

The efficiency of the Norrish Type I reaction also depends on the structure of the molecule as well as the mobility of the radicals formed. In very concentrated solutions or in the solid state these radicals have restricted mobility and experience a cage effect. When large cage effects are involved, the radicals may recombine to reform the original ketone (cage collapse). The cage effect thus reduces the quantum yield of α-cleavage which is therefore favoured at high temperatures in the gas phase where vibrational deactivation is more difficult to achieve.[2] In the gas phase, vibrationally excited acyl radicals, produced from α-cleavage, frequently undergo decarbonylation to produce carbon monoxide. In solution, decarbonylation occurs only if the acyl radical has an adjacent stabilizing group, such as a tertiary alkyl or benzyl group, so as to promote a second α-cleavage.[1,2]

2. **Hydrogen Atom Abstraction**. The excited keto species resulting from the $n \rightarrow \pi^*$ transition abstracts a hydrogen atom either intramolecularly from a C-H unit which is spatially close to it or intermolecularly from a suitable adjacent donor

molecule. The intramolecular abstraction is strongly dependent on the molecular conformation, but both intermolecular and intramolecular abstraction are dependent on the strength of the C-H bond of the hydrogen donor molecule. The excitation energy and electronic configuration of the excited state of the particular ketones also affect the hydrogen abstraction efficiency, e.g. the π,π^* triplet is much less effective in abstraction reactions (i.e. less electrophilic).

The Norrish Type II reaction, the classical hydrogen atom abstraction reaction, is an intramolecular type hydrogen abstraction which occurs at the carbon γ to the carbonyl group. This reaction (shown below) leads to the cleavage of the α-β carbon-carbon bond and results in the formation of a terminal olefin and an enol which rapidly tautomerizes back to a ketone.[2]

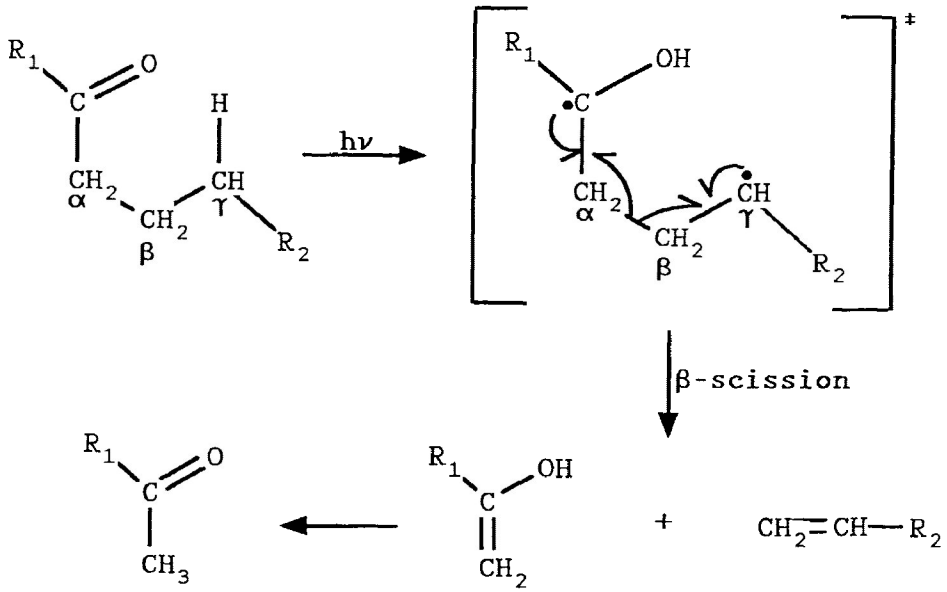

Norrish Type II Reaction (γ-Hydrogen Abstraction)

Yang and Yang[9] first showed that the reaction produced a 1,4-biradical intermediate, and Wagner[10] confirmed its presence through biradical trapping experiments. The 1,4-biradical from γ-methylvalerophenone[11] did, however, undergo other competitive processes (other than β-cleavage). One such process was a cyclization (combination) reaction to form cyclobutanols while another involved a reverse hydrogen transfer to give the ground state ketone. A simplified mechanism is shown below:

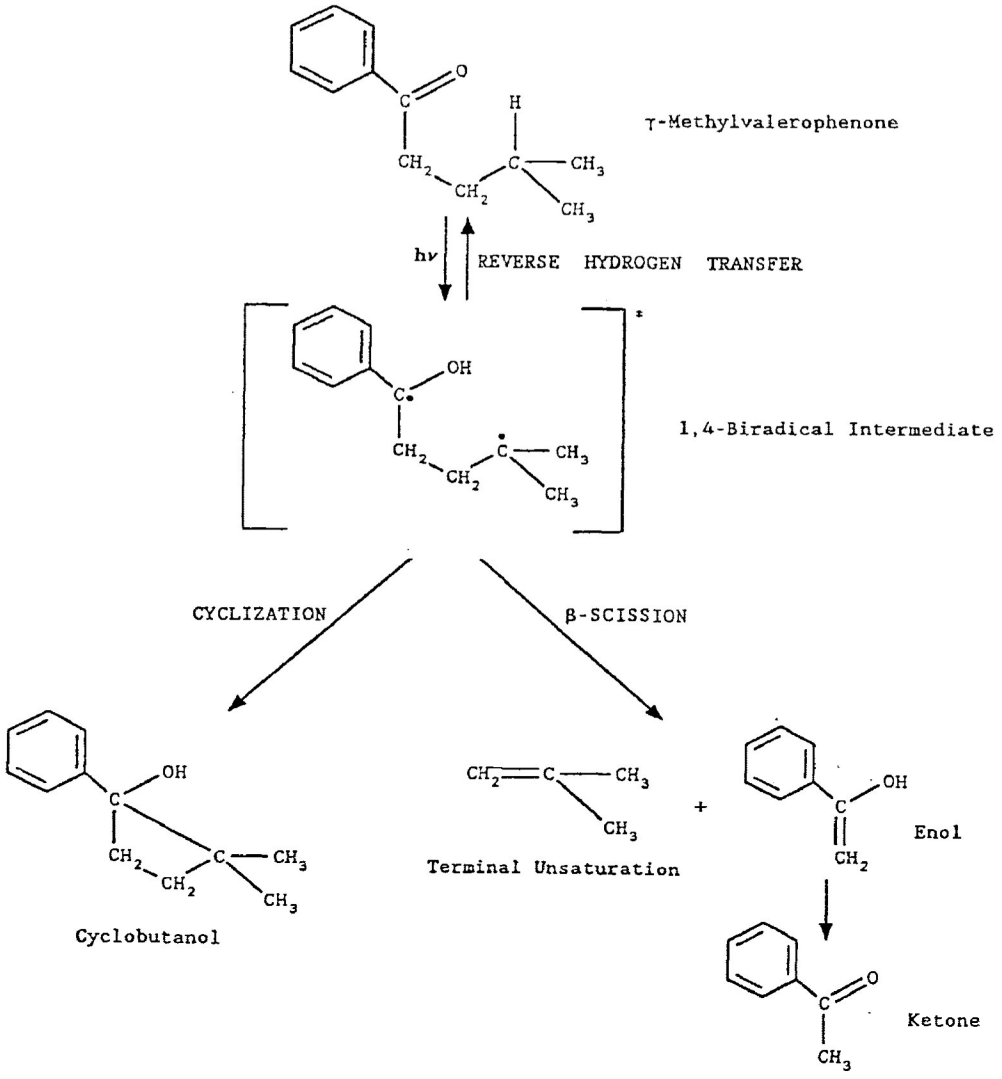

In phenyl alkyl ketones, the lifetimes of the biradicals produced are 30-100 ns.[1] The rate constants for the respective individual processes and the attainment of the conformational equilibrium in the biradical influence reaction selectivities. The efficiency of type II cleavage is dependent upon the degree to which the p-orbitals of the biradical are parallel to the C_α-C_β bond; the more parallel these are, the more overlap of the p-orbitals with the developing π-orbitals of the double bonds.[1] A typical conformation best fulfilling this requirement is as follows:

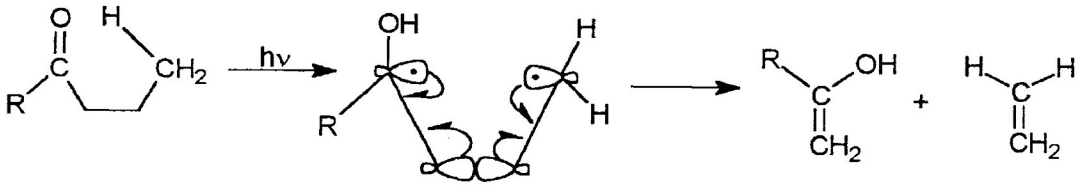

Any feature which inhibits the attainment of the parallel geometry will reduce the cleavage efficiency. On the other hand, the cyclization to produce cyclobutanols requires only interaction of the radical centres; therefore, it is always competitive with the cleavage process.

The use of polar solvents, particularly alcohols, significantly increases type II quantum yields of phenyl alkyl ketones. Hydrogen bonding of the solvent to the hydroxyl function apparently stabilizes the biradical in a conformation

which prevents the reverse hydrogen transfer to give the ground state ketone and also slows the cyclization process.[2]

The efficiency of γ-hydrogen abstraction and formation of the 1,4-biradical is also dependent on the preferred molecular geometry in the ground state, i.e., the proximity of the ketone chromophore to the γ-hydrogen produces a suitable environment for hydrogen abstraction. This imposes conformational control over the biradical formation.[12] The γ-hydrogen must be in the *syn* conformation (relative to the carbonyl function) so as to produce a strain free 6-membered intermediate in the chair configuration. If the γ-hydrogen is in the *anti* conformation, the system must rotate into a *syn* conformation before undergoing a type II reaction.[12] If the triplet lifetime is much shorter than the time it takes for the bond rotation into *syn* conformation, the only ketones that will then react to form the 1,4-biradical are those already in the *syn* conformation. This imposes, what Wagner[12,13] refers to as, ground state control on the system.

This influence of the conformation on the reaction is shown by the photoreactions of 1-methylcyclohexyl phenyl ketone.[14] This system, due to the products obtained from irradiation of this ketone, undergoes both α-cleavage and γ-hydrogen abstraction. Quenching experiments indicated that the products of the two different reactions are quenched with different efficiencies. The measured rate constants for α-cleavage ($k_{\alpha\text{-cleavage}}$) and γ-hydrogen abstraction (k_H) were

2.5×10^7 s^{-1} and 1.7×10^8 s^{-1} respectively.[14] Conclusive evidence is therefore obtained from these quenching experiments that there are two kinetically distinguishable n,π^* triplet states each leading to a different reaction.

From the molecular structures, it is evident that the *anti* conformation is expected to lead to α-cleavage whereas the *syn* conformation is ideally oriented to undergo γ-hydrogen abstraction. Furthermore, both processes are appreciably more rapid than ring inversion; as a result, the product composition and the efficiencies of the processes reflect the population of the ground state conformations. Imposing steric constraints on rotations of the bonds between the carbonyl and the γ-C-H, in order to reduce the proportion of unfavourable conformations, increases rate constants for γ-hydrogen abstraction.[1] The contribution of the *anti* conformer to γ-hydrogen abstraction, therefore, will be determined by the magnitude of energy barrier to rotation of the acyl group. These effects are illustrated by photoisomerization of phenyl alkyl ketones (Figure 1.4).

In addition to there being two distinct triplets arising from conformationally different ground states, two conformationally different photoenols are observed following γ-hydrogen abstraction.[15] Only the *syn* triplet can abstract a hydrogen atom intramolecularly to form a 1,4-biradical; in addition, if its lifetime is long enough, it has time to undergo rotation into the *anti* conformer. The triplet state

process, however, accounts for a little more than 50% of the total enolization reaction; therefore, there is, apparently, an appreciable contribution from the n,π^* singlet state.[1] This can only involve the *syn* conformer since it has the required geometry for γ-hydrogen abstraction. Quenching studies with well known triplet quenchers reveal that about 30% of the total yield of the *syn* photoenol remains while essentially formation of all of the *anti* photoenol is quenched.[1] Thus, only one excited state (the triplet) of the *anti* conformer is able to participate in photoenolization reactions. Furthermore, photoenolization involving the singlet state of the *syn* conformer yields essentially only the *syn* photoenol, and the rate of this reaction competes with the rapid intersystem crossing (Figure 1.4).

Increasing substitution on the γ-carbon increases the abstractability of the H-atom, i.e., the rate of type II cleavage increases as the dissociation energy of the γ-C-H bond decreases. Electron-donating substituents attached to the γ-carbon atom reduce the bond dissociation energy as they make the H-atom more susceptible to electrophilic attack by the carbonyl n,π^* state.[2] Conversely, electron-withdrawing substituents are deactivating.

Electron-donating substituents attached to the aromatic ring decrease the rate of type II cleavage since they favour the formation of low-lying π,π^* triplets. Electron-withdrawing substituents favour the formation of n,π^* triplets, and hence

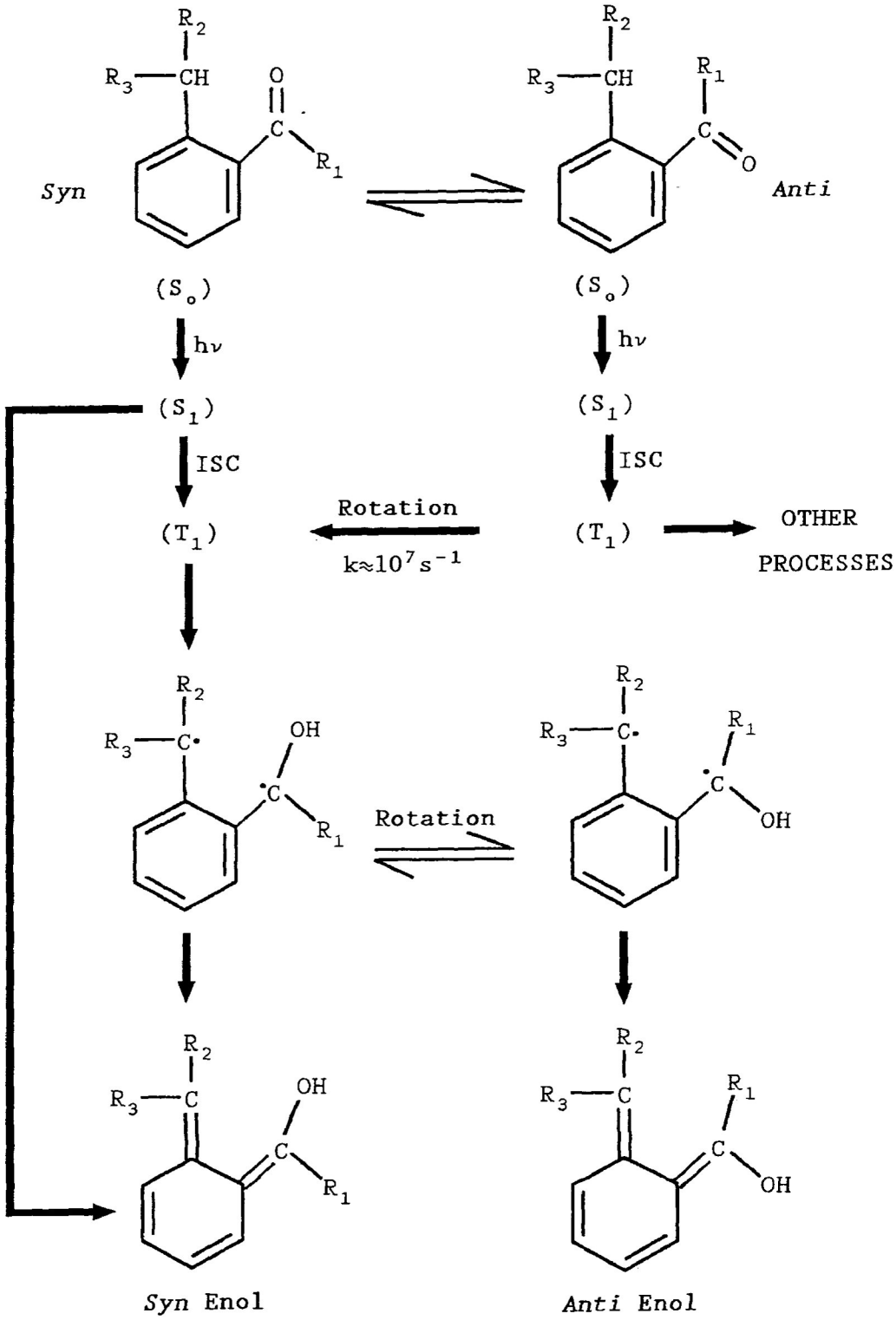

Figure 1.4. Photoisomerization of Phenyl Alkyl Ketones.[1,15]

increase the rate of type II cleavage.

It is also possible for intramolecular abstraction of δ-hydrogens to occur resulting in the formation of a 1,5-biradical which can undergo similar reactions. For example, it can undergo a reverse hydrogen transfer back to the ground state ketone, cyclization to form cyclopentanol, or abstraction reactions with solvent or other ketone molecules, the most common reaction being cyclization. The 1,5-biradical, following cyclization, forms a fairly strain free 5-membered ring; however, the transition state involves a 7-membered ringlike structure which is energetically less favoured than the 6-membered cyclic transition state formed from the 1,4-biradical.[2] It is not possible for the 7-membered transition state to form a relatively strain free chair configuration as is found with the 6-membered transition state. When both γ and δ-hydrogens are present, abstraction occurs primarily from the γ-hydrogens unless steric constraints make the formation of the 6-membered transition state impossible.[2]

Carbonyl compounds which have an n,π^* triplet state as the lowest excited state also abstract hydrogen intermolecularly from donor molecules efficiently (photoreduction). However, when the π,π^* triplet state is the lowest excited state, photoreduction does not occur or has a very low efficiency, the inefficiency being due to the relatively high electron density on the oxygen. Similarly, the

radical-like structure of the n,π^* triplet state is much more electrophilic.[1,2]

Solvent and substitution can influence the nature of the lowest excited state of aromatic carbonyl compounds. In polar solvents, such as isopropanol, the abstraction rate constants increase due to a decrease in the dissociation energy of the C-H bonds. However, ketones, which have a relatively small energy difference between the n,π^* and π,π^* triplet states, are more greatly affected by the polar properties of the solvent and there is an increasing contribution of the unreactive π,π^* triplet state, these states being relatively stabilized in polar solvents. As well, electron-donating substituents on the aromatic ring lower the energy of the π,π^* triplet state below that of the n,π^* triplet state with consequent loss in reactivity to photoreduction. On the other hand, electron-withdrawing substituents increase the energy gap between these respective states and thereby promote hydrogen abstraction by the n,π^* triplet state.[1,2]

D. **Photochemistry of Keto Polymers**

The carbonyl group is important in polymeric systems as it is known to undergo photoreactions upon exposure of these polymers to terrestrial sunlight radiation.[2] The behaviour of the carbonyl chromophore does not change significantly from small ketone molecules to long chain keto polymers. Any differences that do occur are a result of the long chain nature of the polymer and the restricted or more viscous

environment the system imposes on the dynamics of the polymer chain.[2,16]

The photochemistry of polymers can be divided into two steps:

1) Primary Reactions - The major photochemical reactions that originate from the excited n,π^* singlet and triplet states of the carbonyl are:

i) Norrish Type I Reaction: α-Cleavage which results in the production of free radicals.

ii) Norrish Type II Reaction: A photoelimination reaction which results in the formation of an unsaturated molecule and another ketone.

iii) Photoreduction: This hydrogen abstraction reaction by the carbonyl results in the formation of a biradical, and it can be either inter- or intramolecular in nature depending upon the location of the hydrogen atom to be abstracted. Enols may result. Photoisomerization is similar but restricted to molecules in which intramolecular γ or δ abstraction is possible.

2) Secondary Reactions - This involves further reactions of the radicals with each other or with the polymer. These reactions include the cleavage of side groups resulting in the formation of volatile products, chain scission, crosslinking (combination of macroradicals) and cyclization (which involves an intramolecular crosslinking) of the polymer.

The photochemistry of keto polymers was initially studied

by Guillet and Norrish, and they investigated the photolysis of poly(methyl vinyl ketone) (PMVK) in solution.[17,18] PMVK underwent both Norrish type I and II reactions according to the following scheme:

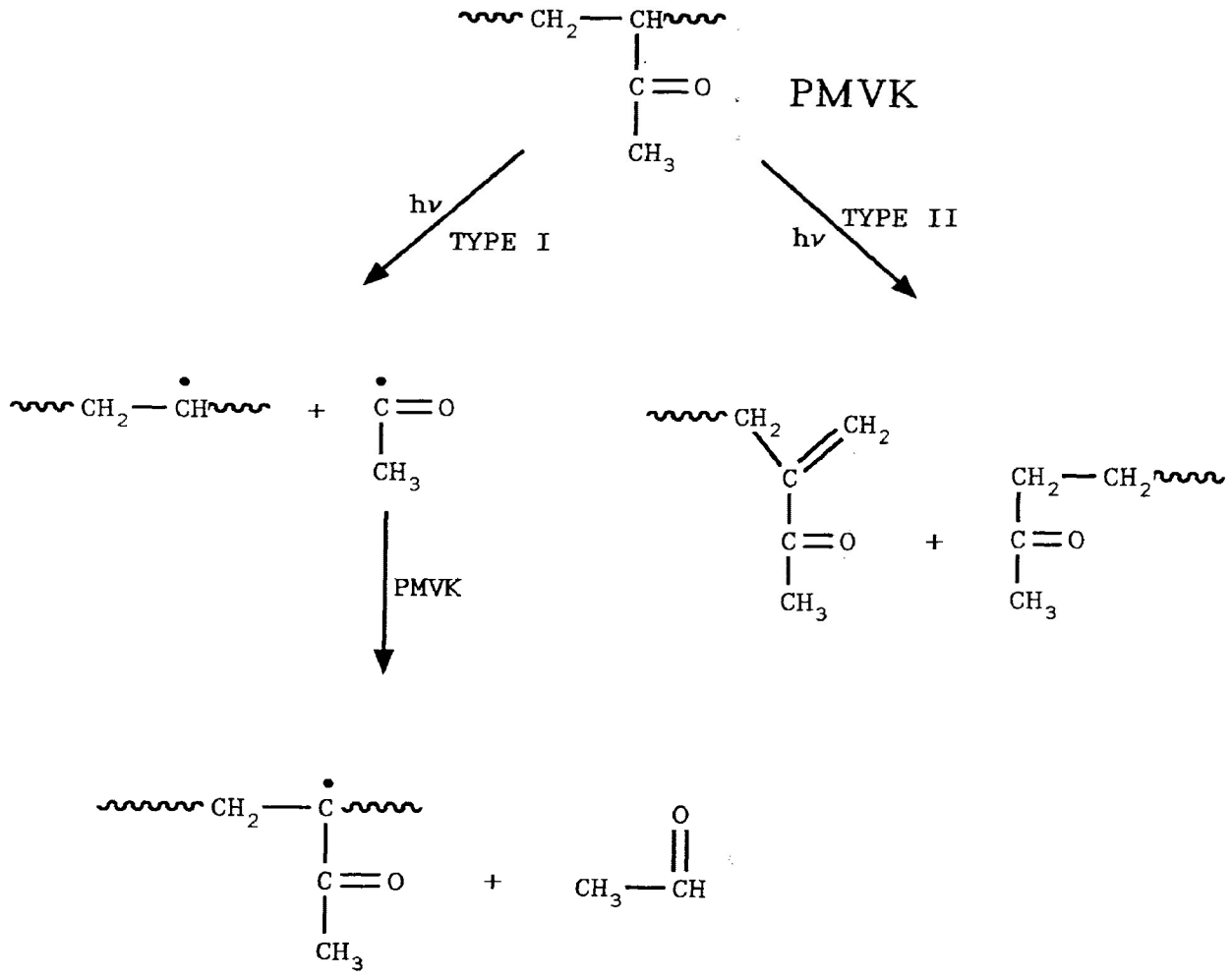

The type I reaction involved α-scission which resulted in the formation of an acetyl radical which subsequently abstracted a hydrogen atom to produce acetaldehyde. The type II reaction, however, involved random chain scission via

γ-hydrogen abstraction with concomitant reduction in the molecular weight of the polymer. A higher quantum yield was obtained for the type II reaction, and it was suggested that the efficiency of the type I reaction is strongly dependent on the stability of the radical formed and on the ability of the radicals to diffuse away from each other before they recombine within the initial cages.[2]

The photodegradation of poly(phenyl vinyl ketone) (PPVK), commonly known as poly(acrylophenone) (PAP), was investigated by Scaiano, and he showed that the principal degradative reaction was a Norrish type II decomposition which resulted in random chain scission.[19,20]

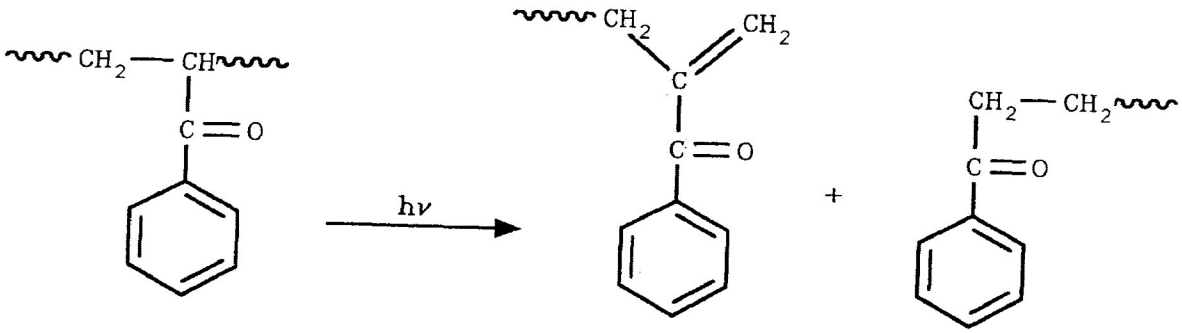

PPVK

Triplet energy transfer in PPVK was also investigated.[20] For triplet-triplet energy transfer to occur, the carbonyl donor and acceptor (quencher) must be in close proximity to allow for sufficient overlap of their orbitals. It was also

shown that the degree of degradation as a function of irradiation time showed an initial sharp increase but leveled off with time. According to Scaiano, intermolecular triplet quenching by the unsaturated chromophores produced from the Norrish type II reaction was responsible. These groups are very good quenchers, their high efficiency being due to fast energy transfer between themselves and the carbonyl triplets.

If a Norrish type II reaction cannot occur, i.e. no γ-hydrogens present, photodegradation of the keto polymers (in solution) can occur either by a Norrish type I reaction or by photoreduction as was shown by Weir *et. al.*[21,22] using poly(vinylacetophenone) (PVAP) and poly(α-methylvinylacetophenone) (PMVAP). The Norrish type I reaction is as follows:

(A)

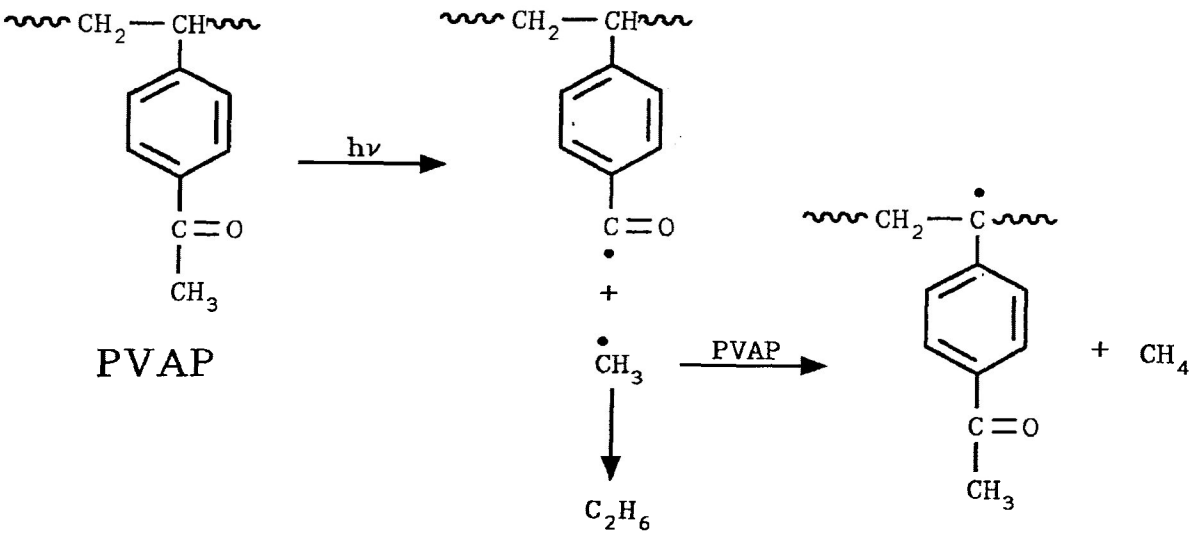

(B)

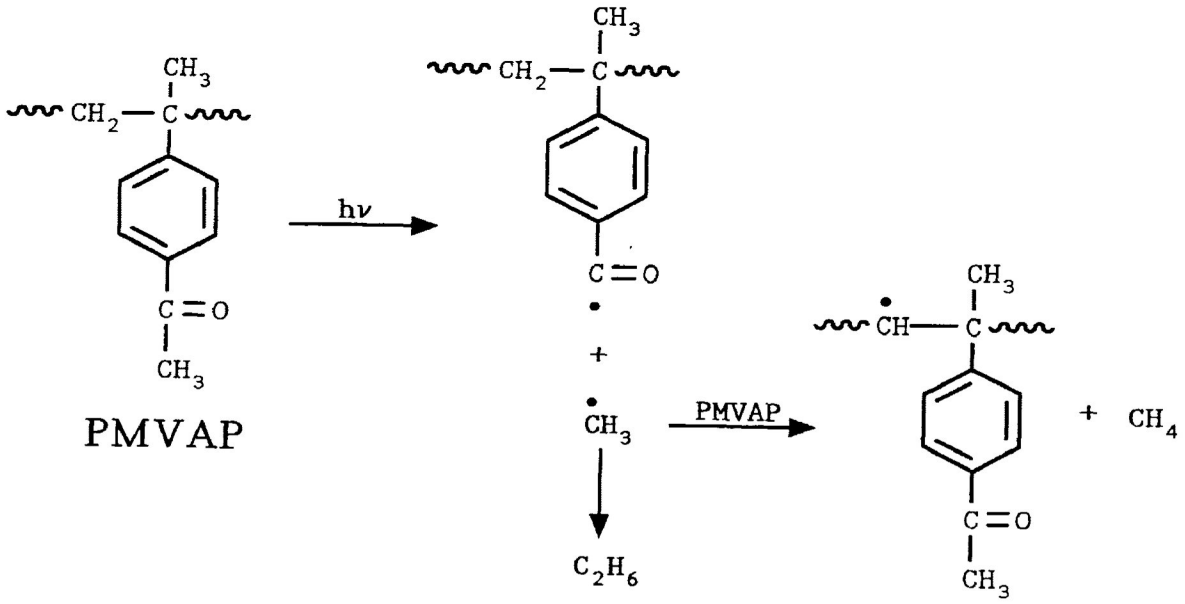

The photodegradation of PVAP (A) resulted in the production of mainly methane and ethane. α-Cleavage (Norrish type I) produced methyl radicals which subsequently abstracted the tertiary H-atom (most energetically favourable) from the polymer backbone. The lack of carbon monoxide and acetaldehyde formation indicates that α-cleavage does not produce an acetyl radical. The loss of a methyl radical leaves a benzoyl radical which can be stabilized by electron delocalization.[21] The product distribution, following similar photodegradation of PMVAP in solution (B), differed from PVAP in that ethane was the more abundant hydrocarbon. The higher ethane yield reflects the greater difficulty of hydrogen abstraction by methyl radicals from PMVAP in which the substitution at the α-carbon atom forces the methyl radicals to abstract at the

less reactive secondary carbon atoms.[22] Nevertheless, the type I reaction for both of these polymers leads to the formation of macroradicals which can undergo crosslinking reactions.[21,22] In these polymers crosslinking has another effect, i.e. it restricts the encounter of a small molecule with the polymer donors. As a result, the efficiency of energy transfer is affected as close proximity and specific relative orientations of donor and acceptor are required for efficient energy transfer.[23,24] This has implications for the use of these polymers as solar energy transfer agents.

Random chain scission was also observed during the photodegradation of both PVAP (I) and PMVAP (II) in dilute solution, and it was attributed to the β-scission of the macroradicals formed by inter- and intramolecular photoreductions involving the carbonyl triplets and the polymer. If the polymer chain is fairly tightly coiled, a hydrogen atom on another part of the same polymer chain is within the reactive range of the excited carbonyl triplet, and thus intramolecular hydrogen abstraction occurs. Similarly, if a hydrogen atom on another polymer chain is sufficiently close to the triplet, intermolecular hydrogen abstraction occurs.[12] In either case, the hydrogen abstraction reaction results in the production of a radical on the polymer backbone and this can lead to secondary reactions (i.e. crosslinking, chain scission). Plausible reaction schemes are summarized (following page).

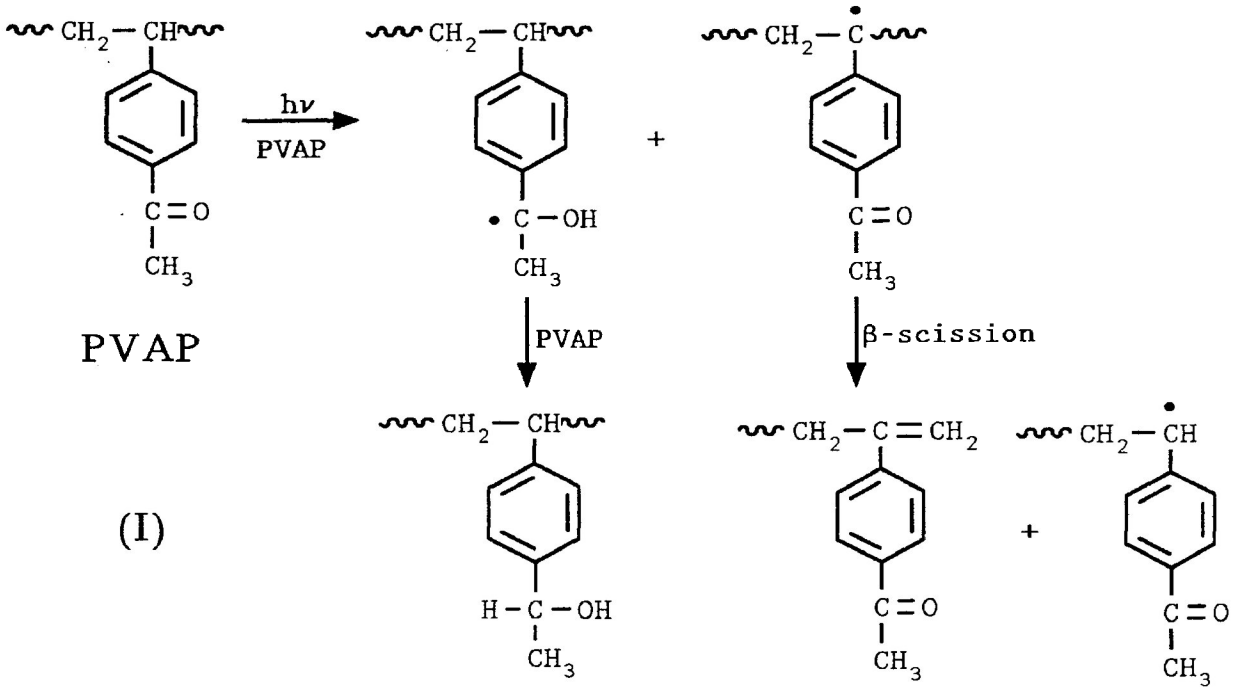
hν
PVAP
PVAP
β-scission
PVAP
(I)

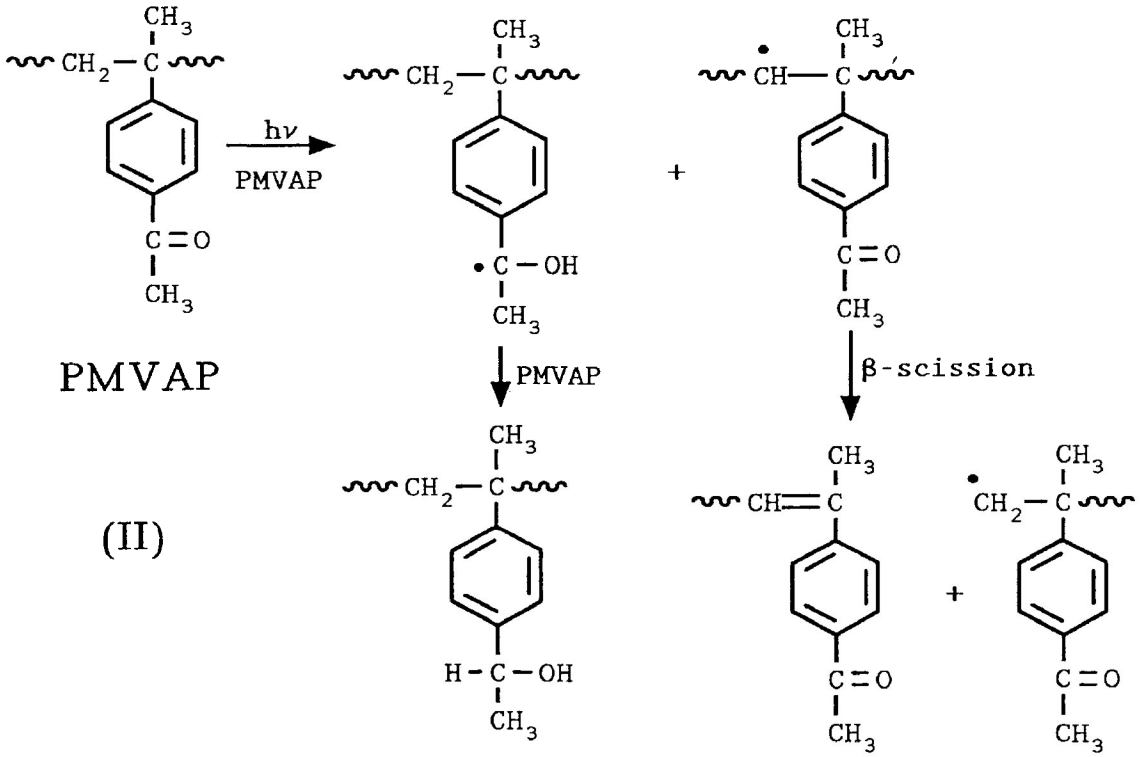
hν
PMVAP
PMVAP
β-scission
PMVAP
(II)

Schnabel[25] investigated the effect of solvent quality on the photochemistry of PPVK. In order for the polymer fragments to diffuse apart they have to disentangle themselves from one another, and the tightness of the coiling and molecular weight will affect the rate of disentanglement. The reduction in solvent quality results in a higher coil density, and this in turn leads to an increase in the rate of entanglement and a reduction in the rate of diffusion of the polymer fragments. Other factors are also involved. With tighter coiling, photoreduction, and perhaps crosslinking, can compete more favourably with chain scission, and the reduction of the interchromophore distance increases the rate of energy transfer and self-quenching.[26,27] These effects will reduce the rate of chain scission. Conversely, as solvent quality increases the coil density decreases, and the rate of disentanglement increases. This is reflected by an increase in the rate of random chain scission.

Scaiano investigated the photochemistry of poly(*o*-tolyl vinyl ketone) (PTVK) and copolymers of *o*-tolylvinylketone and vinylbenzophenone, and it was shown that the *o*-tolylketone units were able to undergo reversible photoenolization. Since this occurred at the expense of other photoprocesses, such as Norrish type II reactions, the extent of photodegradation was reduced.[19,28]

Such photoisomerizations have been observed for keto polymers containing the *o*-methylbenzoyl group and for the

poly(*o*-acylstyrenes). A simplified mechanism is as follows:

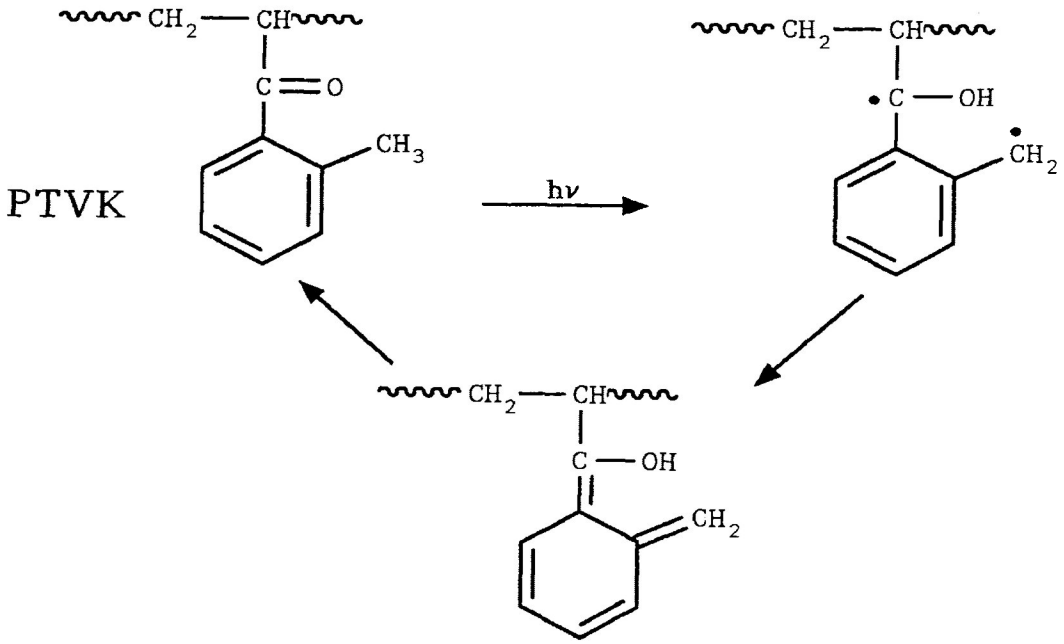

The carbonyl triplets undergo intramolecular hydrogen abstraction to form the biradical which rapidly yields the enol.[19,28,29,30] Two conformationally distinct species, i.e. the *syn* and *anti*, are present in equilibrium in the ground state; as a result, two triplets can be formed. The *syn* conformer, with its adequate geometry, can abstract H-atoms readily; however, the *anti* conformer must first rotate within triplet lifetime. The contribution of the *anti* conformer will then be determined by the magnitude of the energy barrier to rotation of the acetyl group.[29] In both cases, photoisomerization is accomplished at the expense of other photoprocesses; therefore, these polymers have relatively high photostabilities (*cf* the isomeric poly(*p*-tolyl vinyl ketone)

and poly(*p*-acylstyrenes)).

Quantum yields for chain scission tend to be lower for polymers in solid films than for those in solution.[31] This is probably associated with a larger cage effect which imposes restrictions upon the diffusive separation of the fragments resulting from β-scission. In addition, one could expect an increase in the reverse hydrogen abstraction reaction from the 1,4-biradical to regenerate the starting ketone. However, quantum yields for volatile gas formation (CH_4 and C_2H_6) appear to be generally higher for polymers in solid films than for those in solution indicating that photoreduction competes favourably with α-cleavage in solution.[22,29,30,32] Diffusional separation of the radical pairs is easier to achieve in solution, and photoreduction (both inter- and intramolecular) becomes more probable due to the greater rotational flexibility of the molecules in solution. Specific conformational requirements are more readily achievable in solution than in the rigid, solid state.[32]

In another series of studies on the photochemistry of keto polymers in the solid phase,[33,34] it has been shown that the physical state of the polymer defines the rate-determining step for these reactions, the free volume in the polymer matrix being critical.[33] At extremely low temperatures no molecular motion is possible in the polymer, i.e. quantum yields are low; furthermore, the only possible photoprocess is phosphorescence since it requires no molecular motion. As the

temperature is gradually increased, the free volume of the polymer increases and molecular motion takes place, i.e. rotation of phenyl rings, etc. At the glass transition temperature, T_g, segmental motion is also possible, and further increases in temperature beyond T_g result in larger increases in the free volume which lead to the desired conformation required for the photoprocess.[34]

E. **Aims of Present Work**

Poly(acrylophenones) (PAP) have been particularly useful model polymers for photochemical studies because very rapid intersystem crossing occurs in the aromatic ketones so that nearly all of the photochemical and photophysical processes occur from the triplet state. According to Scaiano,[19,20] the principal mode of degradation involved a Norrish type II reaction which led to random chain scission. However, the terminal olefin produced from the type II reaction acted as a quencher for any migrating excitation; therefore, excitation could be quenched both internally and from intra- and intermolecular contacts in solution.

Hrdlovic and Lukac[35] have prepared several different substituted poly(acrylophenones) and determined their quantum yields for chain scission (*cf* unsubstituted polymer). *p*-Alkyl substituents increase the quantum yield for chain scission; however, electron-donating groups such as *p*-methoxy reduce the quantum yield for chain scission while the 3,4-dimethoxy derivative is relatively stable. *p*-Phenyl substitution also

reduces the quantum yield for chain scission to very low values.

Paper today produced from high-yield pulp undergo a yellow discolouration when exposed to sunlight. These pulps contain a high content of lignin which initiate the photo-yellowing process. Earlier studies credited this yellowing to the formation of quinones within the lignin.[36,37] Lignin, being a macromolecular compound, contains a high concentration of a variety of methoxy-substituted acrylophenone moieties.[38] Therefore, the purpose of this work is to carry out a detailed investigation of the photo-yellowing of lignin by studying the long-wave photochemistry of three simple polymeric model compounds: Poly(*p*-methoxyacrylophenone) (PMAP), poly(3,4-dimethoxyacrylophenone) (P34DMAP) and poly(3,5-dimethoxyacrylophenone) (P35DMAP). This work will be carried out in solid (films) and in dilute solution so as to obtain a detailed description of the overall reaction mechanism.

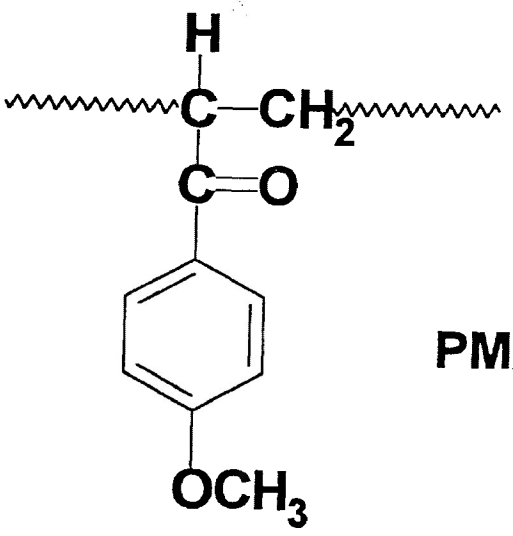

PMAP

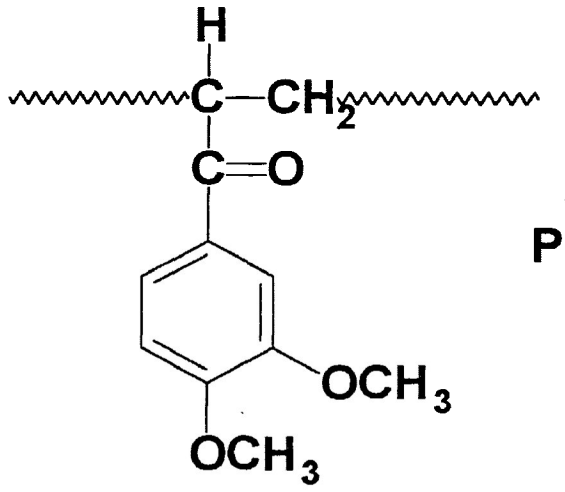

P34DMAP

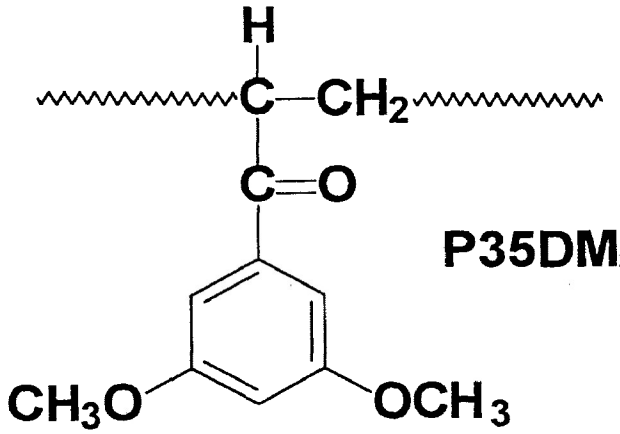

P35DMAP

II. EXPERIMENTAL PROCEDURES

A. Polymer Preparation

Monomers for PMAP, P34DMAP and P35DMAP were synthesized by methods previously described;[39,40] however, anisole was replaced with the molar equivalent of 1,2-dimethoxybenzene (veratrole) in preparing monomeric 3,4-dimethoxyacrylophenone while the molar equivalent of 1,3-dimethoxybenzene replaced anisole in preparing monomeric 3,5-dimethoxyacrylophenone. Bulk polymerization (PMAP and P34DMAP) was carried out at 60°C under high vacuum in the absence of initiator. However, the 3,5-dimethoxyacrylophenone monomer was polymerized in bulk at 60°C under high vacuum in the presence of azobisisobutyronitrile (10^{-3} M). The polymerization was stopped after about 20% conversion, the reaction vessel being immersed in liquid N_2, in order to minimize complications from side reactions. In the absence of initiator, the 3,5-dimethoxyacrylophenone monomer required a long reaction time, and very high molecular weight polymers (>10^7) with large polydispersities (>5) were produced. These tended to gel and characterization by gel permeation chromatography (GPC) became impossible.

The polymers were initially isolated by precipitation, the impure reaction mixture being dissolved in methylene chloride and the resulting solution added to pure methanol. They were then purified by repeated precipitation from

methylene chloride solutions in methanol. After drying at 10^{-5} kPa, the polymers were stored under vacuum in the dark. Molecular weights were obtained by GPC (Table 2.1) using Waters equipment in conjunction with a UV detector and Ultrastyragel® column (7.8 X 300 mm; 7 μm pores). The polymers were run through the column using methylene chloride as the solvent (1.0 cm^3 min^{-1} flow rate) (Figure 2.1).

TABLE 2.1

GPC Analysis of

Methoxy-Substituted Poly(acrylophenones)

POLYMER	Number-Average Molecular Weight ($\overline{M}_n$)	Weight-Average Molecular Weight ($\overline{M}_w$)	POLYDISPERSITY $\left(Y = \frac{\overline{M}_w}{\overline{M}_n}\right)$
PMAP	5.0 X 10^5	1.2 X 10^6	2.40
P34DMAP	2.5 X 10^5	7.8 X 10^5	3.12
P35DMAP	2.5 X 10^6	7.0 X 10^6	2.80

B. **Polymer Characterization**

1. **Infrared Spectroscopy**. The infrared spectra of PMAP, P34DMAP and P35DMAP were recorded on a Perkin Elmer 1320 Infrared Spectrophotometer. Films were prepared on NaCl plates by the slow evaporation of a solution of the polymer in methylene chloride. A strong absorption characteristic of carbonyl stretching is shown for each of these polymers in Figures 2.2a-c and are as follows: PMAP: 1670 cm^{-1}; P34DMAP: 1660 cm^{-1}; P35DMAP: 1650 cm^{-1}.

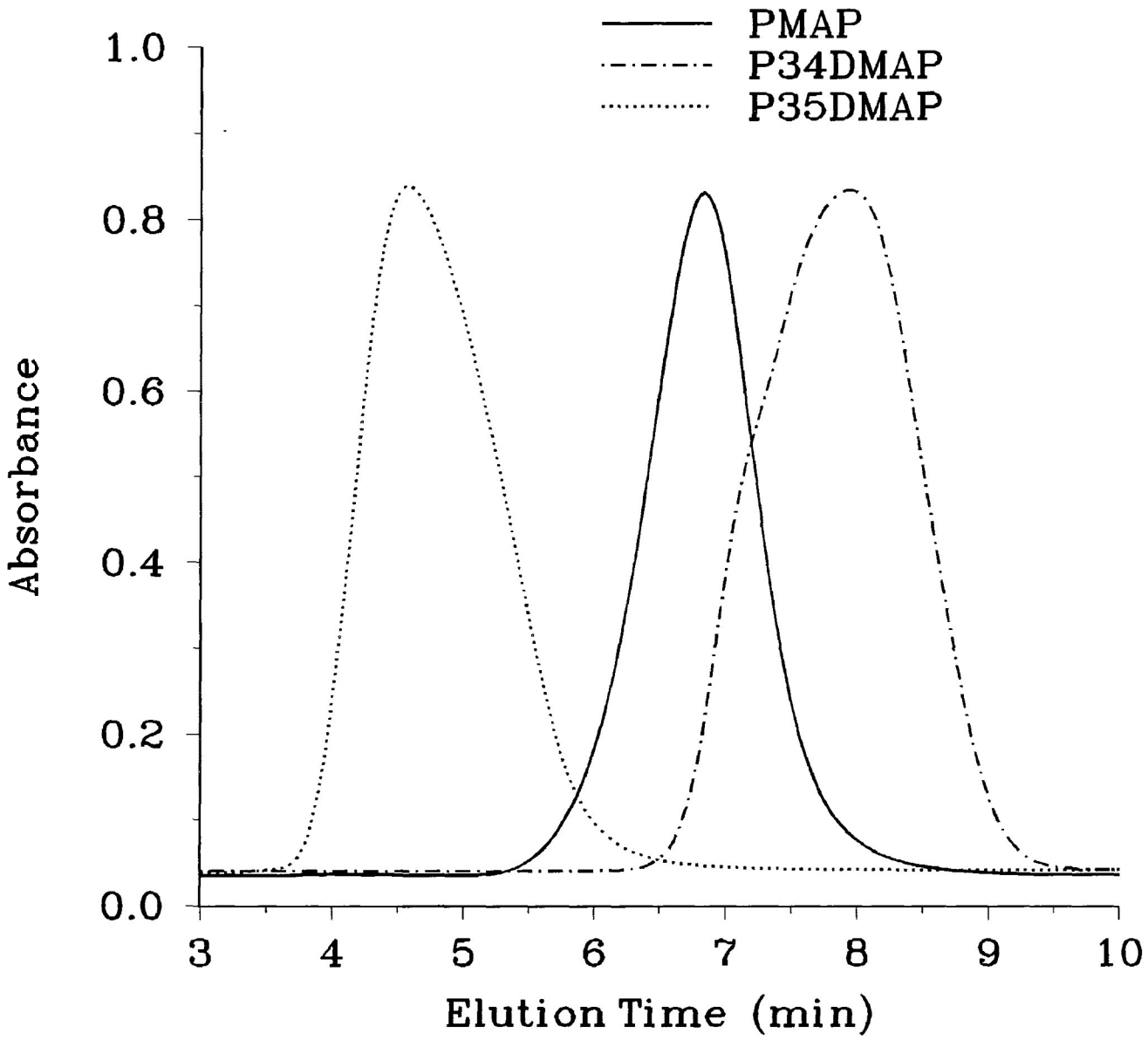

Figure 2.1. GPC Analysis of Methoxy–Substituted Poly(acrylophenones).*

* Run With CH_2Cl_2 Through Ultrastyragel® Linear Column (7 μm pore) at 1.0 cm^3 min^{-1}.

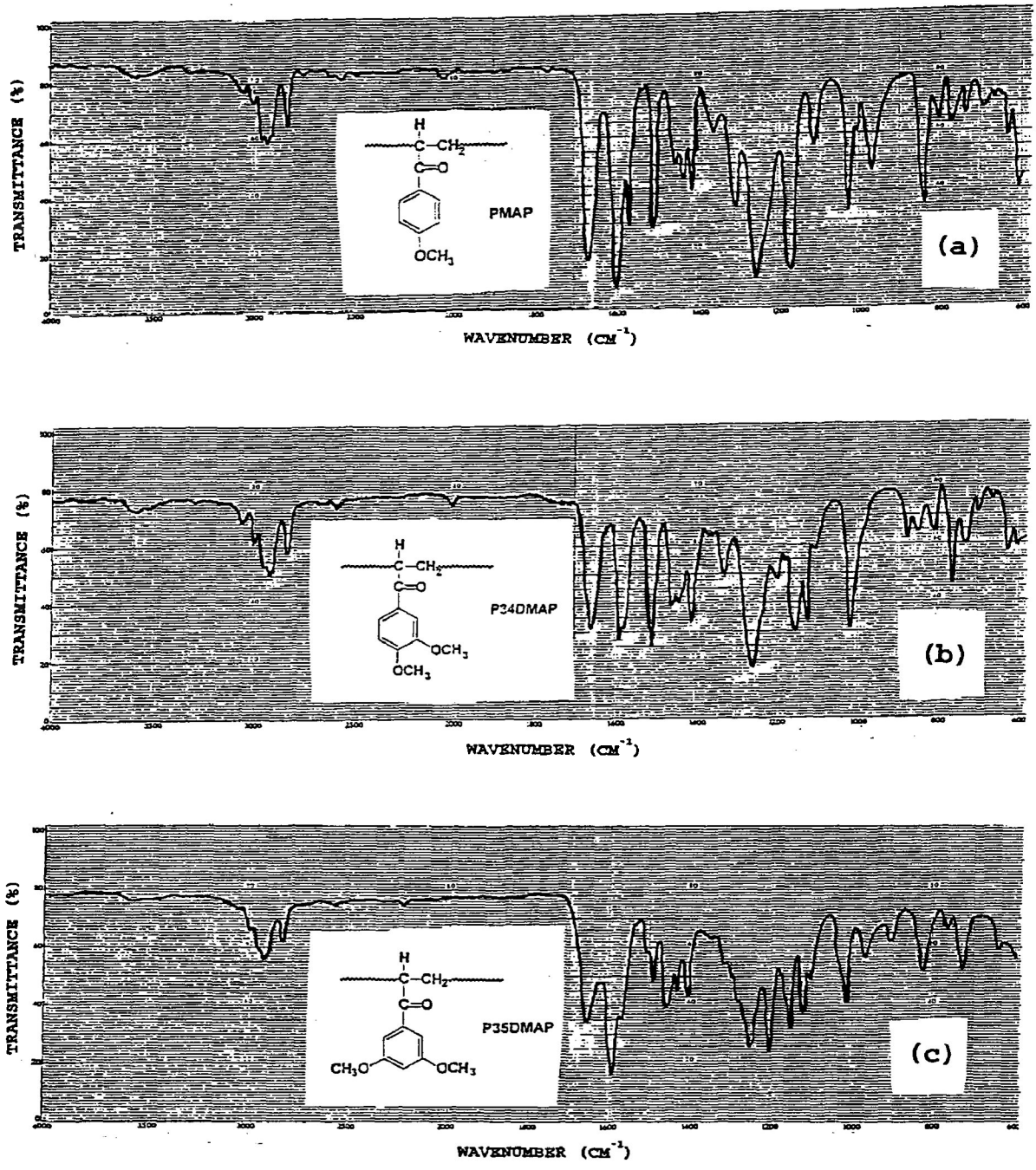

Figure 2.2. Infrared Spectra of (a) PMAP (b) P34DMAP and (c) P35DMAP.

2. **Nuclear Magnetic Resonance**. ^{1}H and ^{13}C NMR assignments (Figures 2.3-2.8) for the corresponding polymers in $CDCl_3$ with tetramethylsilane (TMS) as a standard reference were obtained using a Brüker AC-E 200 MHz NMR, the identities of the individual C-atoms being confirmed by spectral editing using a DEPT (Distortionless Enhancement by Polarization Transfer) sequence.[41] Spectral characteristics of PMAP and P34DMAP were consistent with the expected structures; however, the ^{13}C NMR spectrum of P35DMAP contains additional peaks which could be attributed to traces of the isomeric poly(2,4-dimethoxyacrylophenone) compound.

3. **Ultraviolet Spectroscopy**. The UV spectra of these polymers (CH_2Cl_2 solutions and films) were recorded on a Perkin Elmer Lambda 11 UV/VIS Spectrometer. Thin films were prepared on the inner wall of a quartz cell by slow solvent evaporation, a methylene chloride solution being poured in the cell.

4. **Luminescence Spectroscopy**. Fluorescence (CH_2Cl_2 solutions) and phosphorescence (Glass at 77K) spectra of these polymers, along with their respective phosphorescence lifetimes, were obtained using a Perkin Elmer LS50B Luminescence Spectrometer.

C. **Photochemical Techniques**

Polymers were exposed to long-wave UV ($\lambda \geq 300$ nm) radiation in dilute solutions of CH_2Cl_2 (6×10^{-2} M). Prior to reaction, the solutions were degassed (N_2) rigorously in a

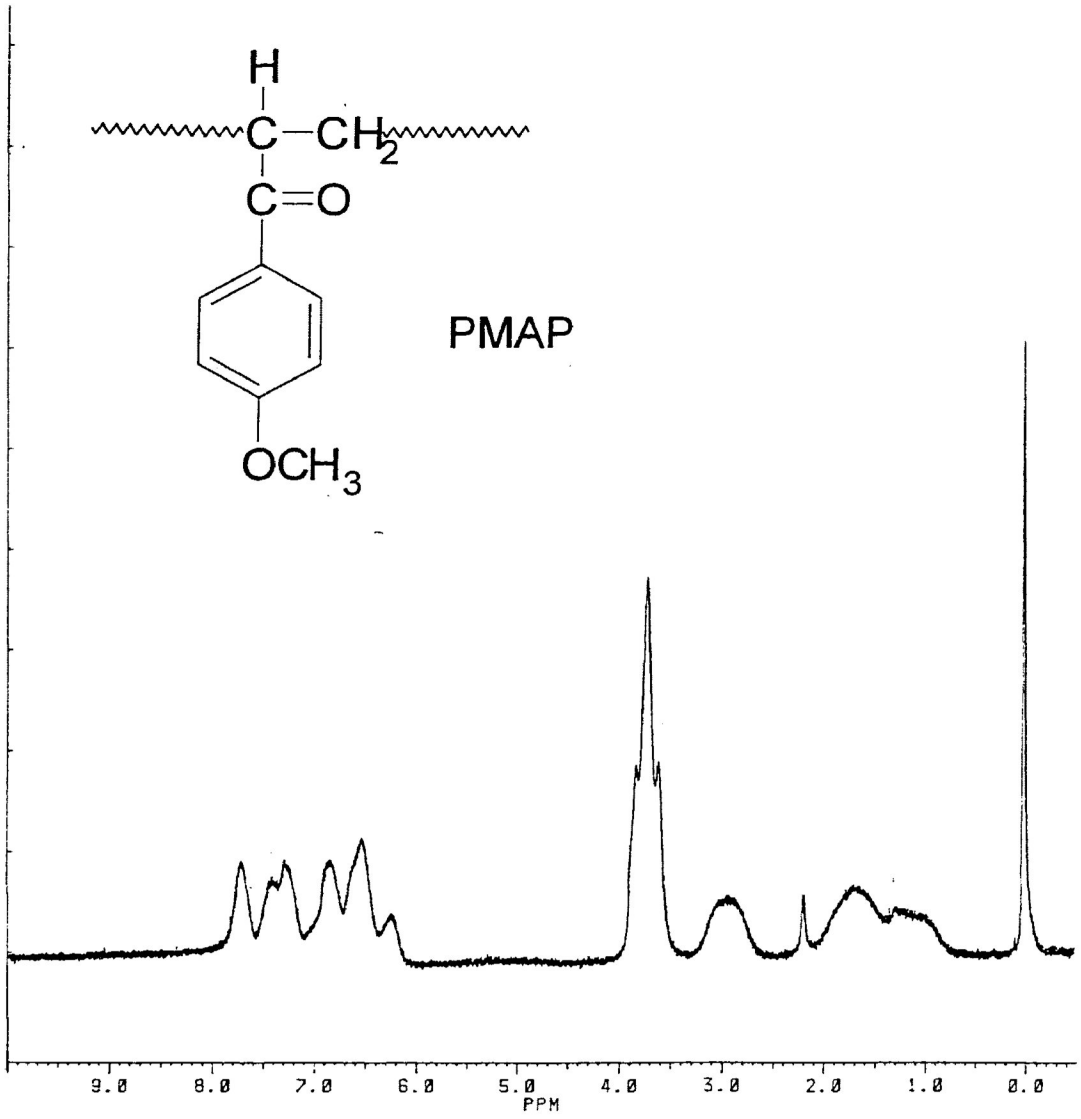

Figure 2.3. ^{1}H NMR Spectrum of PMAP.

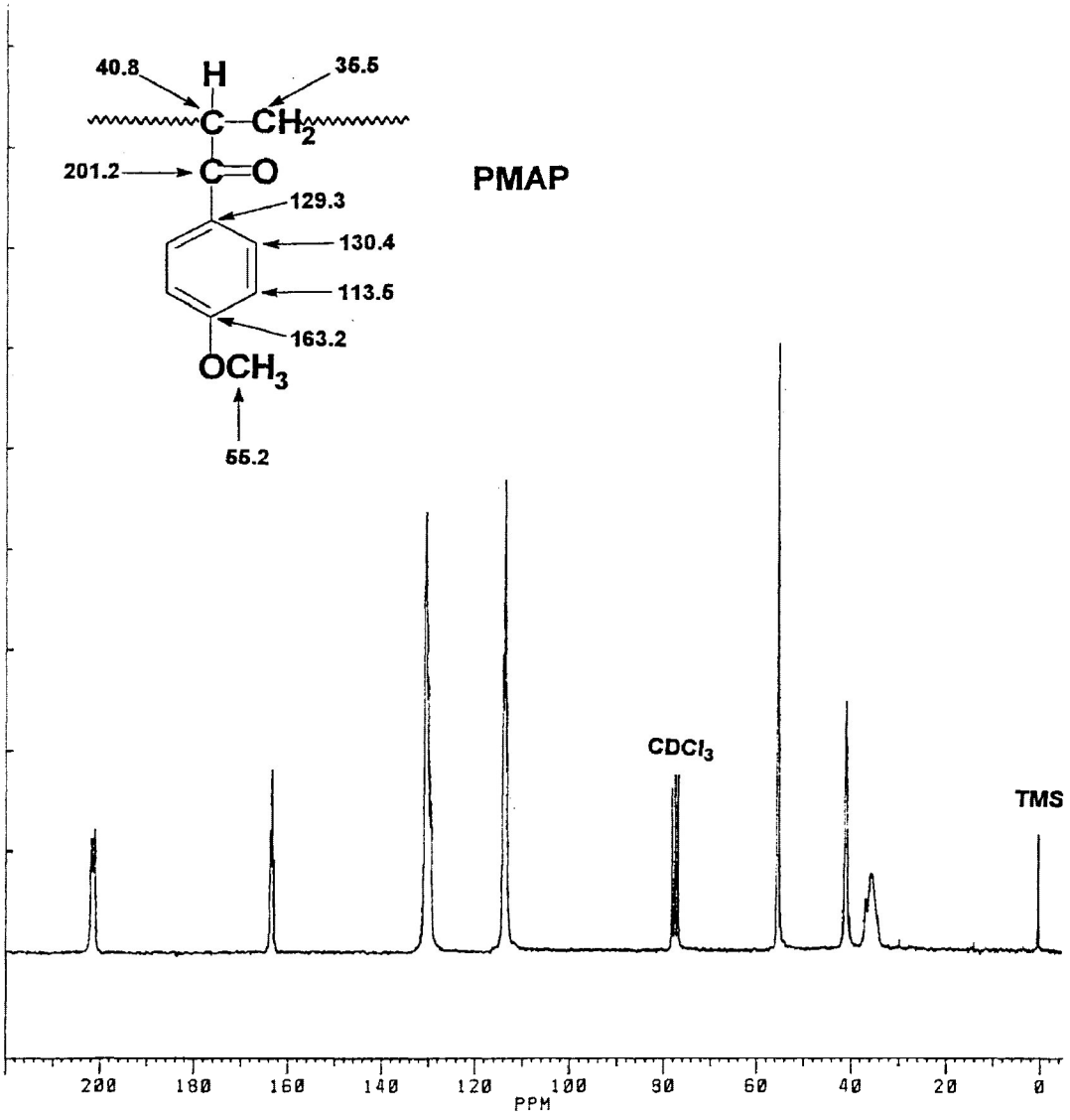

Figure 2.4. ^{13}C NMR Spectrum of PMAP.

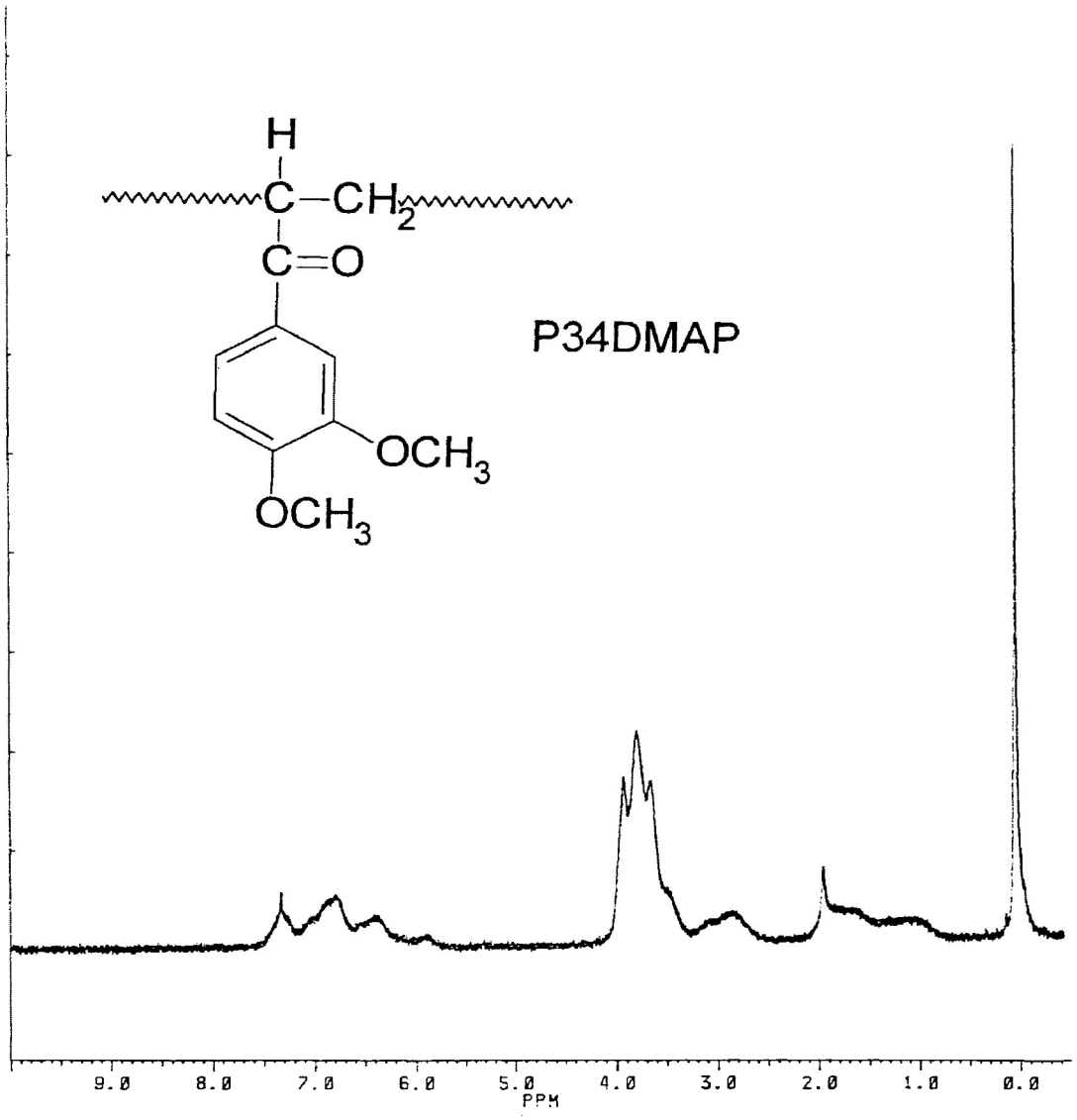

Figure 2.5. ^{1}H NMR Spectrum of P34DMAP.

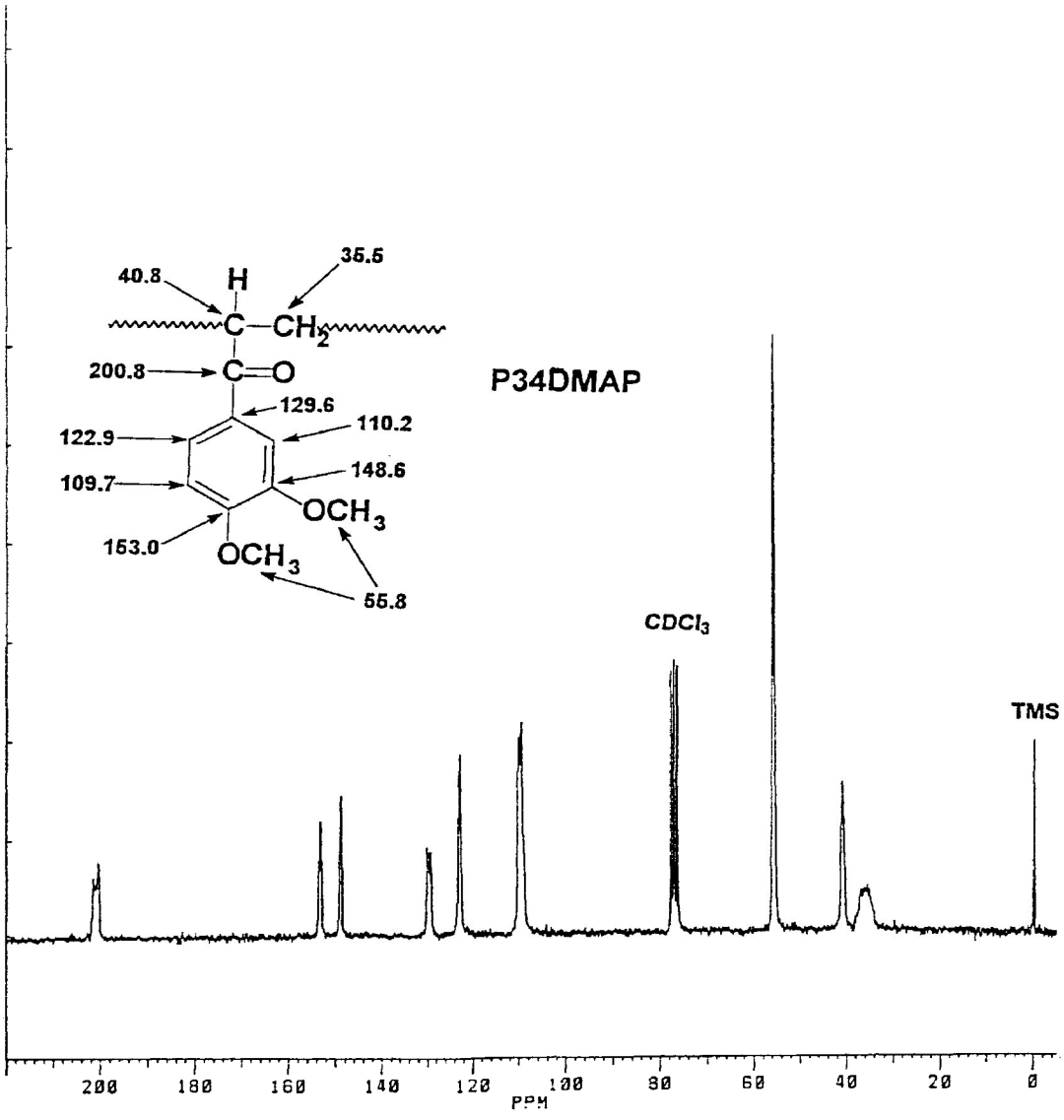

Figure 2.6. ^{13}C NMR Spectrum of P34DMAP.

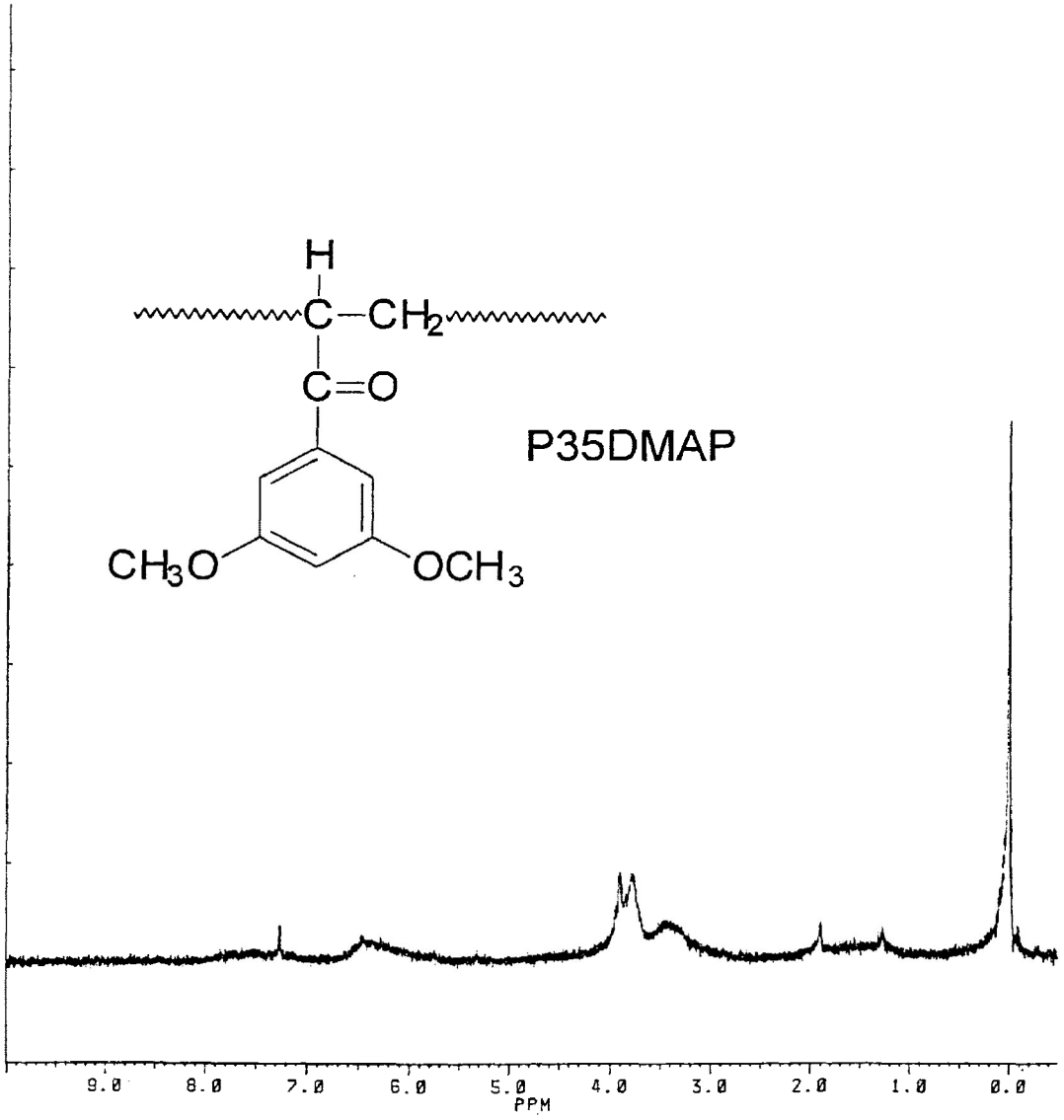

Figure 2.7. ^{1}H NMR Spectrum of P35DMAP.

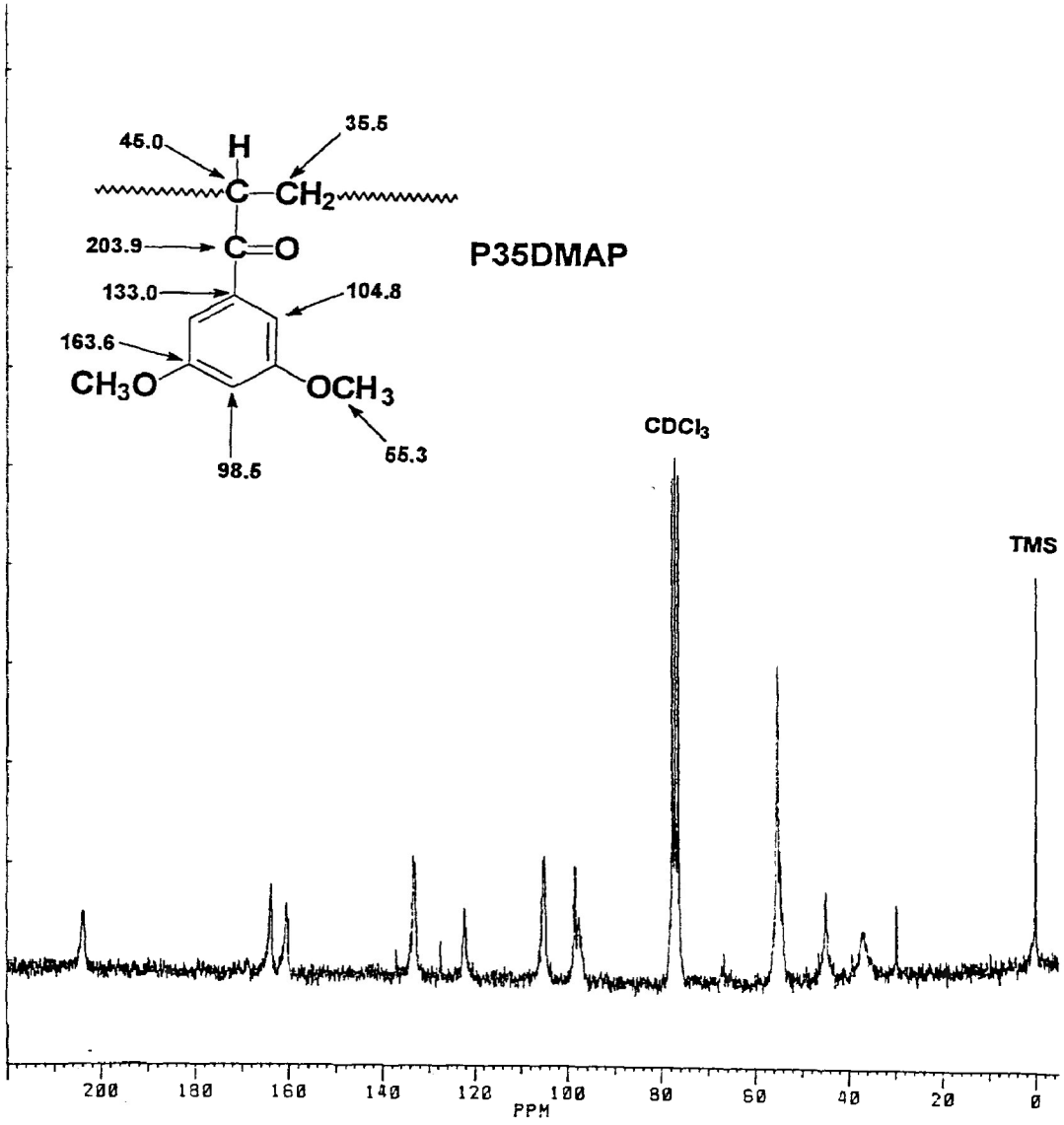

Figure 2.8. ^{13}C NMR Spectrum of P35DMAP.

pyrex reaction vessel sealed to a Ubbelohde viscometer (Figure 2.9); as a result, this eliminated the possibility of photooxidation. Times of flow through the viscometer were obtained for the solvent (t_o) and polymer solutions (t) at 25 ± 1°C before irradiation. The polymer solutions were exposed to a Hanovia 200 W medium pressure Hg arc, the lamp to solution distance being kept constant at 10 cm. The progress of molecular weight change was followed by obtaining times of flow for the polymer solutions (t) after various exposure times. The relative viscosity (η_{rel}), the ratio of the flow time for the polymer solution to the flow time for the pure solvent, is:

$$\eta_{rel} = t/t_o$$

The specific viscosity (η_{sp}), the relative increment in viscosity of the solution over the viscosity of the solvent, is:

$$\eta_{sp} = \eta_{rel} - 1$$

Intrinsic viscosities ($[\eta]$) can then be determined by means of the Solomon-Ciuta equation[2]:

$$[\eta] = \{(\sqrt{2})(\eta_{sp} - \ln \eta_{rel})^{1/2}\}/C$$

where C is the concentration of the polymer solution in g dl^{-1}. The number of chain scissions per original molecule (S) is obtained from the following equation:

$$S = ([\eta]_o/[\eta]_t)^{1/\alpha} - 1$$

where $[\eta]_o$ and $[\eta]_t$ are, respectively, the intrinsic viscosities (dl g^{-1}) before irradiation and after various

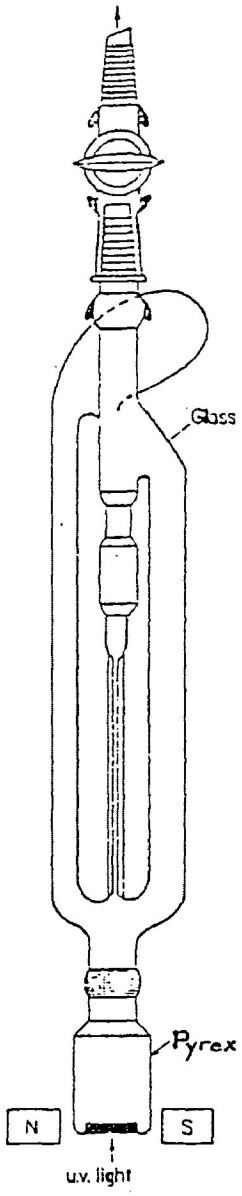

Figure 2.9. Cannon Ubbelohde Viscometer for Photochemical Studies of Polymer Solutions.

intervals of exposure to irradiation, and α is the Mark-Houwink constant (0.75)[40,45]. From the Mark-Houwink equation:

$$[\eta] = KM^{\alpha}$$

where K and α are both constants dependent on the particular polymer at a given temperature in a given solvent, it is possible to relate S to the number-average molecular weights as:

$$S = [(\overline{M}_n)_o/(\overline{M}_n)_t] - 1$$

where $(\overline{M}_n)_o$ and $(\overline{M}_n)_t$ are, respectively, the original number-average molecular weight and that after a degradation period, t. Quantum yields for the various reactions were estimated using photochromic actinometry (Aberchrome 540).[42] Stern-Volmer kinetics were observed for each polymer sample by similarly irradiating dilute degassed solutions of each polymer (6 X 10^{-2} M) in methylene chloride containing various quencher concentrations (naphthalene and *cis*-1,3-pentadiene). Furthermore, the effect of H-donors on each polymer sample were observed by similarly irradiating dilute degassed solutions of each polymer (6 X 10^{-2} M) in methylene chloride containing various H-donor concentrations (isopropanol, n-butanol, *tert*-butanol and cumene).

Polymers were also exposed to long-wave UV ($\lambda \geq 300$ nm) radiation in the form of thin films in order to simulate some of the conditions under which lignin undergoes degradation. Thin films were prepared by slow solvent (CH_2Cl_2) evaporation

on the inner wall of a specially designed pyrex reaction vessel (Figure 2.10), and thoroughly degassed (N_2) before irradiation. The polymer films were exposed to a Hanovia 200 W medium pressure Hg arc, the lamp to film distance being kept constant at 10 cm. Prior to analysis, the irradiated polymer films were kept sealed within the pyrex reaction vessel so as to avoid the presence of O_2 (and photooxidation).

Polymers films, formed on quartz plates by solvent evaporation (CH_2Cl_2), were exposed to long-wave UV ($\lambda \geq 300$ nm) radiation inside a double-walled pyrex reaction vessel under high vacuum (10^{-6} kPa). Details of the equipment and techniques have been published.[43] Thermostatically controlled distilled water (25 ± 1°C) circulated through the outer wall of the reaction vessel to reduce possible thermal effects as the UV source, a medium pressure Hanovia 200 W Hg arc, produced a considerable intensity of infrared radiation. Quantum yields for gaseous product formation were determined using photochromic actinometry (Aberchrome 540).[42]

D. **Analytical Techniques**

These analyses involved the examination of the degraded polymeric residues. Changes in composition, as reflected by changes in spectra, were monitored for each polymer at regular intervals of exposure using a Brüker IFS66 FTIR spectrometer (IR spectra), a Brüker AC-E 200 NMR spectrometer (^1H and ^{13}C NMR spectra, DEPT sequences) and a Perkin Elmer Lambda 11 UV/VIS spectrometer (UV spectra). Changes in molecular weights

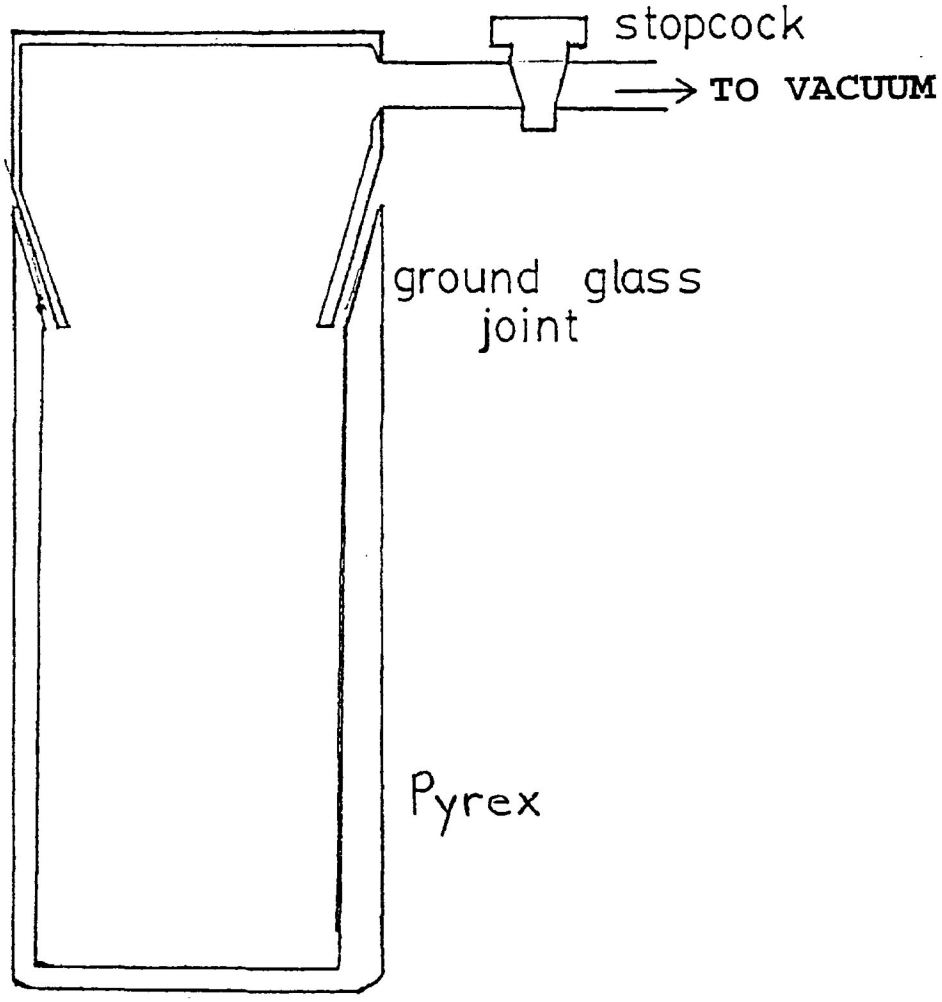

Figure 2.10. Irradiation Cell for Air Free Irradiation of Polymer Films.

were investigated by GPC (Waters) using a linear Ultrastyragel® column (7.8 X 300 mm; 7 μm pores) and methylene chloride as the solvent (1.0 cm^3 min^{-1} flow rate).

E. **Volatile Product Analyses**

Low molecular weight gaseous products were quantitatively analyzed from the polymeric films using an in-line quadrupole mass spectrometer (Spectramass Dataquad 200) which rapidly and repeatedly scanned the range 1 < m/e < 200 amu during the reaction period. As a result, time evolution characteristics were determined from these data.[44] The equipment was calibrated using authentic samples (Matheson) of the volatile products.

III. RESULTS

A. Photophysical Processes

1. **UV Spectral Characteristics**. The UV absorption spectra of PMAP, P34DMAP and P35DMAP in solution (3.0 X 10^{-4} M in CH_2Cl_2), shown in Figure 3.1, are qualitatively very similar to those of thin films.[46] In all cases there is a definite absorbance in the terrestrial solar spectral region ($\lambda \geq 295$ nm). Absorptions attributable to the $\pi \rightarrow \pi^*$ transitions of the aromatic ring are well resolved, and those attributable to the overlapping $n \rightarrow \pi^*$ transitions of the carbonyls are clearly distinguishable in P34DMAP and P35DMAP. However, in PMAP, there is a large degree of overlap of the two absorptions. The UV absorption characteristics are summarized below in Table 3.1.

TABLE 3.1

UV Absorption Characteristics of Methoxy-Substituted Poly(acrylophenones)

POLYMER*	λ_{max} $(n \rightarrow \pi^*)$ (nm)	ϵ (dm^3 mol^{-1} cm^{-1})
PMAP	288	270
P34DMAP	308	6400
P35DMAP	302	5250

* 3.0 X 10^{-4} M Solution in CH_2Cl_2

The very large apparent differences in the value of ϵ for di- and mono-substituted polymers are probably not genuine, but

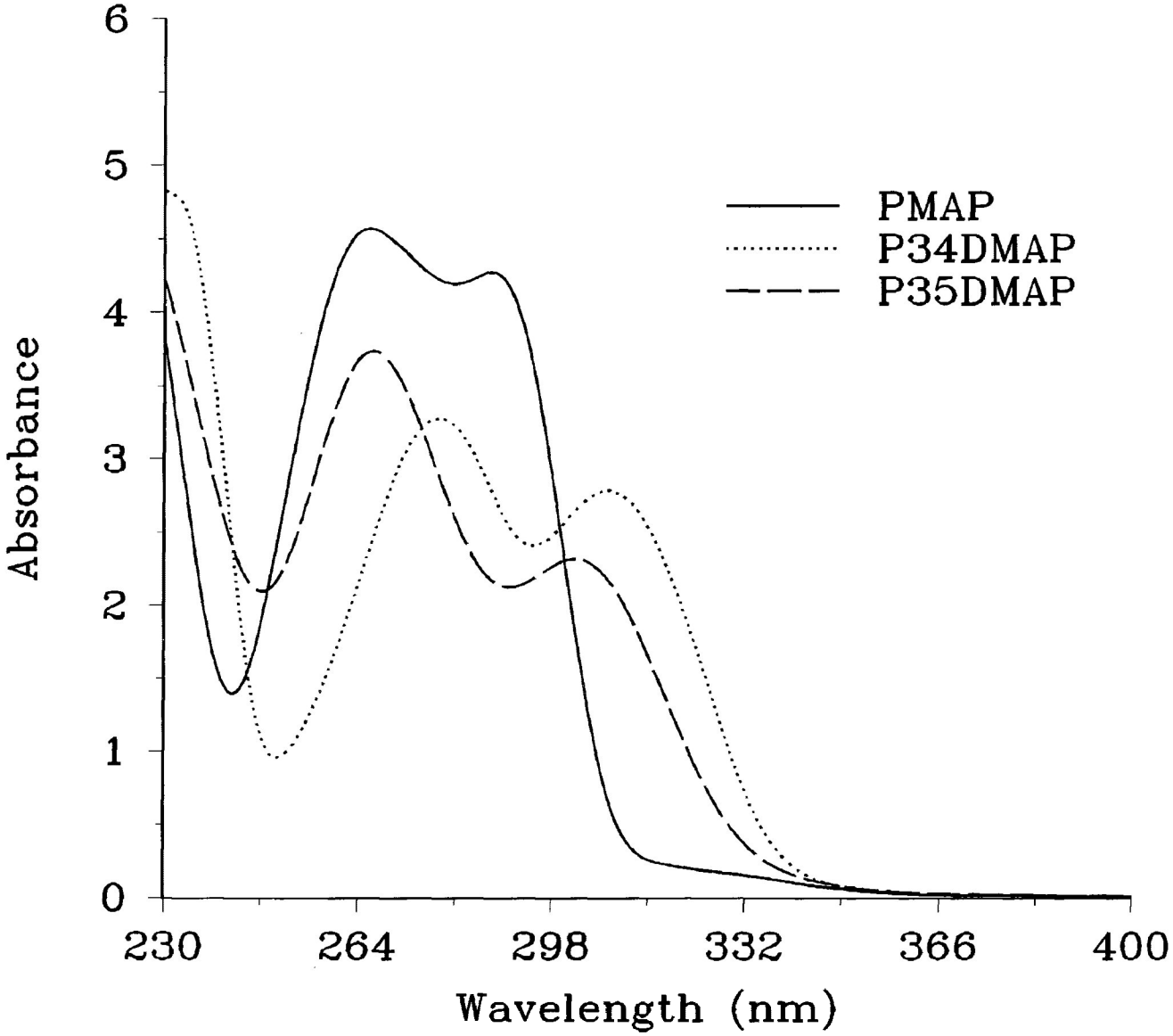

Figure 3.1. UV Absorption Spectra[†‡] of Methoxy–Substituted Poly(acrylophenones).

[†] 3.0×10^{-4} M Solution in CH_2Cl_2.

[‡] Instrument Sensitive to 0.0001 %T.

are the result of the overlap of the two absorptions which cannot readily be deconvoluted.

2. **Emission**. The emission characteristics of PMAP, P34DMAP and P35DMAP are shown in Figures 3.2 (fluorescence) and 3.3 (phosphorescence) along with the excitation spectra. The intensities of fluorescence are quite weak and the quantum yields (estimated by comparison with dibenzyl ketone[47]) are very low (Table 3.2). This is understandable, quantum yields for n,π^* intersystem crossing being unity or very close to unity in such aromatic ketones. Thus, photoreactions proceed mainly from the triplet state[1,2], and the singlet state of the carbonyl does not participate to a significant extent. The fluorescence characteristics are summarized below in Table 3.2.

TABLE 3.2

Fluorescence Characteristics of Methoxy-Substituted Poly(acrylophenones)

POLYMER*	λ_{max} (excitation) (nm)	λ_{max} (emission) (nm)	$\Phi_{fluorescence}$ mol(Einstein)$^{-1}$
PMAP	323	361	1.35×10^{-4}
P34DMAP	346	385	2.42×10^{-5}
P35DMAP	341	381	3.55×10^{-5}

* 5.0×10^{-3} M Solution in CH_2Cl_2

A mirror image relationship is shown between the fluorescence and the excitation spectra (Figure 3.2), and the relatively

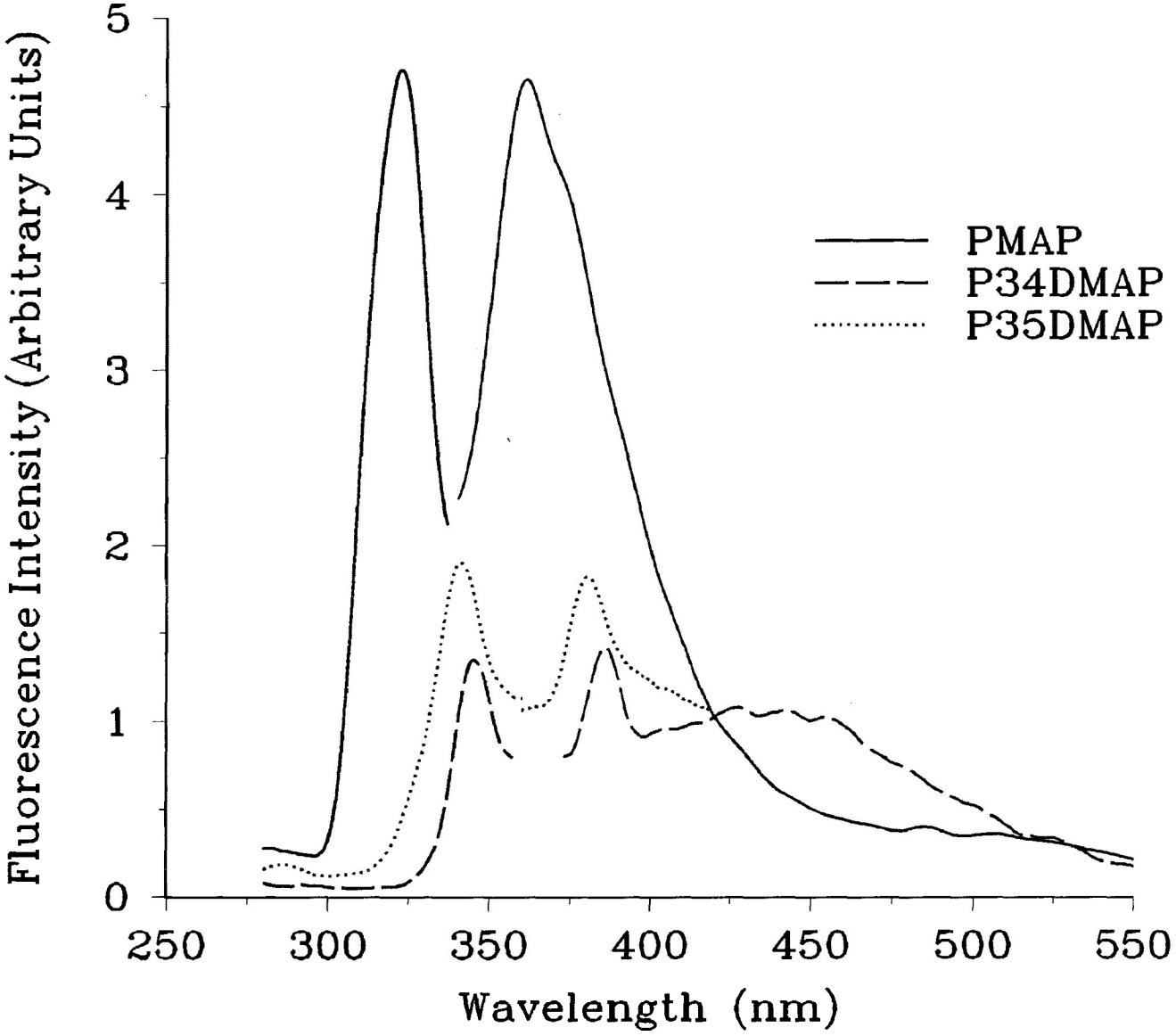

Figure 3.2. Fluorescence Spectra of Polymer Solutions (5.0×10^{-3} M) in CH_2Cl_2 at Room Temperature.

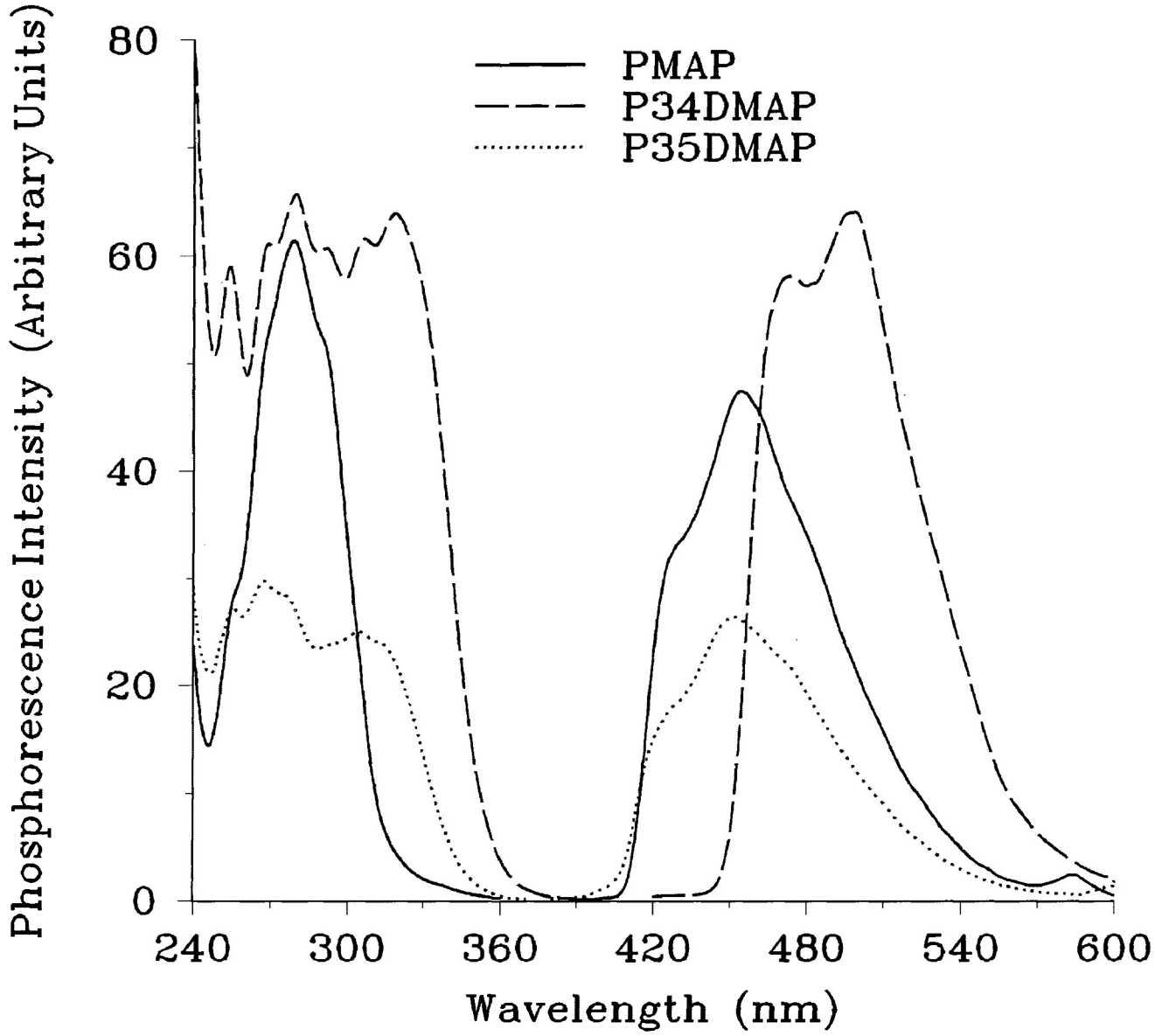

Figure 3.3. Phosphorescence Spectra of Polymers in Glass at 77K.

small Stokes shift (40 nm) reflects the similarity of the geometries of the ground and the singlet (S_1) states.

Much higher phosphorescence intensities are observed (at 77K) (Figure 3.3). It can be seen that the spectra show little vibrational fine structure, and this is characteristic of triplets which have predominantly π,π^* character. The triplet (T_1) energy, defined as the energy difference between the zero vibrational levels in T_1 and the ground state ($E_T(0-0)$), is lower than that of poly(acrylophenone) but comparable with that of alkyl substituted poly(acrylophenones)[48] (Table 3.3).

The effect of polymer concentration on phosphorescence intensity is shown in Figure 3.4. The results indicate that, at low polymer concentrations, a linear relationship exists between phosphorescence intensity and polymer concentration. Deviations from linearity, however, occur at higher polymer concentrations. It can also be seen that the incorporation of a second OCH_3 group into the ring reduces the phosphorescence intensity, the lower reactivity being characteristic of triplets which have predominant π,π^* character.

3. **Lifetimes**. The decay characteristics of the triplets were investigated and are shown in Figures 3.5-3.7. The linearity of the log (phosphorescence intensity) versus time plots (inserts of Figures 3.5-3.7) clearly indicate that a single excited species is undergoing exponential decay, and the triplet lifetimes are shown in Table 3.3.

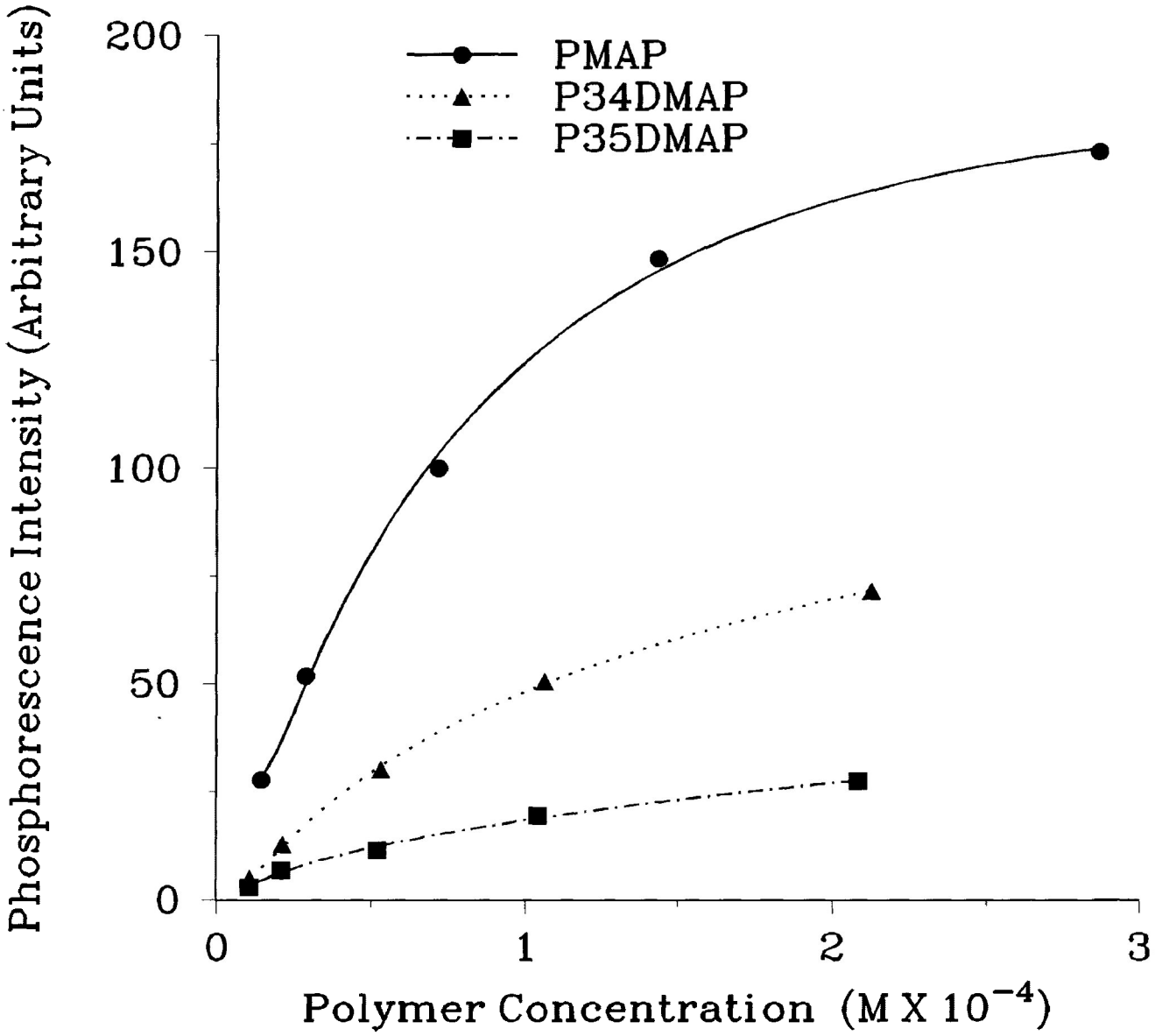

Figure 3.4. Phosphorescence† Intensity as a Function of Polymer Concentration.

† In Glass at 77K.

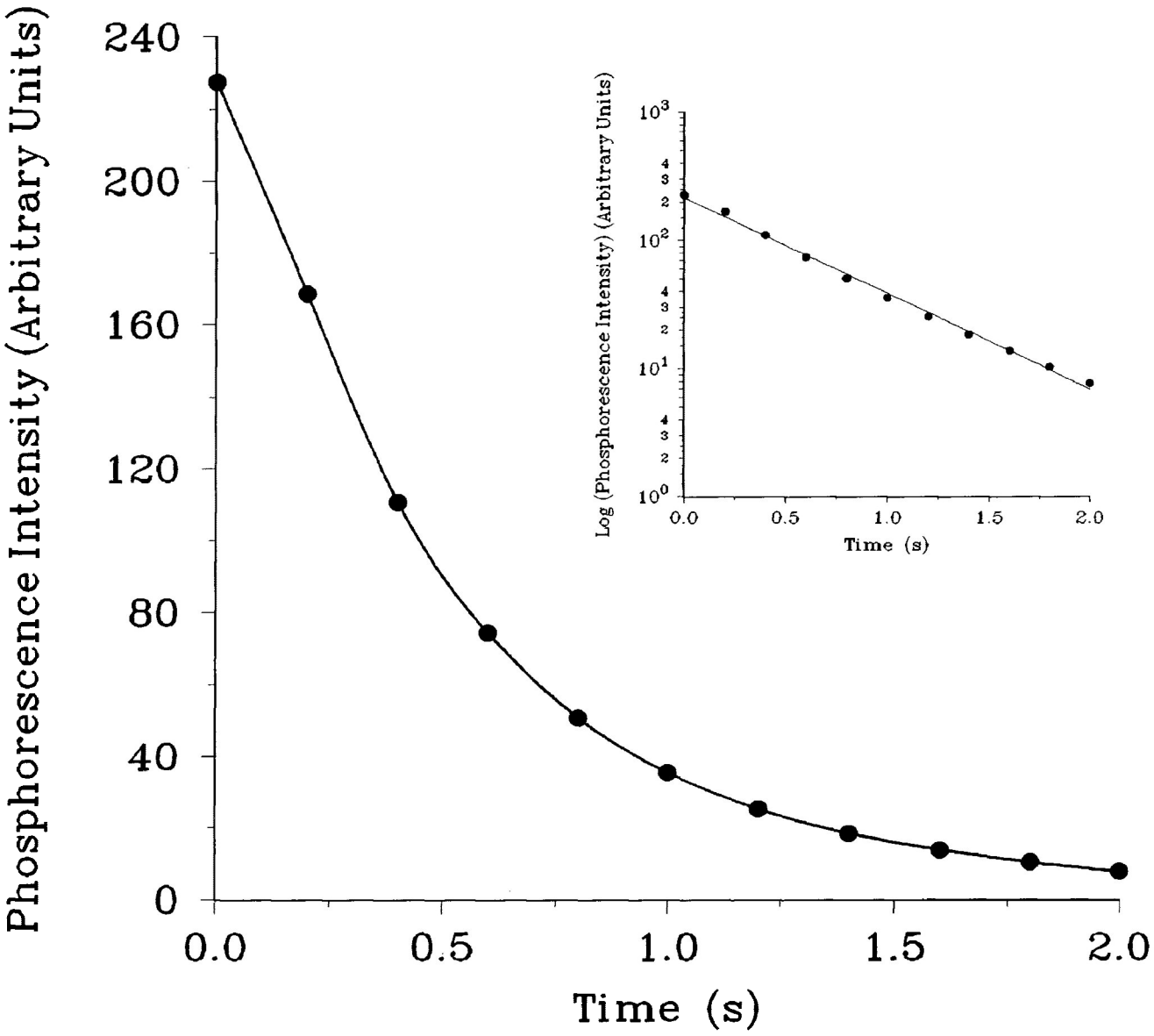

Figure 3.5. Phosphorescence Decay Characteristics of PMAP Triplet. (Insert Represents Semi–Logarithmic Plot)

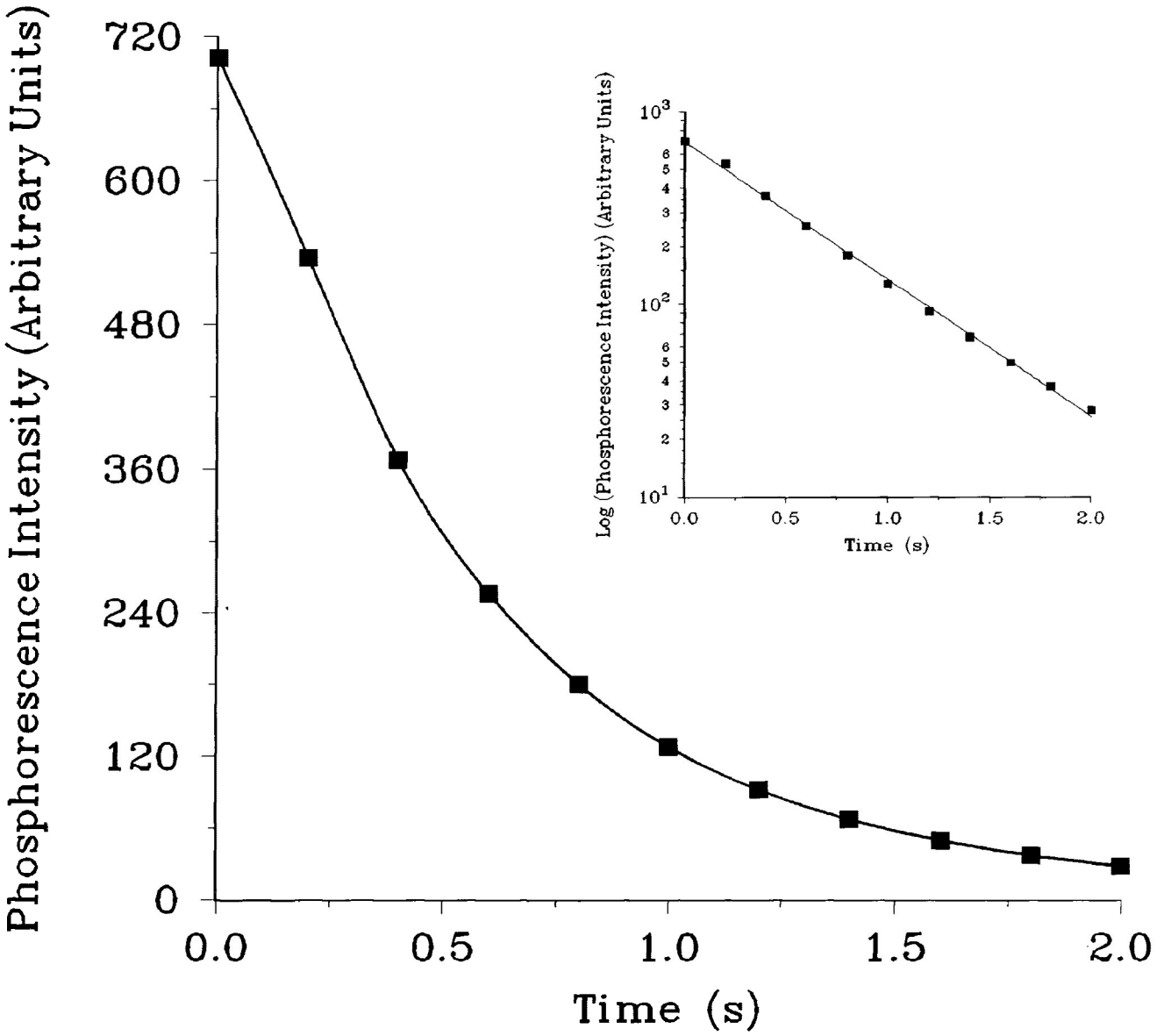

Figure 3.6. Phosphorescence Decay Characteristics of P34DMAP Triplet. (Insert Represents Semi–Logarithmic Plot)

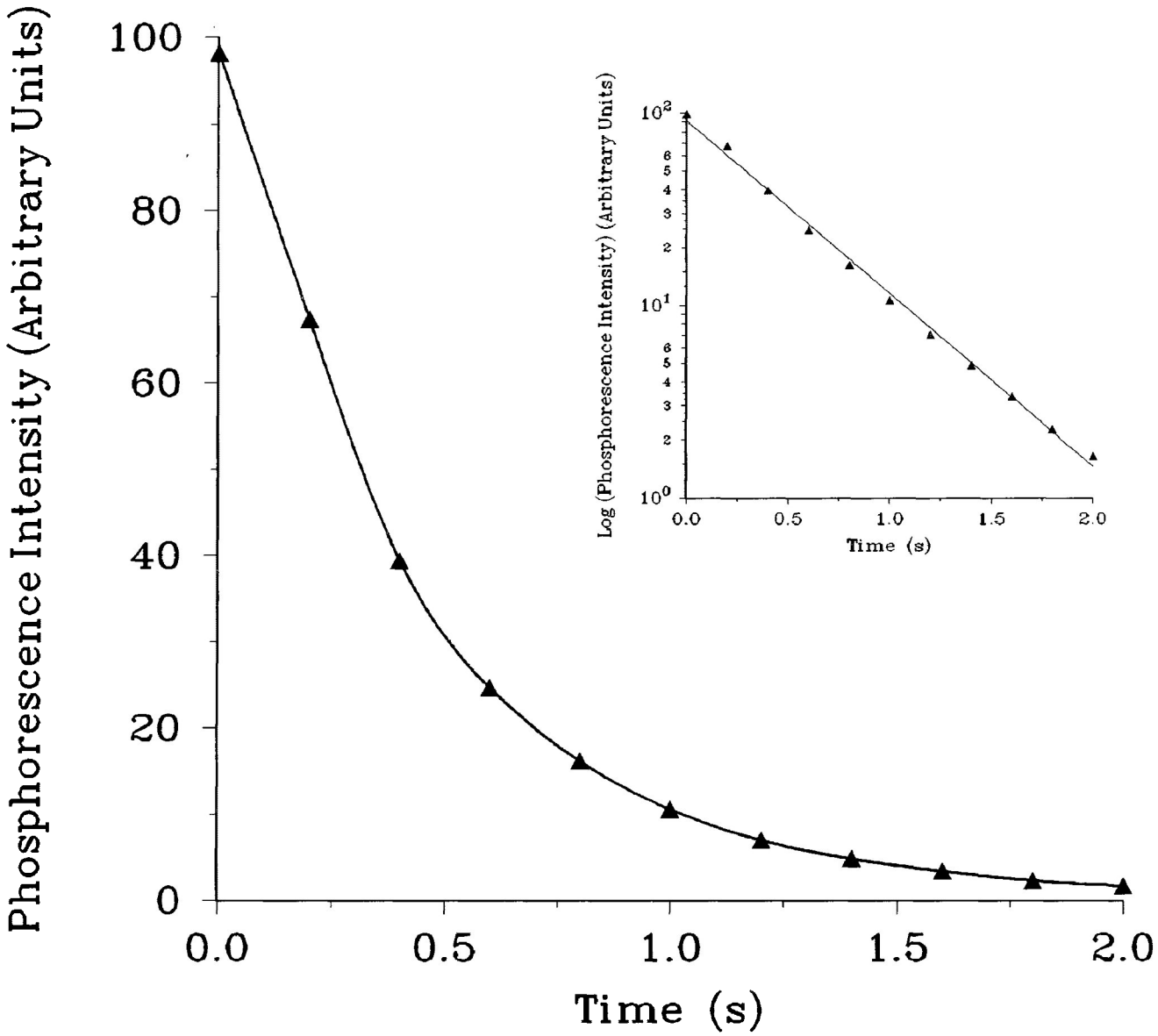

Figure 3.7. Phosphorescence Decay Characteristics of P35DMAP Triplet. (Insert Represents Semi–Logarithmic Plot)

TABLE 3.3

Phosphorescence Characteristics of Methoxy-Substituted Poly(acrylophenones)

POLYMER*	λ_{max}† (nm)		$E_T(0-0)$ kJ mol^{-1}	τ_{phos} (s)
PMAP	454	429†	280	0.33 ± 5%
P34DMAP	497	472	254	0.61 ± 6%
P35DMAP	452	435†	276	0.55 ± 6%

* Glass at 77K

† Indicates Shoulder

4. **Quenching of Phosphorescence**. Direct phosphorescence quenching of PMAP, P34DMAP and P35DMAP triplets by *cis*-1,3-pentadiene was investigated and the results are shown in Figure 3.8 in which the intensity in the presence and absence of the quencher are I_x and I_o respectively. It can be seen that the data conform to Stern-Volmer kinetics. The slopes of the Stern-Volmer quenching plots, (K_{SV}), were determined and are summarized in Table 3.4.

B. **Photochemical Processes**

1. **UV Spectral Changes**. Shown in Figures 3.9-3.11 are the spectral changes associated with irradiation ($\lambda \geq 300$ nm, vacuum) of the various polymers in solution, and Figures 3.12-3.14 show the corresponding changes for identical irradiation of the films. Reduced intensities of both $\pi \rightarrow \pi^*$ and $n \rightarrow \pi^*$ peaks are observed in all cases; however, these changes are

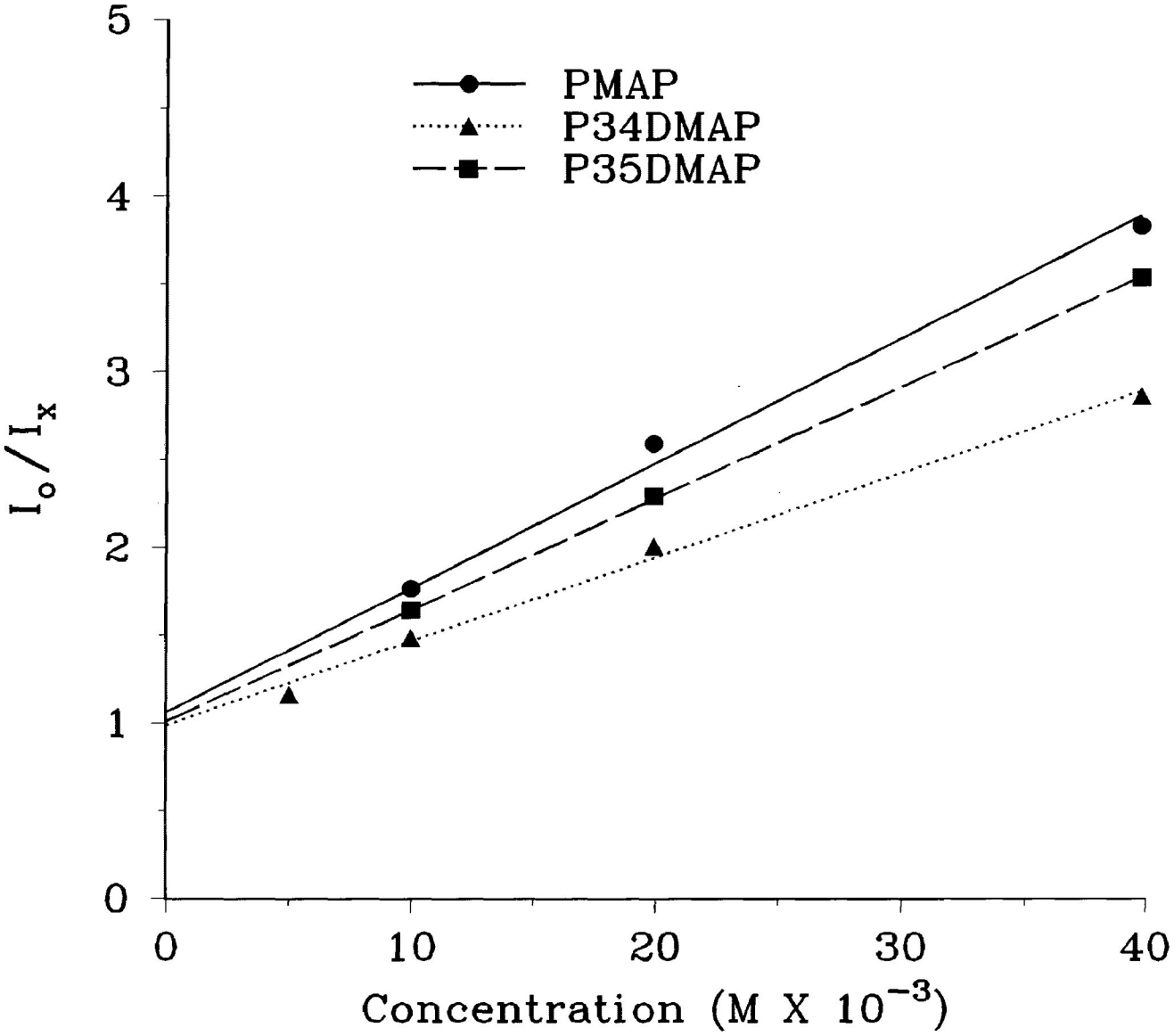

Figure 3.8. Stern–Volmer Data for Direct Quenching of Triplets by *cis*–1,3–Pentadiene.

TABLE 3.4

Phosphorescence Analysis Following

Direct Quenching of Triplets

POLYMER	K_{SV}^{*} $dm^3\ mol^{-1}$
PMAP	71.05 ± 5%
P34DMAP	47.81 ± 5%
P35DMAP	63.52 ± 2%

* With *cis*-1,3-pentadiene

greater in the films. Furthermore, a new broad absorption appears in the long-wave region. Prolonged irradiation not only increases the intensity of this band, but leads to colouration (yellow) and this is reflected by a bathochromic shift (to 400 nm) in the absorption.

2. **Emission Spectral Changes**. Changes in intensities of phosphorescence maxima were particularly noticeable following irradiation ($\lambda \geq 300$ nm, vacuum) of all three polymers (solid state and solution) (Figures 3.15-3.17). Reduced phosphorescence intensities are observed in all cases; however, these changes are greater in solution. These changes closely parallel those observed for UV absorption; however, new long-wave emissions appear upon irradiation of PMAP (Figure 3.15), P34DMAP (Figure 3.16) and P35DMAP (Figure 3.17), and they are possibly associated with the coloured species.

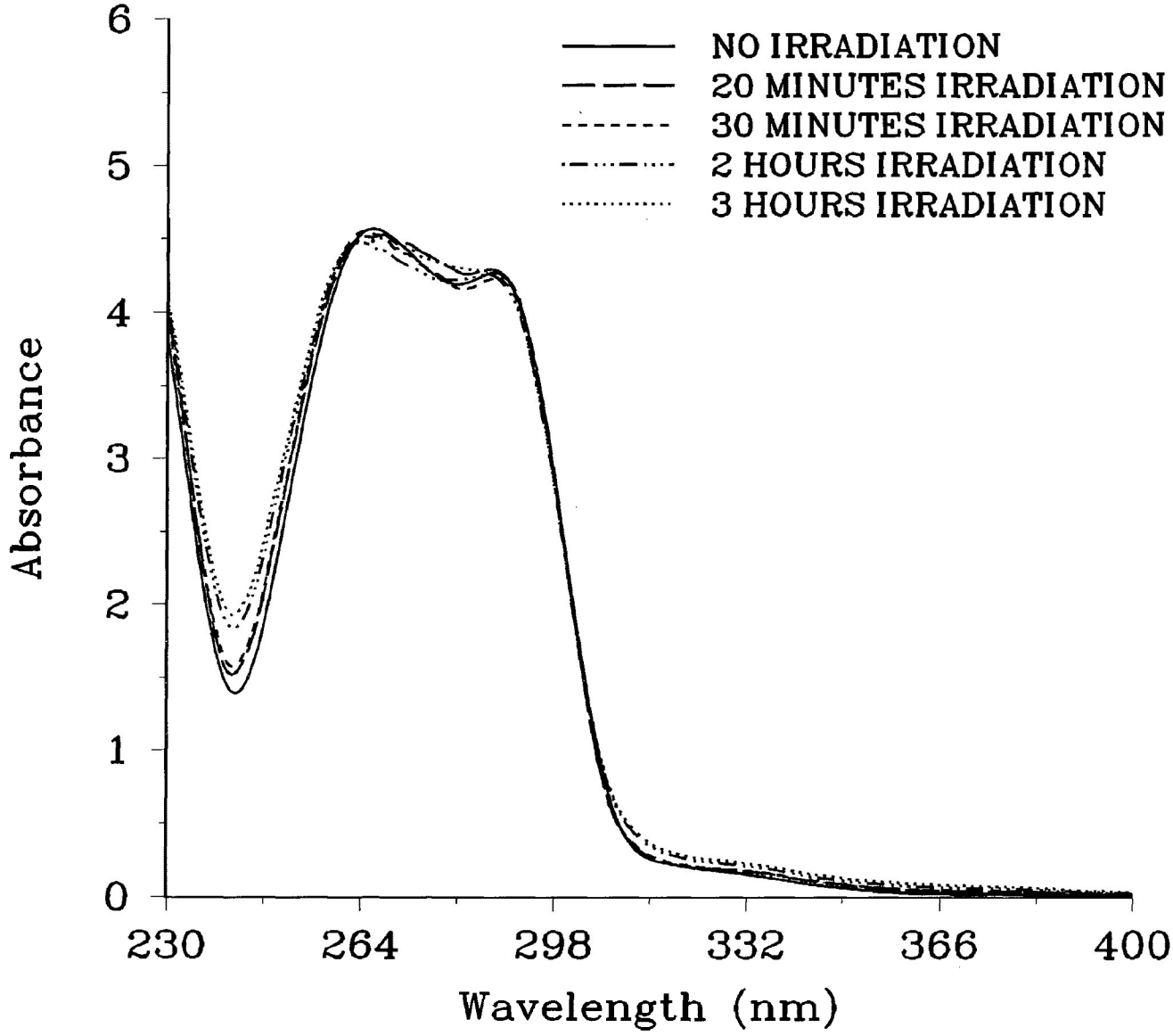

Figure 3.9. UV Absorption Spectrum* of PMAP (3.0×10^{-4} M Solution in CH_2Cl_2) Before and After Irradiation ($\lambda \geq 300$ nm, vacuum).
* Instrument Sensitive to 0.0001 %T.

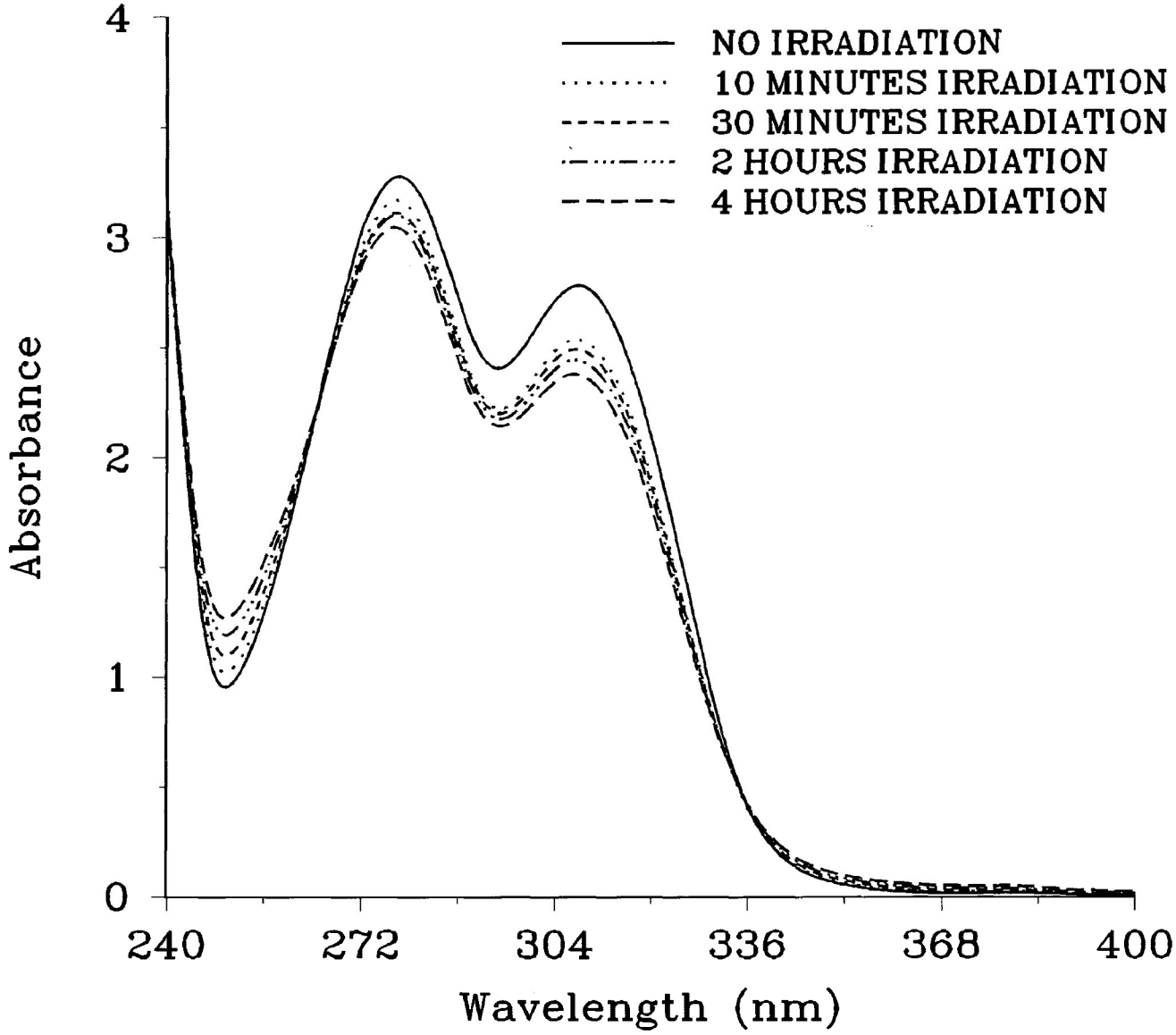

Figure 3.10. UV Absorption Spectrum* of P34DMAP (3.0×10^{-4} M Solution in CH_2Cl_2) Before and After Irradiation ($\lambda \geq 300$ nm, vacuum).

* Instrument Sensitive to 0.0001 %T.

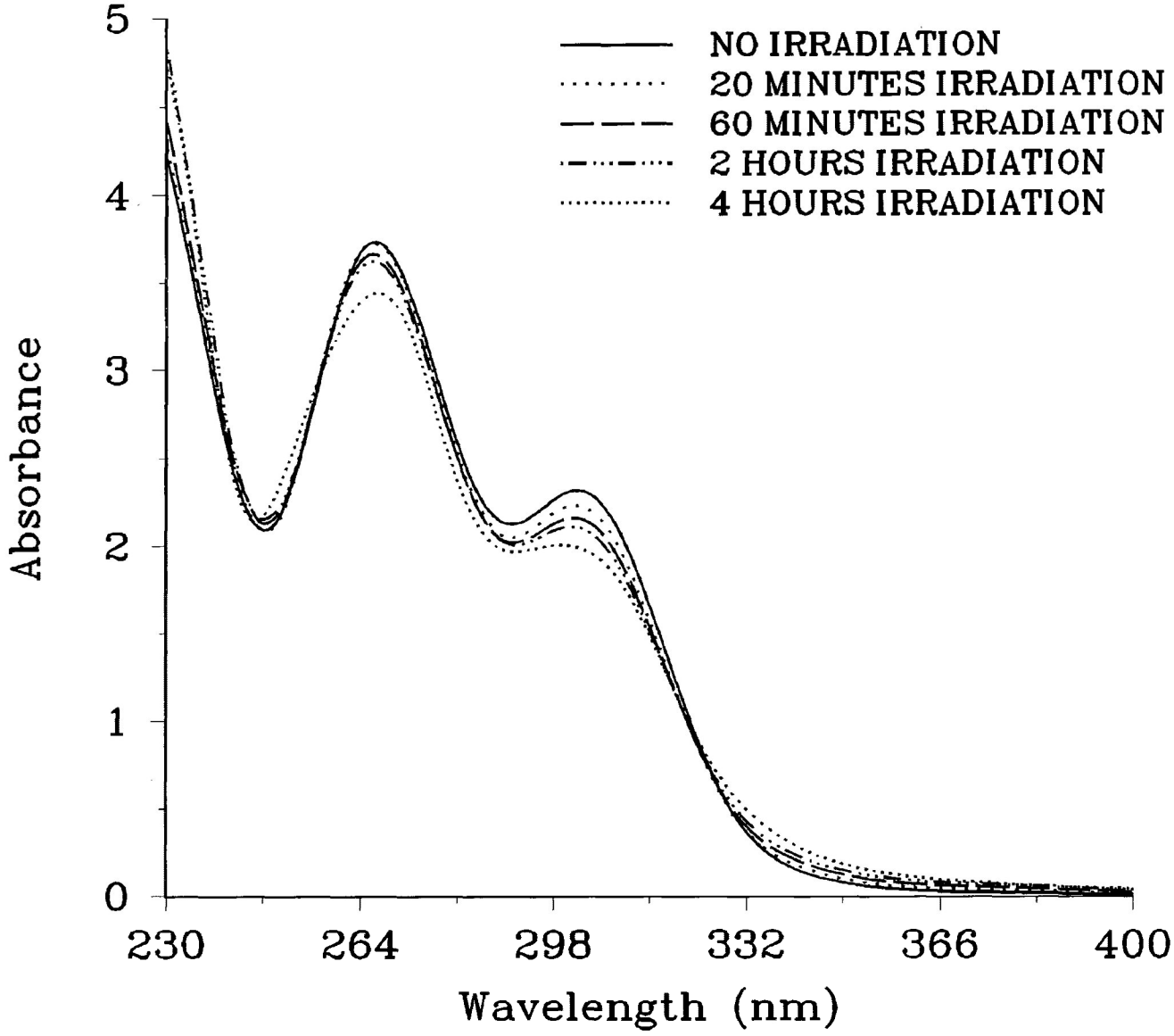

Figure 3.11. UV Absorption Spectrum* of P35DMAP (3.0×10^{-4} M Solution in CH_2Cl_2) Before and After Irradiation ($\lambda \geq 300$ nm, vacuum).

* Instrument Sensitive to 0.0001 %T.

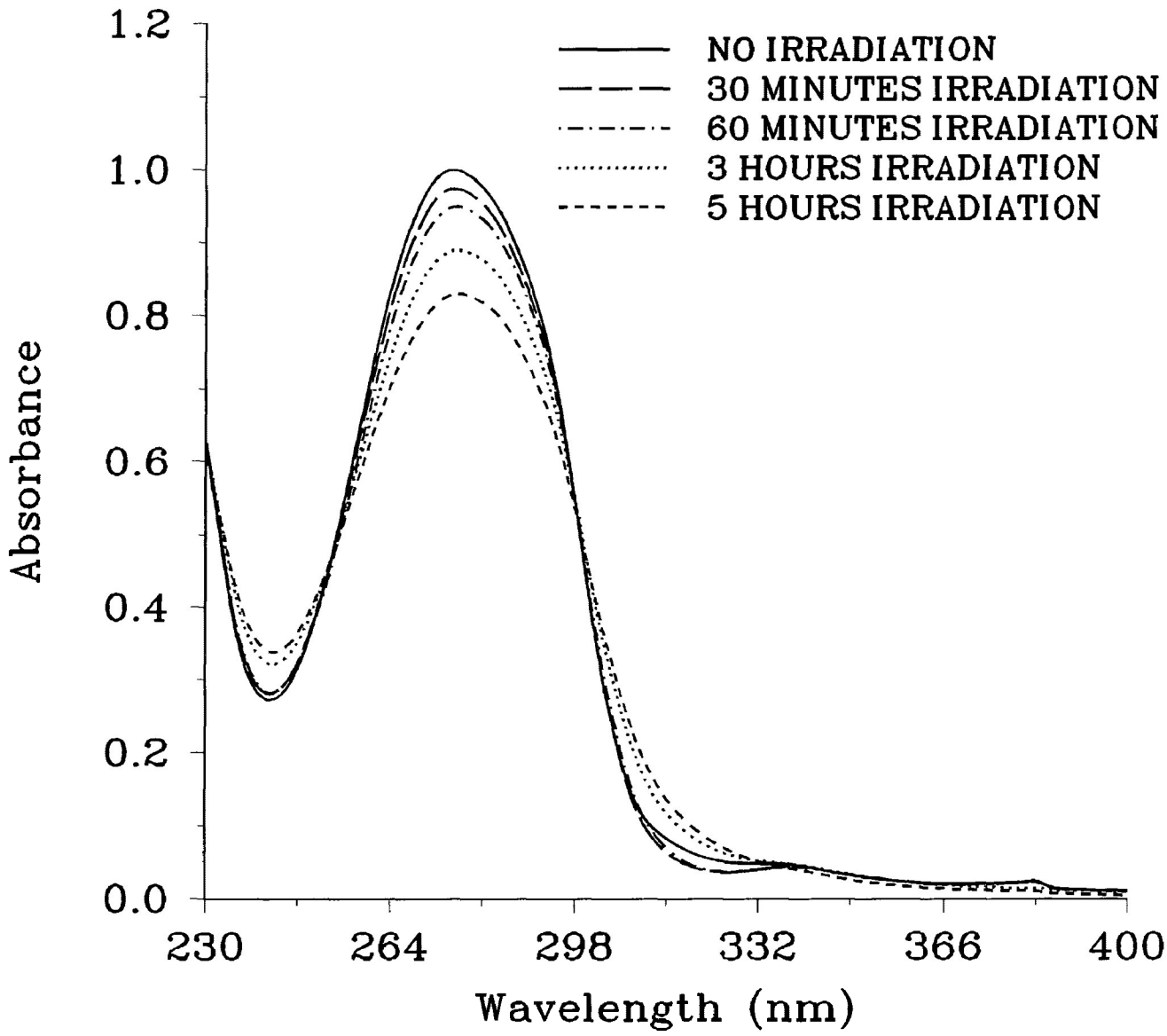

Figure 3.12. UV Absorption Spectrum* of PMAP (thin film) Before and After Irradiation ($\lambda \geq 300$ nm, vacuum).

* Instrument Sensitive to 0.0001 %T.

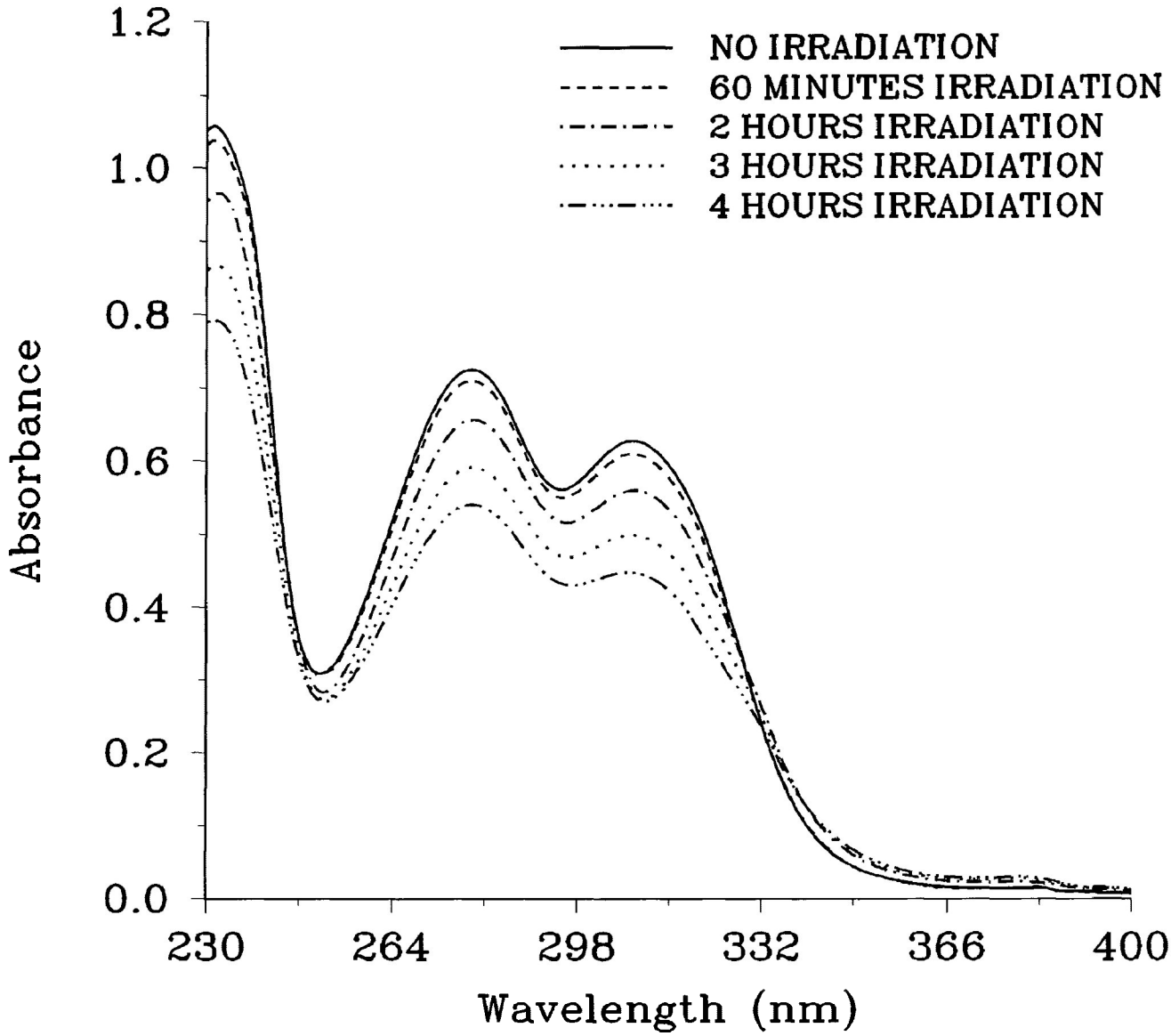

Figure 3.13. UV Absorption Spectrum* of P34DMAP (thin film) Before and After Irradiation ($\lambda \geq 300$ nm, vacuum).

* Instrument Sensitive to 0.0001 %T.

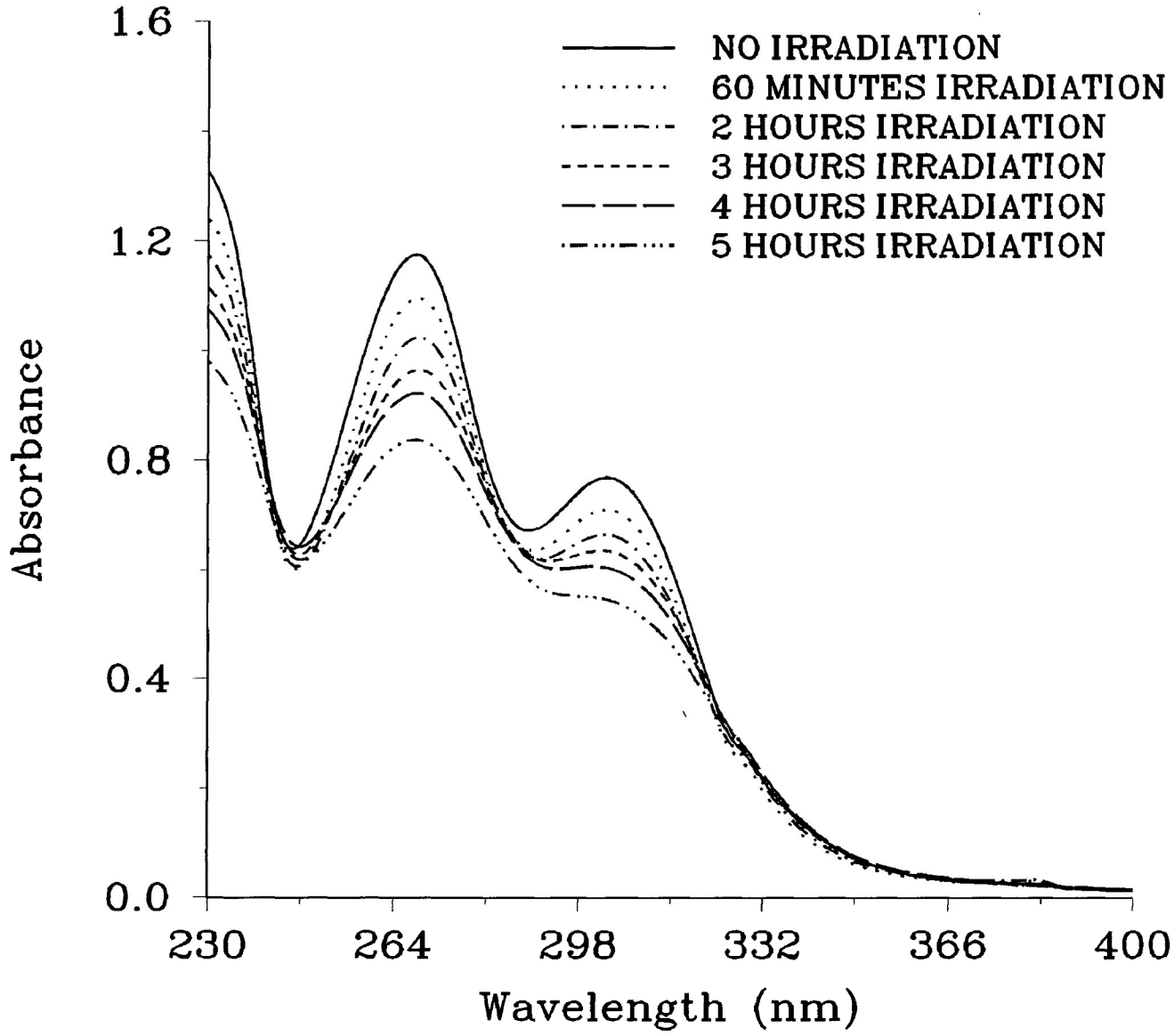

Figure 3.14. UV Absorption Spectrum* of P35DMAP (thin film) Before and After Irradiation ($\lambda \geq 300$ nm, vacuum).

* Instrument Sensitive to 0.0001 %T.

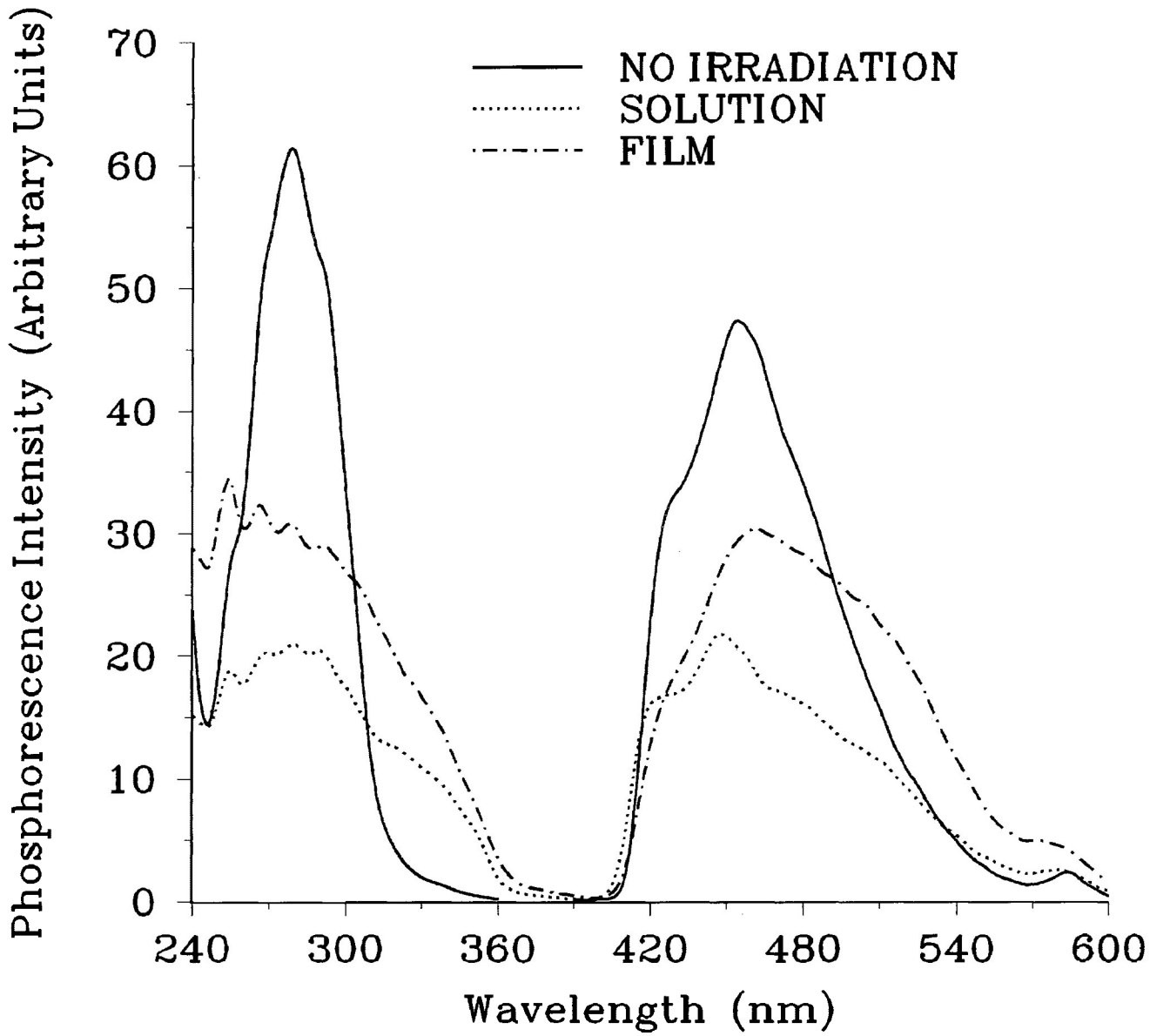

Figure 3.15. Phosphorescence Spectrum* of PMAP Before and After 4 Hours Irradiation ($\lambda \geq 300$ nm, vacuum).

*** In Glass at 77K.**

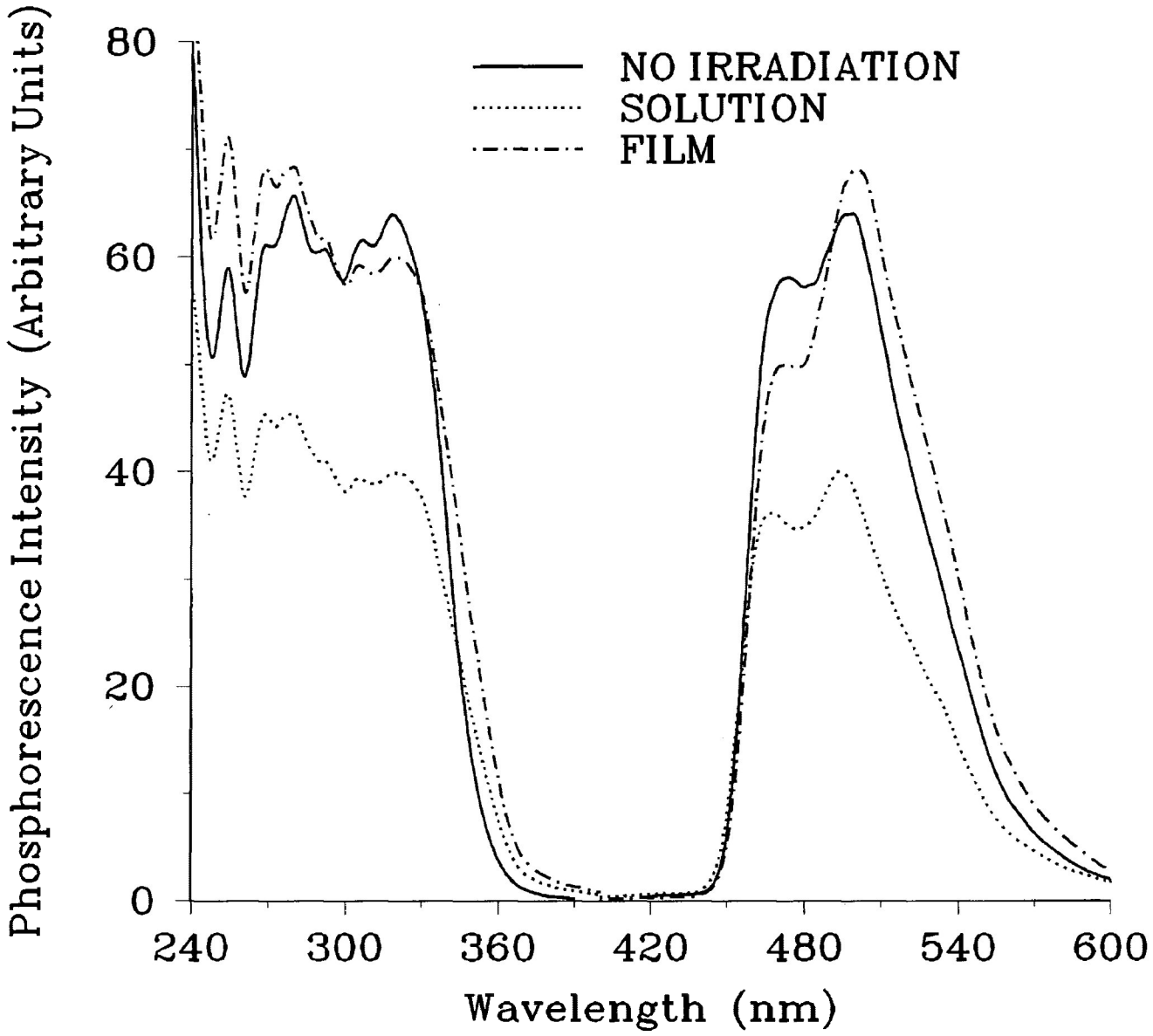

Figure 3.16. Phosphorescence Spectrum* of P34DMAP Before and After 4 Hours Irradiation ($\lambda \geq 300$ nm, vacuum).

*** In Glass at 77K.**

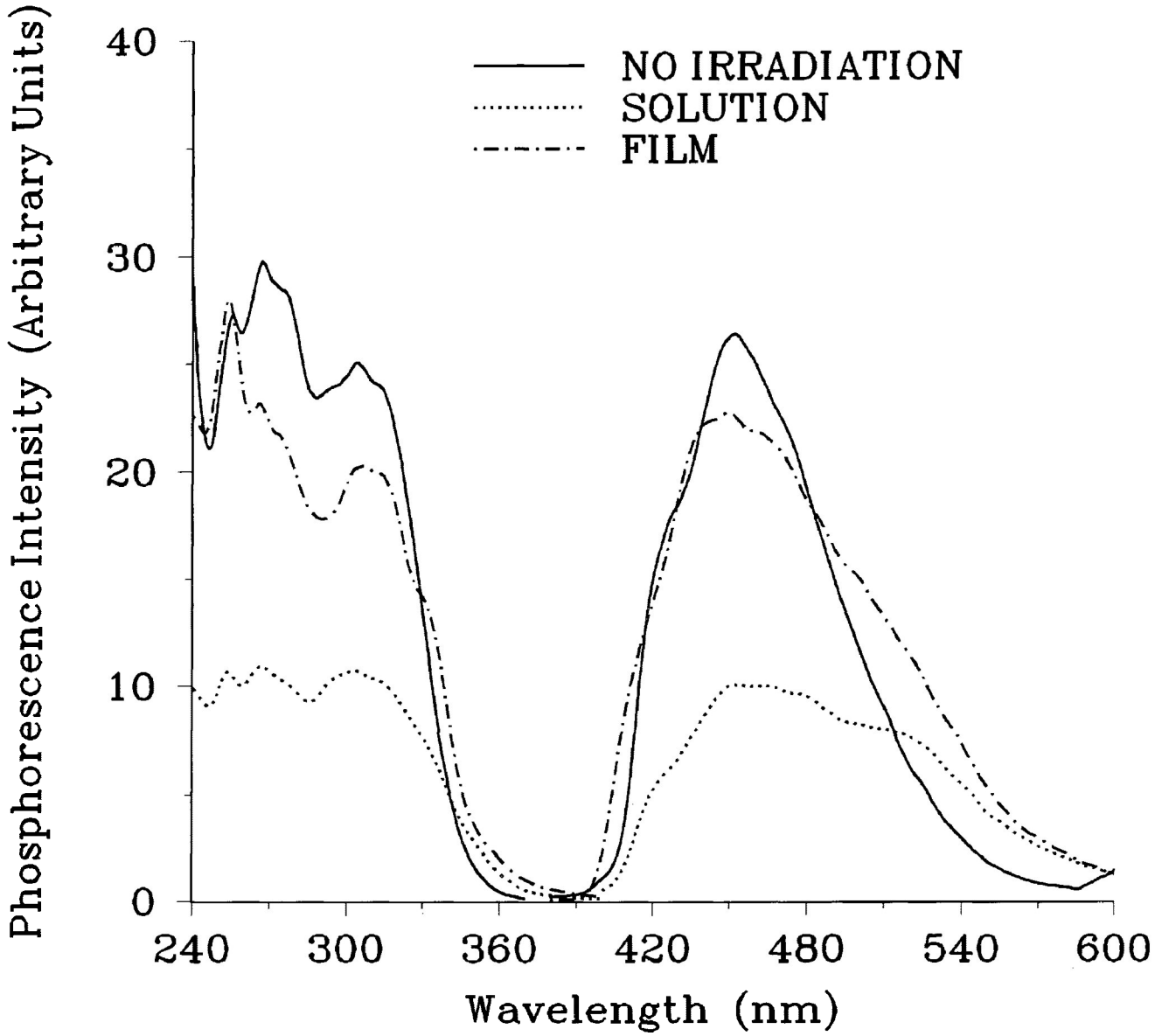

Figure 3.17. Phosphorescence Spectrum* of P35DMAP Before and After 4 Hours Irradiation ($\lambda \geq 300$ nm, vacuum).

*** In Glass at 77K.**

3. **Infrared Spectral Changes**. Irradiation of all three polymers ($\lambda \geq 300$ nm, vacuum) showed increased absorbances in the 1680-1720 cm^{-1} (carbonyl) and 3300-3500 cm^{-1} (hydroxyl) regions of the infrared spectra (Figure 3.18). Furthermore, a slight depletion of the carbonyl concentration in PMAP and P35DMAP was indicated by a decrease in the intensity of the peaks at 1670 cm^{-1} and 1650 cm^{-1} respectively (carbonyl stretching frequency). No significant change, however, was observed in the intensity of the peak at 1660 cm^{-1} for P34DMAP. Otherwise spectra of the non-irradiated and irradiated samples were quite similar.

4. **NMR Spectral Changes**. Major changes in NMR spectra were associated with OCH_3 depletion and the formation of new carbonyl species. Loss of methoxyl protons was confirmed by a decrease in the signal intensity at 3.80 ppm in the ^1H NMR spectrum of all three polymers irradiated in solution. At the same time, a new signal appeared at 5.30 ppm, and this was attributed to the formation of a new unsaturated entity (Figures 3.19-3.21). Loss of the methoxyl carbon was further confirmed by a decrease in the signal intensity at 56 ppm in the ^{13}C NMR spectrum. In addition, a new peak appeared at 184 ppm, and this was attributed to a quinonoid species (Figures 3.22-3.24). The photodegradation of P35DMAP in solution appears to be slightly different from that of PMAP and P34DMAP in that a prominent new CH_2 peak appears in both ^1H NMR (1.25 ppm) and ^{13}C NMR (30 ppm). The identity was

confirmed using a DEPT sequence[41], and the data are shown as inserts in Figures 3.22-3.24. In the other two polymers the intensity of this peak was quite small.

Loss of methoxyl protons at 3.80 ppm was also observed in the film ^{1}H NMR spectrum of PMAP and P34DMAP upon irradiation in solid state. However, intensity of the signal at 5.30 ppm was small indicating little formation of the new unsaturated entity (Figures 3.25-3.26). Loss of the methoxyl carbon was further confirmed by a significant decrease in the 56 ppm signal in the ^{13}C NMR spectrum; furthermore, a new peak appeared at 184 ppm, and this was attributed to formation of a quinonoid species (Figures 3.28-3.29). Solid state photodegradation of PMAP and P34DMAP produced prominent CH_2 peaks at 1.25 ppm (^{1}H NMR) and at 30 ppm (^{13}C NMR). Similar irradiation of P35DMAP resulted in the complete loss of the methoxyl protons at 3.80 ppm in the ^{1}H NMR (Figure 3.27). In addition, a new signal appeared at 2.60 ppm. Complete loss of the methoxyl carbons was confirmed by the disappearance of the 56 ppm signal in the ^{13}C NMR spectrum (Figure 3.30). A very weak signal was observed at 184 ppm following prolonged exposure, indicating the possibility of crosslinking, and the CH_2 peak at 1.25 ppm (^{1}H NMR) and 30 ppm (^{13}C NMR) was not as prominent as in solution degradation. Changes are also summarized in Tables 3.5-3.16 (below diagrams).

5. **Low Molecular Weight Gaseous Products**. The only detectable low molecular weight products from the vacuum

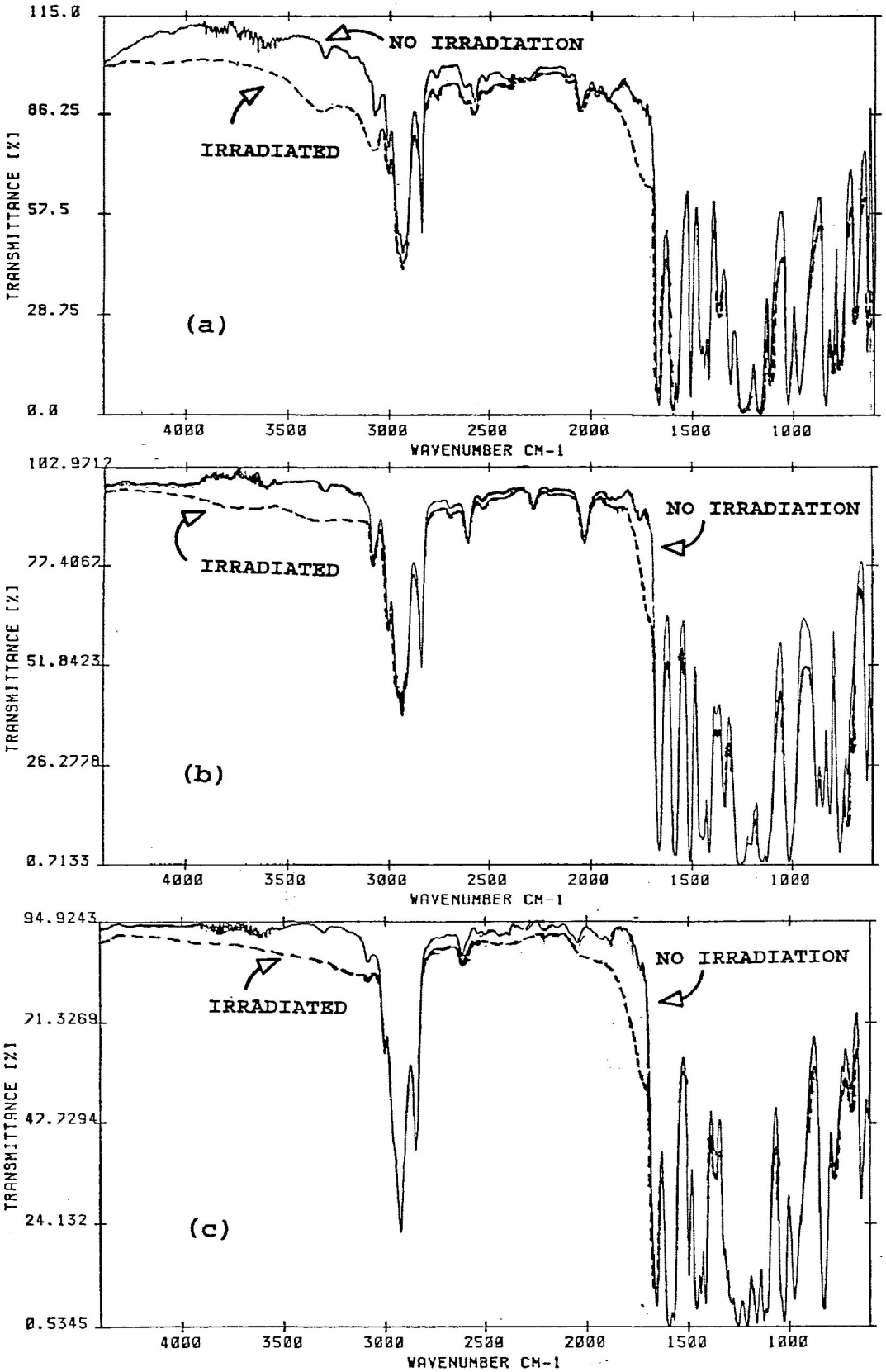

Figure 3.18. Infrared Spectral Changes of (a) PMAP (b) P34DMAP and (c) P35DMAP After 12 Hr Irradiation ($\lambda \geq 300$ nm, vacuum).

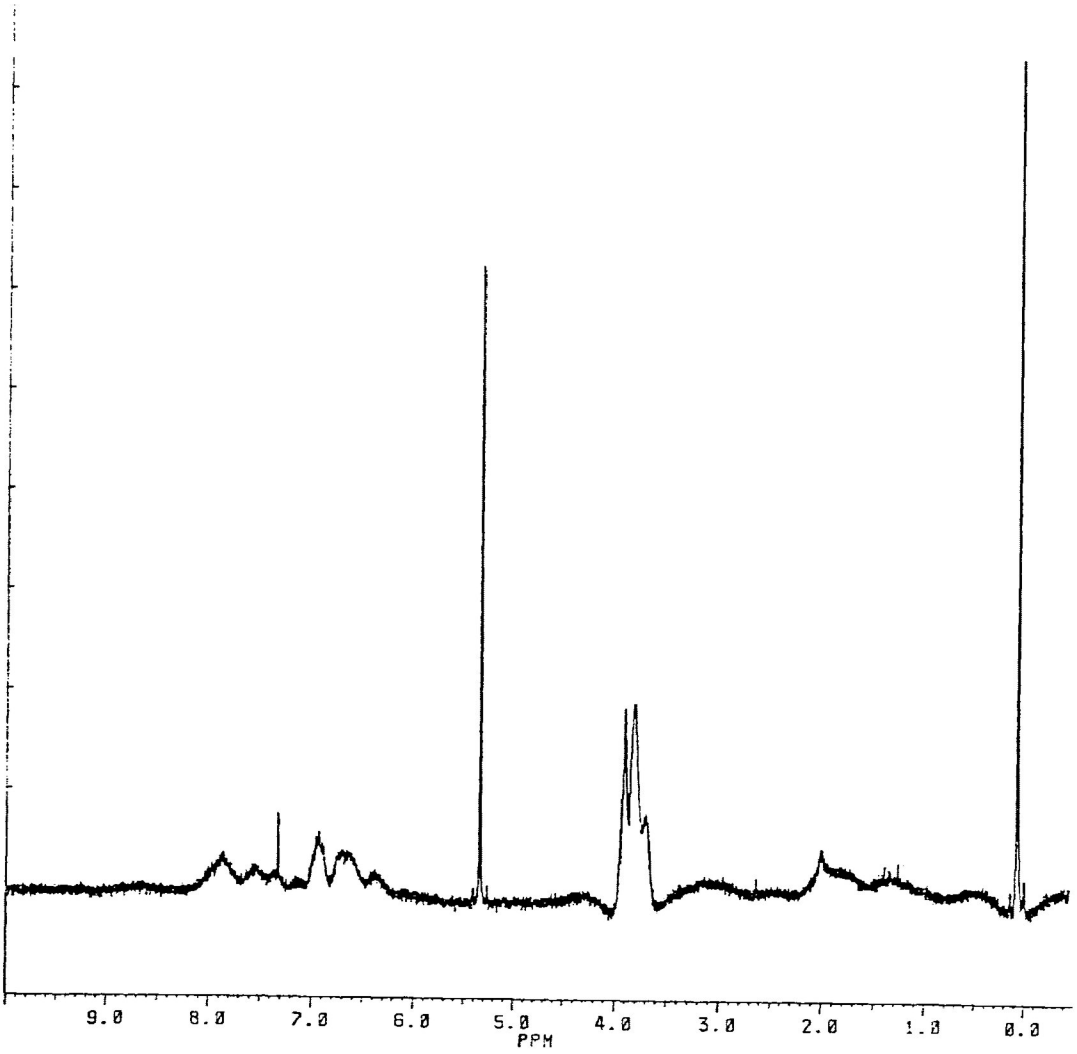

Figure 3.19. ^1H NMR Spectrum of Irradiated PMAP Solution. (6.0×10^{-2} M in CH_2Cl_2) After 12 Hours Exposure ($\lambda \geq 300$ nm, vacuum).

TABLE 3.5

^1H NMR Spectral Changes of PMAP Solution After 12 Hr Exposure ($\lambda \geq 300$ nm, vacuum)

Depletion		Formation	
Chemical Shift (δ) (ppm)	Assignment	Chemical Shift (δ) (ppm)	Possible Assignment
3.80	$O-CH_3$	5.30 (strong)	$=CH-$, $=CH_2$
		1.25 (weak)	$-CH_2-$

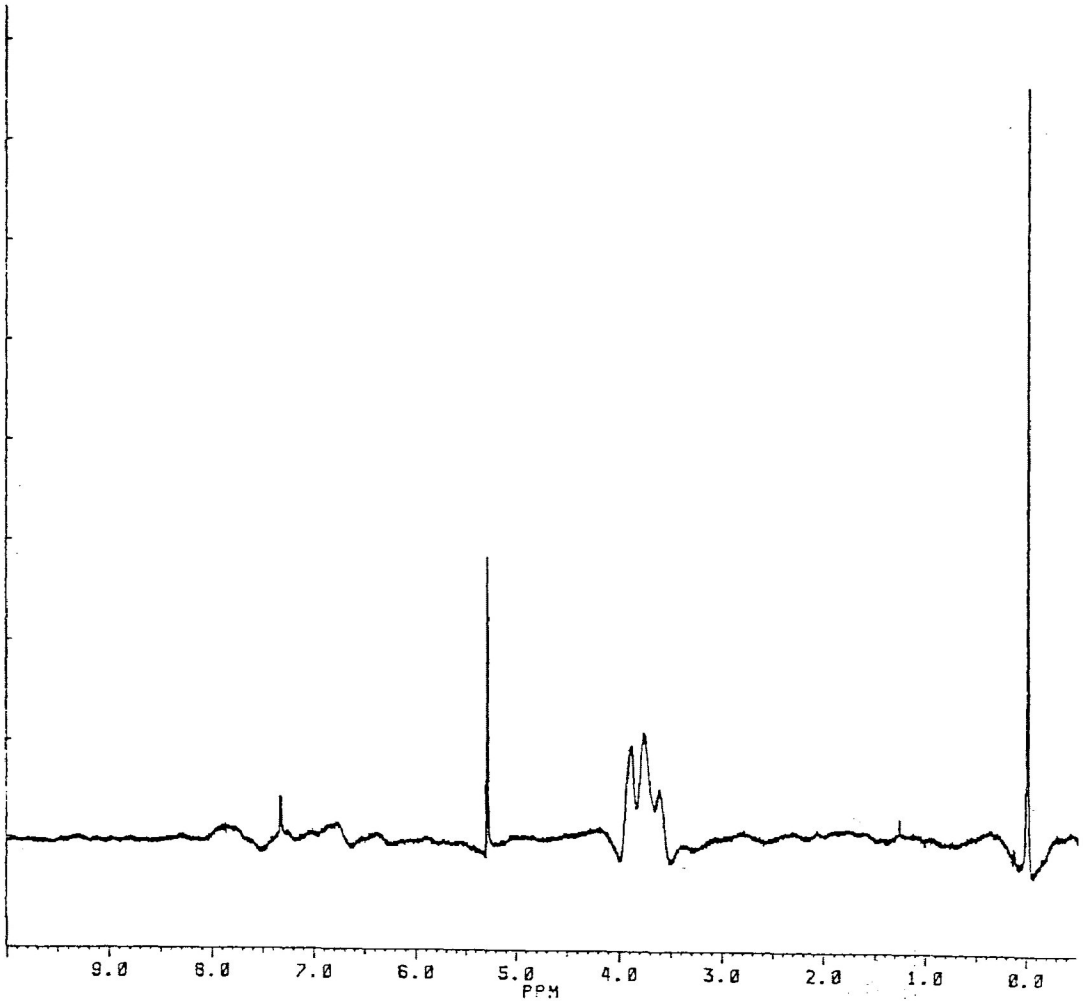

Figure 3.20. ^1H NMR Spectrum of Irradiated P34DMAP Solution (6.0×10^{-2} M in CH_2Cl_2) After 12 Hours Exposure ($\lambda \geq 300$ nm, vacuum).

TABLE 3.6

^1H NMR Spectral Changes of P34DMAP Solution After 12 Hr Exposure ($\lambda \geq 300$ nm, vacuum)

Depletion		Formation	
Chemical Shift (δ) (ppm)	Assignment	Chemical Shift (δ) (ppm)	Possible Assignment
3.80	$O-CH_3$	5.30 (strong)	$=CH-$, $=CH_2$
		1.25 (weak)	$-CH_2-$

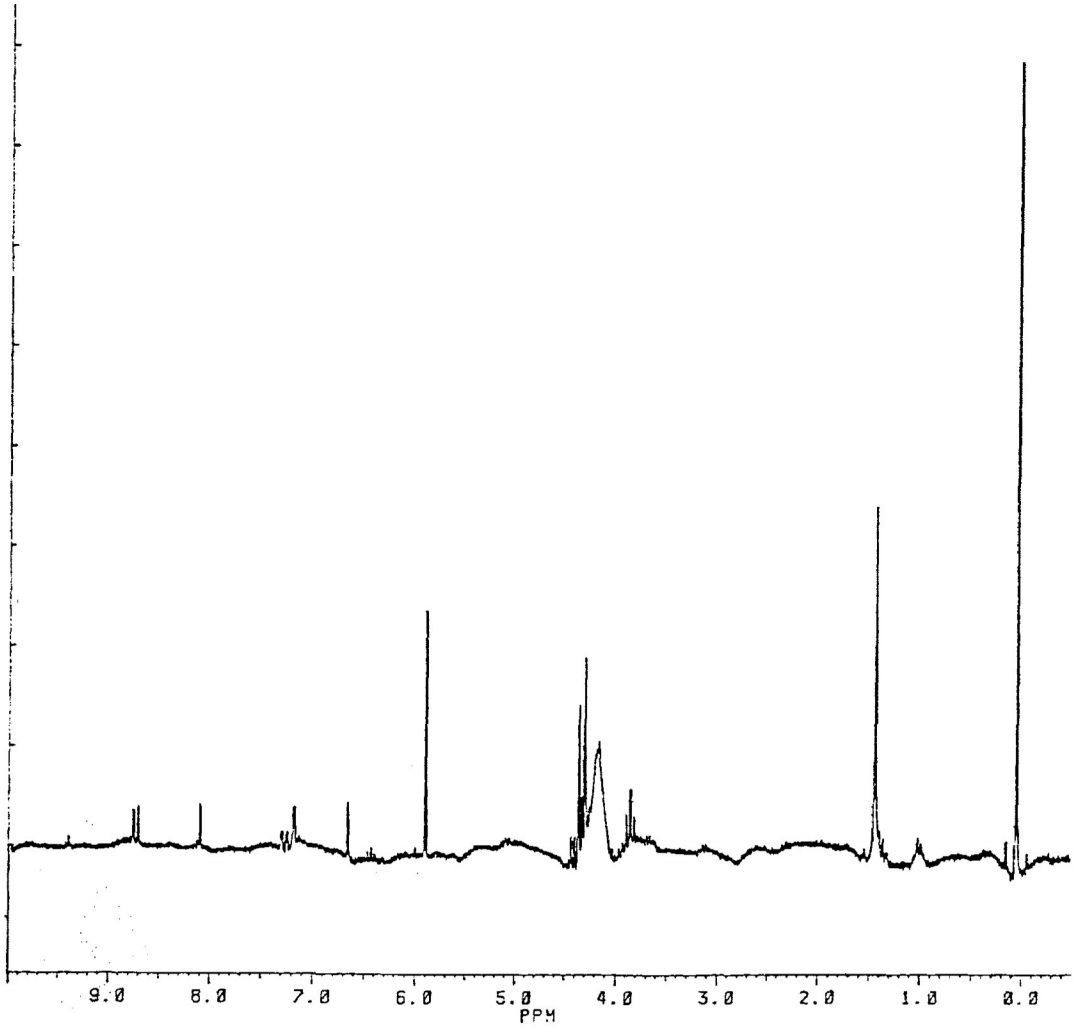

Figure 3.21. ^{1}H NMR Spectrum of Irradiated P35DMAP Solution (6.0×10^{-2} M in CH_2Cl_2) After 12 Hours Exposure ($\lambda \geq 300$ nm, vacuum).

TABLE 3.7

^{1}H NMR Spectral Changes of P35DMAP Solution After 12 Hr Exposure ($\lambda \geq 300$ nm, vacuum)

Depletion		Formation	
Chemical Shift (δ) (ppm)	Assignment	Chemical Shift (δ) (ppm)	Possible Assignment
3.80	$O-CH_3$	5.30 (strong)	$=CH-$, $=CH_2$
		1.25 (strong)	$-CH_2-$

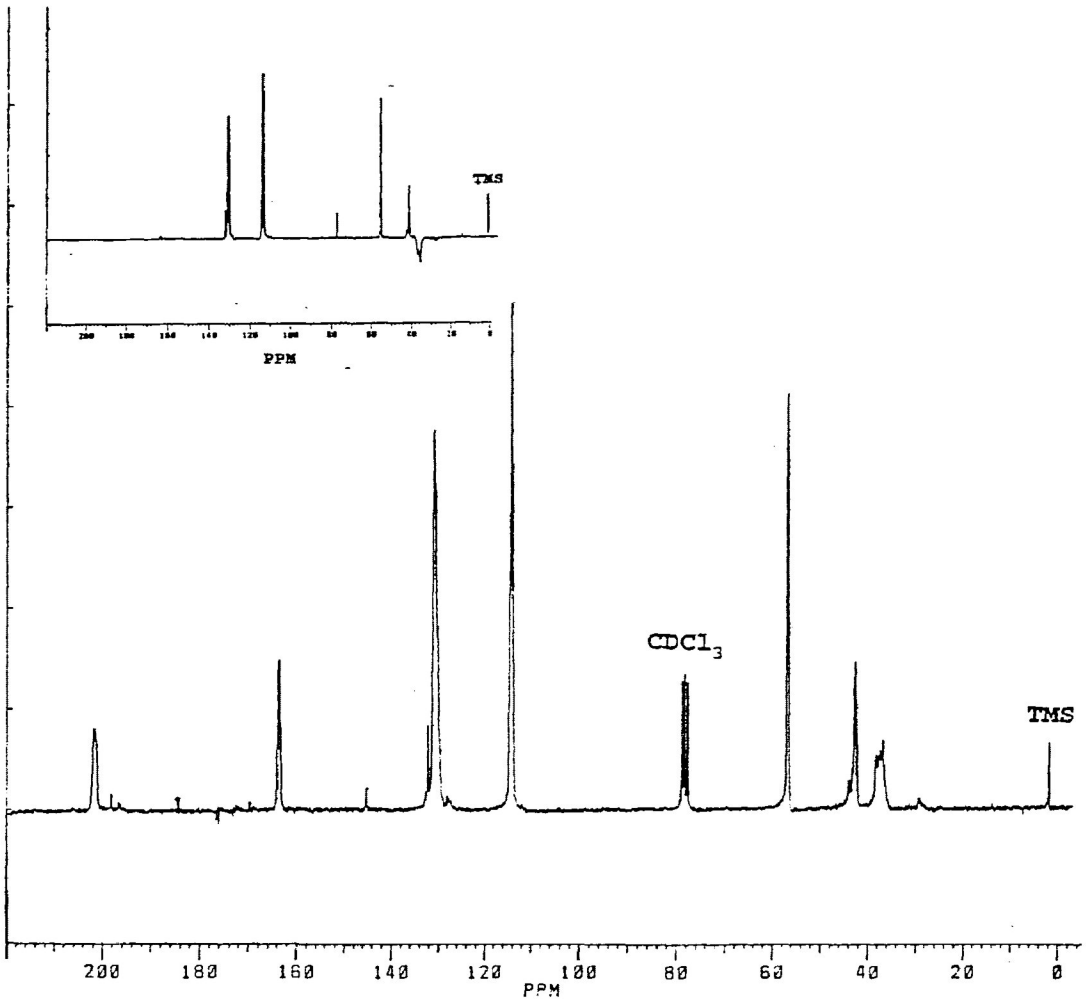

Figure 3.22. ^{13}C NMR Spectrum of Irradiated PMAP Solution (6.0×10^{-2} M in CH_2Cl_2) After 12 Hours Exposure ($\lambda \geq 300$ nm, vacuum). (Insert Represents DEPT Sequence[41])

TABLE 3.8

^{13}C NMR Spectral Changes of PMAP Solution After 12 Hr Exposure ($\lambda \geq 300$ nm, vacuum)

Depletion		Formation	
Chemical Shift (δ) (ppm)	Assignment	Chemical Shift (δ) (ppm)	Possible Assignment
56	O-**C**H_3	184 (weak)	**C**=O (quinone)
41	-**C**H-CH_2	30 (weak)	-**C**H_2-
		128 (weak)	=**C**H_2

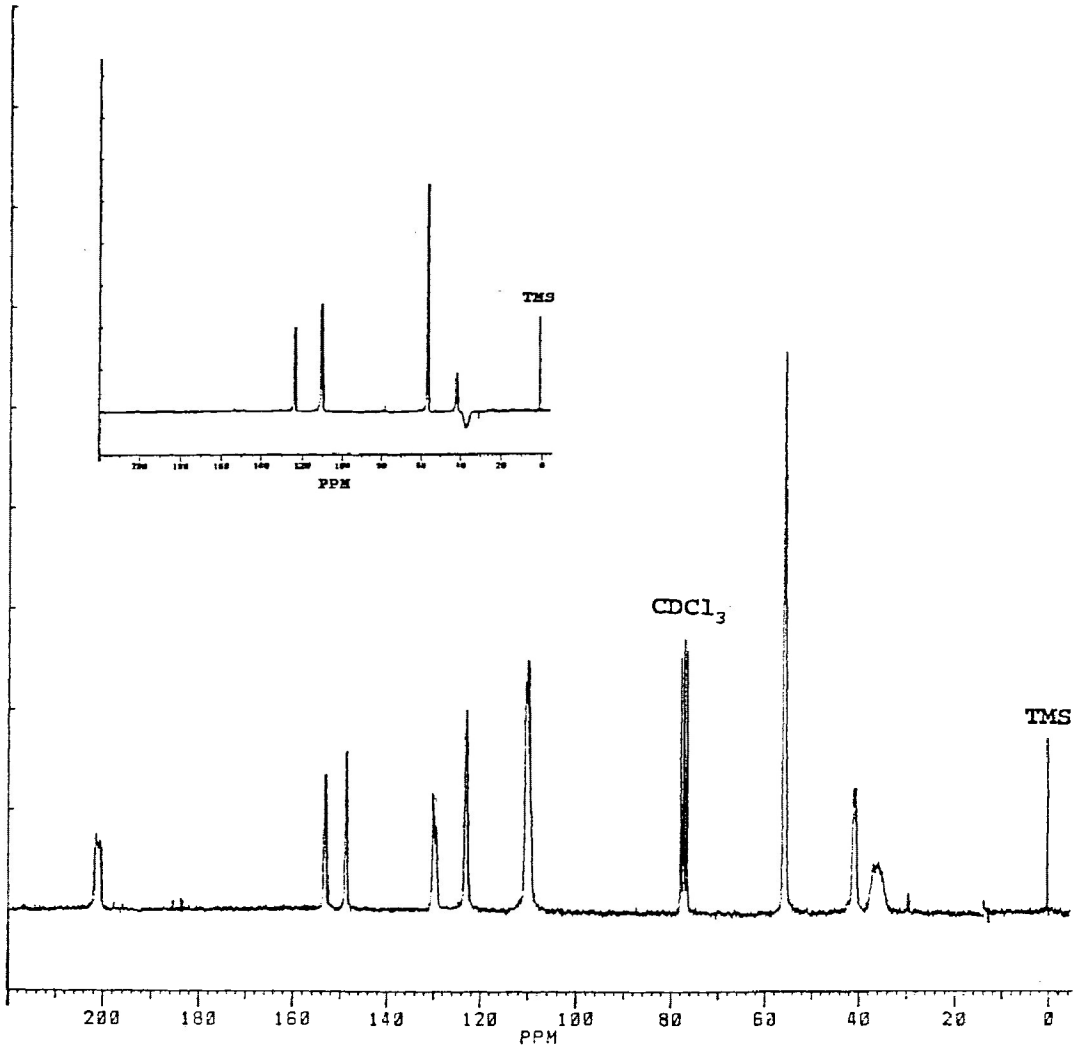

Figure 3.23. ^{13}C NMR Spectrum of Irradiated P34DMAP Solution (6.0×10^{-2} M in CH_2Cl_2) After 12 Hours Exposure ($\lambda \geq 300$ nm, vacuum). (Insert Represents DEPT Sequence[41]) .

TABLE 3.9

^{13}C NMR Spectral Changes of P34DMAP Solution After 12 Hr Exposure ($\lambda \geq 300$ nm, vacuum)

Depletion		Formation	
Chemical Shift (δ) (ppm)	Assignment	Chemical Shift (δ) (ppm)	Possible Assignment
56	O-**C**H_3	184 (weak)	**C**=O (quinone)
41	-**C**H-CH_2-	30 (weak)	-**C**H_2-

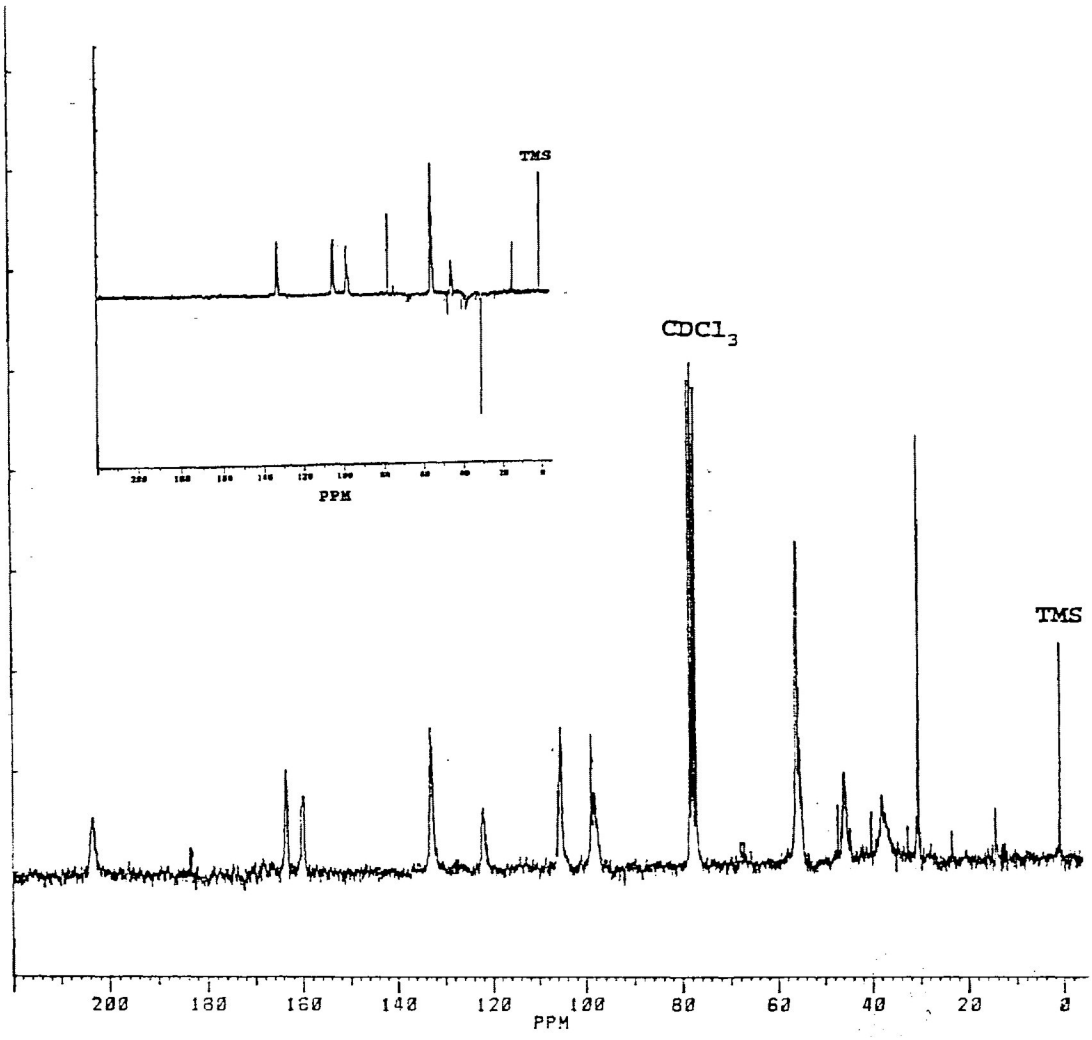

Figure 3.24. ^{13}C NMR Spectrum of Irradiated P35DMAP Solution (6.0×10^{-2} M in CH_2Cl_2) After 12 Hours Exposure ($\lambda \geq 300$ nm, vacuum). (Insert Represents DEPT Sequence[41])

TABLE 3.10

^{13}C NMR Spectral Changes of P35DMAP Solution After 12 Hr Exposure ($\lambda \geq 300$ nm, vacuum)

Depletion		Formation	
Chemical Shift (δ) (ppm)	Assignment	Chemical Shift (δ) (ppm)	Possible Assignment
56	O-**C**H_3	184 (weak)	**C**=O (quinone)
45	-**C**H-CH_2-	30 (strong)	-**C**H_2-
		14 (medium)	-**C**H_3

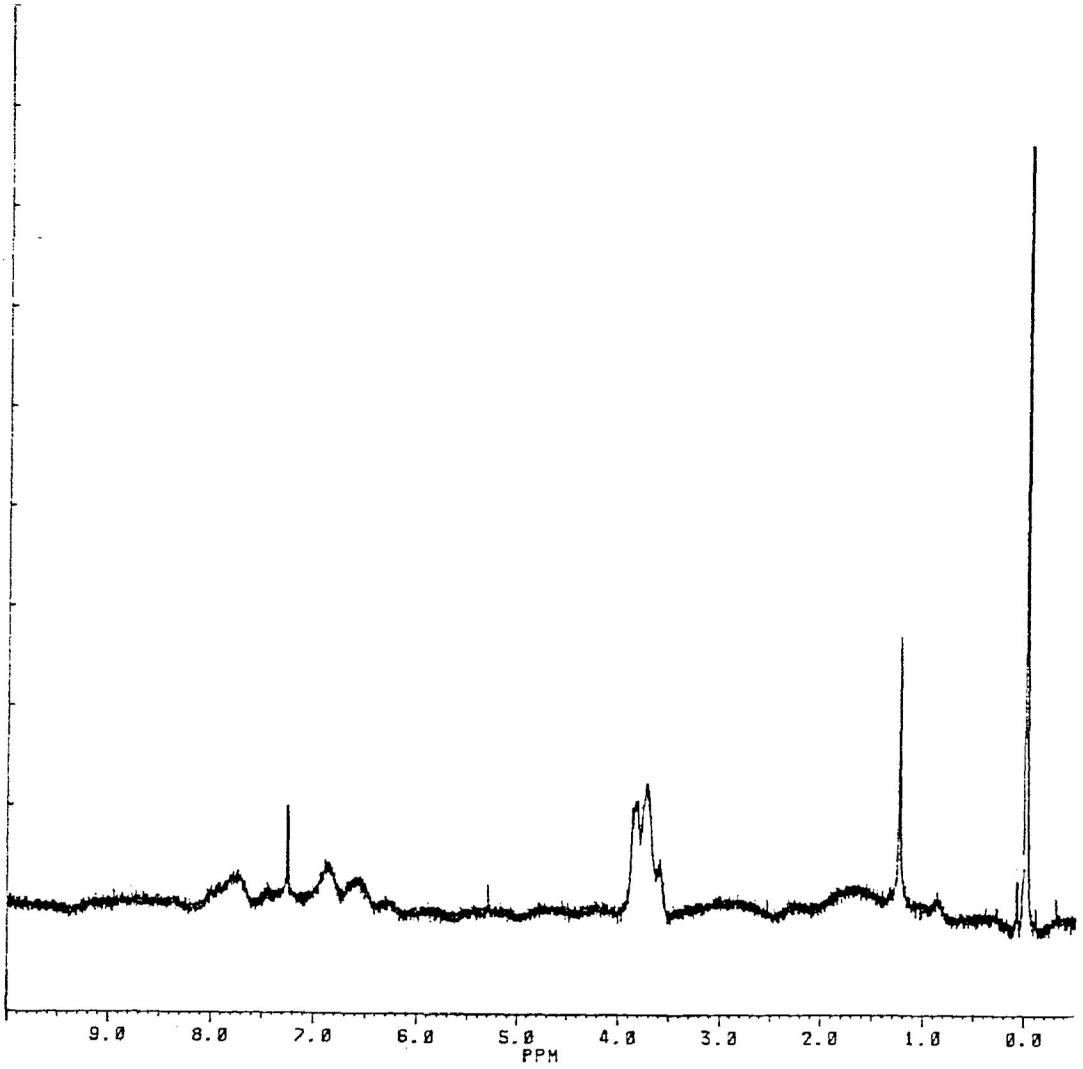

Figure 3.25. ^{1}H NMR Spectrum of Irradiated PMAP Film After 12 Hours Exposure ($\lambda \geq 300$ nm, vacuum).

TABLE 3.11

^{1}H NMR Spectral Changes of PMAP Film After 12 Hr Exposure ($\lambda \geq 300$ nm, vacuum)

Depletion		Formation	
Chemical Shift (δ) (ppm)	Assignment	Chemical Shift (δ) (ppm)	Possible Assignment
3.80	$O-CH_3$	5.30 (weak)	$=CH-$, $=CH_2$
		1.25 (strong)	$-CH_2-$

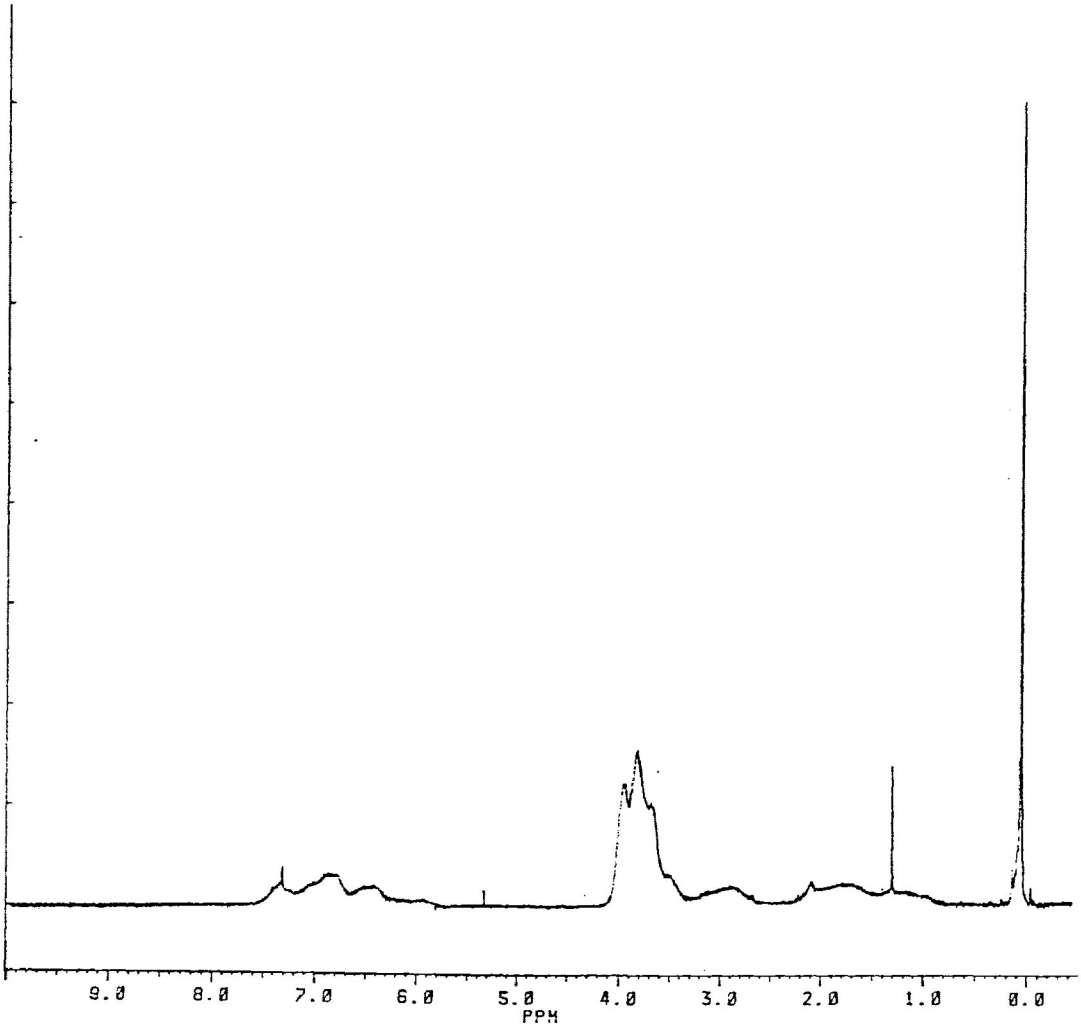

Figure 3.26. ^{1}H NMR Spectrum of Irradiated P34DMAP Film After 12 Hours Exposure ($\lambda \geq 300$ nm, vacuum).

TABLE 3.12

^{1}H NMR Spectral Changes of P34DMAP Film After 12 Hr Exposure ($\lambda \geq 300$ nm, vacuum)

Depletion		Formation	
Chemical Shift (δ) (ppm)	Assignment	Chemical Shift (δ) (ppm)	Possible Assignment
3.80	$O-CH_3$	5.30 (weak)	$=CH-$, $=CH_2$
		1.25 (strong)	$-CH_2-$

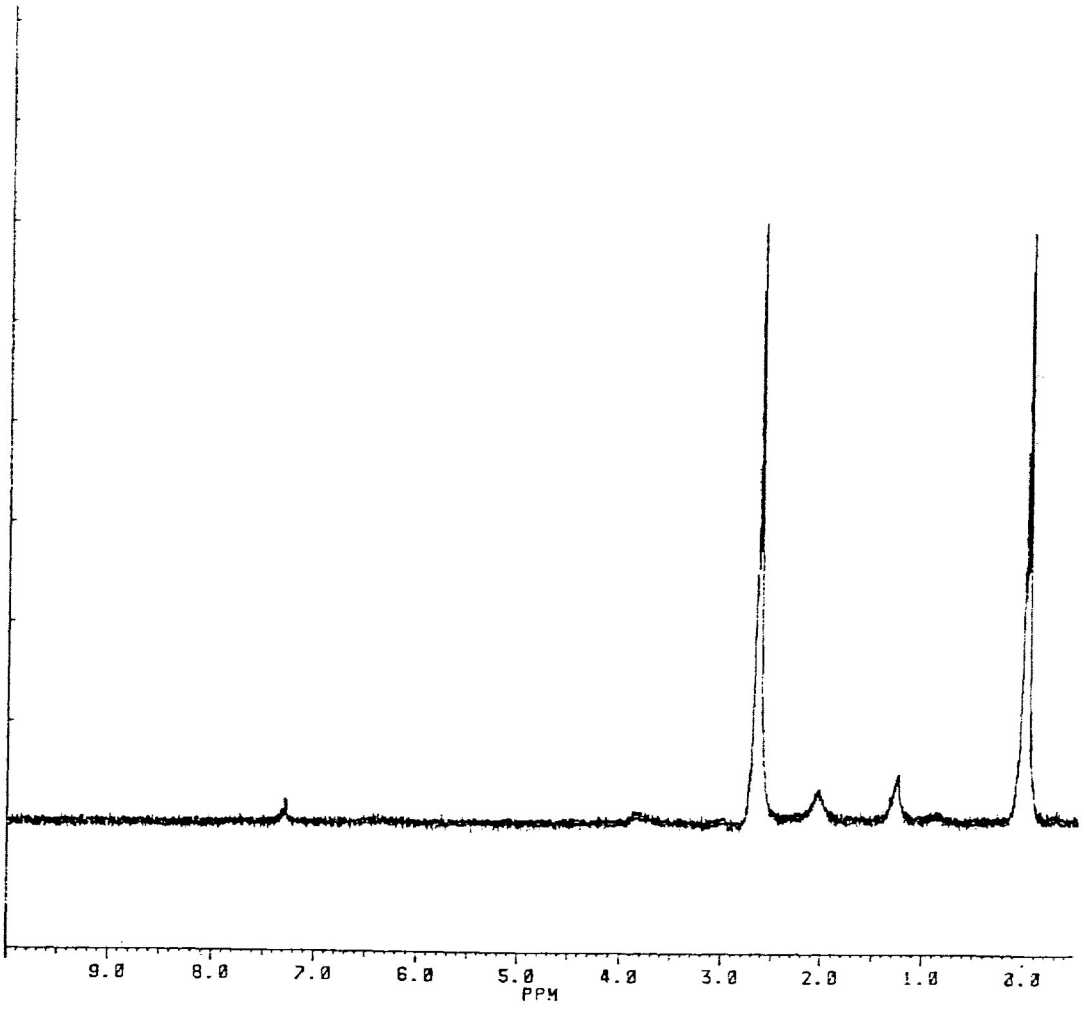

Figure 3.27. ^{1}H NMR Spectrum of Irradiated P35DMAP Film After 12 Hours Exposure ($\lambda \geq 300$ nm, vacuum).

TABLE 3.13

^{1}H NMR Spectral Changes of P35DMAP Film After 12 Hr Exposure ($\lambda \geq 300$ nm, vacuum)

Depletion		Formation	
Chemical Shift (δ) (ppm)	Assignment	Chemical Shift (δ) (ppm)	Possible Assignment
3.80 (intense)	$O-CH_3$	1.25 (weak)	$-CH_2-$
		2.60 (strong)	-C-CH-CO-Ar

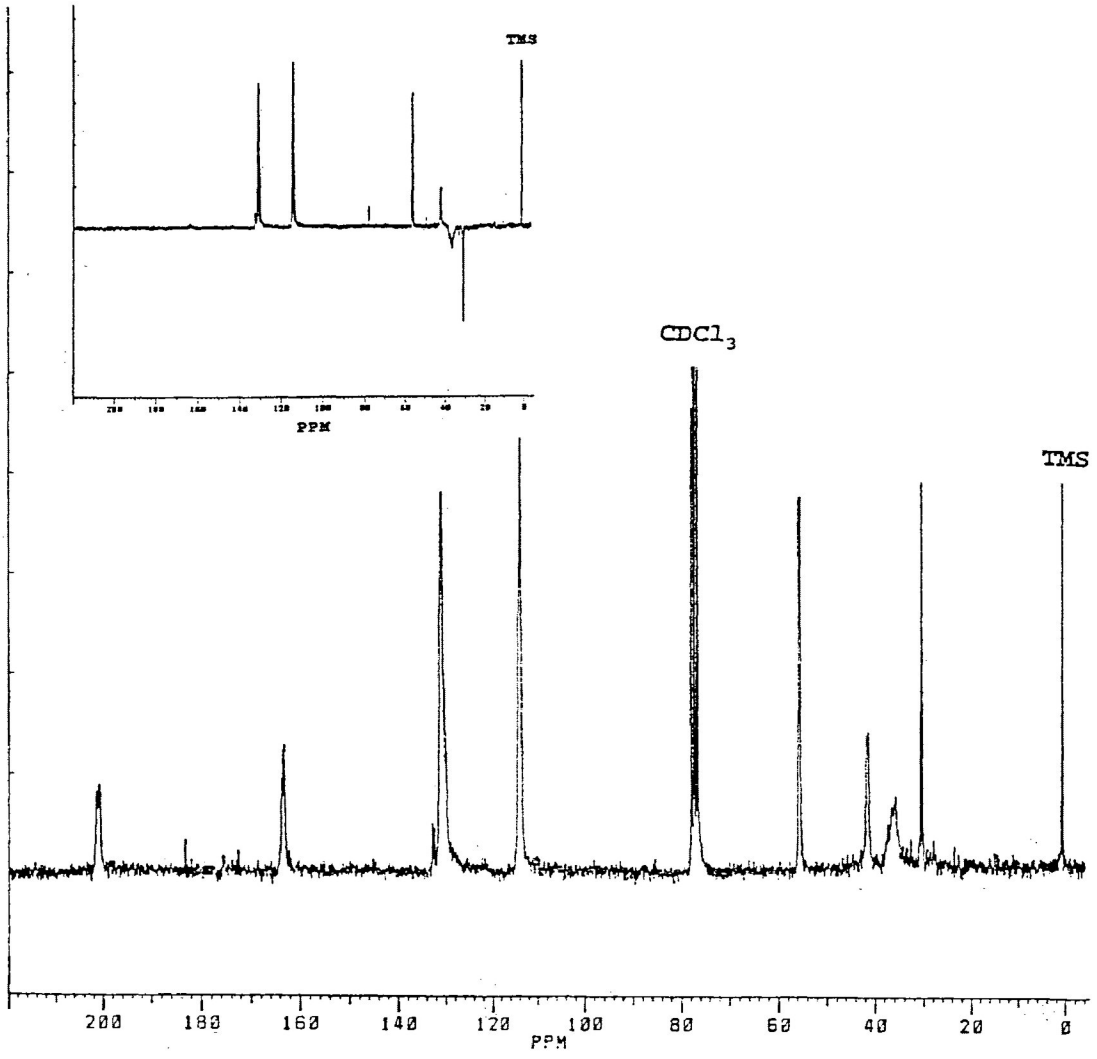

Figure 3.28. ^{13}C NMR Spectrum of Irradiated PMAP Film After 12 Hours Exposure ($\lambda \geq 300$ nm, vacuum). (Insert Represents DEPT Sequence[41])

TABLE 3.14

^{13}C NMR Spectral Changes of PMAP Film After 12 Hr Exposure ($\lambda \geq 300$ nm, vacuum)

Depletion		Formation	
Chemical Shift (δ) (ppm)	Assignment	Chemical Shift (δ) (ppm)	Possible Assignment
56	O-CH_3	184 (weak)	C=O (quinone)
41	-CH-CH_2	30 (strong)	-CH_2-

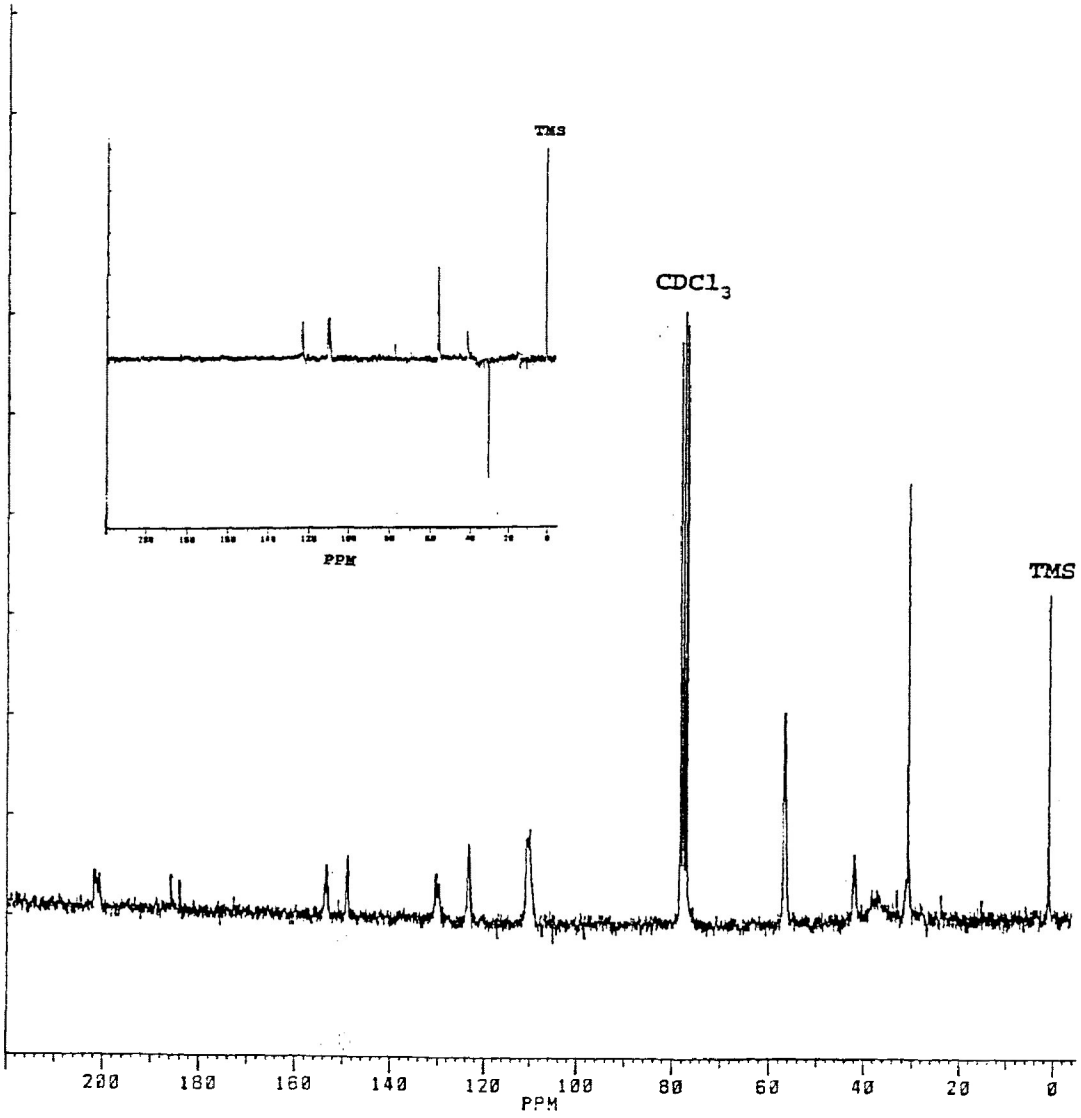

Figure 3.29. ^{13}C NMR Spectrum of Irradiated P34DMAP Film After 12 Hours Exposure ($\lambda \geq 300$ nm, vacuum). (Insert Represents DEPT Sequence[41])

TABLE 3.15

^{13}C NMR Spectral Changes of P34DMAP Film After 12 Hr Exposure ($\lambda \geq 300$ nm, vacuum)

Depletion		Formation	
Chemical Shift (δ) (ppm)	Assignment	Chemical Shift (δ) (ppm)	Possible Assignment
56	O-**C**H_3	184 (weak)	**C**=O (quinone)
41	-**C**H-CH_2	30 (strong)	-**C**H_2-

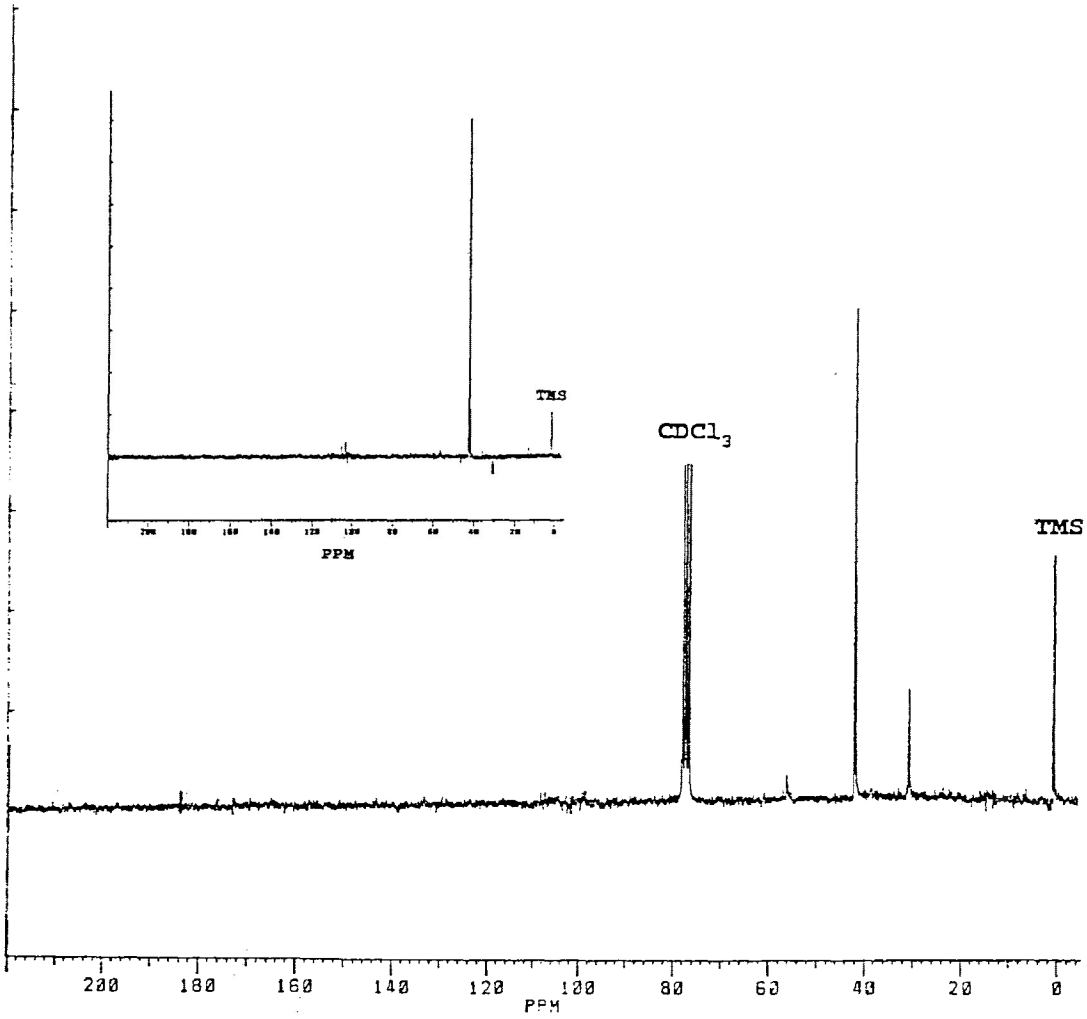

Figure 3.30. ^{13}C NMR Spectrum of Irradiated P35DMAP Film After 12 Hours Exposure ($\lambda \geq 300$ nm, vacuum). (Insert Represents DEPT Sequence[41])

TABLE 3.16

^{13}C NMR Spectral Changes of P35DMAP Film After 12 Hr Exposure ($\lambda \geq 300$ nm, vacuum)

Depletion		Formation	
Chemical Shift (δ) (ppm)	Assignment	Chemical Shift (δ) (ppm)	Possible Assignment
56 (intense)	O-CH_3	184 (weak)	C=O (quinone)
45, 36 (intense)	-CH-, -CH_2-	30 (weak)	-CH_2-
204 (intense)	C=O	41 (strong)	-CH-
99-164 (intense)	ring carbons		

irradiation of the polymers in solid state are methane and ethane, and the time evolution characteristics are shown in Figure 3.31. The data qualitatively resemble those obtained for a number of polymers in that after an initial linear period the rates fall off.[43,49] Quantum yields for the formation of the gaseous products were determined, the quantum yield for formation of x (Φ_x) being given by the relation:

$$\phi_x = \frac{\textit{Rate of formation of X in the film}}{\textit{Rate of absorption of quanta by film}}$$

$$= \frac{d(X) \; / \; dt}{I_o[1 - \exp(-\beta L)]A}$$

where I_o is the incident UV intensity (in quanta s^{-1} per unit area), β is the absorption coefficient (equivalent to ϵc) and L and A are the thickness and area of the film respectively. Since β is small, the quantum yield can be estimated with minimal error as:

$$\phi_X = \frac{d(X) \; / \; dt}{I_o \beta L A}$$

Quantum yields (± 10%) were estimated and are shown in Table 3.17.

6. **Molecular Weight Changes**. The effect of long-wave UV radiation on the molecular weights of PMAP, P34DMAP and P35DMAP (all 6.0 X 10^{-2} M in CH_2Cl_2) can be seen in Figure 3.32 in which S, the number of chain scissions per original

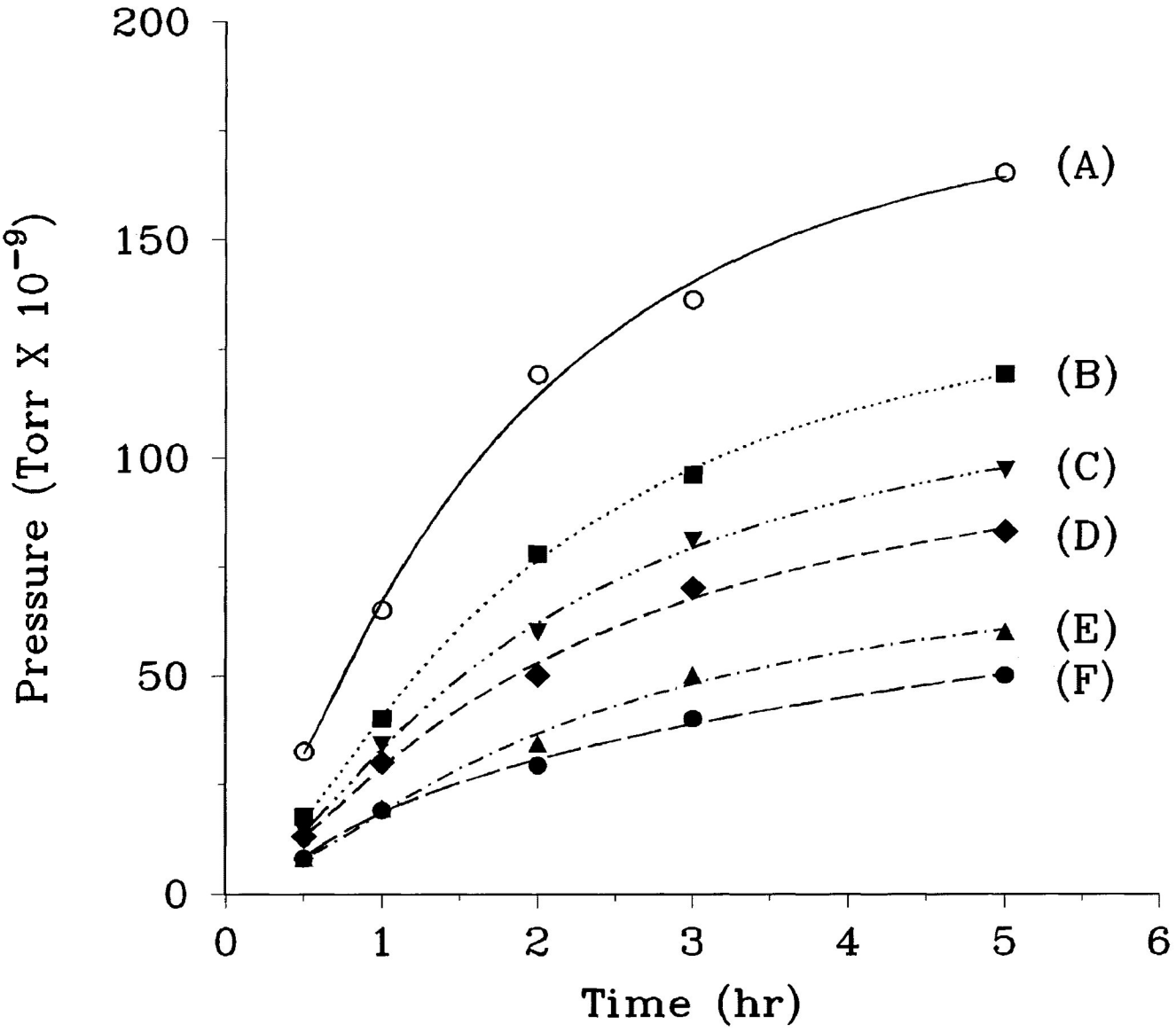

Figure 3.31. Low Molecular Weight Product Evolution as a Function of Time of Irradiation ($\lambda \geq 300$ nm, vacuum).

(A) C_2H_6 from P35DMAP

(B) CH_4 from P35DMAP

(C) C_2H_6 from P34DMAP

(D) CH_4 from P34DMAP

(E) C_2H_6 from PMAP

(F) CH_4 from PMAP

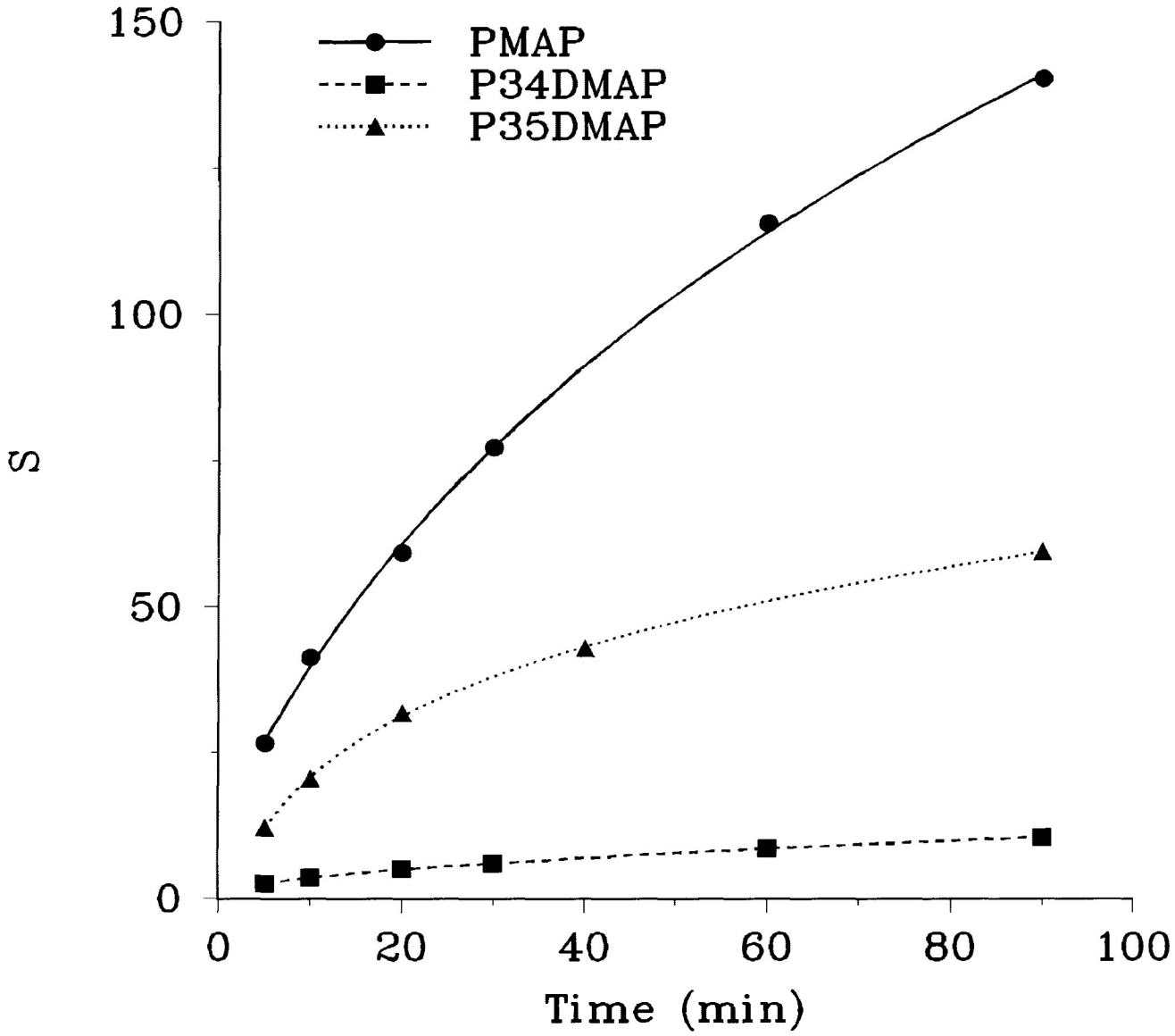

Figure 3.32. Number of Chain Scissions Per Molecule (S) as a Function of Irradiation Time ($\lambda \geq 300$ nm, vacuum).
Polymer Concentration = 6.0×10^{-2} M in CH_2Cl_2.

TABLE 3.17

Quantum Yields for Gaseous Product Formation from Polymer Films Upon Irradiation ($\lambda \geq 300$ nm, vacuum)

POLYMER	ΦCH_4 (± 10%) **mol(Einstein)$^{-1}$**	ΦC_2H_6 (± 10%) **mol(Einstein)$^{-1}$**
PMAP	2.0×10^{-4}	2.3×10^{-4}
P34DMAP	3.8×10^{-4}	4.4×10^{-4}
P35DMAP	4.3×10^{-4}	6.4×10^{-4}

molecule, is plotted as a function of irradiation time, t. The results indicate that random chain scission occurs in the early stages of the photolysis, but on prolonged exposure competing reactions, such as crosslinking, can play a more significant role. It can also be seen that the incorporation of a second OCH_3 group into the ring reduces the rate of chain scission, P34DMAP being relatively stable. That these polymers were undergoing photodecomposition in solution into lower molecular weight fragments was demonstrated by GPC and this is shown in Figure 3.33 (PMAP), Figure 3.34 (P34DMAP) and Figure 3.35 (P35DMAP). It can be seen that new lower molecular weight fragments appear with PMAP (Figure 3.33) and P34DMAP (Figure 3.34) after increasing times of irradiation; furthermore, their molecular weight distributions became narrower with prolonged exposure. However, more high molecular weight material is formed from P35DMAP upon longer irradiation times, and this is reflected by a broadened molecular weight

distribution (Figure 3.35).

The quantum yield for chain scission, Φ_{CS}, is given by the relation:[2]

$$\phi_{cs} = \frac{n}{I_A t}$$

where n is the number of moles of chain scissions in time, t, and I_A is the number of einsteins of photons absorbed by the polymer solution in unit time. In addition, n is related to the molecular weights by:[16]

$$n = \frac{w}{(\bar{M}_n)_o}\left\{\frac{(\bar{M}_n)_o}{(\bar{M}_n)_t} - 1\right\}$$

in which w is the mass of polymer undergoing photolysis. I_A is related to the incident intensity, I_o, as:

$$I_A = I_o\{1 - \exp-(\epsilon c l)\}$$

where ϵ is the molar absorption coefficient, c is the (molar) concentration and l is the effective path length of the solution. As a result, the overall expression for Φ_{CS} is related to the experimentally determined quantities as:

$$\phi_{cs} = \frac{w\{(\bar{M}_n)_o / (\bar{M}_n)_t - 1\}}{(\bar{M}_n)_o I_o\{1 - \exp-(\epsilon c l)\}t}$$

Quantum yields for chain scission were determined from the linear portions of the S versus t plots and are summarized in Table 3.18. It appears that chain scission is less probable in the dimethoxy-substituted polymers.

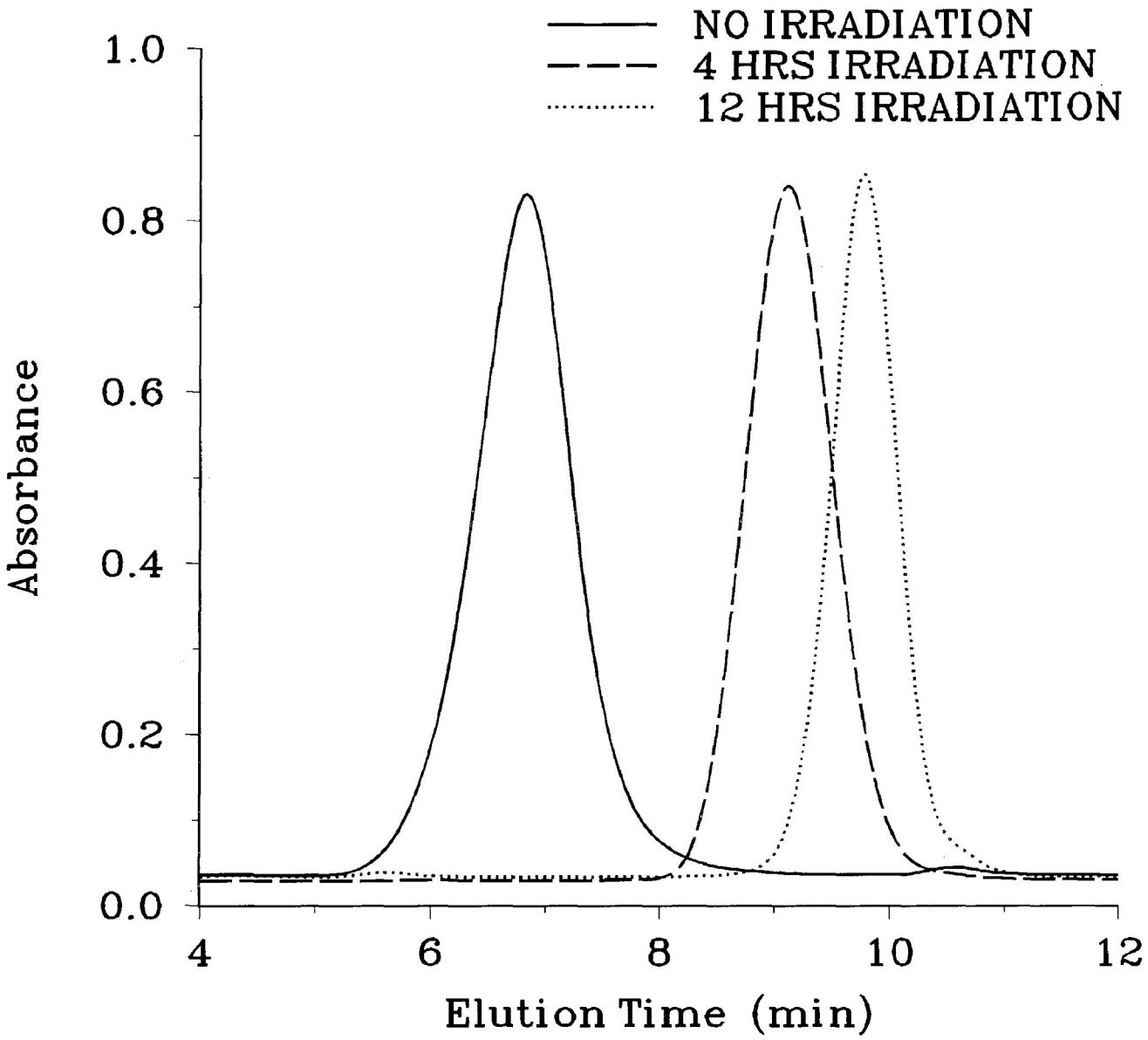

Figure 3.33. Gel Permeation Chromatograph* of PMAP Following Irradiation ($\lambda \geq 300$ nm, vacuum) in Solution (6.0×10^{-2} M in CH_2Cl_2).

* Run With CH_2Cl_2 Through Ultrastyragel® Linear Column (7 μm pore) at 1.0 cm^3 min^{-1}.

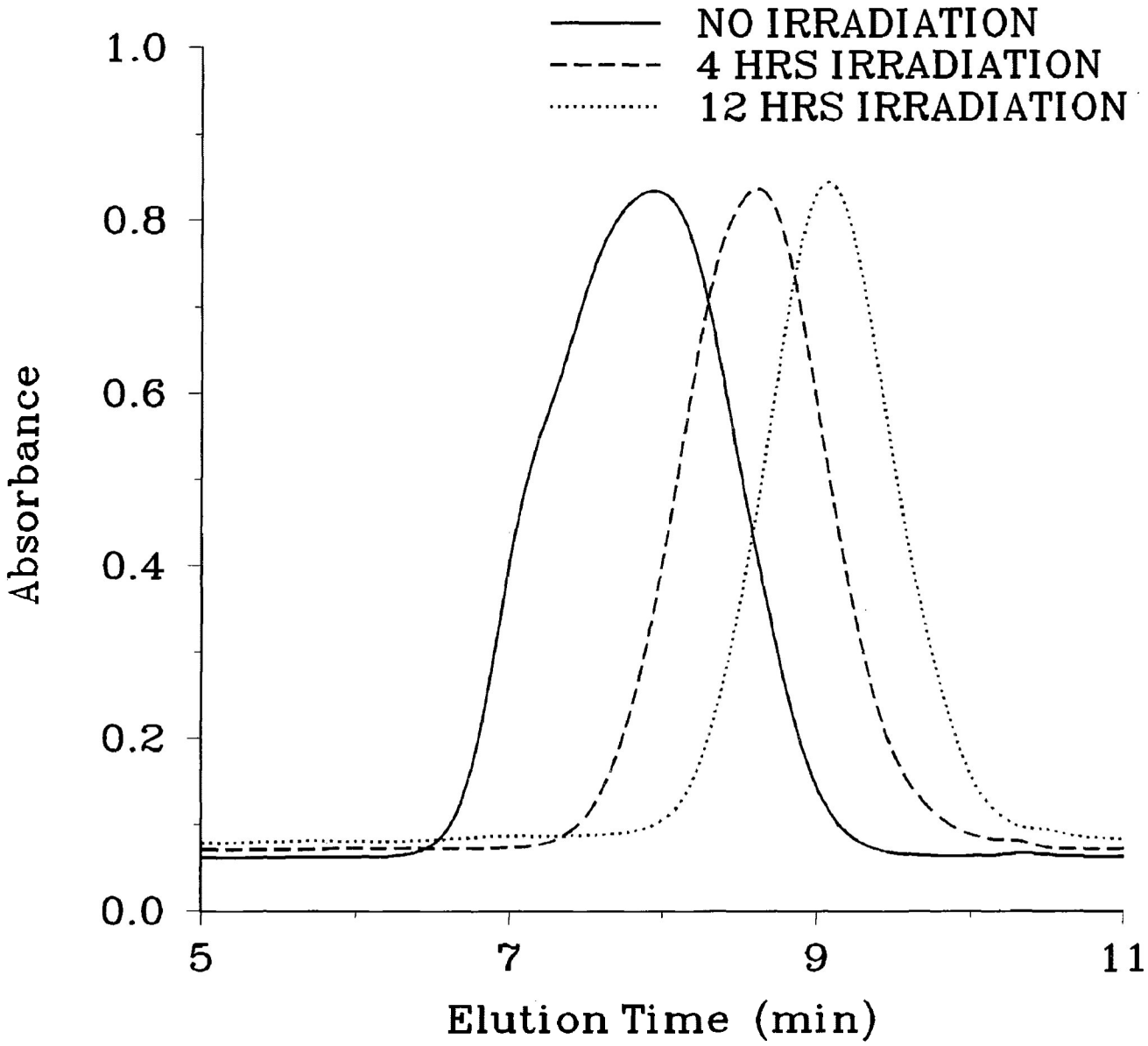

Figure 3.34. GPC Data for P34DMAP Solution (6.0×10^{-2} M in CH_2Cl_2) Before and After Irradiation. (Same Conditions as in Figure 3.33).

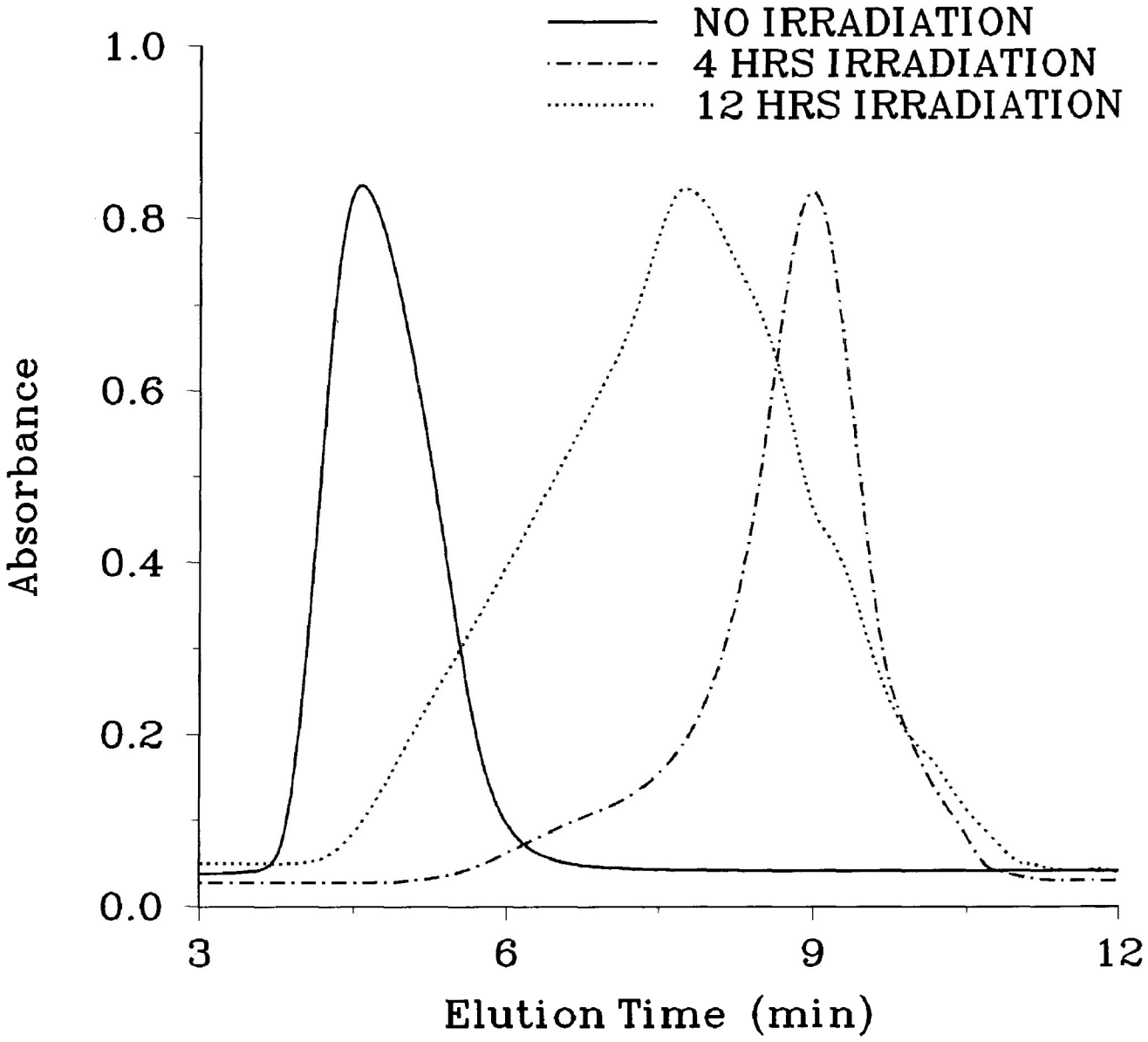

Figure 3.35. GPC Data for P35DMAP Solution (6.0×10^{-2} M in CH_2Cl_2) Before and After Irradiation. (Same Conditions as in Figure 3.33).

TABLE 3.18

Quantum Yields for Chain Scission (Irradiation: $\lambda \geq 300$ nm, vacuum) of Polymer Solution (6.0×10^{-2} M in CH_2Cl_2)

POLYMER	Φ_{CS} (± 10%) mol(Einstein)$^{-1}$
PMAP	10^{-1}
P34DMAP	1.1×10^{-4}
P35DMAP	1.0×10^{-4}

The effects of well known triplet quenchers (naphthalene and *cis*-1,3-pentadiene) on chain scission are shown in Figures 3.36-3.37 (PMAP), Figures 3.38-3.39 (P34DMAP) and Figures 3.40-3.41 (P35DMAP). While the rates of chain scission are reduced significantly for all polymers by both naphthalene and *cis*-1,3-pentadiene, naphthalene appears to be the more efficient quencher (Figures 3.42-3.44). The effects of these triplet quenchers on rates of chain scission are also shown in Figure 3.45 (PMAP), Figure 3.46 (P34DMAP) and Figure 3.47 (P35DMAP) in which the ratios of quantum yields for chain scission (Φ_o/Φ) are shown as functions of quencher concentration. It can be seen that all sets of data conform well to the Stern-Volmer equation:

$$\frac{\phi_o}{\phi} = 1 + K_{SV}[Q]$$

in which K_{SV} is the Stern-Volmer constant, [Q] is the quencher concentration, Φ_o is the quantum yield for chain scission in

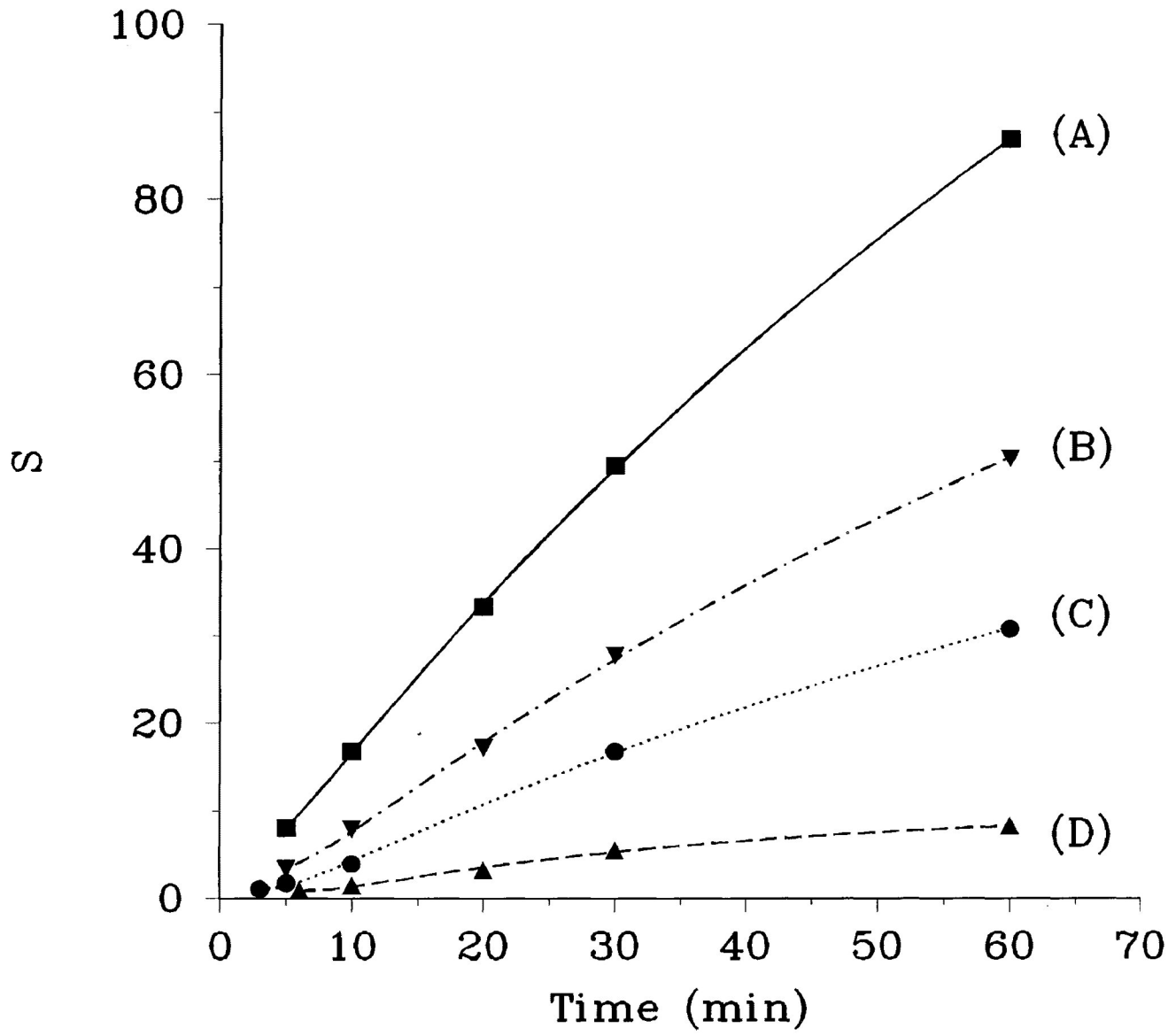

Figure 3.36. Number of Chain Scissions Per Molecule (S) as a Function of Irradiation Time ($\lambda \geq 300$ nm, vacuum).
PMAP Concentration = 6.0×10^{-2} M in CH_2Cl_2.
(A) Pure PMAP
(B) + 5.5×10^{-4} M Naphthalene
(C) + 1.5×10^{-3} M Naphthalene
(D) + 4.7×10^{-3} M Naphthalene

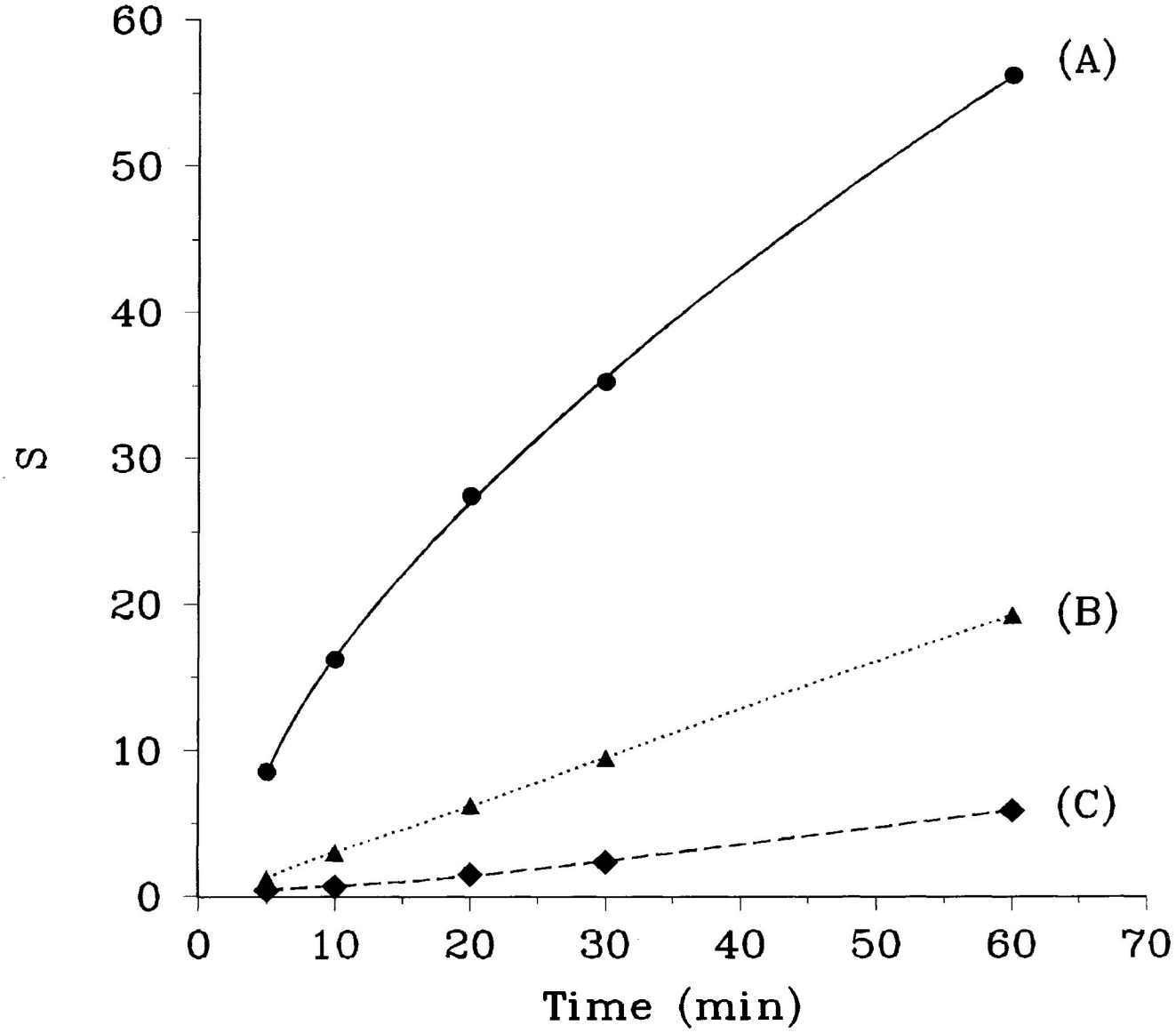

Figure 3.37. Chain Scission Data for PMAP in the Presence of *cis*–1,3–Pentadiene. (Same Conditions as in Figure 3.36).
(A) Pure PMAP
(B) + 9.9 X 10^{-3} M *cis*–1,3–pentadiene
(C) + 2.0 X 10^{-2} M *cis*–1,3–pentadiene

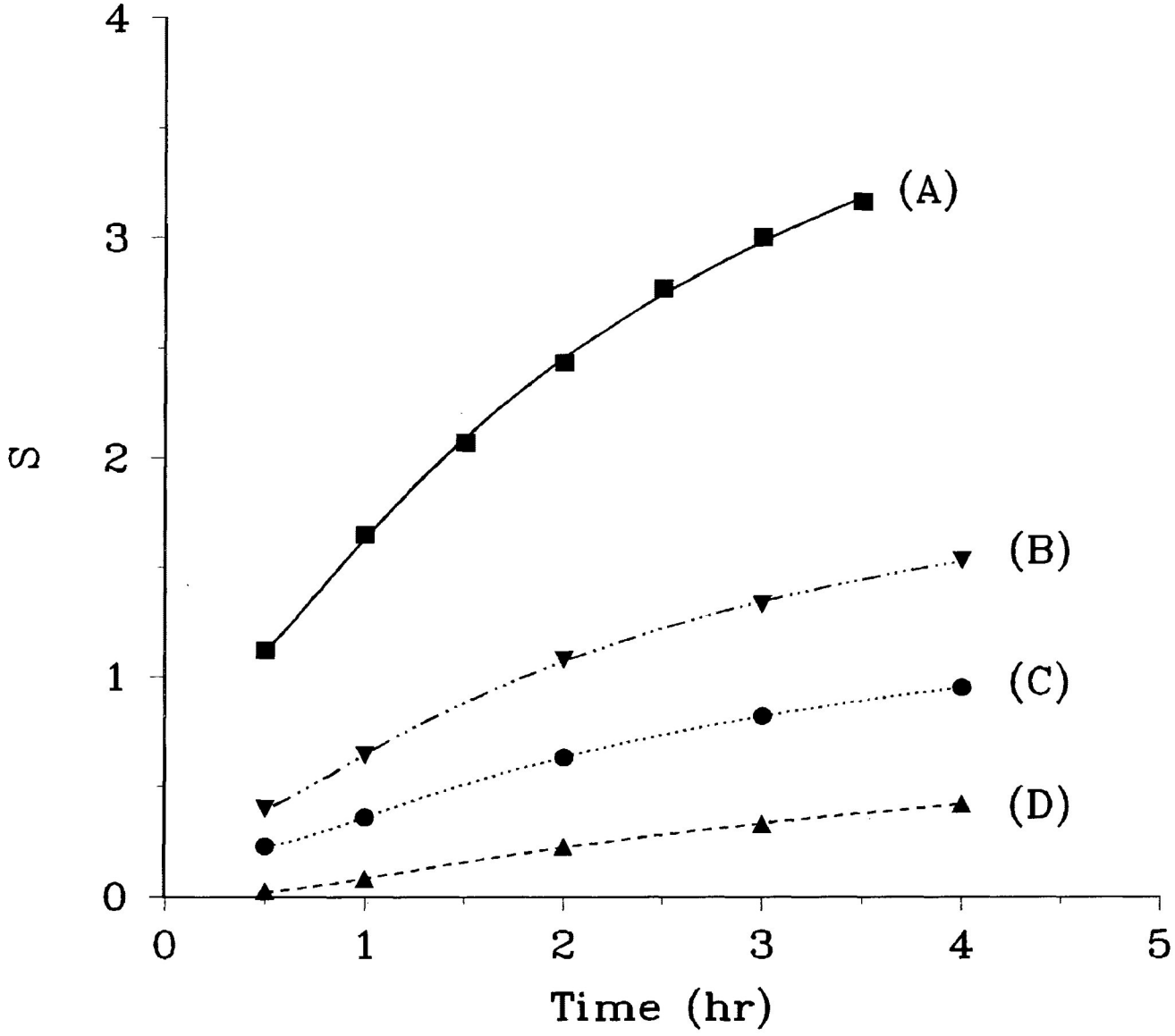

Figure 3.38. Chain Scission Data for P34DMAP in the Presence of Naphthalene. (Same Conditions as in Figure 3.36).
(A) Pure P34DMAP
(B) + 3.1 X 10^{-4} M Naphthalene
(C) + 7.8 X 10^{-4} M Naphthalene
(D) + 4.2 X 10^{-3} M Naphthalene

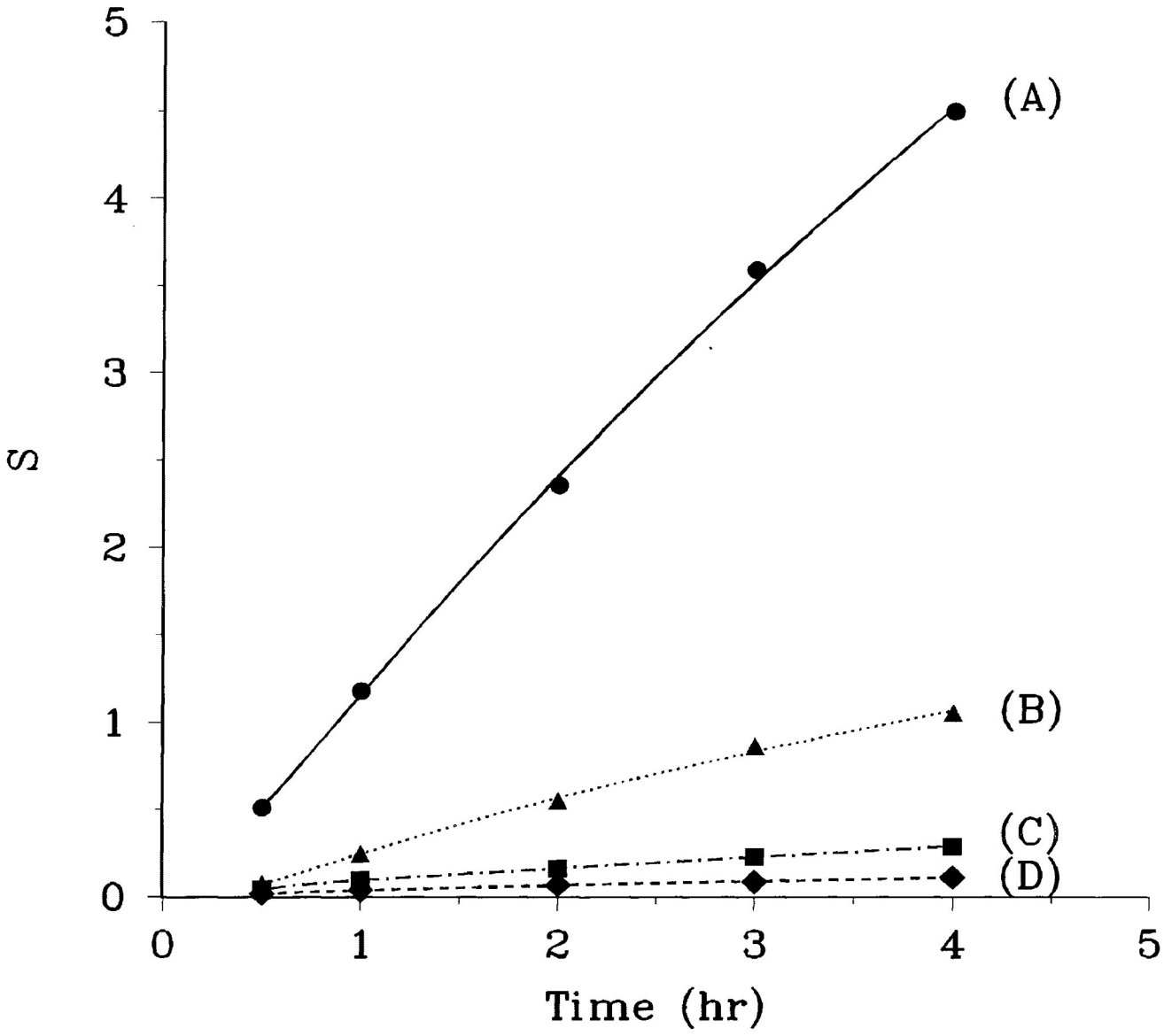

Figure 3.39. Chain Scission Data for P34DMAP in the Presence of *cis*−1,3−Pentadiene. (Same Conditions as in Figure 3.36).
(A) Pure P34DMAP
(B) + 5.0×10^{-3} M *cis*−1,3−pentadiene
(C) + 9.9×10^{-3} M *cis*−1,3−pentadiene
(D) + 2.5×10^{-2} M *cis*−1,3−pentadiene

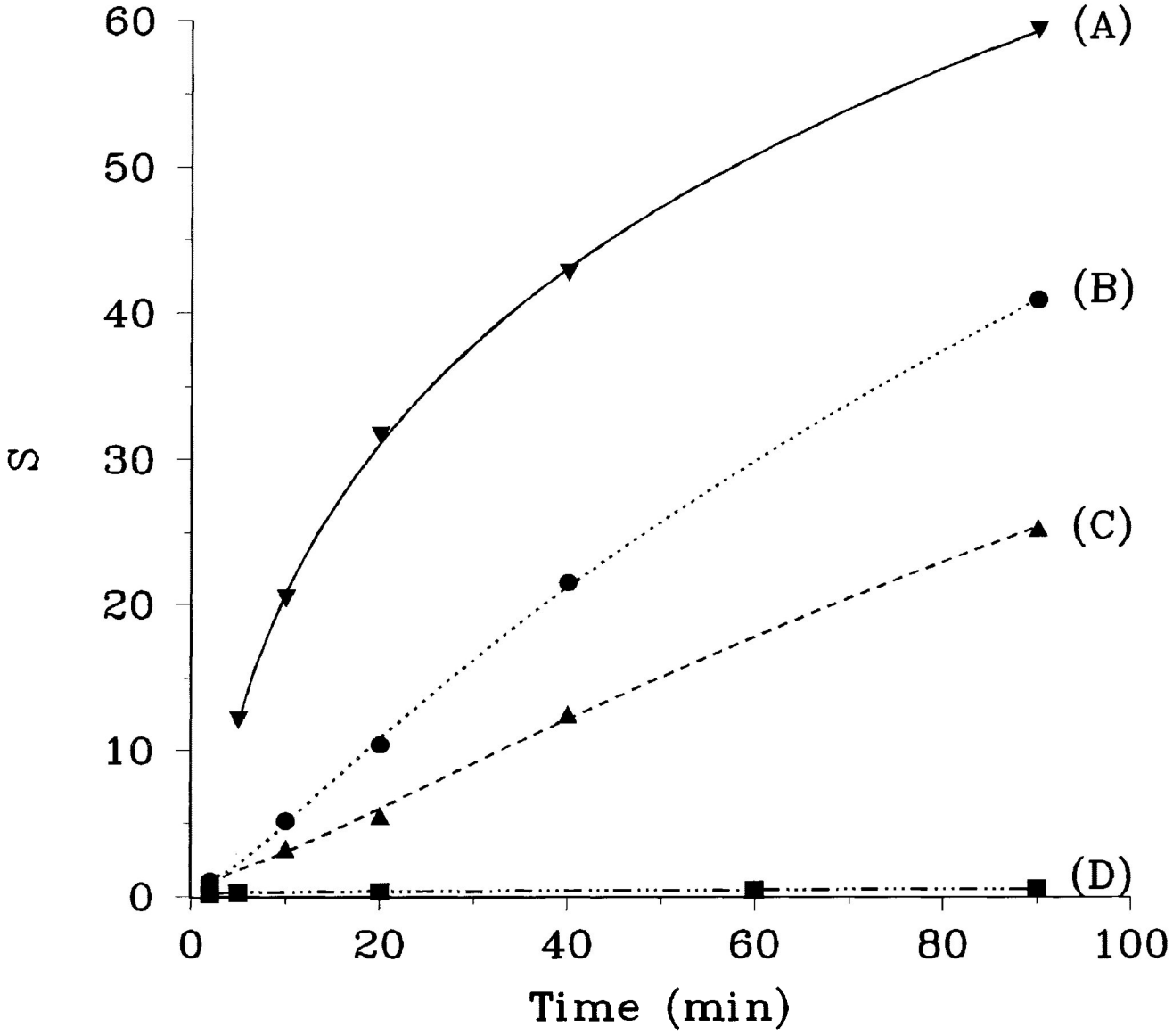

Figure 3.40. Chain Scission Data for P35DMAP in the Presence of Naphthalene. (Same Conditions as in Figure 3.36).
(A) Pure P35DMAP
(B) + 3.9×10^{-4} M Naphthalene
(C) + 6.6×10^{-4} M Naphthalene
(D) + 1.8×10^{-3} M Naphthalene

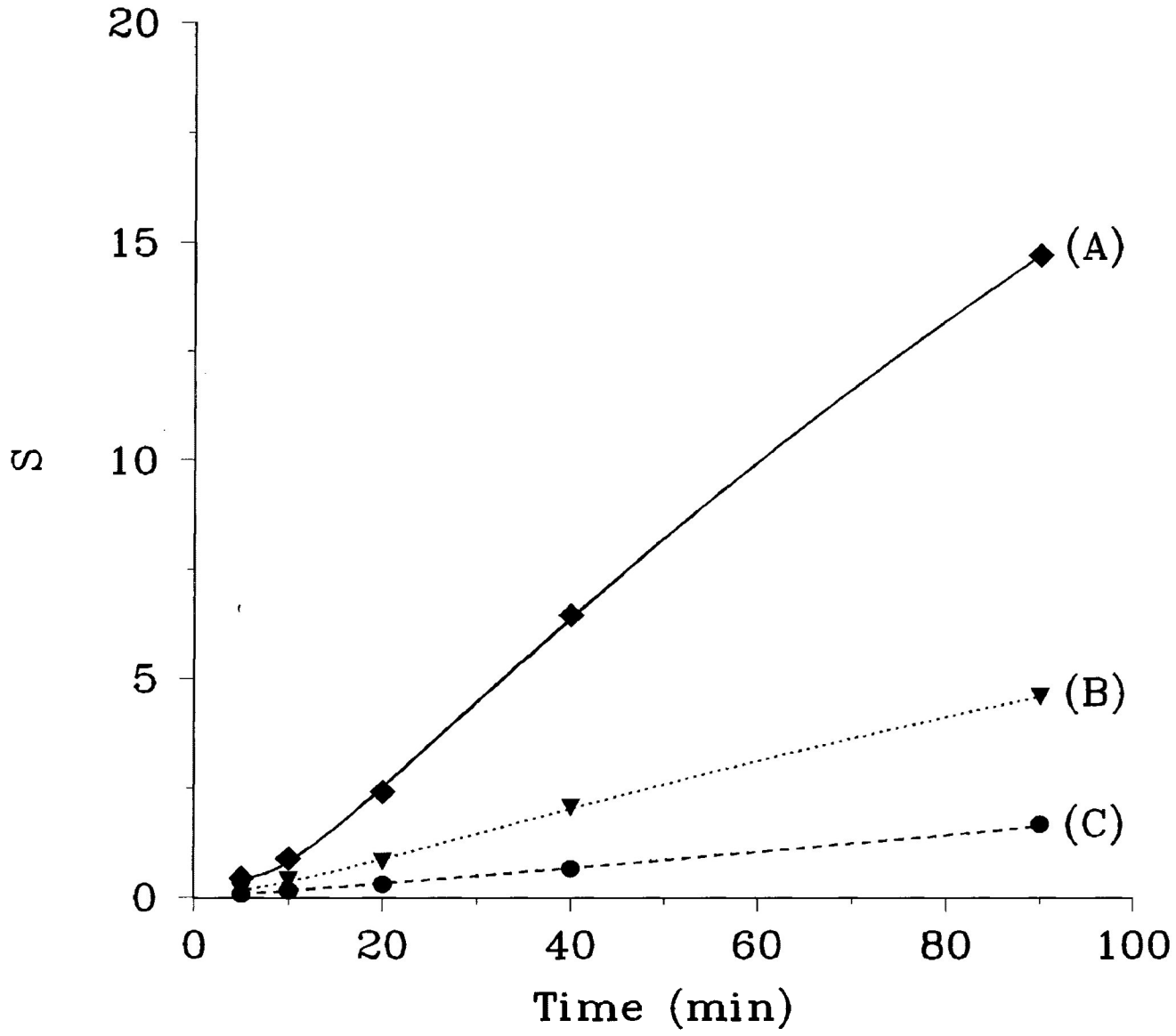

Figure 3.41. Chain Scission Data for P35DMAP in the Presence of *cis*–1,3–Pentadiene. (Same Conditions as in Figure 3.36).
(A) Pure P35DMAP
(B) + 5.0 X 10^{-3} M *cis*–1,3–pentadiene
(C) + 9.9 X 10^{-3} M *cis*–1,3–pentadiene

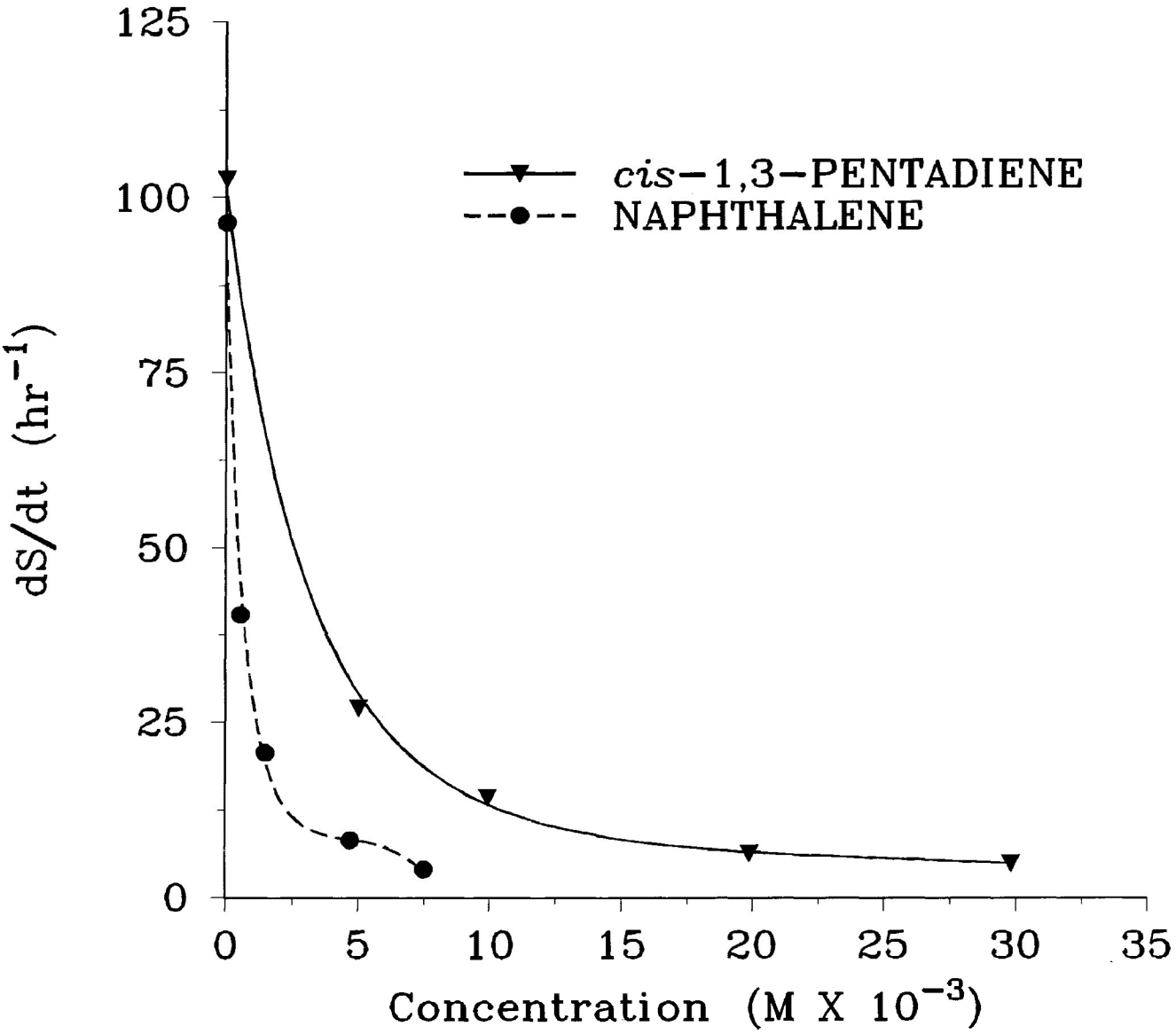

Figure 3.42. Rate of Chain Scission of PMAP (i.e. Number of Chain Scissions Per Hour) as a Function of Quencher Concentration. (Irradiation: $\lambda \geq 300$ nm, vacuum).

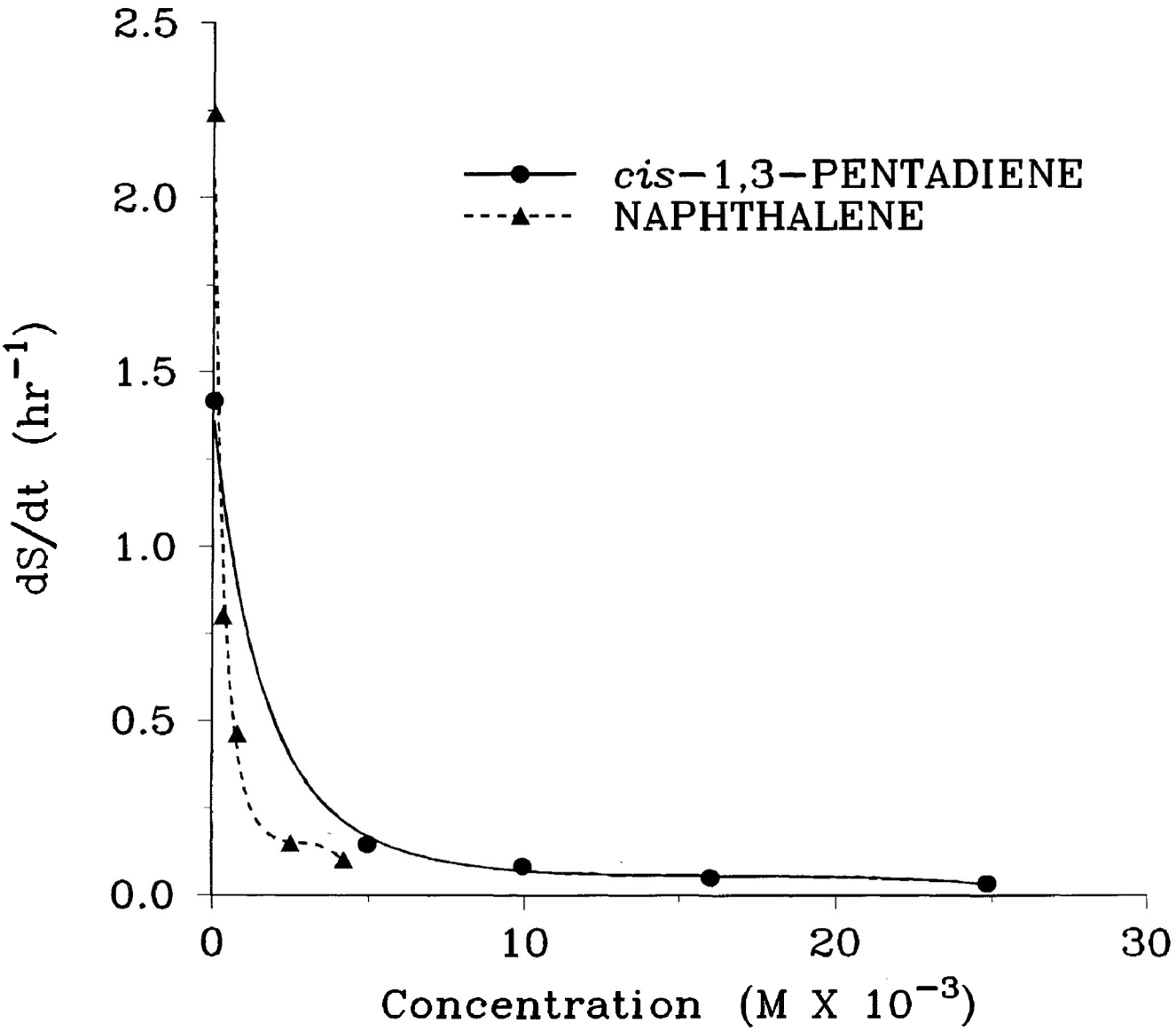

Figure 3.43. Rate of Chain Scission of P34DMAP as a Function of Quencher Concentration.
(Irradiation: $\lambda \geq 300$ nm, vacuum).

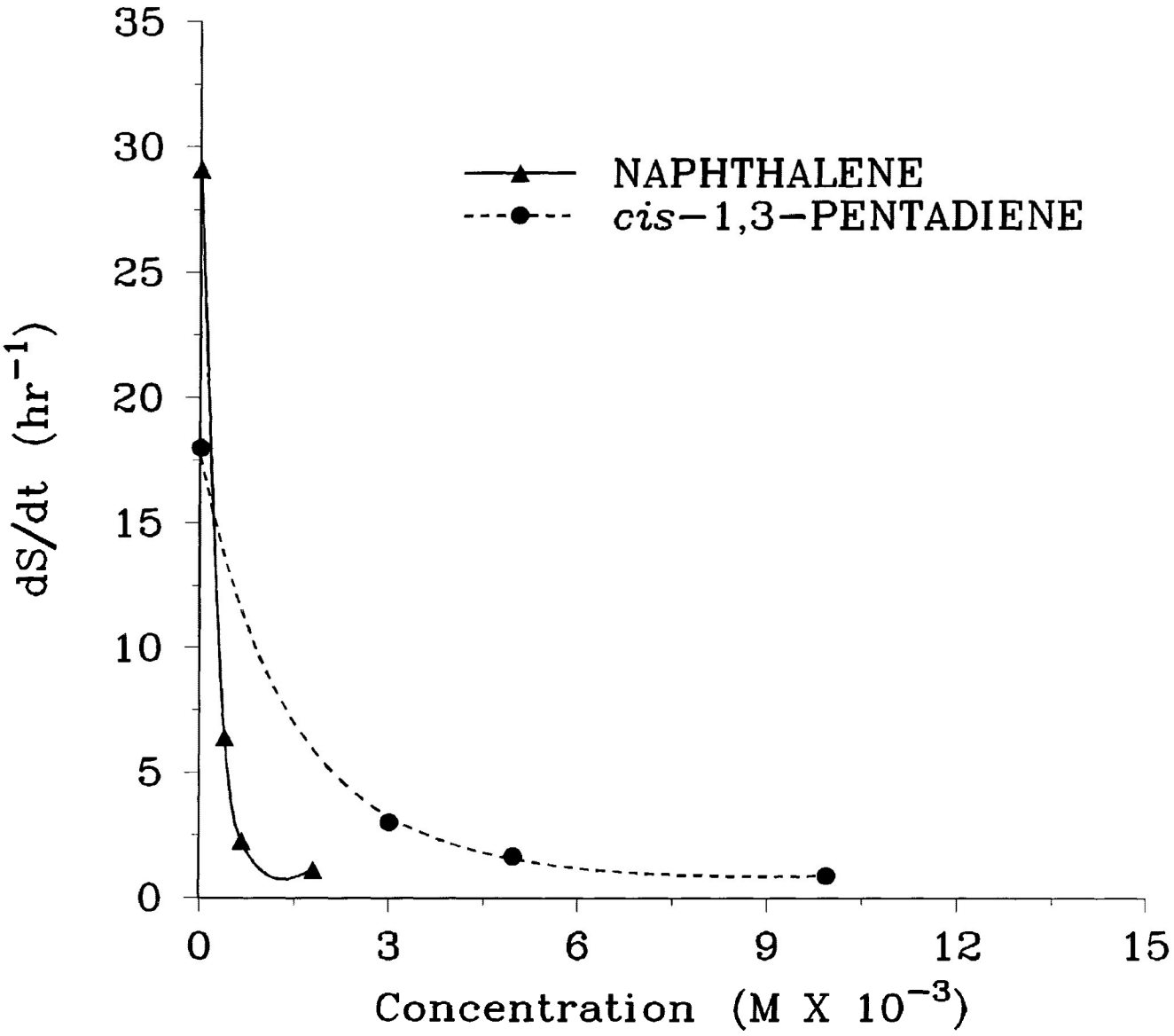

Figure 3.44. Rate of Chain Scission of P35DMAP as a Function of Quencher Concentration. (Irradiation: $\lambda \geq 300$ nm, vacuum).

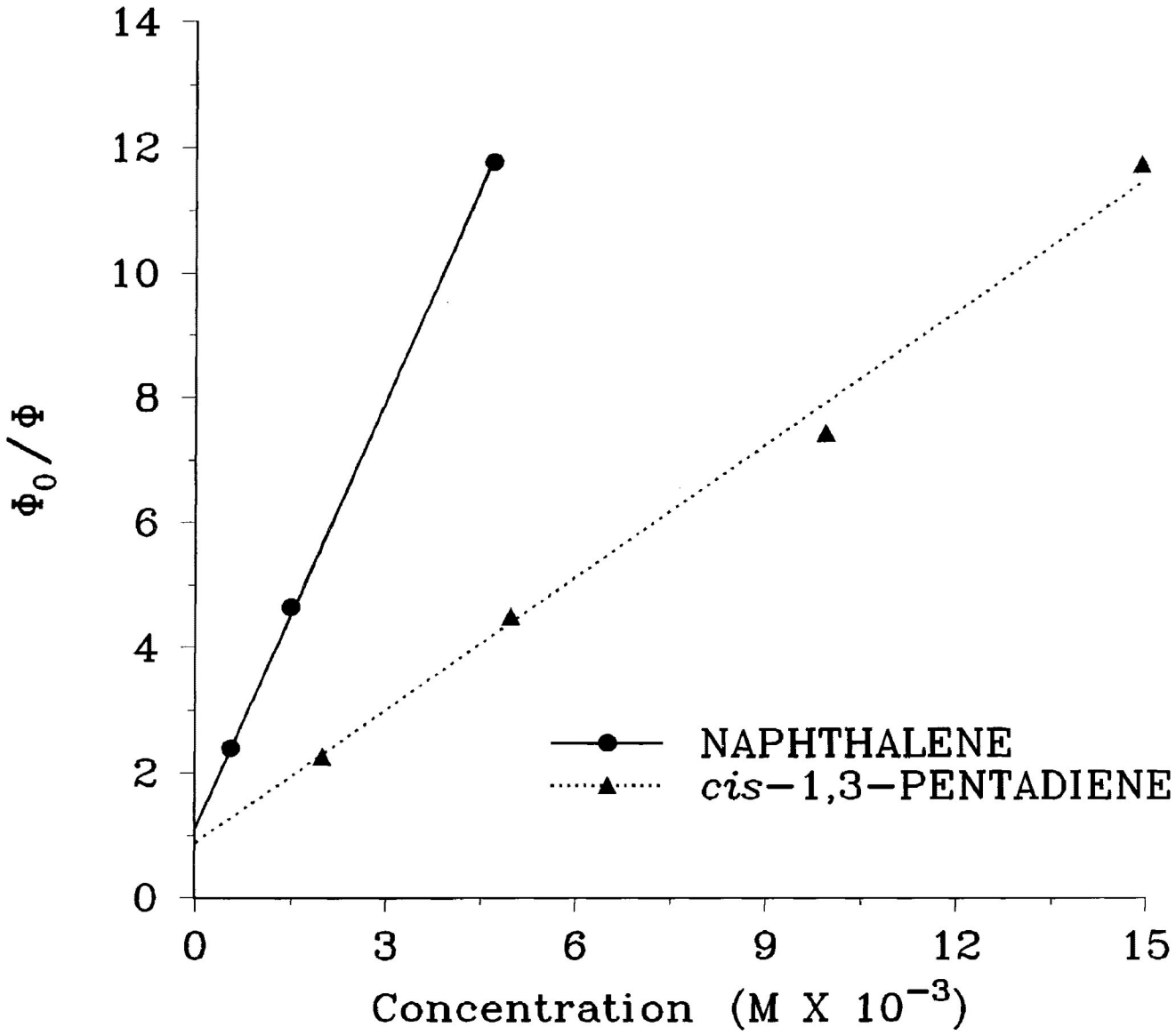

Figure 3.45. Stern−Volmer Plots for Quenching of PMAP Triplet.

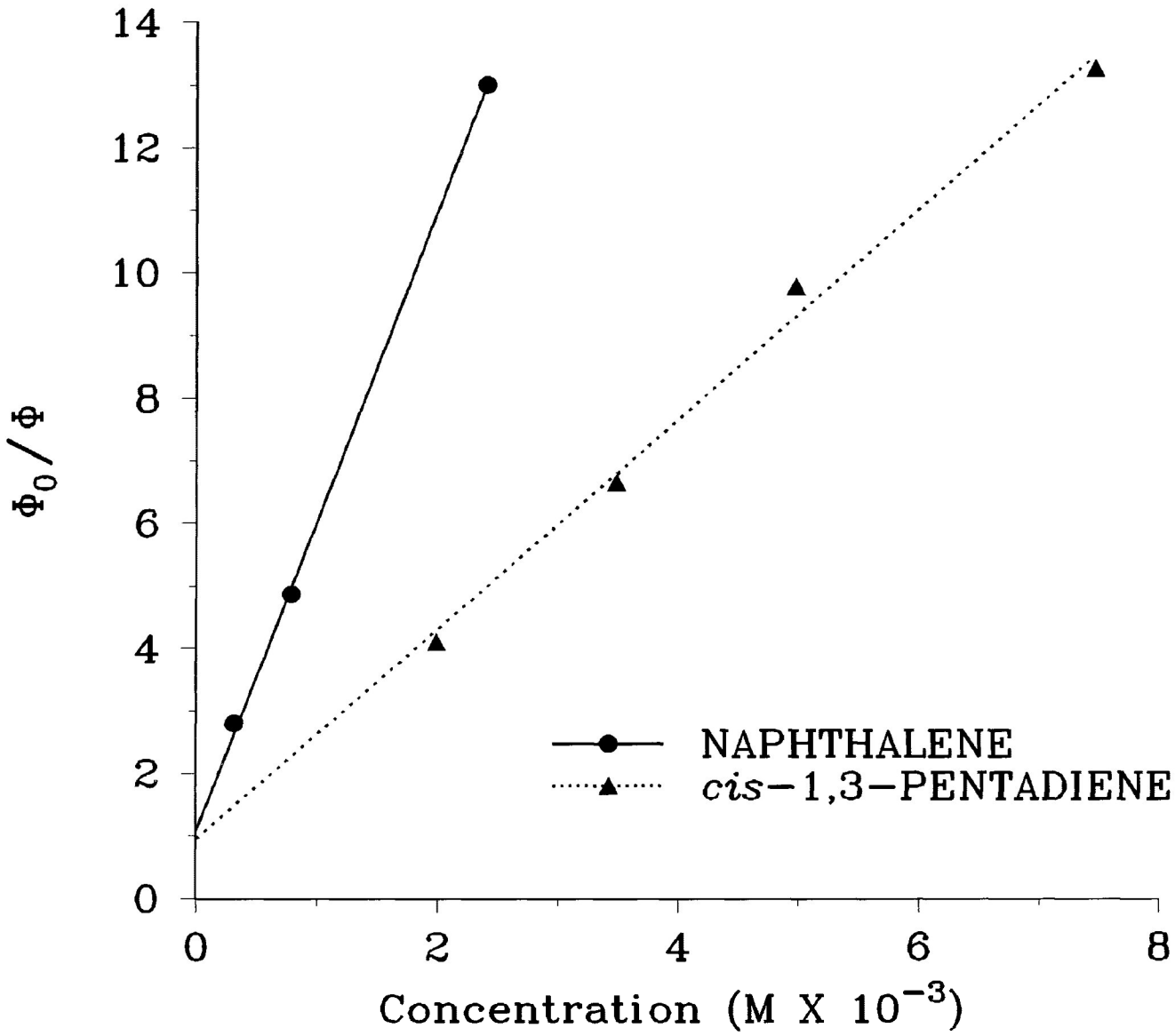

Figure 3.46. Stern–Volmer Plots for Quenching of P34DMAP Triplet.

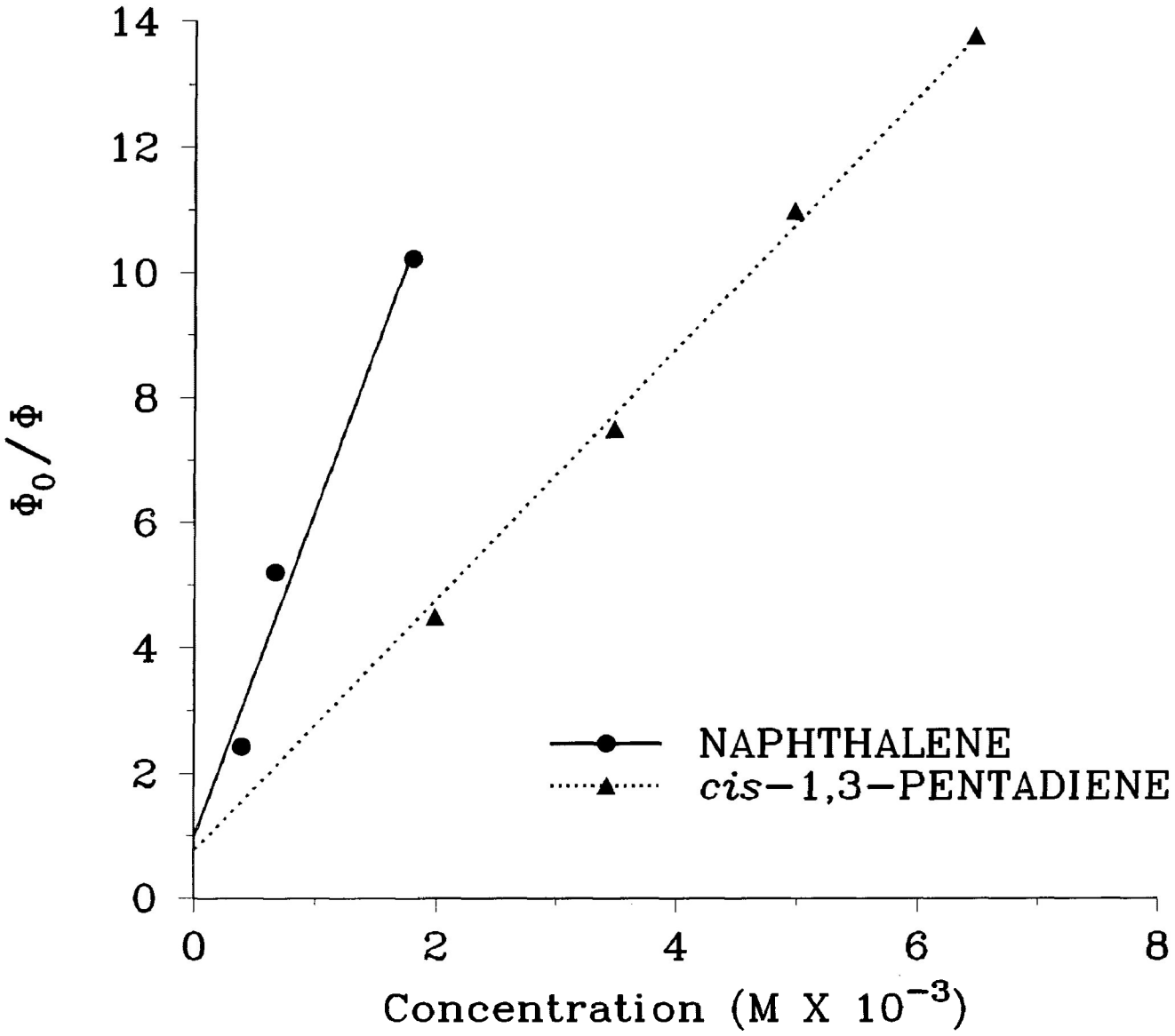

Figure 3.47. Stern–Volmer Plots for Quenching of P35DMAP Triplet.

the absence of a quencher and Φ is the quantum yield for chain scission in the presence of a quencher. The slopes of the Stern-Volmer, i.e. K_{SV}, plots were determined and are summarized below in Table 3.19.

TABLE 3.19

Quenching Constants for the Photolysis (λ ≥ 300 nm, vacuum) of Carbonyl Polymers in Solution (6.0 X 10^{-2} M in CH_2Cl_2)

POLYMER	K_{SV} (dm^3 mol^{-1})	
	NAPHTHALENE	*cis*-1,3-Pentadiene
PMAP	2300 ± 2%	710 ± 4%
P34DMAP	4950 ± 2%	1680 ± 4%
P35DMAP	5200 ± 10%	2000 ± 4%

The inhibiting effects of naphthalene and *cis*-1,3-pentadiene on the triplet states of the polyketones in solution are also demonstrated by GPC data which are shown in Figure 3.48 (PMAP), Figure 3.49 (P34DMAP) and Figure 3.50 (P35DMAP). It can be seen that both naphthalene and *cis*-1,3-pentadiene reduce the rate of photodecomposition, the curves being displaced to shorter elution times (*cf* irradiation of polymer without quencher (Figures 3.33-3.35)), and naphthalene appears to be the more effective triplet quencher.

The effect of polymer concentration on chain scission is shown in Figure 3.51 (PMAP), Figure 3.52 (P34DMAP) and Figure 3.53 (P35DMAP). In all cases, the rates of chain

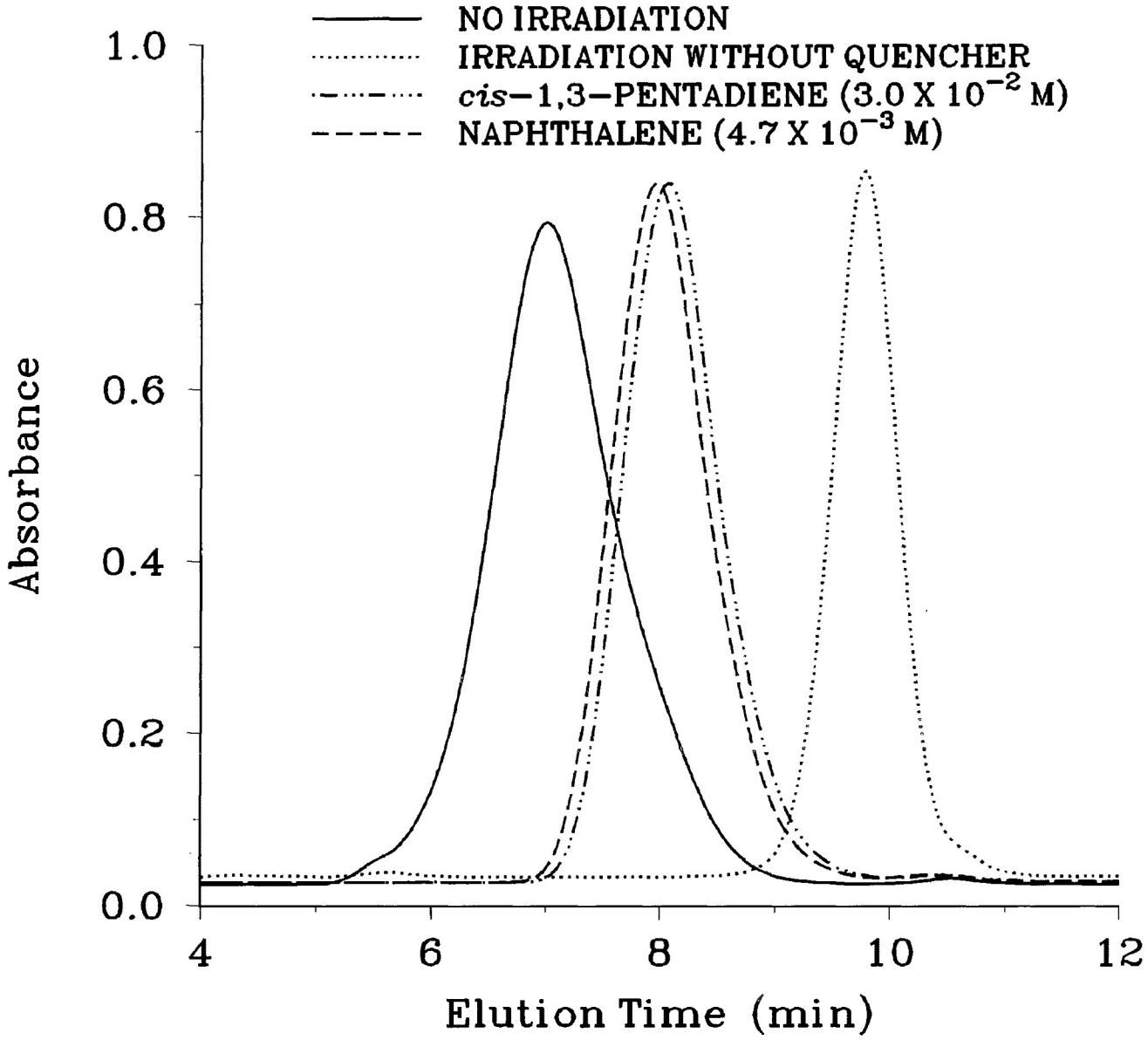

Figure 3.48. GPC Data for PMAP Solution (6.0 X 10^{-2} M in CH_2Cl_2) Before and After Irradiation in the Presence of Triplet Quenchers. (Same Conditions as in Figure 3.33).

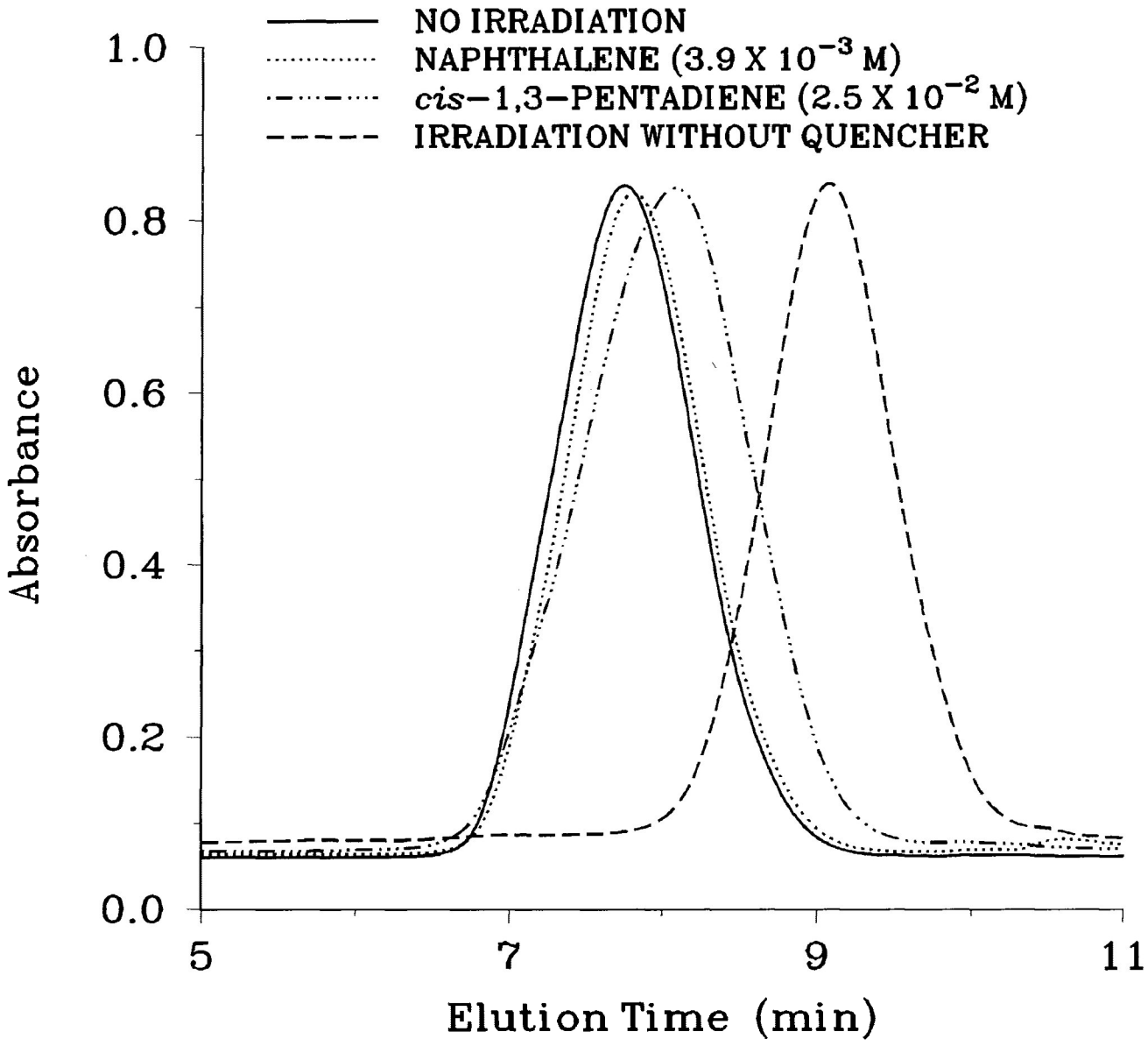

Figure 3.49. GPC Data for P34DMAP Solution (6.0 X 10^{-2} M in CH_2Cl_2) Before and After Irradiation in the Presence of Triplet Quenchers. (Same Conditions as in Figure 3.33).

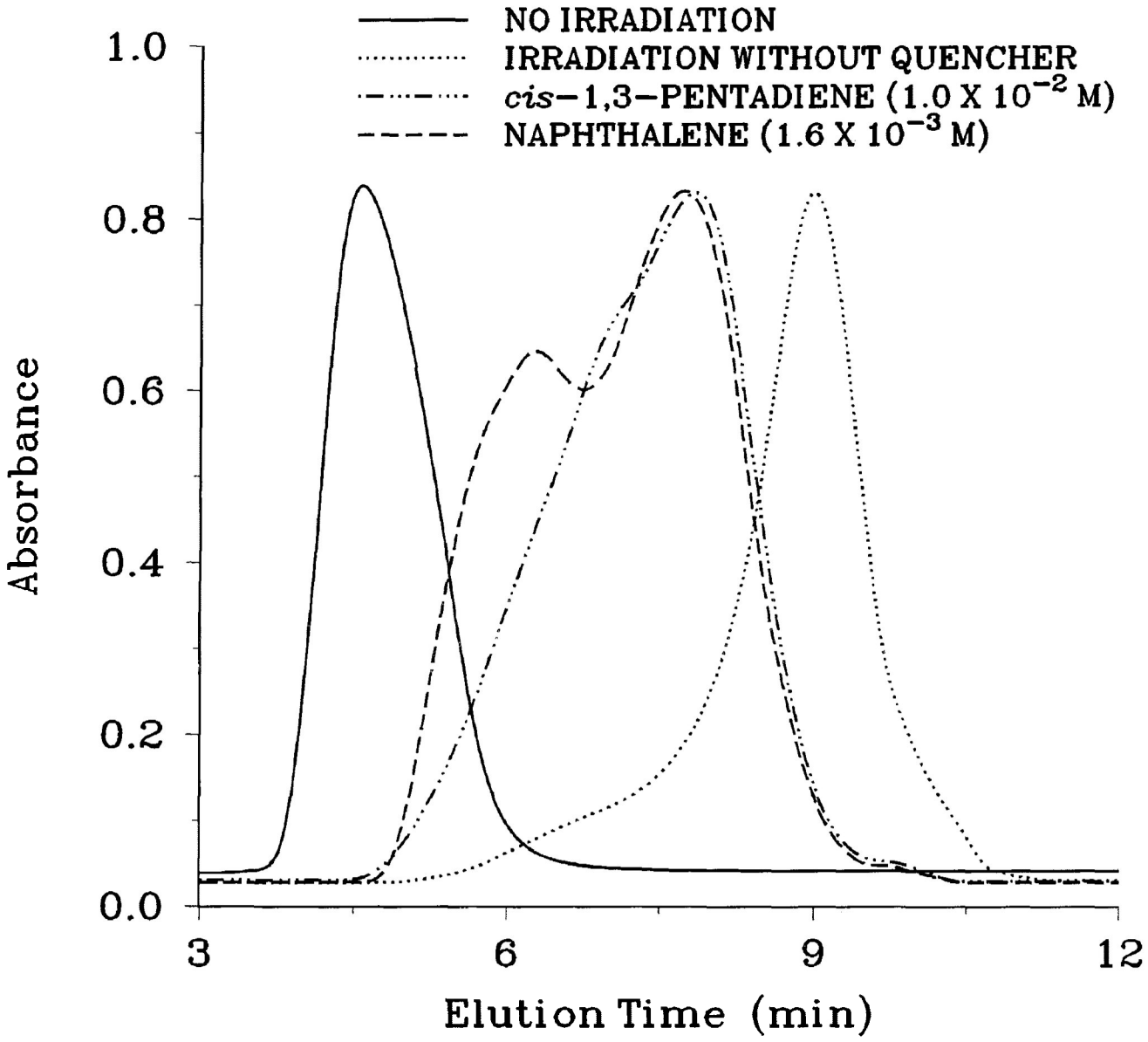

Figure 3.50. GPC Data for P35DMAP Solution (6.0 X 10^{-2} M in CH_2Cl_2) Before and After Irradiation in the Presence of Triplet Quenchers. (Same Conditions as in Figure 3.33).

scission decrease with increasing polymer concentration. If the rate of chain scission was controlled by bimolecular collisions of the carbonyl triplet (or methyl radical) with the polymer[22], a stronger dependence of the rate of chain scission on polymer concentration would be expected. However, Figures 3.54-3.55 indicate that an inverse relationship exists, and this suggests that chain scission is strongly influenced by other physical factors.

Triplet states of polyketones are also quenched by isopropanol and other good (H-atom) transfer agents, and this has been reflected in molecular weight changes in a number of other polymers.[21,22,50,51] The effects of isopropanol on chain scission are shown in Figure 3.56 (PMAP), Figure 3.57 (P34DMAP) and Figure 3.58 (P35DMAP), and similar effects of cumene are shown in Figure 3.59 (PMAP), Figure 3.60 (P34DMAP) and Figure 3.61 (P35DMAP). It can be seen that both isopropanol and cumene are effective in reducing the rate of chain scission. Cumene is, however, more effective in reducing chain scission in PMAP (Figure 3.68) and P34DMAP (Figure 3.69), and isopropanol is more effective in reducing chain scission in P35DMAP (Figure 3.70). Similar qualitative effects are observed in all the polymers with less reactive transfer agents such as n-butanol (Figures 3.62-3.64) and *tert*-butanol (Figures 3.65-3.67).

On the basis of previous observations of photoreductions of ketones, it has been observed that less reactive transfer

agents are generally less effective in quenching the triplets.[22] However, this is not the case in PMAP (Figure 3.68) and P34DMAP (Figure 3.69). It is apparent that these molecules are playing additional roles to that of transfer agents, the expected linearity between the rate of decrease of chain scission and the concentration of transfer agent not being observed. These results could be attributable to indirect effects such as solvent quality since both hydrocarbons and alcohols are poor solvents for the polymers. The effects of transfer agents on the chain scission process in solution were demonstrated by GPC and are shown in Figure 3.71 (PMAP), Figure 3.72 (P34DMAP) and Figure 3.73 (P35DMAP). All transfer agents, including n-butanol and *tert*-butanol, appear to quench the degradation in solution, the curves being displaced to shorter elution times (*cf* irradiation without H-donor (Figures 3.33-3.35)).

The results of the photoreactions of these polymers in thin films are demonstrated by GPC changes and are shown in Figure 3.74 (PMAP), Figure 3.75 (P34DMAP) and Figure 3.76 (P35DMAP). It can be seen that new higher and lower molecular weight species appear from PMAP (Figure 3.74) and P34DMAP (Figure 3.75), and this is reflected by a broadening of the molecular weight distribution, particularly in P34DMAP. However, the narrower molecular weight distribution (Figure 3.76) indicates that more lower molecular weight material is formed upon irradiation of P35DMAP.

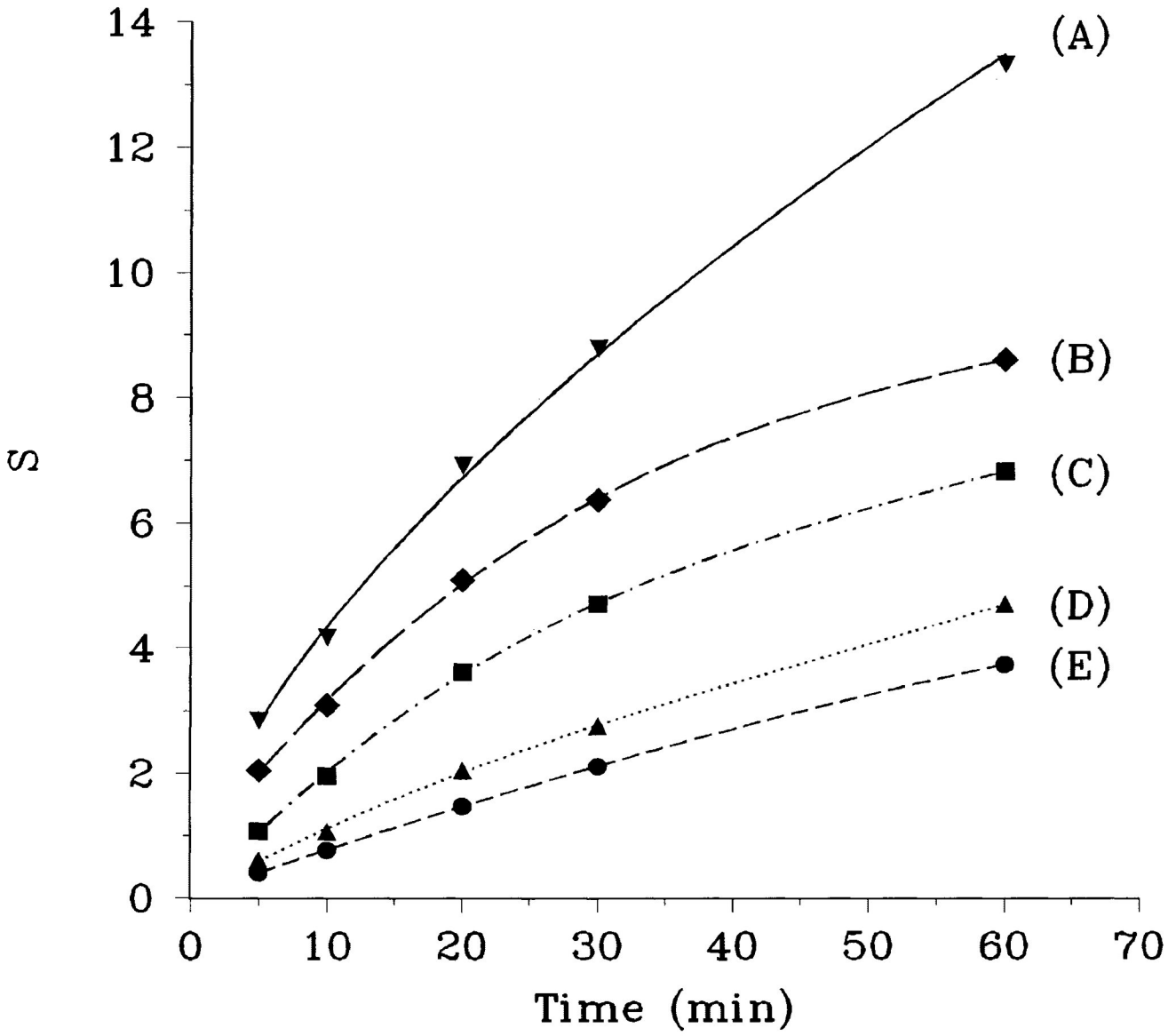

Figure 3.51. Number of Chain Scissions Per Molecule (S) as a Function of Irradiation Time of PMAP ($\lambda \geq 300$ nm, vacuum) in Solution (CH_2Cl_2).
(A) 1.2×10^{-2} M PMAP
(B) 3.1×10^{-2} M PMAP
(C) 6.2×10^{-2} M PMAP
(D) 1.2×10^{-1} M PMAP
(E) 1.8×10^{-1} M PMAP

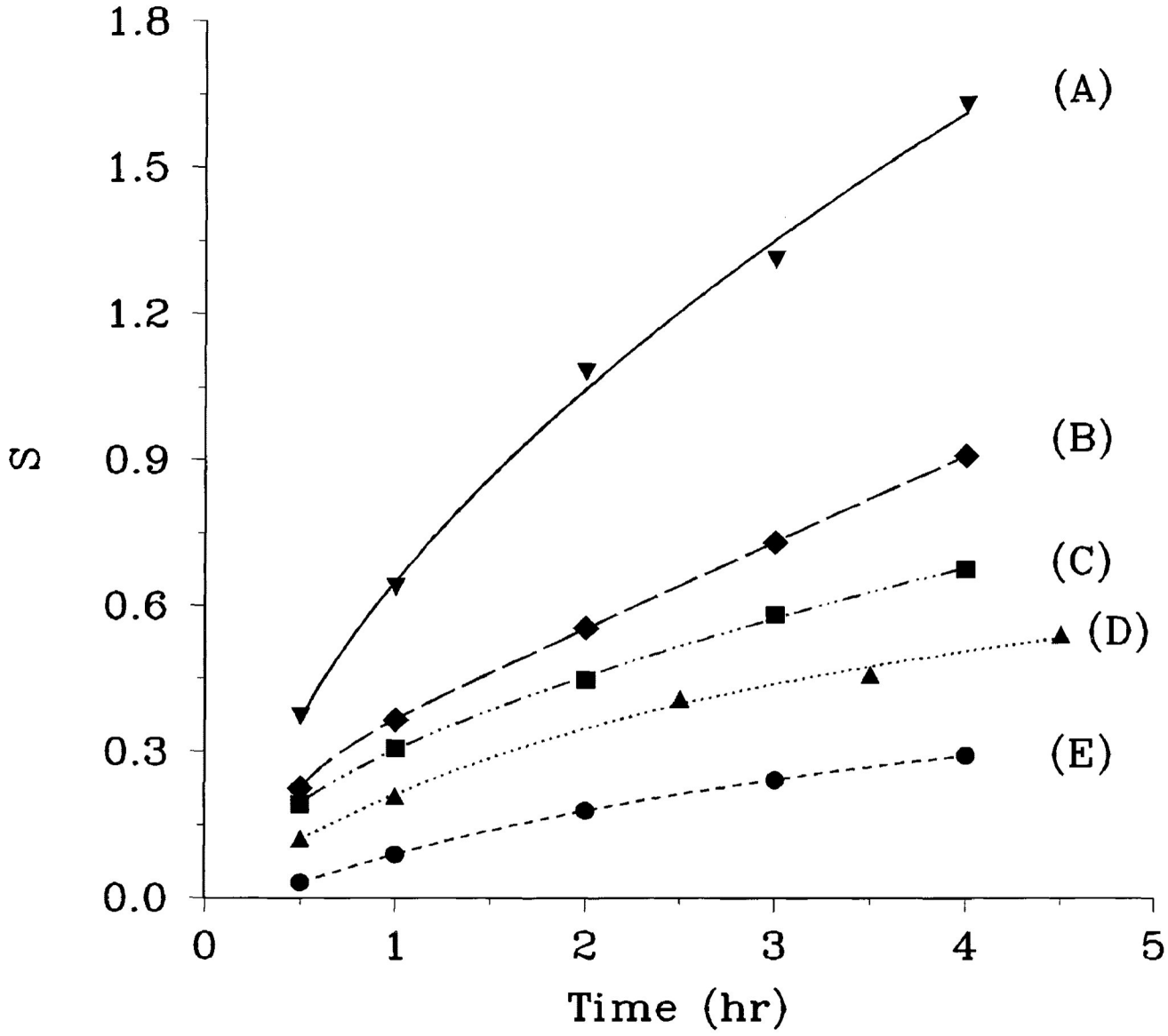

Figure 3.52. Chain Scission Data for P34DMAP in Solution (CH_2Cl_2).
(Same Conditions as in Figure 3.51).
(A) 1.1 X 10^{-2} M P34DMAP
(B) 2.6 X 10^{-2} M P34DMAP
(C) 5.2 X 10^{-2} M P34DMAP
(D) 1.0 X 10^{-1} M P34DMAP
(E) 1.6 X 10^{-1} M P34DMAP

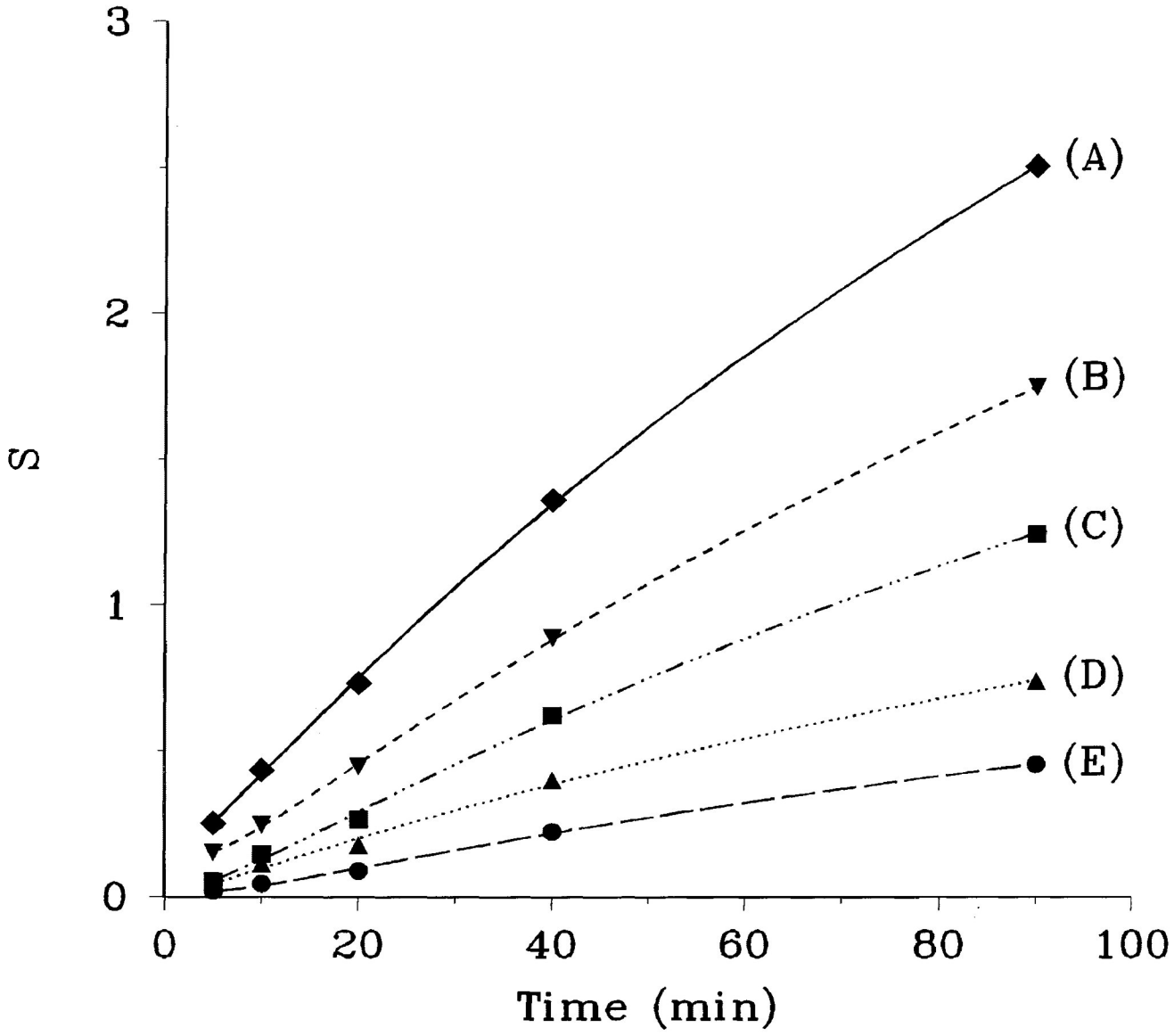

Figure 3.53. Chain Scission Data for P35DMAP in Solution (CH_2Cl_2).
(Same Conditions as in Figure 3.51).
(A) 1.0×10^{-2} M P35DMAP
(B) 1.8×10^{-2} M P35DMAP
(C) 2.6×10^{-2} M P35DMAP
(D) 5.2×10^{-2} M P35DMAP
(E) 1.0×10^{-1} M P35DMAP

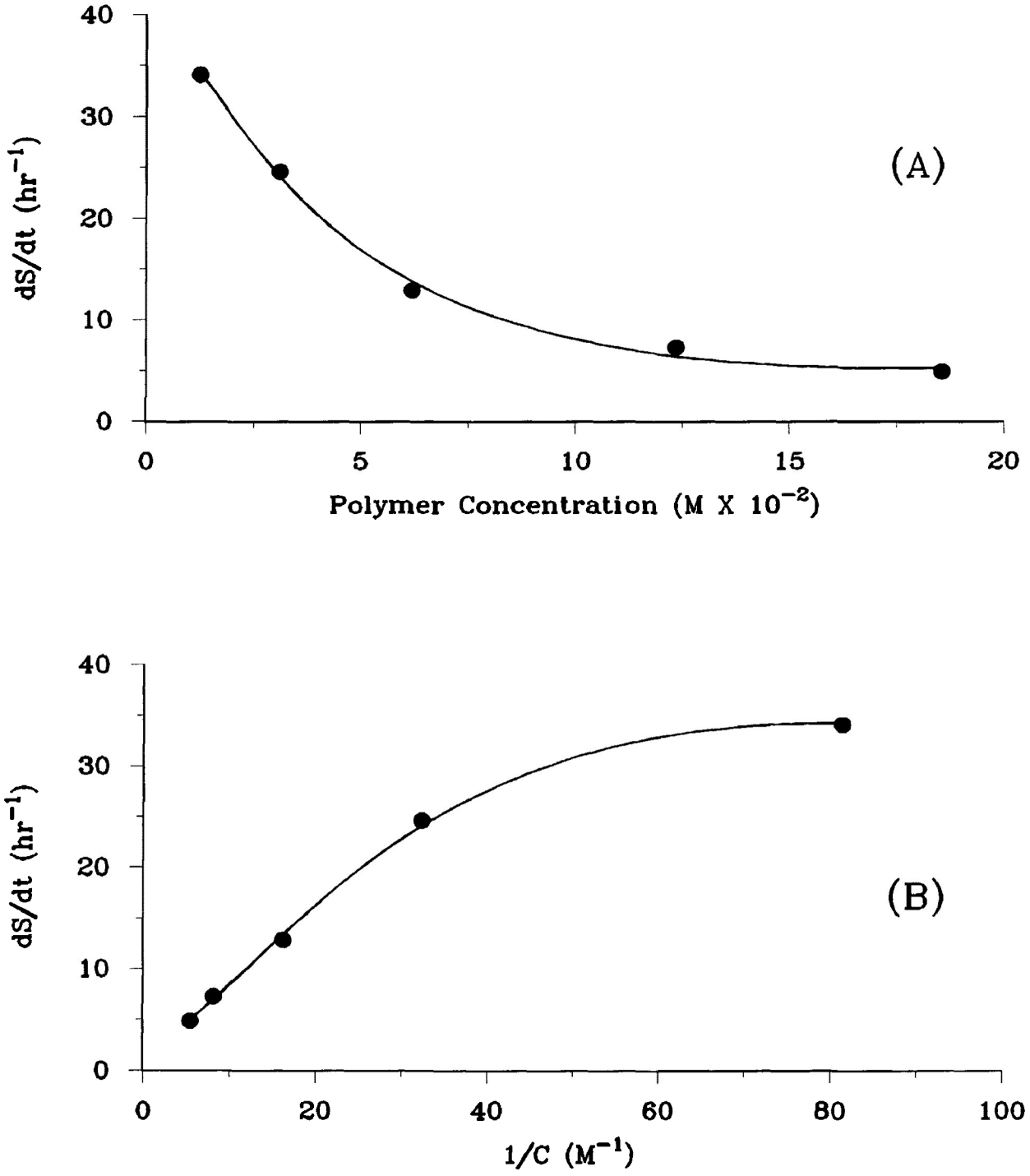

Figure 3.54. Rate of Chain Scission as a Function of (A) PMAP Concentration and (B) PMAP Reciprocal Concentration. (Irradiation: $\lambda \geq 300$ nm, vacuum).

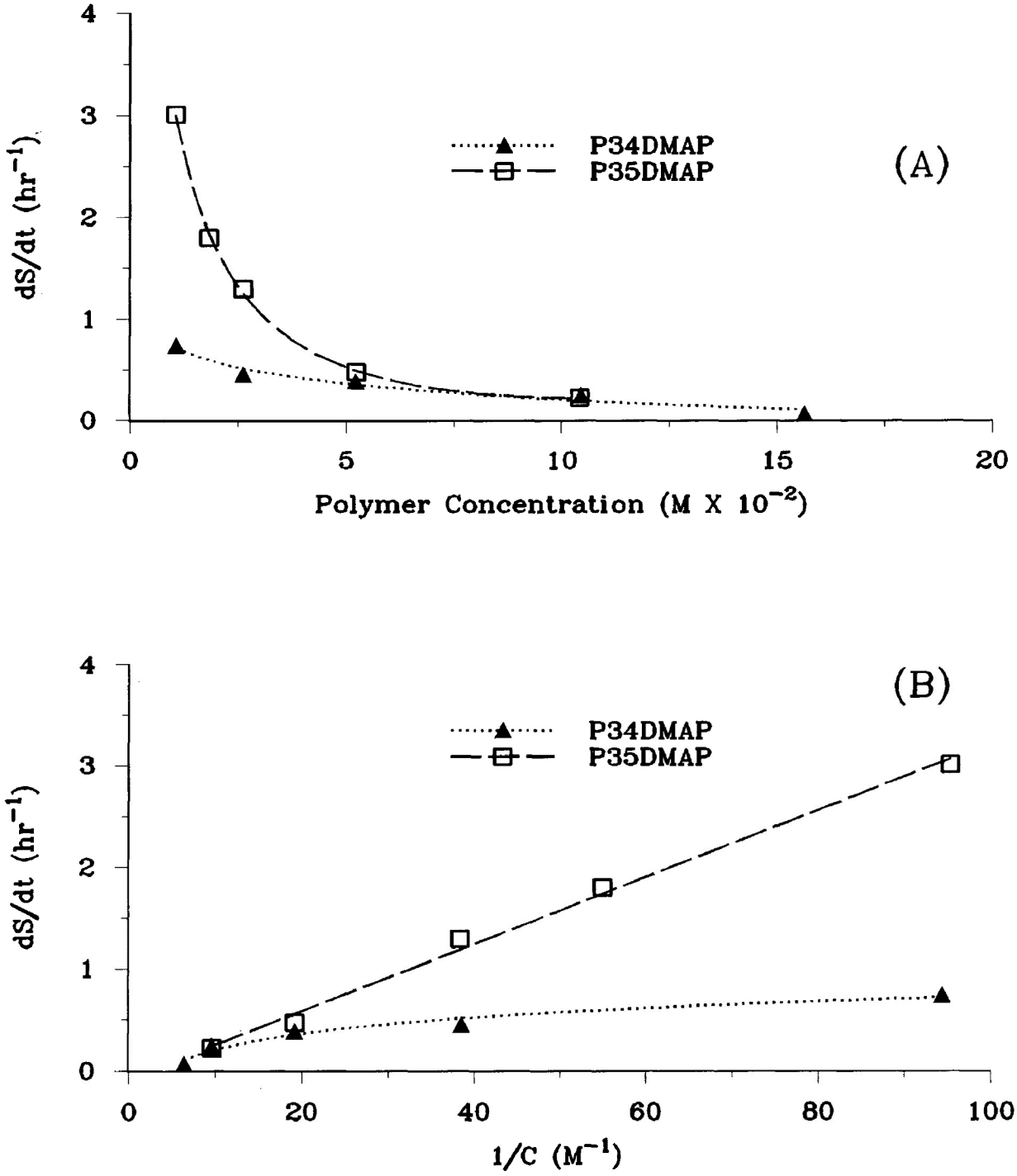

Figure 3.55. Rate of Chain Scission as a Function of (A) Polymer (P34DMAP, P35DMAP) Concentration and (B) Their Reciprocal Concentration. (Irradiation: $\lambda \geq 300$ nm, vacuum).

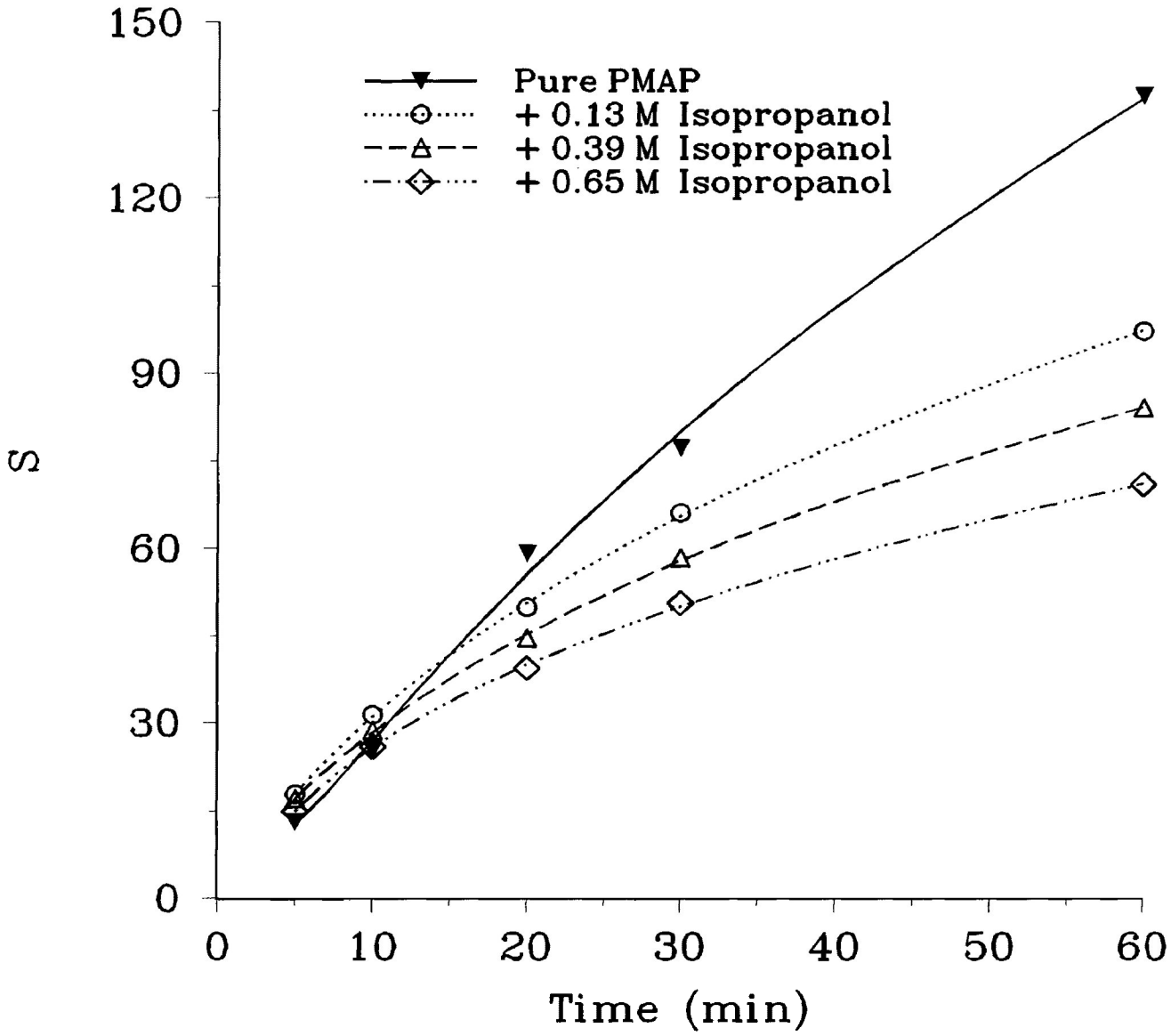

Figure 3.56. Number of Chain Scissions Per Molecule (S) as a Function of Irradiation Time ($\lambda \geq 300$ nm, vacuum).
PMAP Concentration = 6.0×10^{-2} M in CH_2Cl_2.

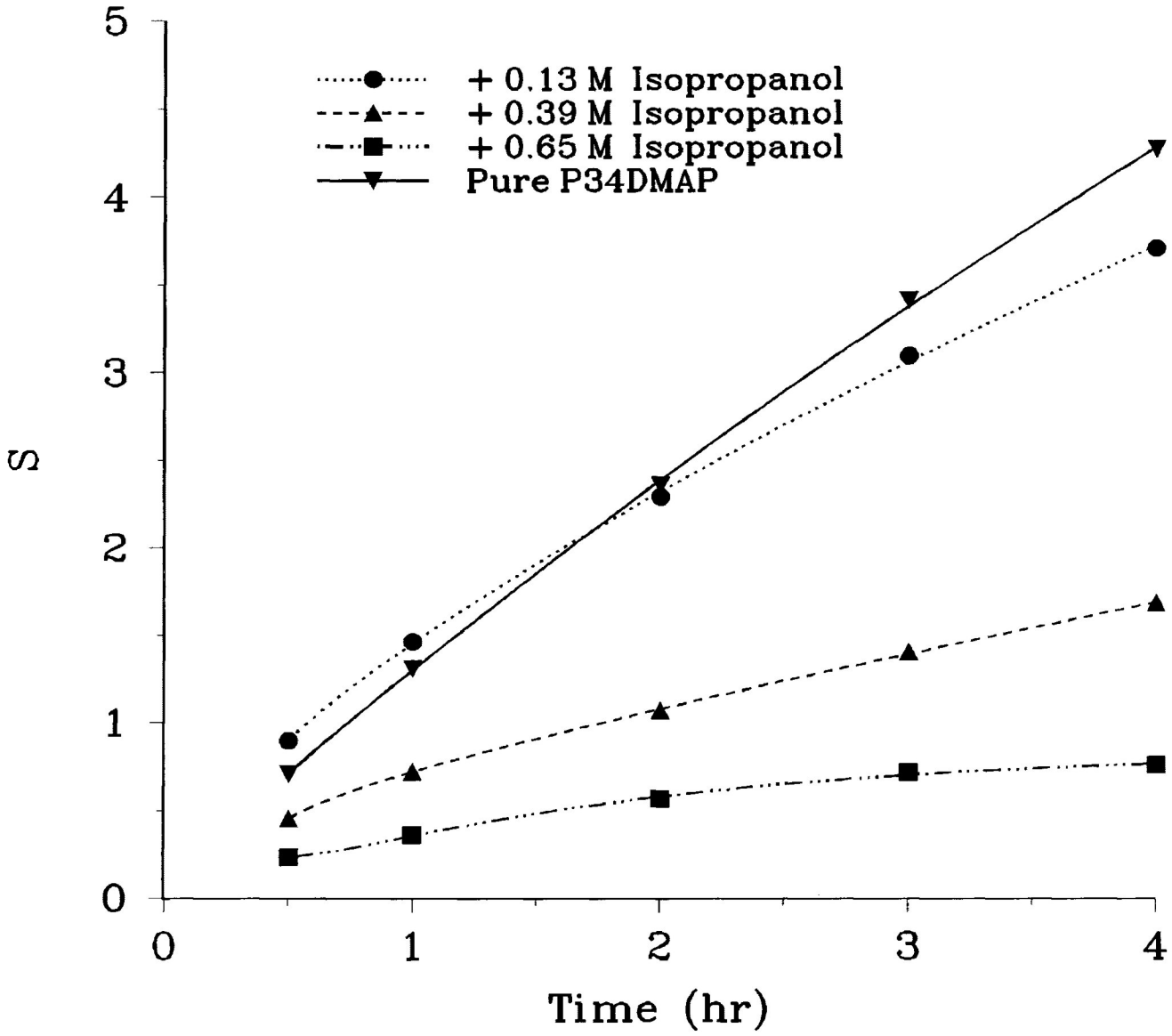

Figure 3.57. Number of Chain Scissions Per Molecule (S) as a Function of Irradiation Time ($\lambda \geq 300$ nm, vacuum).
P34DMAP Concentration = 6.0×10^{-2} M in CH_2Cl_2.

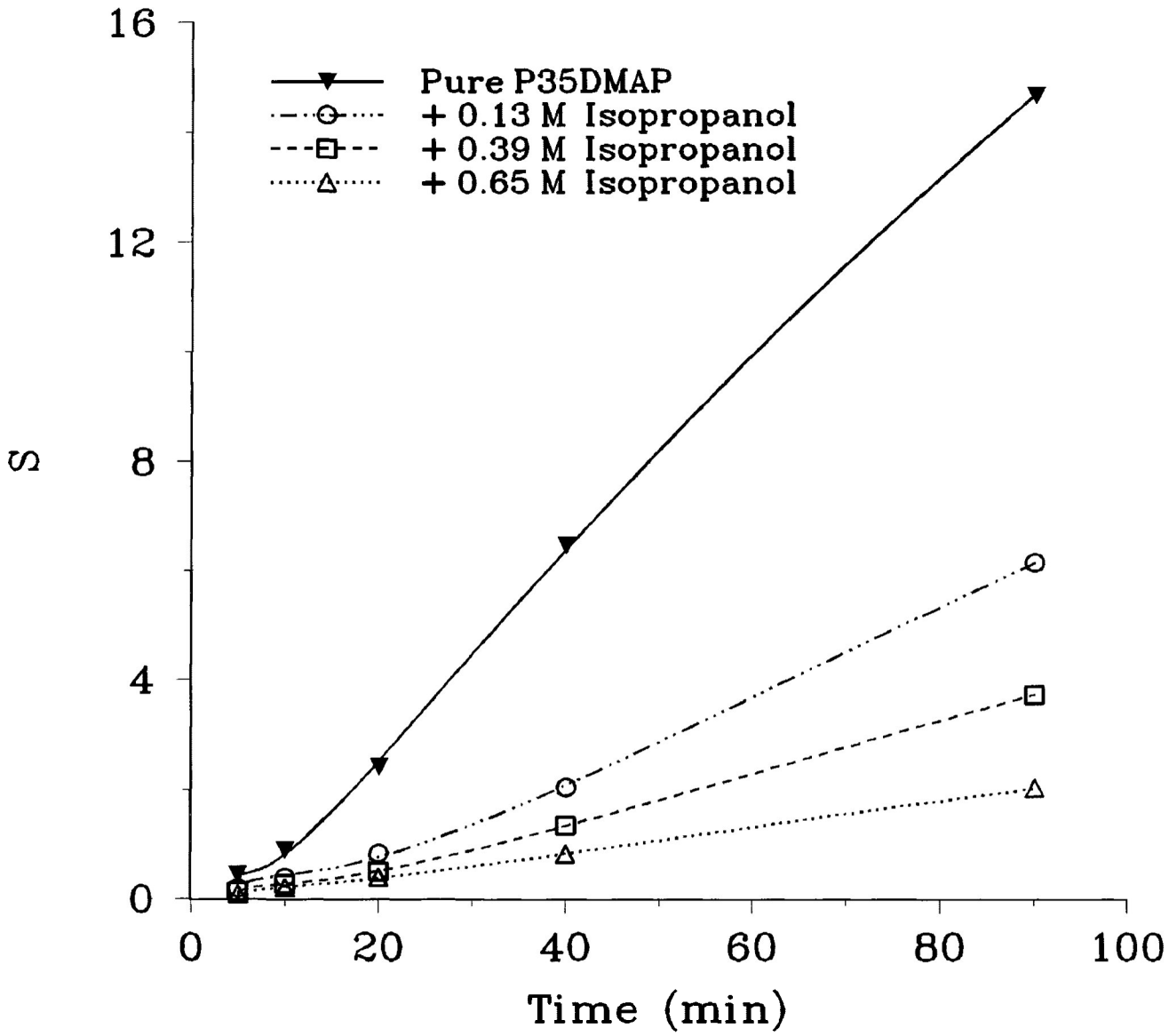

Figure 3.58. Number of Chain Scissions Per Molecule (S) as a Function of Irradiation Time ($\lambda \geq 300$ nm, vacuum).
P35DMAP Concentration = 6.0×10^{-2} M in CH_2Cl_2.

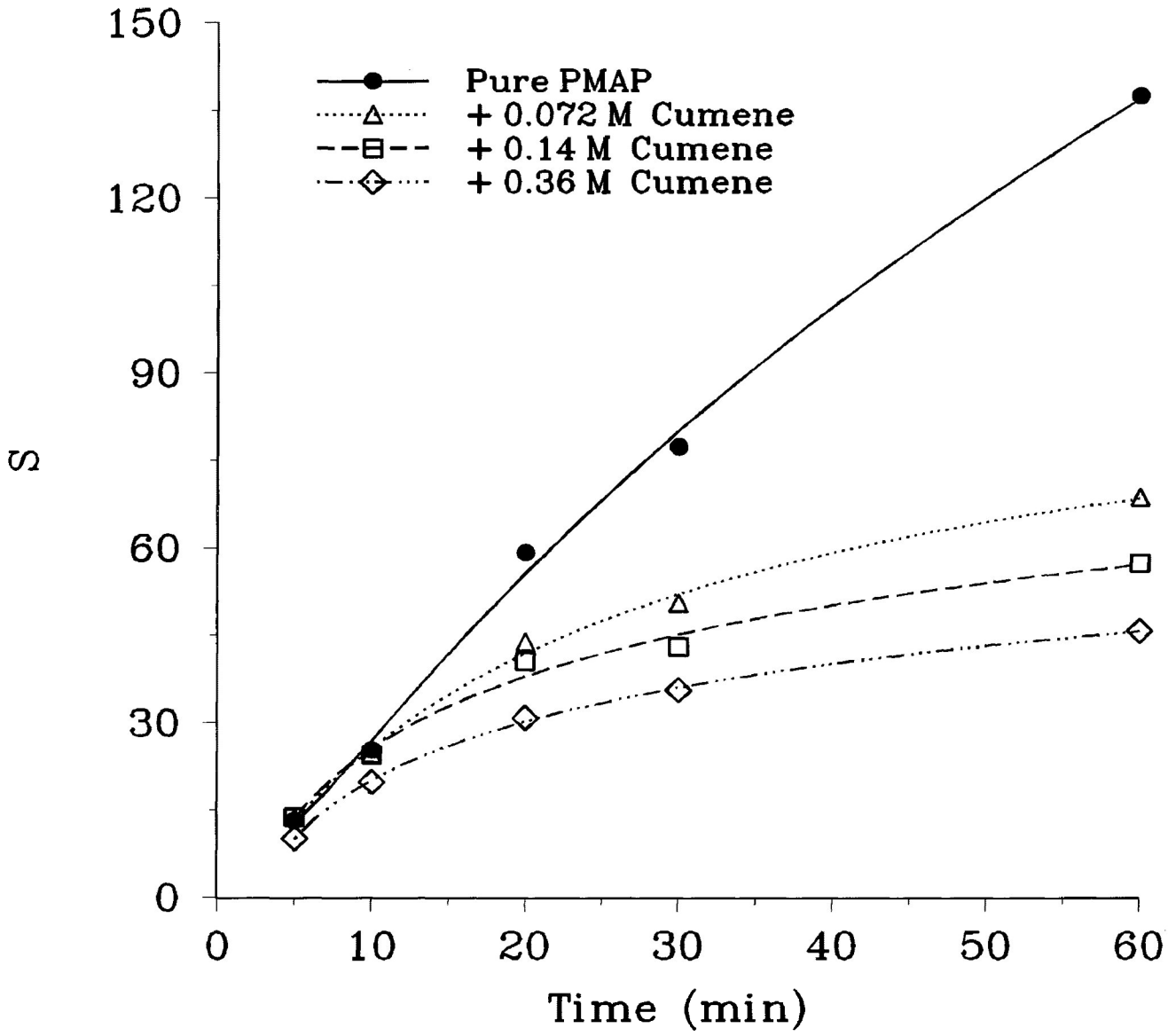

Figure 3.59. Chain Scission Data for PMAP (6.0×10^{-2} M in CH_2Cl_2). (Same Conditions as in Figure 3.56).

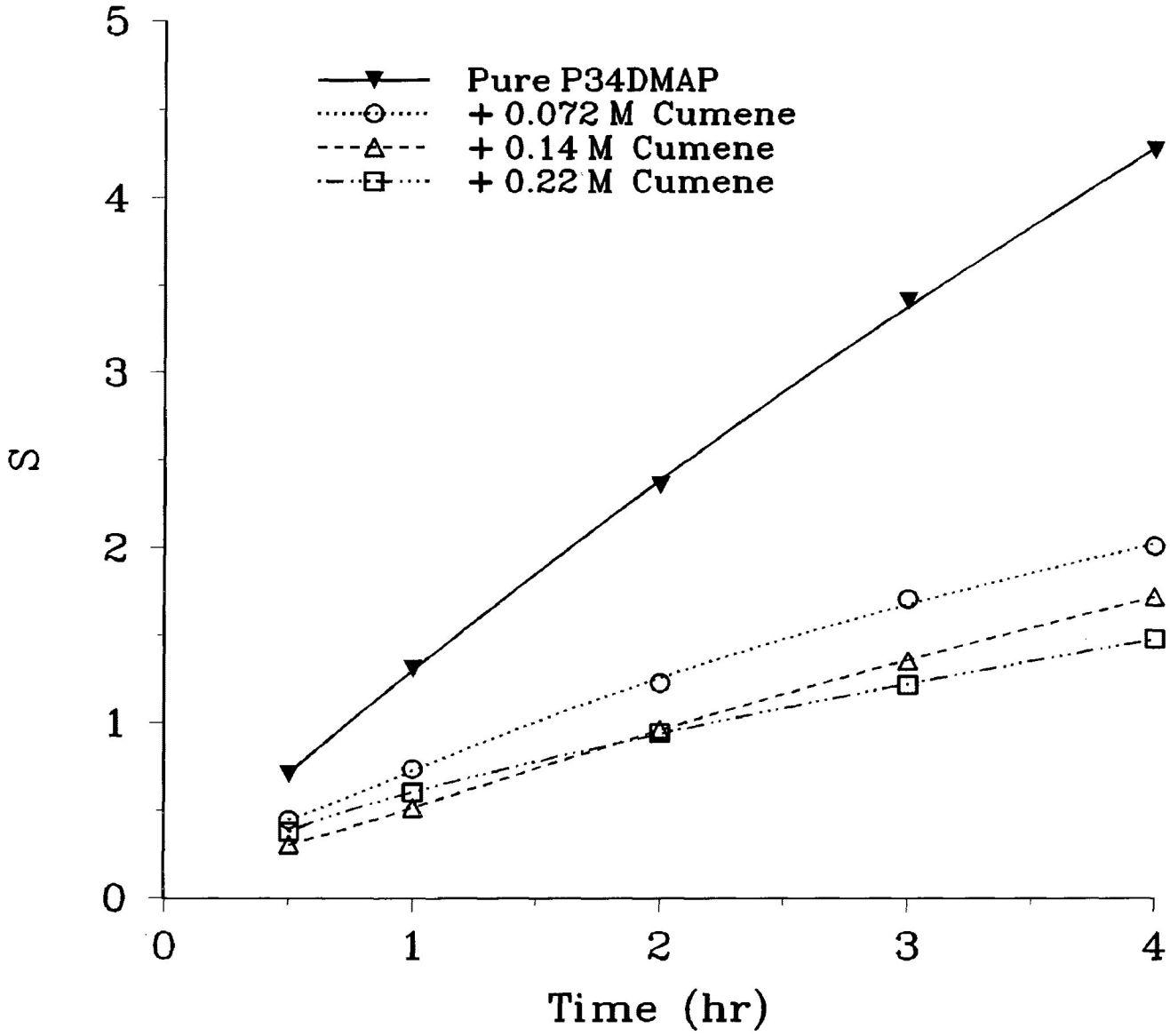

Figure 3.60. Chain Scission Data for P34DMAP (6.0×10^{-2} M in CH_2Cl_2). (Same Conditions as in Figure 3.57).

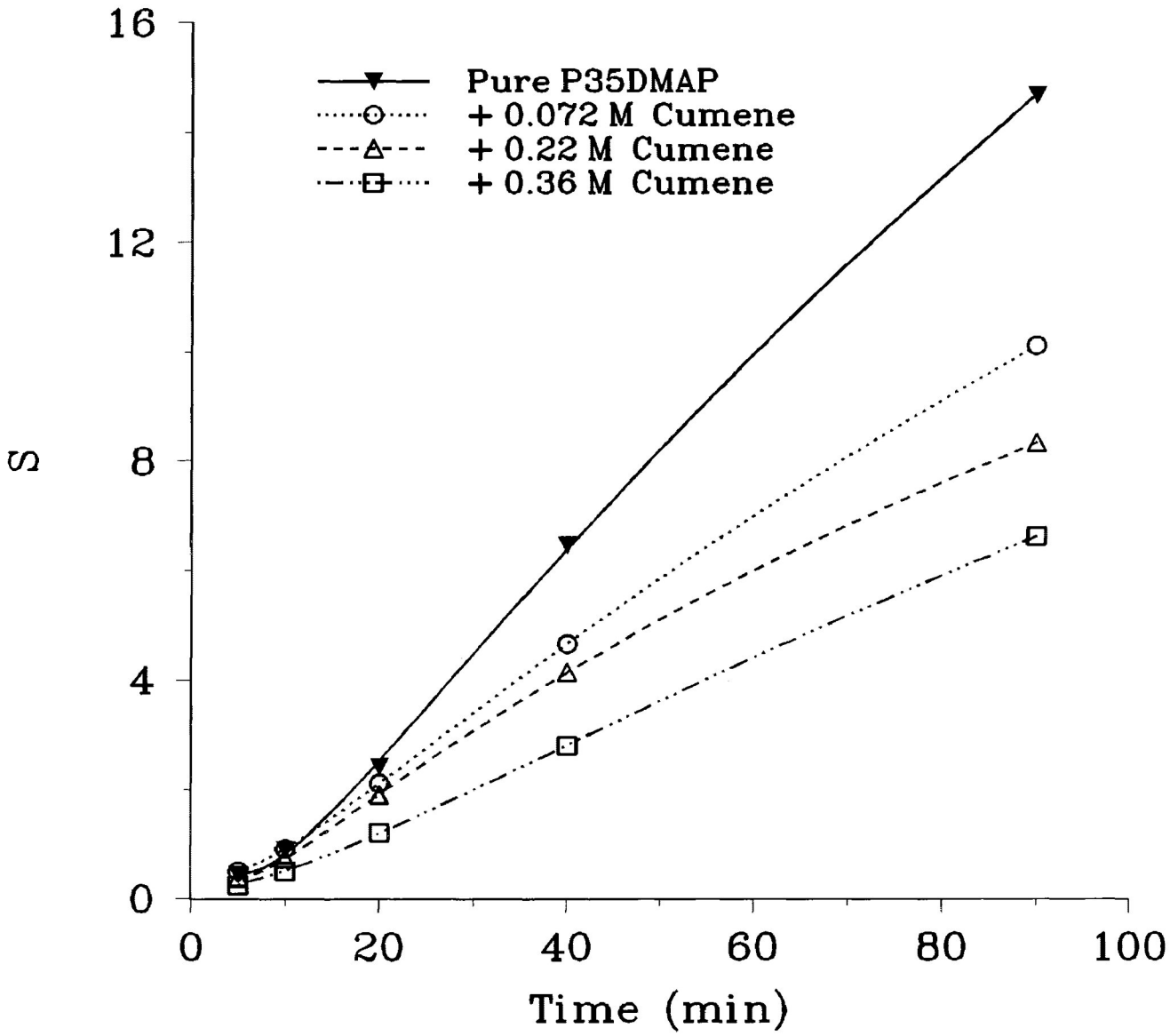

Figure 3.61. Chain Scission Data for P35DMAP (6.0×10^{-2} M in CH_2Cl_2). (Same Conditions as in Figure 3.58).

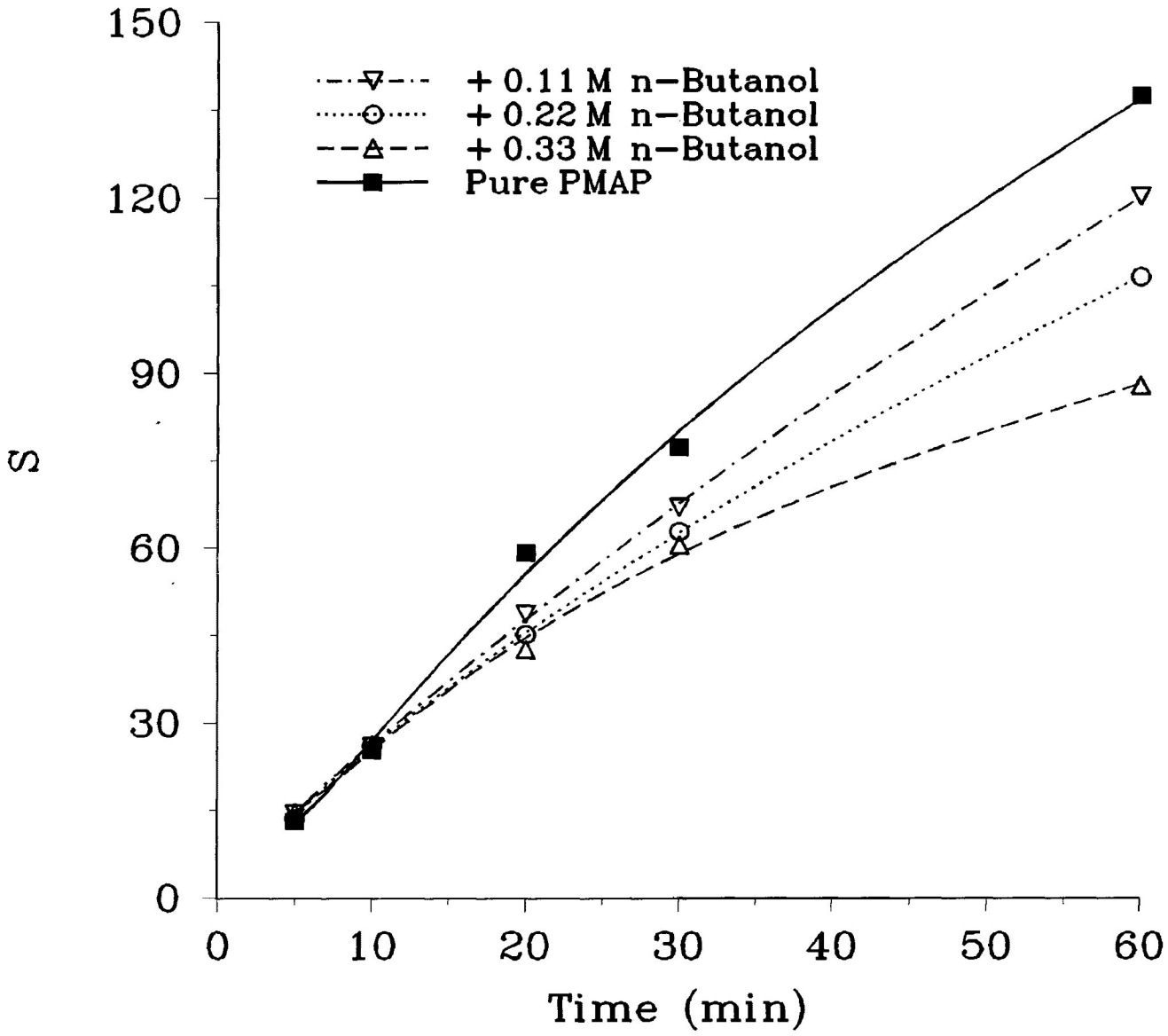

Figure 3.62. Chain Scission Data for PMAP (6.0×10^{-2} M in CH_2Cl_2). (Same Conditions as in Figure 3.56).

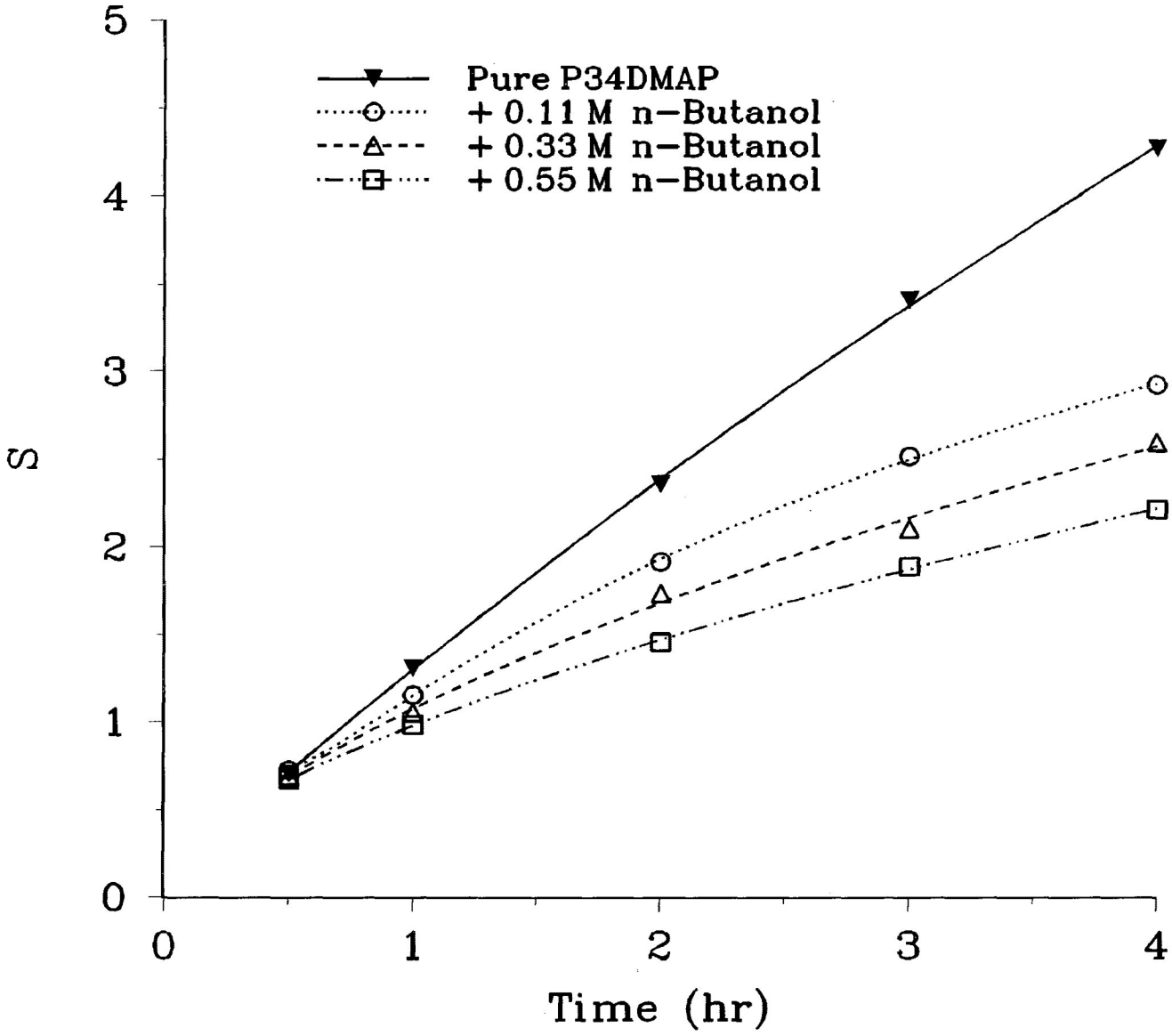

Figure 3.63. Chain Scission Data for P34DMAP (6.0×10^{-2} M in CH_2Cl_2). (Same Conditions as in Figure 3.57).

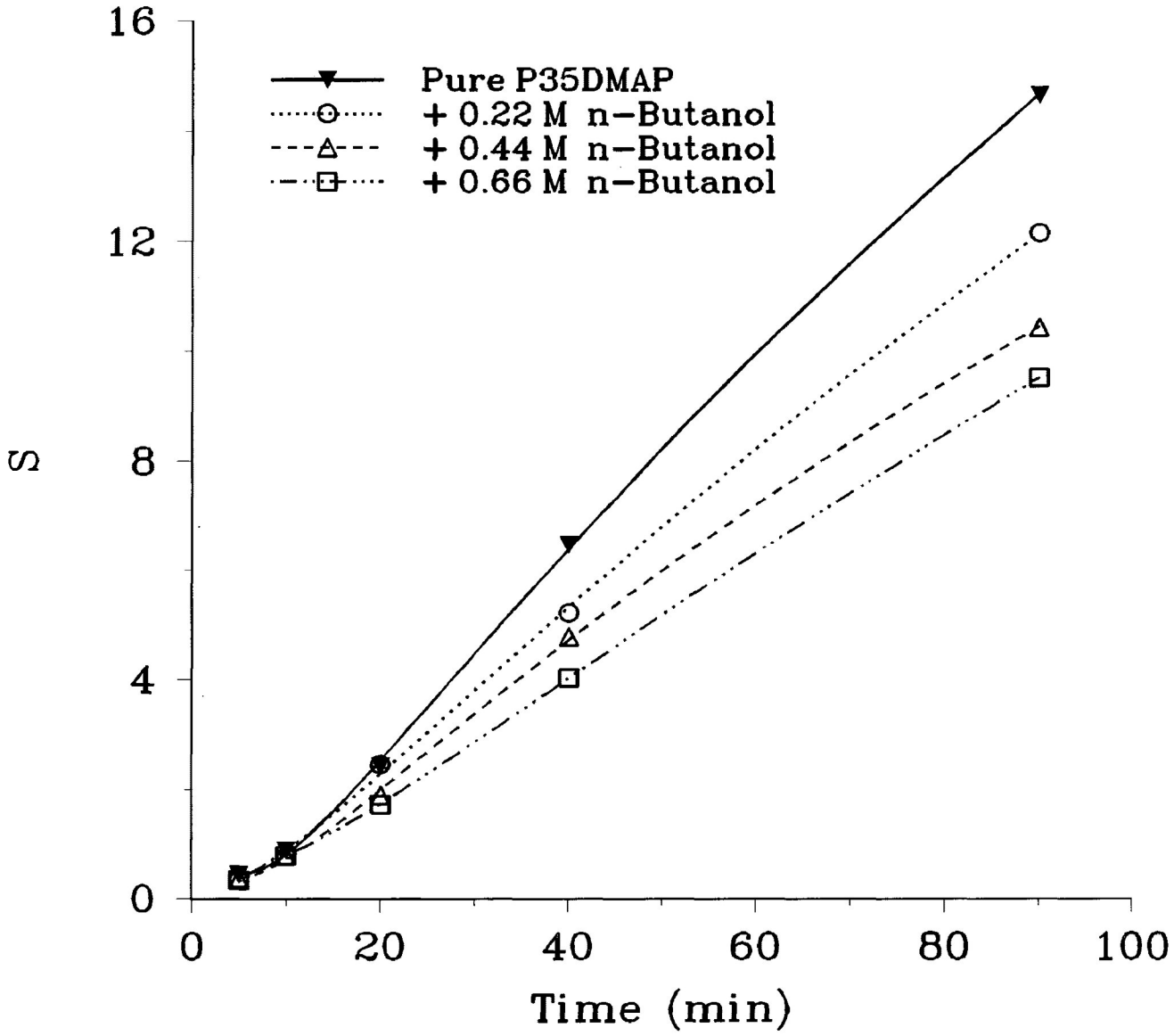

Figure 3.64. Chain Scission Data for P35DMAP (6.0×10^{-2} M in CH_2Cl_2). (Same Conditions as in Figure 3.58).

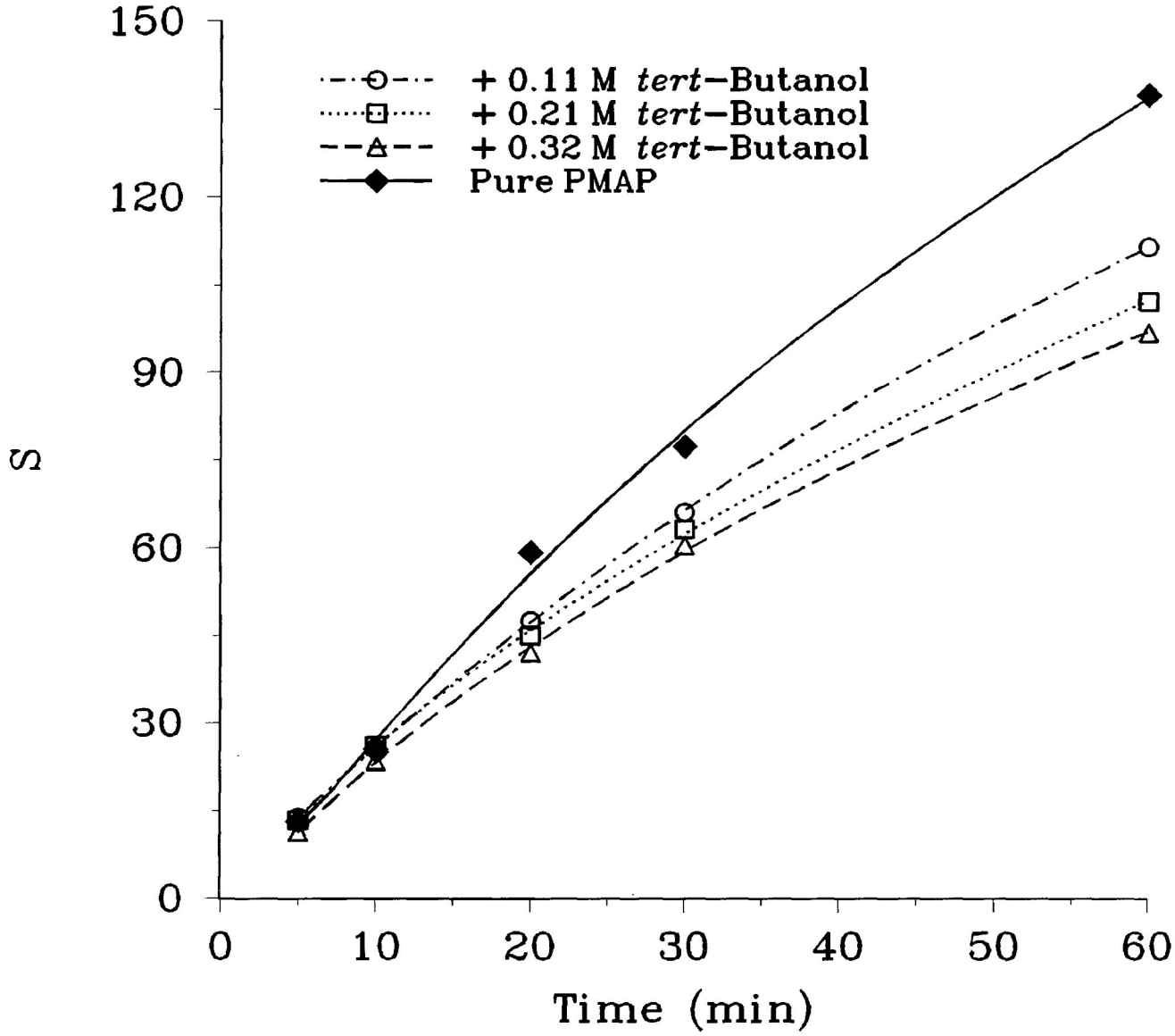

Figure 3.65. Chain Scission Data for PMAP (6.0×10^{-2} M in CH_2Cl_2). (Same Conditions as in Figure 3.56).

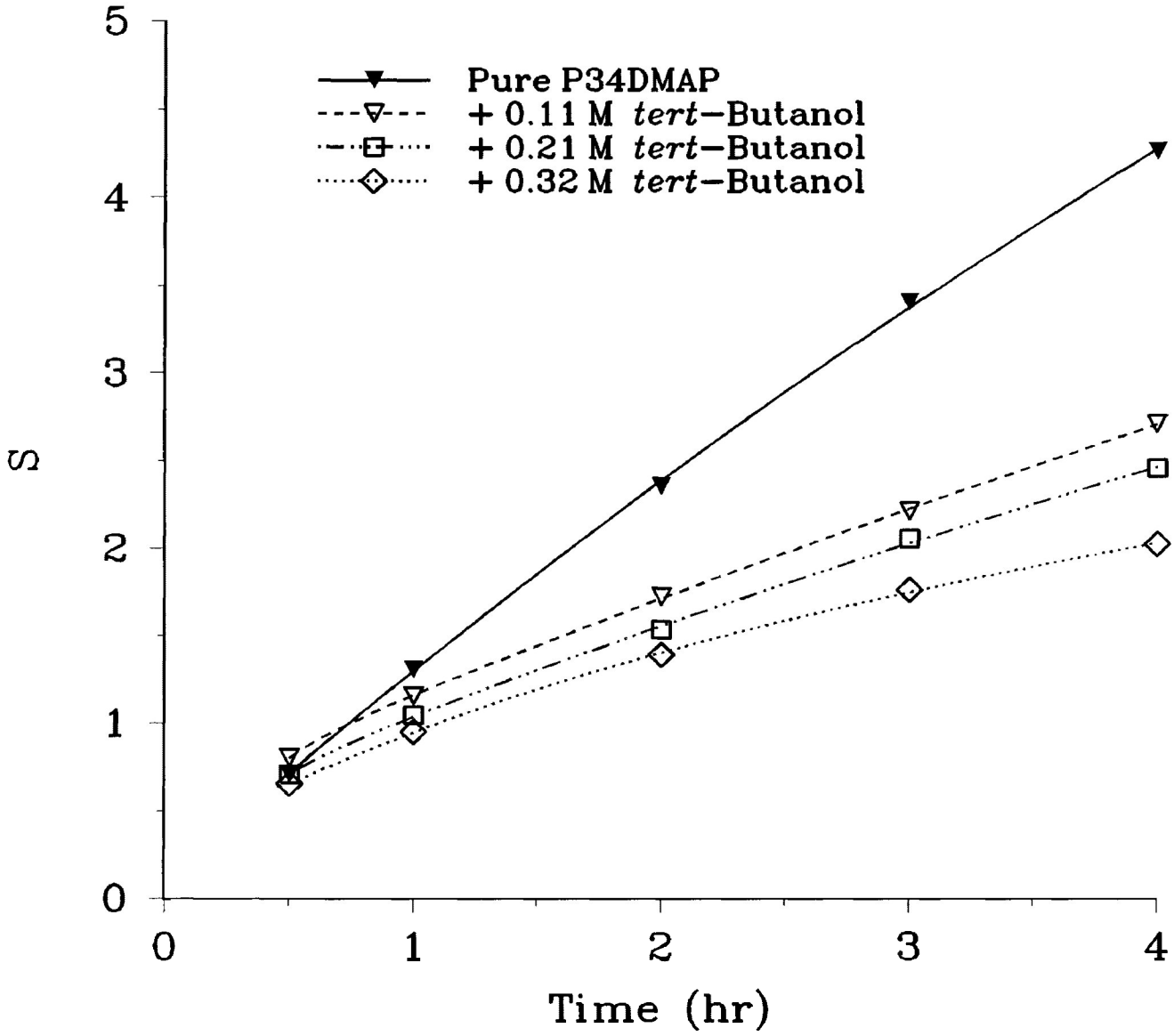

Figure 3.66. Chain Scission Data for P34DMAP (6.0×10^{-2} M in CH_2Cl_2). (Same Conditions as in Figure 3.57).

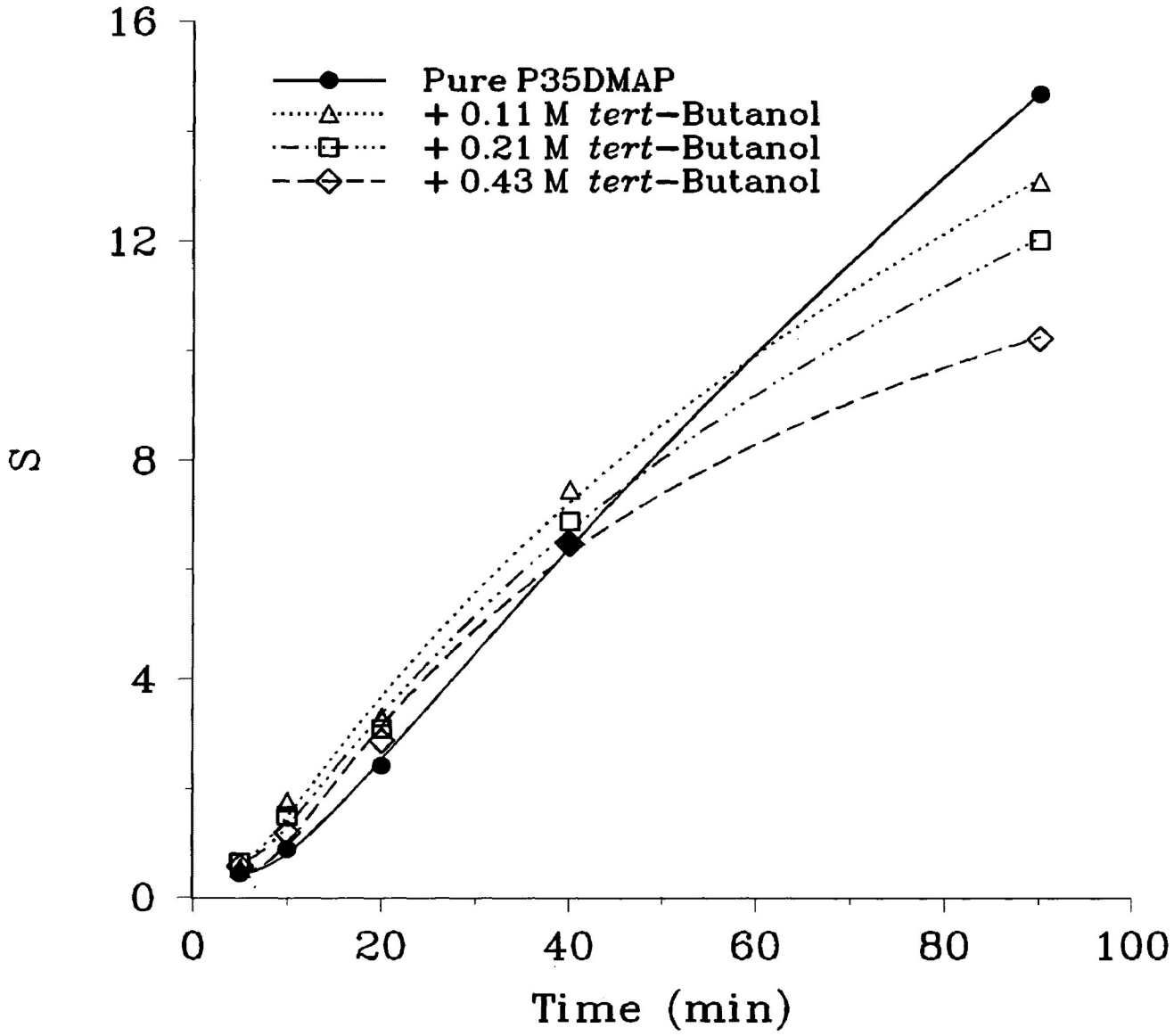

Figure 3.67. Chain Scission Data for P35DMAP (6.0×10^{-2} M in CH_2Cl_2). (Same Conditions as in Figure 3.58).

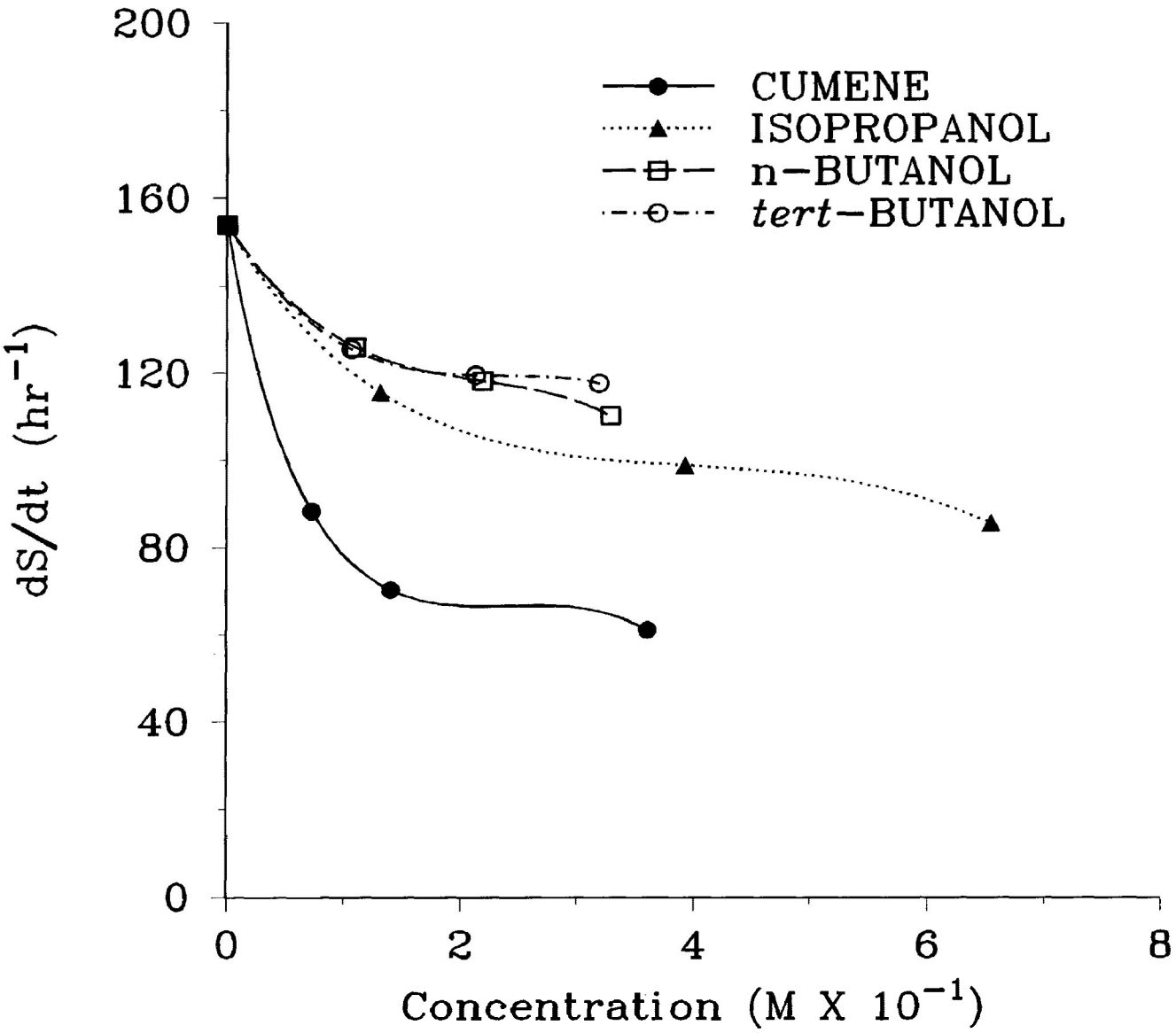

Figure 3.68. Rate of Chain Scission of PMAP as a Function of Concentration of Transfer Agent. (Irradiation: $\lambda \geq 300$ nm, vacuum).

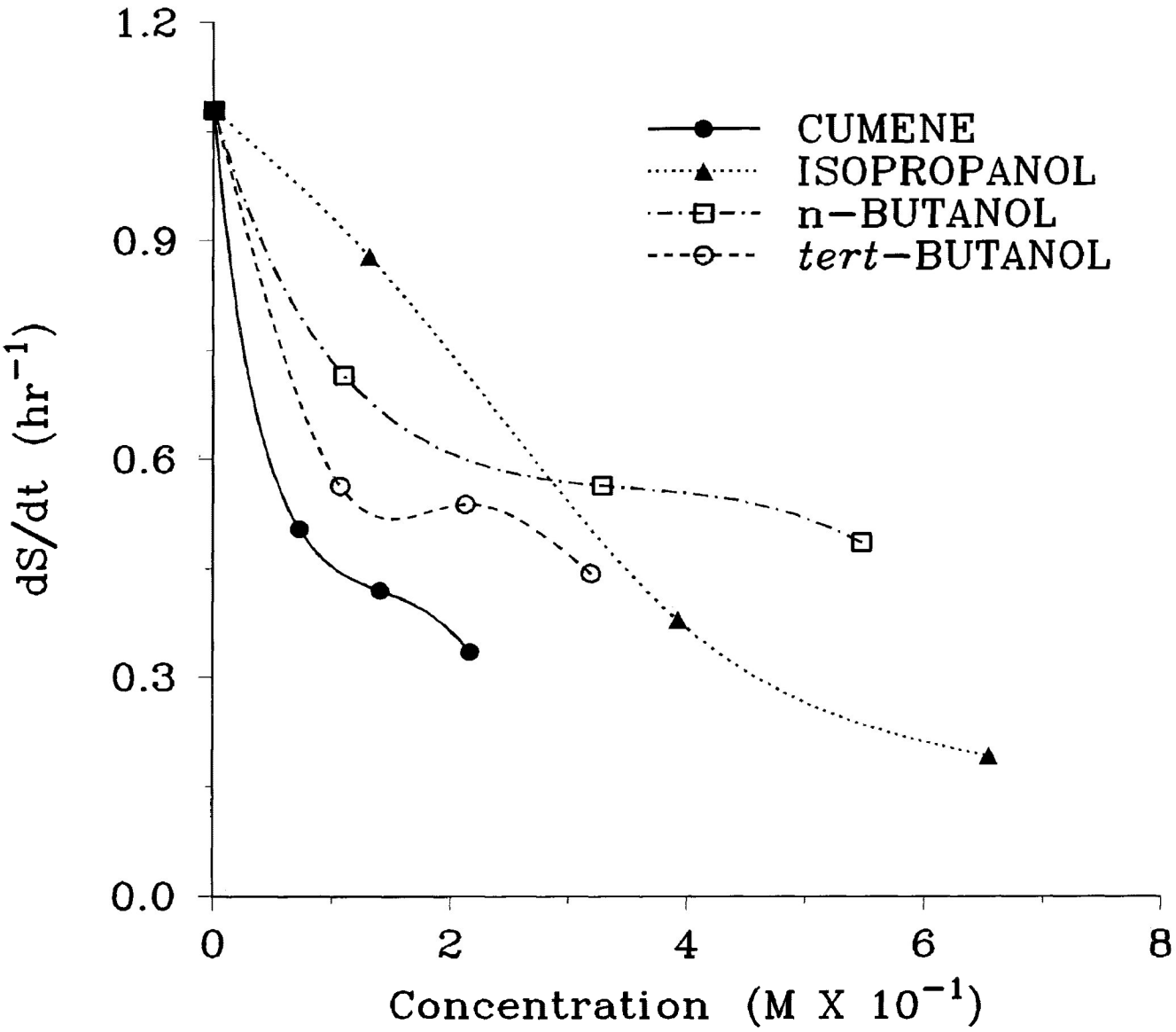

Figure 3.69. Rate of Chain Scission of P34DMAP as a Function of Concentration of Transfer Agent. (Irradiation: $\lambda \geq 300$ nm, vacuum).

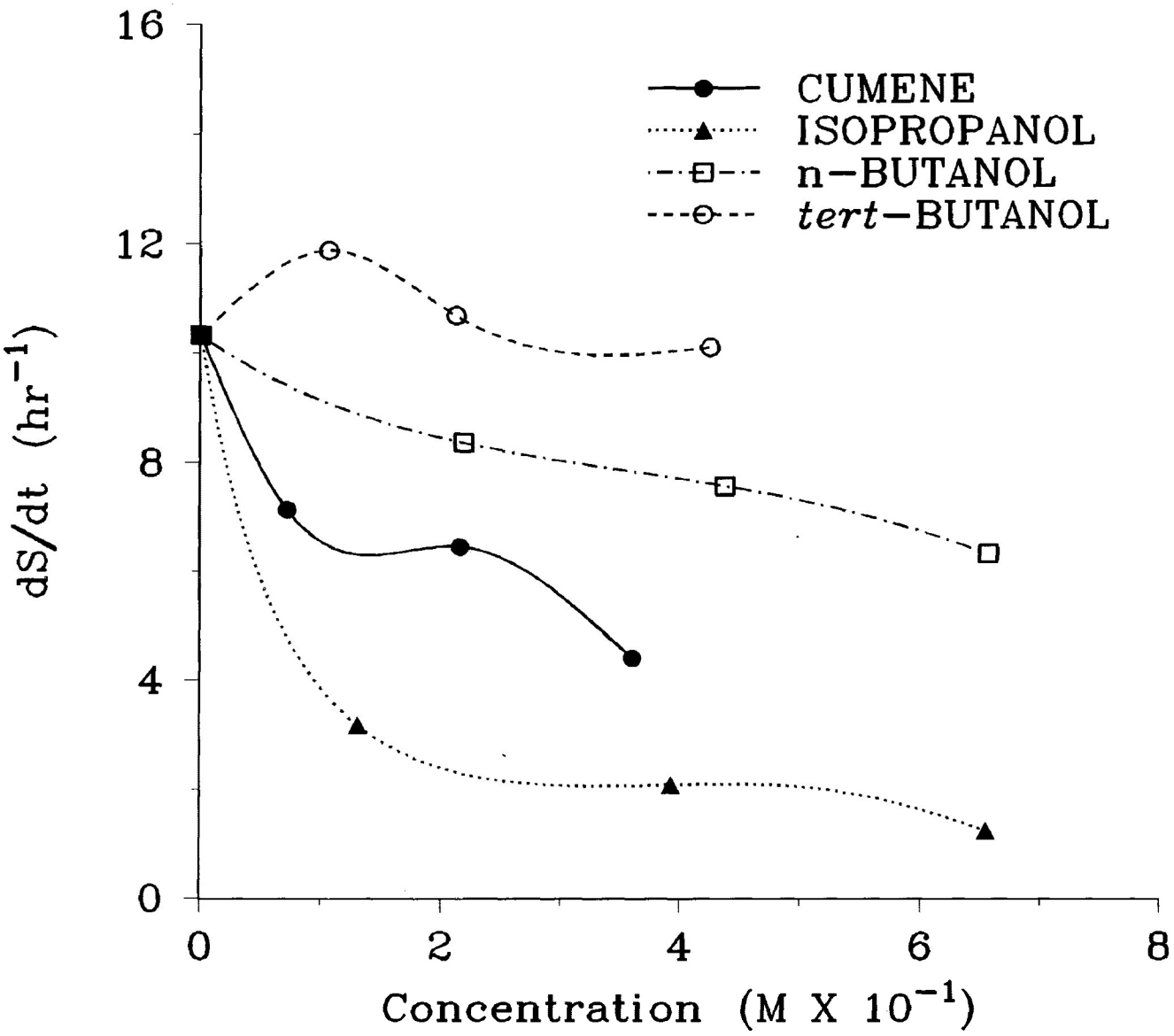

Figure 3.70. Rate of Chain Scission of P35DMAP as a Function of Concentration of Transfer Agent. (Irradiation: $\lambda \geq 300$ nm, vacuum).

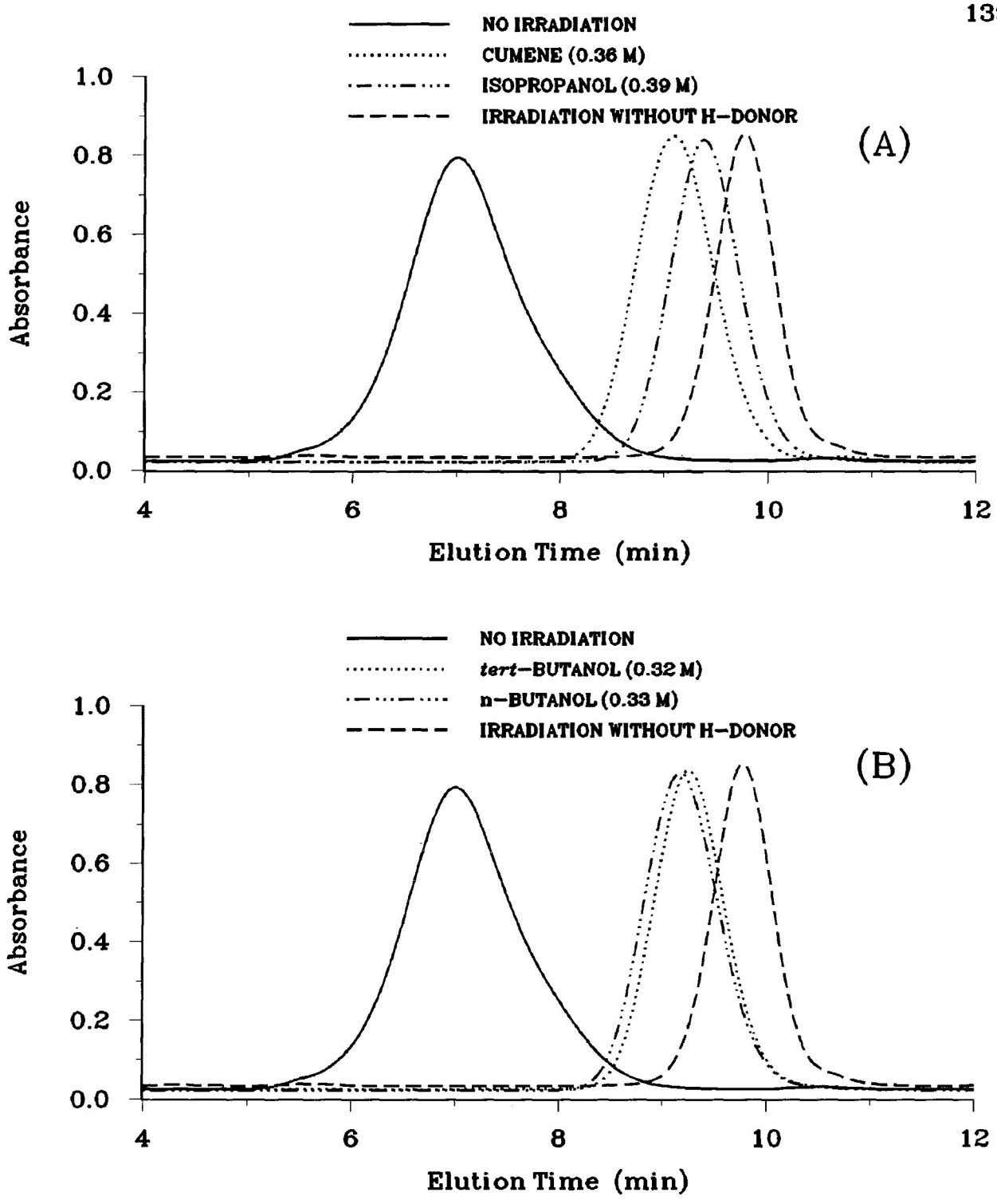

Figure 3.71. GPC Data for PMAP Solution (6.0×10^{-2} M in CH_2Cl_2) Before and After Irradiation in the Presence of Transfer Agents. (Same Conditions as in Figure 3.33).

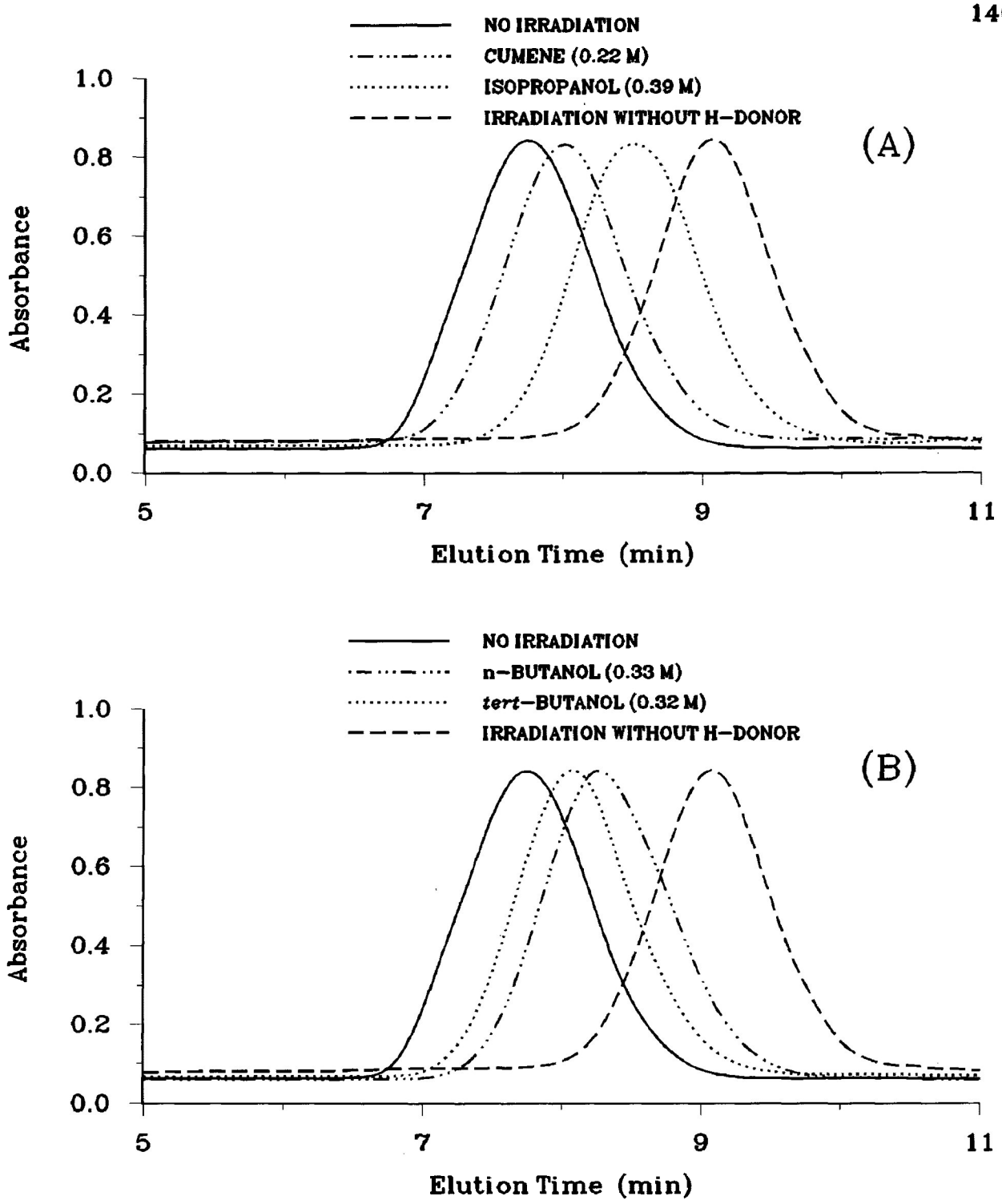

Figure 3.72. GPC Data for P34DMAP Solution (6.0×10^{-2} M in CH_2Cl_2) Before and After Irradiation in the Presence of Transfer Agents. (Same Conditions as in Figure 3.33).

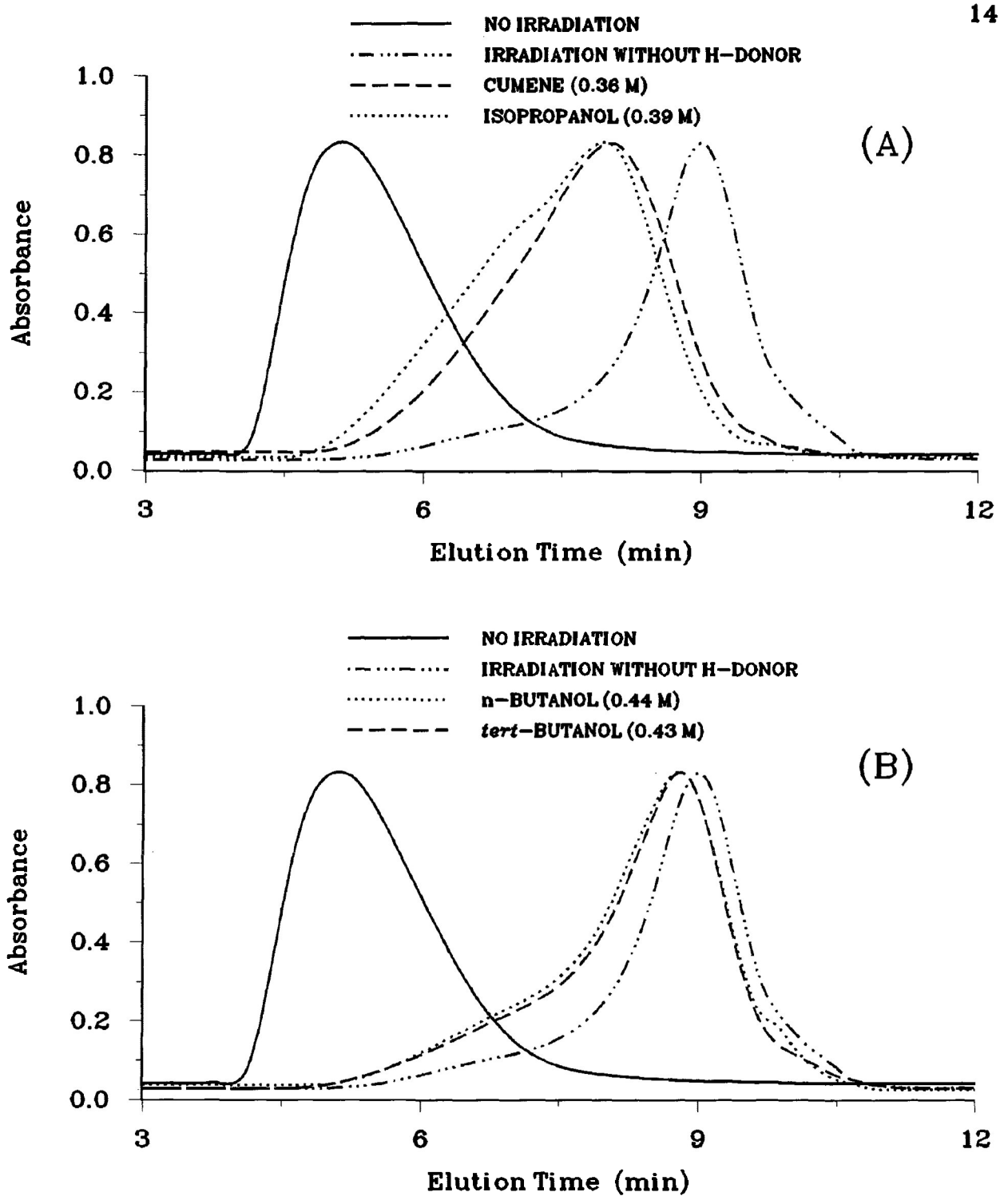

Figure 3.73. GPC Data for P35DMAP Solution (6.0×10^{-2} M in CH_2Cl_2) Before and After Irradiation in the Presence of Transfer Agents. (Same Conditions as in Figure 3.33).

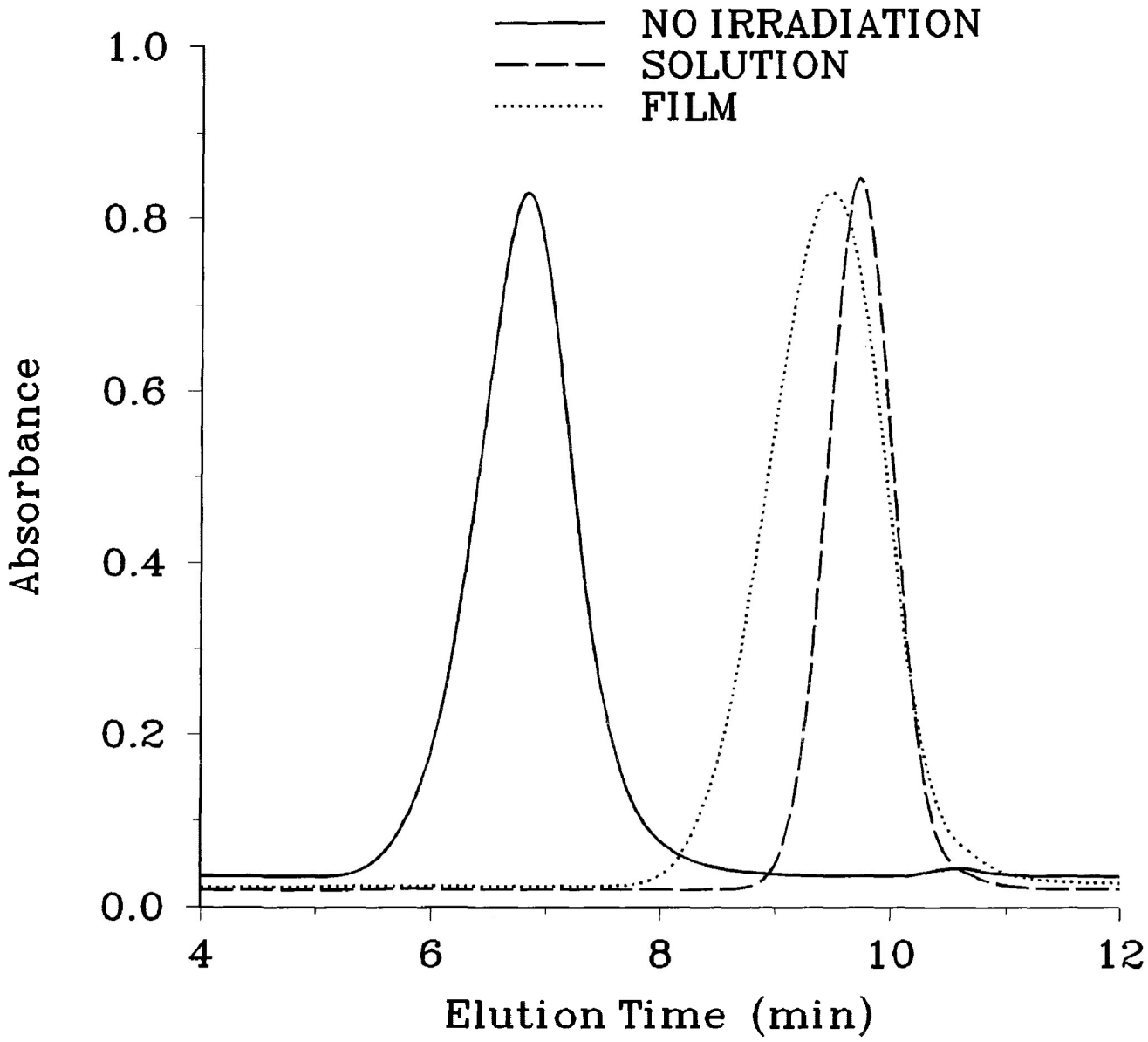

Figure 3.74. Gel Permeation Chromatographs of PMAP Before and After 12 Hour Irradiation ($\lambda \geq 300$ nm, vacuum). (Same Conditions as in Figure 3.33).

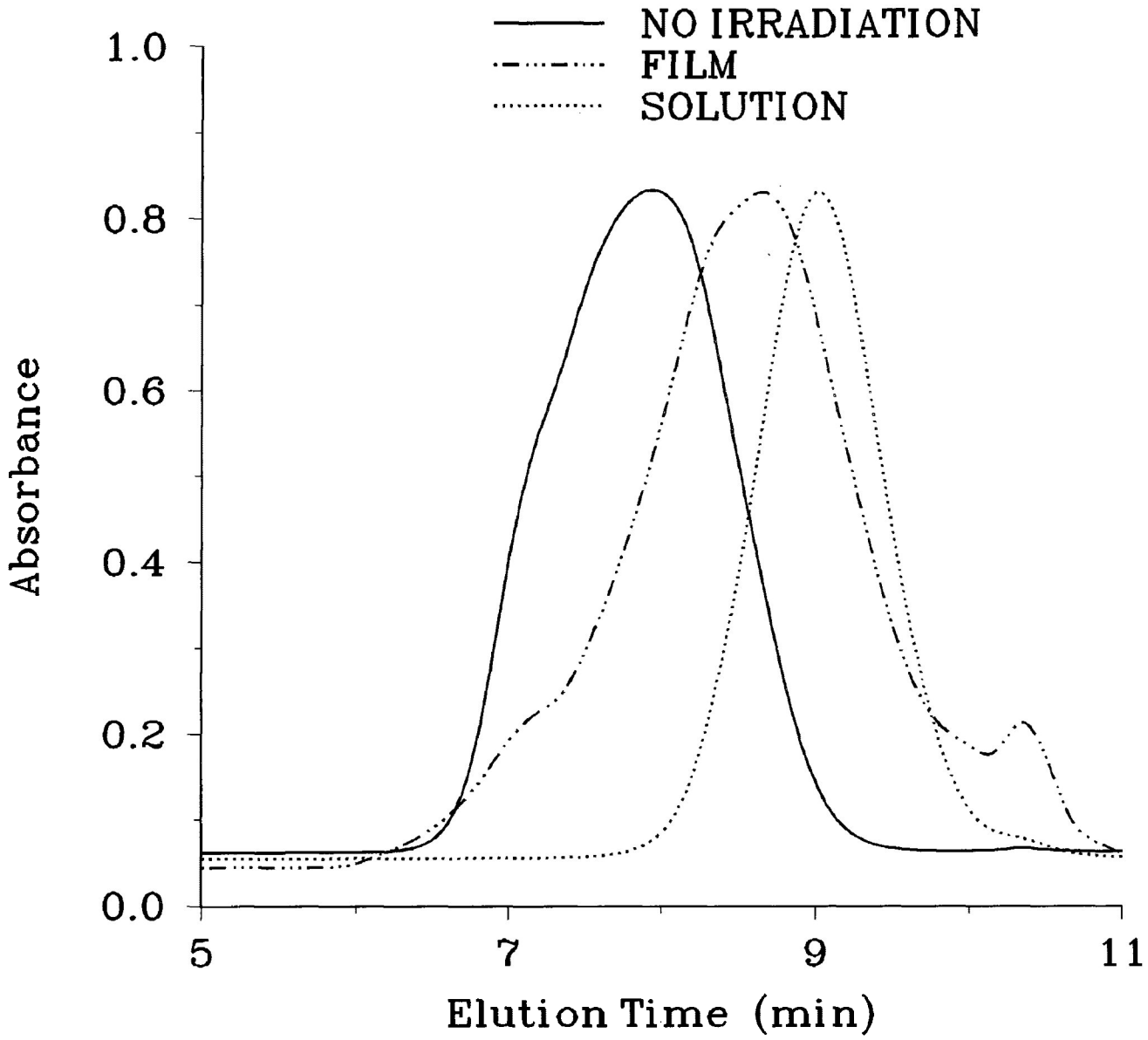

Figure 3.75. GPC Data for P34DMAP Before and After 12 Hour Irradiation ($\lambda \geq 300$ nm, vacuum). (Same Conditions as in Figure 3.33).

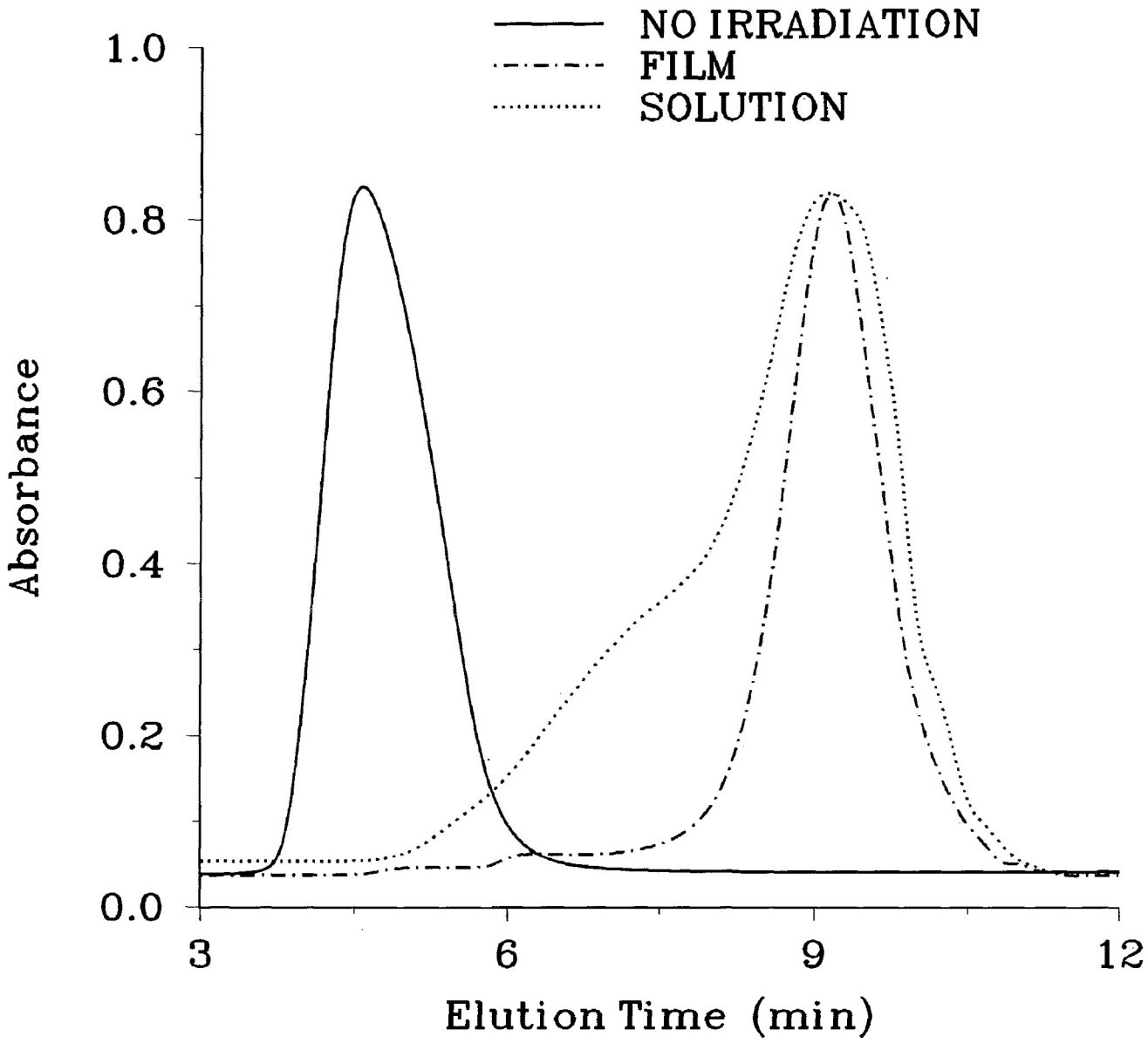

Figure 3.76. GPC Data for P35DMAP Before and After 12 Hour Irradiation ($\lambda \geq 300$ nm, vacuum). (Same Conditions as in Figure 3.33).

IV. DISCUSSION

Absorption of long-wave UV radiation ($\lambda \geq 300$ nm) by aromatic ketones results in the formation of the n,π^* singlet state which proceeds rapidly to the n,π^* triplet state, the quantum yield for intersystem crossing (ISC) approaching unity.[1,2] Electron-donating substituents (OCH_3) attached to the aromatic ring, however, favour the formation of carbonyl triplets in which the π,π^* character increases with increasing methoxy substitution.[52,53] Investigation of the polymeric lignin models (PMAP, P34DMAP and P35DMAP) reveals modified UV absorption characteristics as a result of the electron-donating OCH_3 groups. The energies of the π-molecular orbitals of the aromatic ring are perturbed, and this results not only in a red-shifting of the symmetry forbidden $\pi \rightarrow \pi^*$ transitions but also in considerable overlapping of these peaks with the carbonyl n $\rightarrow \pi^*$ absorptions.[54] While some resolution of the bands is observed in P34DMAP and P35DMAP, there is almost complete overlap in PMAP (Figure 3.1); as a result, a composite long-wave chromophore is observed.

The methoxy-substituted aromatic ketones, particularly the dimethoxy species, have low-lying, relatively unreactive π,π^* triplets (especially in abstraction reactions).[54,55] The triplet state reactivity of ketones with low-lying π,π^* triplets decreases as the energy gap between the π,π^* and n,π^* triplets increases.[54] Since the carbonyl n,π^* and aromatic π,π^* triplets are energetically similar, they are subject to

configurational mixing. This, along with vibronic coupling, increases the π,π^* character of the carbonyl triplet.[23,54] The excitation of the carbonyl chromophore can then be delocalized into the aromatic π system. The greater reactivity of PMAP (*cf* P34DMAP and P35DMAP) (Figure 3.4) reflects the higher degree of overlap of the two absorptions and the higher n,π^* character of the triplet.

Similar bathochromic shifts are observed in the phosphorescence spectra of PMAP, P34DMAP and P35DMAP (Figure 3.3). While poly(acrylophenone) (PAP) possesses a vibronically well resolved emission spectrum (characteristic of a ketone which has n,π^* character),[56] the methoxy-substituted derivatives possess very little vibrational fine structure, and this is typical of π,π^* triplets. In addition, the triplet state energies (energy of the 0,0 band) of the polymers under study are lower than that of the unsubstituted polymer. At the same time, the lifetimes of P34DMAP and P35DMAP are longer than that of PAP (Table 3.3), and this confirms the increased π,π^* character. The linearity of the log (phosphorescence intensity) versus time plots (Figures 3.5-3.7) clearly indicate that a single excited species (i.e. the triplet) is undergoing exponential decay in all three polymers. The weak fluorescence intensities (Figure 3.2) along with their small fluorescence quantum yields (10^{-4}) (Table 3.2) confirm that the principal excited species are the triplet states.

In addition to being deactivated by radiationless decay to the ground state, the triplets may also participate in a number of photochemical processes which give rise to the observed results, two principal degradation reactions being (a) O-CH_3 fission and (b) chain scission. The former, which is more limited and which was studied in less detail, is discussed first. The volatile product distributions (Figure 3.31) clearly show that methyl radical formation (O-CH_3 fission) is occurring in solid state photodegradation of PMAP, P34DMAP and P35DMAP. In addition, phenoxy radicals (R_1) are presumably also formed (Schemes I, II and III). Similar photochemistry occurs when the degradation takes place in solution; however, quantum yields for these reactions are much lower than those of chain scission. Such fissions are probably the result of internal conversions,[46,57] energy from the excited aromatic system being transferred into the vibrational modes of the O-C bond. Ethane can be formed by combination of the resulting methyl radicals, and methane by methyl radical abstraction of H-atoms from the polymer, the most probable point of attack (on energetic grounds) being the α-C-atom.[58] This abstraction reaction results in the formation of a tertiary radical (R_3) which can undergo further reactions including β-scission, which has previously been observed,[8,21] or crosslinking. Despite the lack of direct evidence, this form of degradation cannot be completely ruled out.

Phenoxy radicals (R_1), resulting from O-CH_3 fission, can

give rise to new carbonyl species. Due to electron delocalization, these radicals are relatively stable; therefore, they have sufficiently long lifetimes to participate in a number of other reactions including quinone formation (R_2).[59] O-CH_3 fission rates are undoubtedly affected by phenoxy radical stabilities, and this is particularly so in P34DMAP. It is possible, therefore, that in P34DMAP repeated photolysis will occur leading to a di-phenoxy species (R_4) which can rearrange to an *o*-quinone (Scheme II). PMAP and P35DMAP, however, can only form quinones (Schemes I and III). Evidence for quinone formation is provided by various spectroscopic data. The increased long-wave absorbance and emissions resulting from colouration (yellow) is consistent with the presence of quinones and is present in all cases. The new infrared absorbances at 1680-1720 cm^{-1} and the new ^{13}C NMR peaks at 184 ppm are also consistent with the formation of quinones. Plausible reaction schemes (Schemes I, II and III) to account for the various products are summarized.

The other degradation mechanism is random chain scission as indicated by decreasing molecular weights. Typical results are shown in Figure 3.32 where, for all three polymers, S, the number of chain scissions per original molecule, is plotted against the time of long-wave UV irradiation ($\lambda \geq 300$ nm). Chain scission can be attributed to a Norrish type II decomposition (as shown in Schemes I, II and III). For example, the Norrish type II reaction for PMAP is:

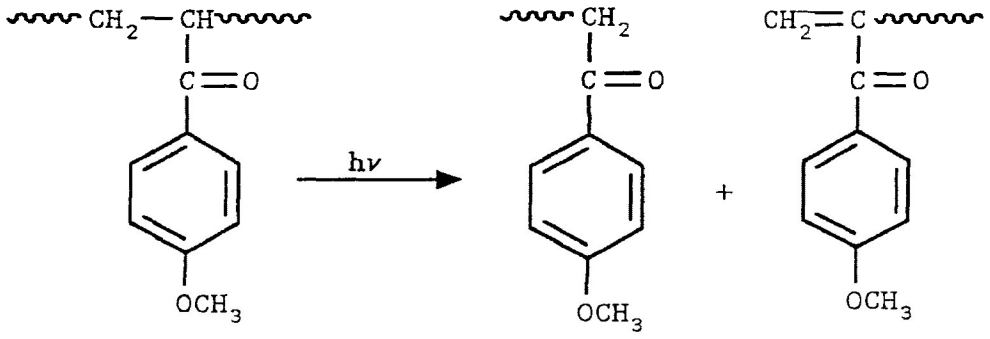

PMAP CHAIN SCISSION (Norrish Type II)

The new ^{1}H NMR peak at 5.30 ppm is indicative of the presence of a terminal unsaturation. The quantum yield for chain scission for PMAP is lower than that of the unsubstituted polymer, the effect being explained by lower reactivity of the methoxy-substituted triplet towards abstraction.[40] In addition, the quantum yields for chain scission for P34DMAP and P35DMAP are three orders of magnitude lower than that of PMAP (Table 3.18). This is very characteristic of low-lying π,π^* triplets,[60,61] and it can be explained in terms of the relative reactivities of the triplets in H-abstraction, γ-H-abstraction being the prerequisite to the formation of the biradical which collapses into the two fragments. Similar photochemistry occurs when the degradation takes place in the solid state (films); however, the quantum yields for chain scission are decreased. The greater rotational freedom of the molecules in solution ensures that the specific conformational requirements for γ-H-abstraction by the triplet are more easily met than in the rigid solid state at sub-T_g

temperatures. Furthermore, the rigid solid state makes the collapse of the biradicals (β-scission) more difficult.[62]

It can be seen that the S versus t plots (Figure 3.32) are non-linear at longer exposure times. This is probably the result of self-quenching, the terminally unsaturated ketones formed in the Norrish type II process acting as traps for the migrating triplet energy.[35] Since their concentrations increase during degradation, the reactions become increasingly subject to self-quenching, and this is reflected in the molecular weight data (Figures 3.33-3.35). This type of inhibition of degradation during prolonged irradiation is a feature of these polymers, and it is more pronounced in solution (Figures 3.9-3.11) than in film (Figures 3.12-3.14). In solid state degradation a more linear response is obtained, and this reflects the lower probability of formation of the terminally unsaturated ketones (less Norrish type II decomposition).

Because of the increased probability of separation of fragments in solution (*cf* film), the characteristics of molecular weight changes are different in the solid and in solution. Data are shown for PMAP and P34DMAP in both solution (Figures 3.33-3.34) and in films (Figures 3.74-3.75). Gelling is observed after prolonged exposures in solution; therefore, crosslinking is not impossible even though narrower molecular weight distributions are observed for photolyzed PMAP and P34DMAP (Figures 3.33-3.34). It could be argued, however, that

very high molecular weight material is not eluted but is trapped in the column.

An alternative reaction, which is similar to crosslinking, may also occur since the rotational flexibility of the polymer segments is higher in solution.

CYCLIZATION (INTRAMOLECULAR CROSSLINKING)

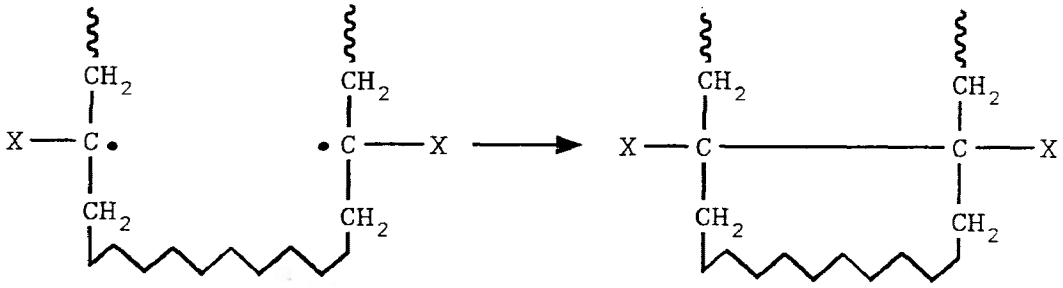

(X = methoxy-substituted benzoyl derivative)

The effects of cyclization on molecular weight are unlikely to be large, but they do effectively alter the balance in favour of chain scission by competing with intermolecular radical combinations. The probability of crosslinking increases in solid state photodegradation as a result of the increased difficulty of the diffusional separation of the macroradicals, and this could account for the broader molecular weight distributions, particularly in photolyzed P34DMAP (Figure 3.75). In addition, because of their relatively long lifetimes, phenoxy radicals can participate in crosslinking reactions.[59]

Molecular weight may also influence these reactions. The high degree of polymerization of P35DMAP will lead to increased entanglement in solution, and this could further restrict the mobility of the chromophores. As a result, specific conformational requirements for γ-H-abstraction (Norrish type II) may not be readily attainable, and this will decrease the rate of chain scission which results in a less rapid decrease in the molecular weight (Figure 3.35). In addition, the rates of diffusive separation, because of entanglement of the macroradical fragments, are decreased. This again alters the balance between crosslinking and chain scission (apparently favouring crosslinking), and this could account for the broader molecular weight distributions observed in photolyzed P35DMAP, especially after prolonged exposures (Figure 3.35).

Solid state photodegradation of P35DMAP is complex. Since crosslinking is favoured by the increased difficulty of the diffusional separation of the macroradical fragments, a broader molecular weight distribution should be observed. However, GPC results (Figure 3.76) indicate a low molecular weight species having a narrower molecular weight distribution than that observed for solution degradation. Furthermore, NMR spectroscopy showed the presence of a completely new species with no aromatic, methoxy or carbonyl peaks. The irradiated material was highly gelled, and GPC and NMR studies were carried out on the soluble material extractable from the gel.

Clearly, other reactions were occurring, but these were restricted to P35DMAP and were not investigated further.

The effects of well known triplet quenchers (naphthalene and *cis*-1,3-pentadiene) were investigated both from the points of view of chain scission and intensity of phosphorescence. All polymeric ketone triplets are readily quenched by naphthalene and *cis*-1,3-pentadiene (Figures 3.36-3.41), and the data for chain scission conform well to Stern-Volmer kinetics (Figures 3.45-3.47). The high Stern-Volmer constants (Table 3.19) are indicative of the long lifetimes of the triplet states responsible for main chain scission in these polymers. For example, the Stern-Volmer constant for PMAP quenched by naphthalene is comparable to that obtained in previous work,[56,61] and it is about 25 times that of PAP (naphthalene quencher). This indicates that the lifetime of the PMAP triplet is considerably longer than that of PAP,[61] and this reflects the lower reactivity of the PMAP triplet towards abstraction. In addition, the Stern-Volmer constants for P34DMAP and P35DMAP are approximately 2-3 times that of PMAP. These results indicate increasing π,π^* character and lower reactivity of the carbonyl triplets, the result of increasing methoxy substitution.

It is often assumed that triplet energy transfer is so efficient that every encounter in solution between donor and acceptor molecules results in energy transfer; therefore, the rate of energy transfer is limited by the rate of diffusion

together of donor and acceptor (i.e. diffusion control).[63,64] It is evident, from Table 3.19, that the Stern-Volmer constants, K_{SV}, are different for the two quenchers. That *cis*-1,3-pentadiene is a less effective quencher than naphthalene (Figures 3.42-3.44) can be explained by reversible energy transfer.[65] This indicates that the rate of quenching is not only determined by the diffusion constant but also by energetic and steric factors.[66] Similar results have been obtained by Scaiano,[61] but a general explanation has not yet been given. However, steric limitations of quenching abilities are not unknown.[67]

There is also a large difference between the Stern-Volmer constants based on the inhibition of degradation (Table 3.19) and those obtained by direct triplet quenching (Table 3.4), the former being considerably larger by a factor of ten for PMAP and by a factor of 35 for P34DMAP and P35DMAP. The Norrish type II decomposition leads to the formation of terminally unsaturated groups which quench some of the triplets (self-quenching). On the other hand, no such self-quenching of the triplet is possible when quenching of the phosphorescence intensity is measured, i.e. no degradation occurs during the measurement of phosphorescence intensity. It follows then that the apparent quenching efficiency of these solutes (based on chain scission) are lower, i.e. the products formed during degradation are participating in the quenching process.

The triplets may also be quenched by H-donors in hydrogen abstraction reactions (or photoreduction), i.e.

$$(RCO^*)^3 + YH \rightarrow \underset{(A)}{RC\dot{O}H} + \underset{(B)}{Y\bullet}$$

The reactivity of the π,π^* carbonyl triplets is decreased by methoxy substitution and also as the solvent polarity increases.[1,2]

Hydrogen abstraction by the polymer triplets occurs from good H-donors (cumene and isopropanol), and the data are shown in Figures 3.56-3.61. In addition, the effects of these H-donors on the rates of chain scission (dS/dt) are shown in Figures 3.68-3.70. It is clear that the triplets are being deactivated by the H-donors, the rates varying with H-donor concentration (Figures 3.56-3.61). The character of the carbonyl triplets is once again indicated by the different behaviour of the polymers, the PMAP triplet being obviously more reactive in abstraction (Figures 3.68-3.70). At the same time, the lower reactivities of P34DMAP and P35DMAP can be rationalized in terms of lower reactivity of the predominantly π,π^* triplet.

In the presence of transfer agents, the rate of degradation is decreased. The competing reactions are summarized in the following scheme in which YH and RCO are, respectively, the transfer agent and the polymer, and X is the

aromatic system.

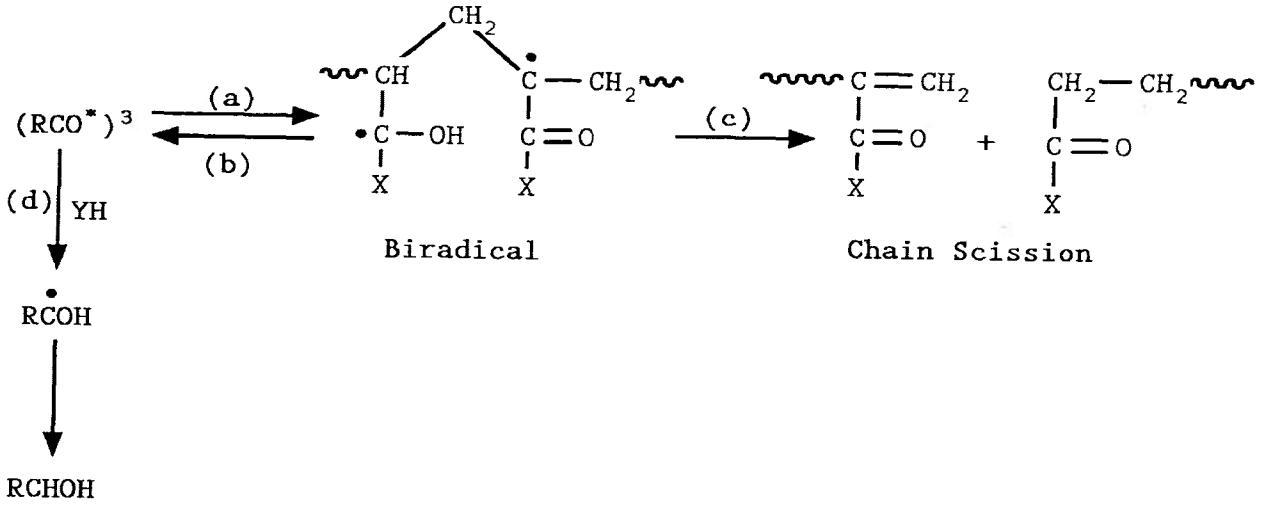

Process (b) involves a reverse hydrogen abstraction, and (d) competes with chain scission (c) and leads to the formation of a ketyl radical (A) which subsequently abstracts a hydrogen atom.

The effects of the various additives on the rates of chain scission can be understood, in a general sense, in terms of the above scheme. The competition between H-abstraction (from YH) (d) and biradical formation (a) is most obvious in the cases of cumene and isopropanol, and this can be ascribed to their high transfer abilities which, in turn, reflect their dissociation energies of the C-H bond, e.g. D_{C-H} for cumene $\approx$ 290 kJ mol^{-1} and that for isopropanol is 381 kJ mol^{-1}.[68] Similarly, the inhibiting effects of the other alcohols are less significant on account of their higher C-H dissociation energies.

In the case of P34DMAP and P35DMAP, the rates of chain scission are not only lower but the effects of the additives are smaller. These two observations are directly attributable to the π,π^* character, and hence to the lack of reactivity in abstraction, of the carbonyl triplets. In addition, the relative stabilization of the π,π^* state in polar media further reduces their reactivity towards the alcohols. The reverse situation applies in PMAP in which the triplet is not predominantly π,π^*, i.e. the triplet has relatively higher n,π^* character.

It is clear from the shapes of the curves (Figures 3.68-3.70) that the rates of degradation are not wholly dependent upon single competition shown in the scheme. Instead, they result from the interplay of a number of other variables (not necessarily independent) which produce the complex behaviour shown in Figures 3.68-3.70. It is known[16] that polar solvents stabilize (by H-bonding) the biradical and, at the same time, reduce the extent of reverse hydrogen abstraction (b). Thus, in solutions containing alcohols, the rate of degradation can be increased so that the inhibitory effect of the transfer agent can be opposed. Isopropanol appears to be less reactive in H-transfer than cumene with PMAP and P34DMAP (Figures 3.68-3.69) despite the fact that its transfer constant (C_s) is greater than that of cumene.[45] This is perhaps the result of compensation from biradical stabilization. A similar explanation may be made for the

apparent levelling off of the rates of degradation shown in a number of cases (Figures 3.68-3.70).

A further factor which is difficult to quantify must be considered, i.e. solvent quality. All of the additives are poor solvents for the polymers, and this will cause coil contraction which, in turn, will decrease the rate of Norrish type II decomposition by restricting the access of the C=O chromophore to an abstractable H-atom.[16] At the same time, there are more coil-coil contacts and this can lead to self-quenching and to inter- and intramolecular photoreductions which produce biradicals; however, they do not necessarily all undergo chain scission. The overall effect will be a reduction in the rate of chain scission, i.e. a less rapid decrease in the molecular weight (Figures 3.71-3.73).

P35DMAP appears to be anomalous in that the effects of isopropanol and cumene are reversed and the rate of degradation in the presence of *tert*-butanol increases. Since the effects of solvent polarity and quality on P35DMAP are expected to be similar to those of P34DMAP, it is unlikely that these factors are responding. However, steric effects may be more important, particularly since P35DMAP has a higher molecular weight, and increased polymer contacts and entanglement will restrict the rates of collision of the additives with the carbonyl chromophore.

The unusual effect of polymer concentration (Figures 3.54-3.55) is perhaps also explicable in terms of

increasing molecular entanglement which can lead to more self-quenching. The rates of separation and disentanglement are decreased because of an increased number of polymer-polymer contacts; hence, chain scission is inhibited. An increase in polymer concentration will also give rise to stronger cage effects. As a result, reverse hydrogen abstraction will be favoured and, at the same time, the diffusive separation of the two macrofragments formed by biradical collapse will be impeded.

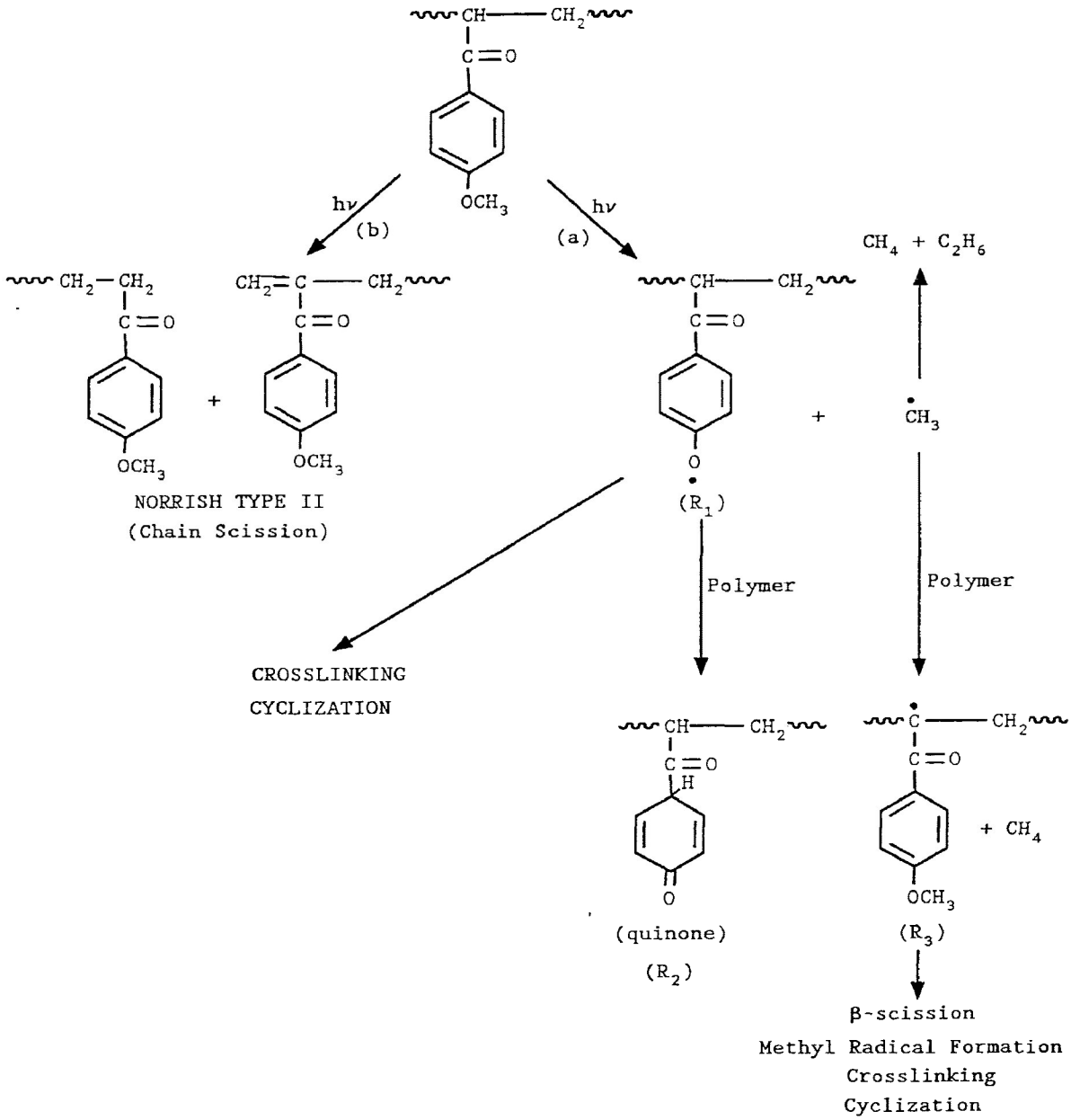
hν
(b)
hν
(a)
NORRISH TYPE II
(Chain Scission)
CROSSLINKING
CYCLIZATION
Polymer
Polymer
CH4 + C2H6
(R1)
(quinone)
(R2)
(R3)
+ CH4
β-scission
Methyl Radical Formation
Crosslinking
Cyclization

SCHEME I

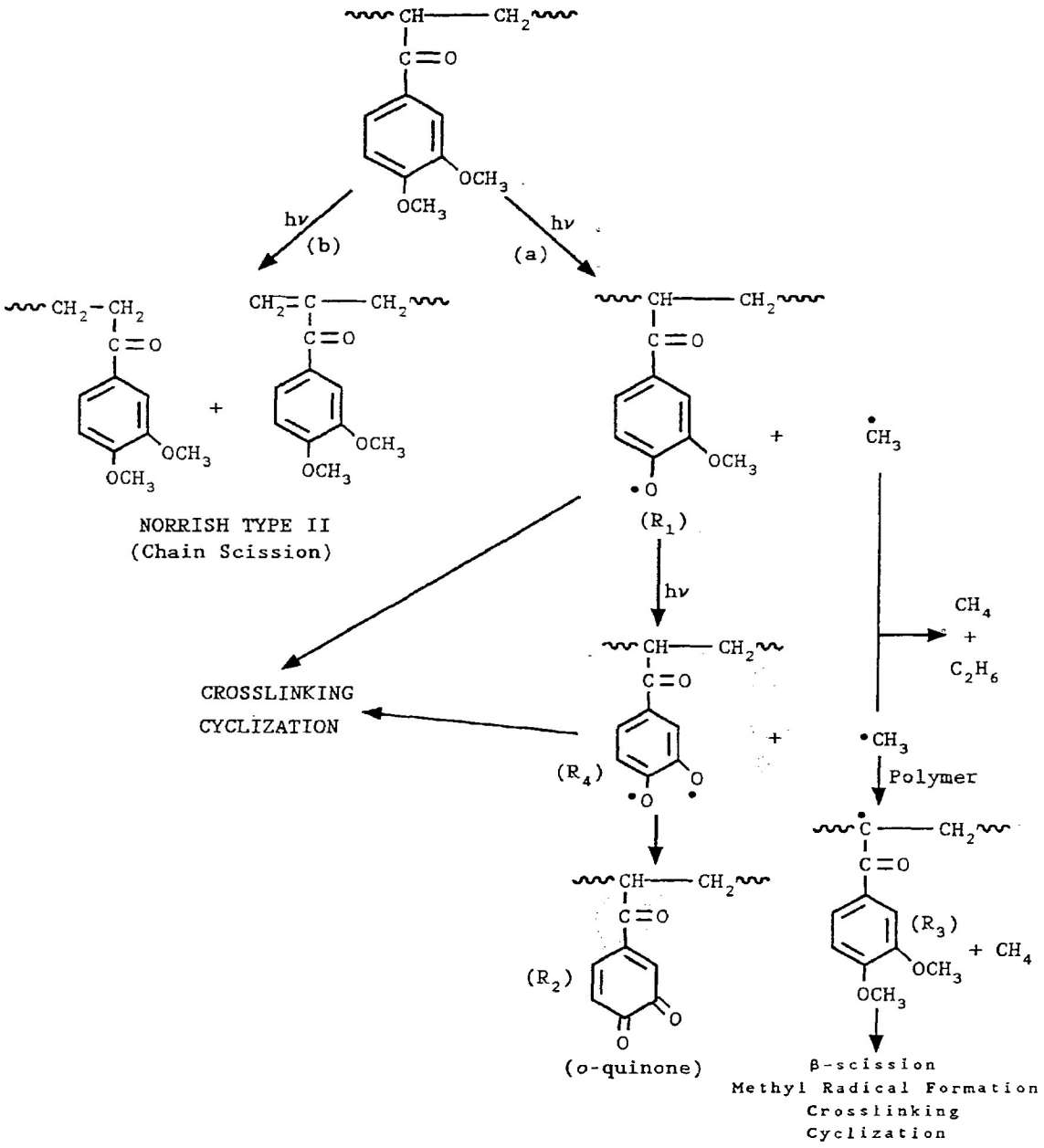
hν
(b)
hν
(a)
NORRISH TYPE II
(Chain Scission)
(R1)
hν
CROSSLINKING
CYCLIZATION
(R4)
CH4
+
C2H6
•CH3
Polymer
(R2)
(o-quinone)
(R3)
+ CH4
β-scission
Methyl Radical Formation
Crosslinking
Cyclization

SCHEME II

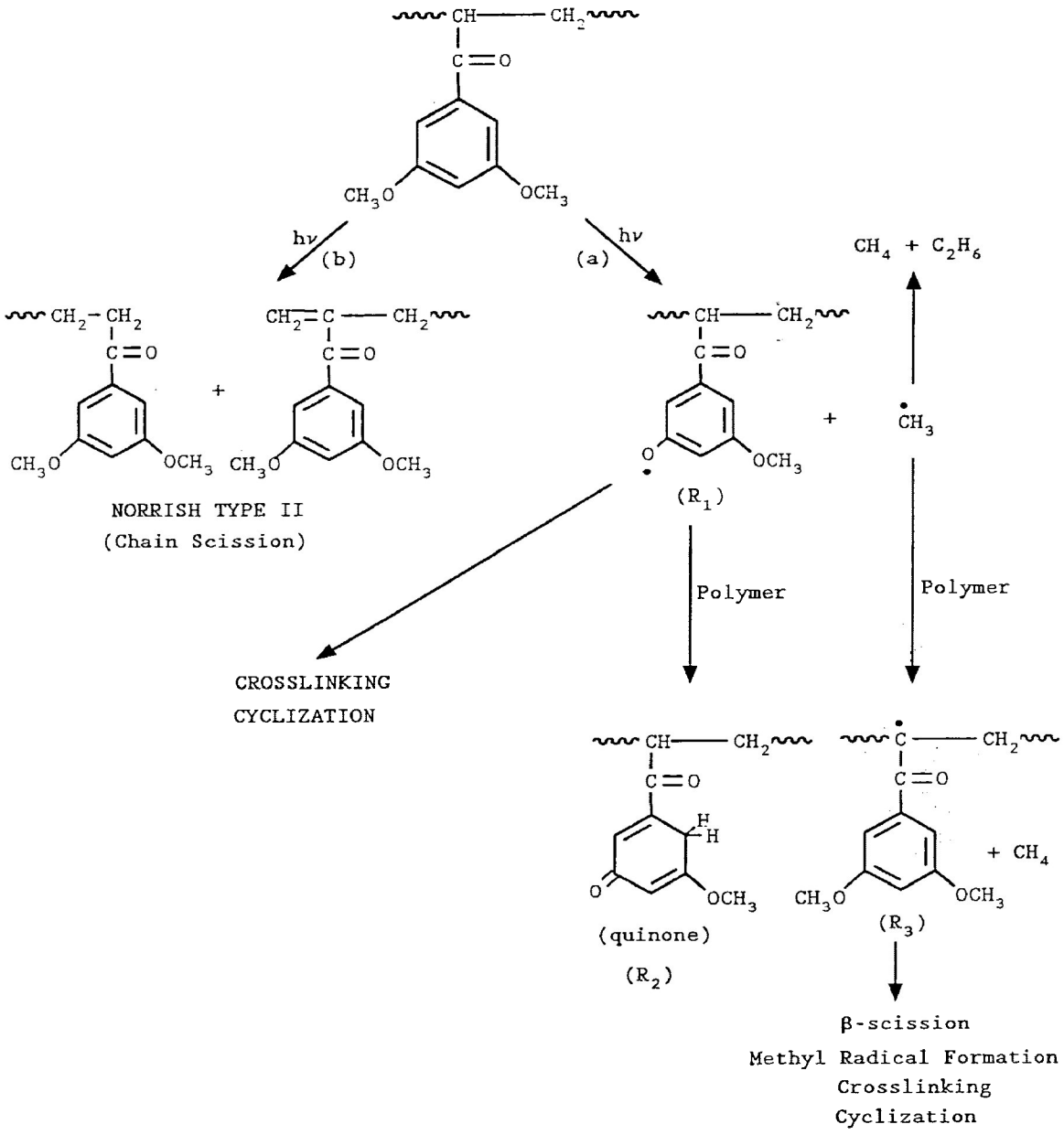
hν
(b)
hν
(a)
NORRISH TYPE II
(Chain Scission)
CROSSLINKING
CYCLIZATION
Polymer
Polymer
CH4 + C2H6
(R1)
(quinone)
(R2)
(R3)
+ CH4
β-scission
Methyl Radical Formation
Crosslinking
Cyclization

SCHEME III

V. CONCLUSIONS

This work demonstrates that methoxylated poly(acrylophenones) undergo a number of photo-processes upon exposure to long-wave UV radiation under anaerobic conditions, the principal photoreactions being sensitive to reaction conditions. Norrish type II photodecomposition dominates when the reaction is carried out in solution; however, in the solid state photodegradation, compounds whose spectral characteristics are consistent with the presence of quinones are formed. These can be derived from phenoxy radicals which are, in turn, produced by fission of O-CH_3 bonds.

The results indicate that increasing substitution of methoxy groups into the benzene ring of poly(acrylophenone) leads to increasing π,π^* character of the carbonyl triplets in the polymer. The rates of chain scission reflect the triplet character, the dimethoxy-substituted polymers (P34DMAP, P35DMAP) having quantum yields for chain scission three orders of magnitude lower than that of the methoxy-substituted derivative (PMAP).

The rates of chain scission are also sensitive to the presence of additives such as alcohols and hydrocarbons. However, these molecules do not inhibit chain scission by acting as transfer agents only. They can also alter the polarity and solvent quality, and complex chain scission behaviour is observed.

From the point of view of the photo-yellowing of lignin,

it may also be concluded that some of the colouration of lignin could be associated with pure photoreactions involving the production of quinones from phenoxy radicals which are, in turn, produced by O-CH_3 fission.

REFERENCES

1. A. Gilbert and J. Baggott. *Essentials of Molecular Photochemistry*. Blackwell Publications, London (1991).

2. J. Guillet. *Polymer Photophysics and Photochemistry*. Cambridge University Press, London (1985).

3. W.M. Horspool. *Aspects of Organic Photochemistry*. Academic Press, London (1976).

4. J.G. Calvert and J.N. Pitts, Jr. *Photochemistry*. Wiley, New York (1966).

5. B. Ranby and J.F. Rabek. *Photodegradation, Photooxidation and Photostabilization of Polymers*. Wiley, New York (1975).

6. J.A. Barltrop and J.D. Coyle. *Principles of Photochemistry*. Wiley, New York (1978).

7. D.L. Pavia, G.M. Lampman and G.S. Kriz, Jr. *Introduction to Spectroscopy*. Saunders College, Philadelphia (1979).

8. N.A. Weir and K. Whiting. *J. Polym. Sci. Part A: Polym. Chem.* **30,** 1601 (1992).

9. N.C. Yang and D.H. Yang. *J. Am. Chem. Soc.* **80,** 2913 (1958).

10. P.J. Wagner, P.A. Kelso and R.G. Zepp. *J. Am. Chem. Soc.* **94,** 7480 (1972).

11. J.C. Scaiano. *Acc. Chem. Res.* **15,** 252 (1982).

12. P.J. Wagner. *Acc. Chem. Res.* **16,** 461 (1983).

13. P.J. Wagner. *Meth. Stereochem. Anal.* **3,** 374 (1983).

14. F.D. Lewis, R.W. Johnson and D.E. Johnson. *J. Am. Chem. Soc.* **96,** 6090 (1974).

15. N.A. Weir, J. Arct and A. Ceccarelli. *J. Photochem. Photobiol. A: Chem.* **72,** 87 (1993).

16. J.E. Guillet and H.C. Ng. *Macromolecules* **18,** 2294 (1985).

17. J.E. Guillet and R.G.W. Norrish. *Nature* **173,** 625 (1954).

18. J.E. Guillet and R.G.W. Norrish. *Proc. R. Soc. London, Ser. A* **233,** 153 (1955).

19. J.P. Bays, M.V. Encinas and J.C. Scaiano. *Macromolecules* **13,** 815 (1980).

20. M.V. Encinas, K. Funabashi and J.C. Scaiano. *Macromolecules* **12,** 1167 (1979).

21. N.A. Weir and K. Whiting. *Eur. Polym. J.* **26,** 991 (1990).

22. N.A. Weir, A. Ceccarelli and J. Arct. *Eur. Polym. J.* **29,** 737 (1993).

23. N.J. Turro. *Modern Molecular Photochemistry*. Benjamin, Menlo Park, CA (1978).

24. P.J. Wagner, B.P. Giri, P. Pabon and S.B. Singh. *J. Am. Chem. Soc.* **109,** 8104 (1987).

25. S. Tagawa and W. Schnabel. *Macromolecules* **12,** 663 (1979).

26. T.J.K.S. Siu and R.D. Burkhart. *Macromolecules* **22,** 236 (1989).

27. W.J. Leigh, J.C. Scaiano, C.I. Paraskevopoulos, G.M. Charette and S.E. Sugamori. *Macromolecules* **18,** 2148 (1985).

28. J.P. Bays, M.V. Encinas and J.C. Scaiano. *Macromolecules* **12,** 348 (1979).

29. P.J. Wagner, B.P. Giri, J.C. Scaiano, D.L. Ward, E. Gabe and G.L. Lee. *J. Am. Chem. Soc.* **107,** 5483 (1985).

30. N.A. Weir, J. Arct and K. Whiting. *Eur. Polym. J.* **26,** 341 (1990).

31. P. Hrdlovic and J.E. Guillet. *Polym. Photochem.* **7,** 423 (1986).

32. N.A. Weir, J. Arct and K. Whiting. *Eur. Polym. J.* **27,** 423 (1991).

33. F.W. Deeg, J. Pinsl and C. Brauckle. *J. Phys. Chem.* **90,** 5715 (1986).

34. J.E. Guillet, S.K. Li and H.C. Ng. *A.C.S. Symp. Ser.* **266,** 165 (1984).

35. P. Hrdlovic and I. Lukac. In: *Developments in Polymer Degradation-4.* N. Grassie (ed.), Elsevier Applied Science Publishers, London, 1982, p. 101.

36. G.J. Leary. *Nature* **217,** 672 (1968).

37. S.Y. Lin and K.P. Kringstad. *Norsk. Skogindustri.* **25,** 252 (1971).

38. S.Y. Lin and K.P. Kringstad. *Tappi* **53,** 658 (1970).

39. D.J. Casey and C.S. Marvel. *J. Org. Chem.* **24,** 1022 (1959).

40. I. Lukac, M. Moravcik and P. Hrdlovic. *J. Polym. Sci.: Polym. Chem. Edn.* **12,** 1913 (1974).

41. N.A. Weir and J. Arct. *J. Polym. Sci. Part A: Polym. Chem.* **25,** 3459 (1987).

42. H.G. Heller and J.R. Langan. *J. Chem. Soc. Perkin Trans. II* 341 (1981).

43. N.A. Weir and T.H. Milkie. *J. Polym. Sci.: Polym. Chem. Edn.* **17,** 3723 (1979).

44. N.A. Weir and T.H. Milkie. *Polym. Degrad. Stab.* **1,** 105 (1979).

45. J. Brandrup and E.H. Immergut. (eds.) *Polymer Handbook.* 3rd edn. Wiley, New York (1989).

46. N.A. Weir, J. Arct, A. Ceccarelli and A. Siren. *Eur. Polym. J.* **30,** 701 (1994).

47. T. Noh, E. Step and N.J. Turro. *J. Photochem. Photobiol. A: Chem.* **72,** 133 (1993).

48. I. Lukac, S. Chmela and P. Hrdlovic. *J. Photochem.* **11,** 301 (1979).

49. N.A. Weir and J. Arct. *J. Polym. Sci. Part A: Polym. Chem.* **25,** 191 (1987).

50. G. Sanchez, G. Weill and R. Knoesl. *Makromolek. Chem.* **179,** 131 (1978).

51. R. Knoesl and G. Weill. *Polym. Photochem.* **2,** 167 (1982).

52. J.C. Selwyn and J.C. Scaiano. *Polymer* **21,** 1365 (1980).

53. J.C. Selwyn and J.C. Scaiano. *Macromolecules* **14,** 1723 (1981).

54. P.J. Wagner, A.E. Kemppainen and H.N. Schott. *J. Am. Chem. Soc.* **95,** 5604 (1973).

55. M.V. Encinas, E.A. Lissi, E. Lemp, A. Zanocco and J.C. Scaiano. *J. Am. Chem. Soc.* **105,** 1856 (1983).

56. P. Hrdlovic, J. Danecek, D. Berek and I. Lukac. *Eur. Polym. J.* **13,** 123 (1977).

57. N.A. Weir, J. Arct and A. Ceccarelli. *Polym. Degrad. Stab.* **43,** 409 (1994).

58. N.A. Weir and M. Rujimethabhas. *Eur. Polym. J.* **18,** 813 (1982).

59. J. Pospisil. *Polym. Degrad. Stab.* **40,** 217 (1993).

60. I. Lukac and P. Hrdlovic. *Eur. Polym. J.* **14,** 339 (1978).

61. P. Hrdlovic, J.C. Scaiano, I. Lukac and J.E. Guillet. *Macromolecules* **19,** 1637 (1986).

62. E. Dan and J.E. Guillet. *Macromolecules* **6,** 230 (1973).

63. P.J. Wagner and I. Kochevar. *J. Am. Chem. Soc.* **90,** 2232 (1968).

64. F. Wilkinson. *Fluorescence: Theory, Instrumentation and Practice*. Dekker, New York (1967).

65. P.J. Wagner. *J. Am. Chem. Soc.* **89,** 2820 (1967).

66. D. Bellus, D.R. Kearns and K. Schaffner. *Helv. Chim. Acta* **52,** 971 (1969).

67. B. Guerin and L.J. Johnston. *Can. J. Chem.* **67,** 473 (1989).

68. S.L. Murov, I. Carmichael and G.L. Hug. *Handbook of Photochemistry*. 2nd edn. Dekker, New York (1993).